MINISTRY OF EDUCATION AND SCIENCE UKRAINE
ODESSA NATIONAL I. I. MECHNIKOV UNIVERSITY

ФОТОЭЛЕКТРОНИКА

PHOTOELECTRONICS
INTER-UNIVERSITIES SCIENTIFIC ARTICLES

Founded in 1986

Number 22

Odessa
ONU
2013

UDC 621.315.592:621.383.51:537.221

« PHOTOELECTRONICS »
№ 22–2013

INTER-UNIVERSITIES SCIENTIFIC ARTICLES

Founded in 1986

Certificate of State Registration KB No 15953

« ФОТОЭЛЕКТРОНИКА »
№ 22–2013

МЕЖВЕДОМСТВЕННЫЙ НАУЧНЫЙ СБОРНИК

Основан в 1986 г.

Свидетельство о Государственной регистрации КВ № 15953

The results of theoretical and experimental studies in problems of the semiconductor and microelectronic devices physics, opto- and quantum electronics, quantum optics, spectroscopy and photophysics of nucleus, atoms, molecules and solids are presented in the issue. New directions in the photoelectronics, stimulated by problems of the super intense laser radiation interaction with nuclei, atomic systems and substance, are considered.

For lecturers, scientists, post-graduates and students.

У збірнику наведено результати теоретичних і експериментальних досліджень з питань фізики напівпровідників та мікроелектронних приладів, опто- та квантової електроніки, квантової оптики, спектроскопії та фотофізики ядра, атомів, молекул та твердих тіл. Розглянуто нові напрямки розвитку фотоелектроніки, пов'язані із задачами взаемодії надінтенсивного лазерного випромінювання з ядром, атомними системами, речовиною.

Для викладачів, наукових працівників, аспірантів, студентів.

В сборнике приведены результаты теоретических и экспериментальных исследований по вопросам физики полупроводников и микроэлектронных приборов, опто- и квантовой электроники, квантовой оптики, спектроскопии и фотофизики ядра, атомов, молекул и твердых тел. Рассмотрены новые направления развития фотоэлектроники, связанные с задачами взаимодействия сверхинтенсивного лазерного излучения с ядром, атомными системами, веществом.

Для преподавателей, научных работников, аспирантов, студентов.

The issue is introduced to the List of special editions of the Ukrainian Higher Certification Commission in physics-mathematics and technical sciences. Scientific articles «Photoelectronics» collection abstracted in ВИНИТИ and «Джерело», and are in scientificmetric base INDEX COPERNICUS with ICV 5.19.

Збірник включено до Переліку спеціальних видань ВАК України з фізико-математичних та технічних наук. Збірник «Photoelectronics» реферується у ВІНІТІ (Москва) та «Джерело» (Київ) і знаходиться у науковометричній базі INDEX COPERNICUS з ICV 5.19.

Сборник включен в Список специальных изданий ВАК Украины по физико-математическим и техническим наукам. Сборник «Photoelectronics» реферируется в ВИНИТИ (Москва) и «Джерело» (Киев) и находится в наукометричной базе INDEX COPERNICUS с ICV 5.19.

Address of editorial board:
Odessa National I. I. Mechnikov University 42, Pasteur str., Odessa, 65026, Ukraine
e-mail: wadz@mail.ru, tel.: +38-048765 32 16.

Information is on the site: http://www.photoelectronics.onu.edu.ua

TABLE OF CONTENTS:

Valentyn A. Smyntyna
Doctor of Physical and Mathematical Sciences, Full Professor,
Honoured Scientist of Ukraine,
Laureate of State Premium of Ukraine in the field of Science and Technology

Valentyn Smyntyna was born on September 8, 1948, in the village Vyshneve (Tatarbunary district of Odessa region). In 1966 he graduated with honors from Tuzlovski secondary school and was enrolled in the Faculty of Physics of Odessa I. I. Mechnikov State University (now Odessa National I. I. Mechnikov University, ONU), from which he graduated with honors in 1971. He has successfully completed post-graduate studies in ONU in 1974 (with the title of Candidate of Sciences (PhD) in 1977); in 1988 he took the degree of Doctor of Physical and Mathematical Sciences, and in 1992 – the title of Full Professor. He is permanently working in ONU, being consequently Vice-Dean for science and research of the Faculty of Physics, Head of the Department of Experimental Physics, Advisor to the Rector, Vice-Rector for international cooperation, Rector.

In 1995 Valentyn Smyntyna was elected and appointed as rector ONU and thereafter effectively stimulates the active development of this university during 15 years till 2010. During the period of Valentyn Smyntyna terms of office (tenure), ONU was awarded the status of National University in 2000, in 2006 its' achievements were recognized by Diploma of the Cabinet of Ministers of Ukraine, and in 2009 it was nominated as the best classic university of independent Ukraine; the University was awarded numerous Grand Prix, gold, silver and bronze medals in international and national exhibitions and competitions, it was included into first 2000 of the most famous universities in the world according to the Webometrics rating and into 120 research universities in the world, it has become the first classical university of independent Ukraine which signed Bologna Magna Charter.

In 1989 Valentyn Smyntyna has found scientific research laboratory of sensor electronics, later – research and training center of medical

and biological physics and in 2008 – interagency Physicotechnical Centre of double submission to Ministry of Education and Science and National Academy of Sciences of Ukraine; he is effectively managing and supervising activities of all these structures. In 1996 he implemented the first in Ukraine unique complex "School - College - University", the model of which was reproduced by leading universities of Ukraine in frames of their structures. Since 1995 Valentyn Smyntyna has created and developed a network of educational units of ONU located in 9 cities in the south of Ukraine; he has opened 10 faculties and institutes, over 20 educational departments and as many new fields of studies in Odessa National University; the quality of students' training has considerably improved: the number of Doctors of Sciences, Professors, increased from 95 to nearly 200, and Candidates of Sciences, Associate Professors - from 375 to about 800.

Valentyn Smyntyna is well-known distinguished physicist, whose studies are widely recognised in Ukraine and abroad, he is the author of over 700 scientific works, 11 scientific monographs (4 - personal, 2 of them in English published in New York), 27 patents for inventions, 12 textbooks (5 personal) recommended by Ministry of Education and Science of Ukraine, including the first in Ukraine "Course of general physics" in 6 volumes.

Valentin Smyntyna is recognised leader of scientific school for physics of semiconductor's surface which determines development of this branch in Southern Ukraine and makes significant impact on these studies in Ukraine in the whole. He is the Head of specialized scientific council for examination of dissertations for a degree of Doctor of Sciences in Physics in four specialties; 5 Doctor of Sciences and over 10 Candidate (PhD) dissertations were prepared under his supervision.

The main scientific results were achieved by Valentyn Smyntyna in the field of study of electron-molecular phenomena on the surface and in the bulk of semiconductor polycrystalline films and nanostructured materials, layers of oxide semiconductors and compound semiconductor materials, in which he has discovered the new type of electrical heterogeneity (chemisorptional-electric domain); he has put forward, explained and validated its model and electron-molecular nature.

In 2007 Valentyn Smyntyna was awarded by the State Premium of Ukraine in the field of science and technology; in addition, two more State Premium of Ukraine in the field of science and technology were awarded in 2009 and 2011 for two other research projects realized in frames of headed by him Physicotechnical Center.

The most important results of scientific research of Valentyn Smyntyna are published in international peer-review editions with high Scopus citation index, and *h*-index and in those ones recognized by the American Institute of Physics.

Valentyn Smyntyna is well-known in Ukraine and abroad public figure acting as Vice-President and since 2013 as a Coordinating Council member of Ukrainian Physical Society, chairman of its Southern Branch, member of the State Accreditation Committee of Ukraine (2003-2006), vice-head of scientific council for semiconductor physics of Presidium of National Academy of Sciences, member of Committee for State Awards of Ukraine in the field of science and technology, deputy head of Southern Scientific Centre of National Academy of Sciences (1995-2010), scientific supervision of regional seminar on problems of physics and the Head of the Coordination board on Semiconductor Physics of Southern Scientific Center of NAS of Ukraine.

During 1980-1992 he was member of Ukrainian and Southern regional boards of scientific and technical societies analytical instrumentation and Ukrainian Republican Council of analytical instrumentation, in 1997-2000, - supervisor of nationwide coordination plan for semiconductor physics and metals; in 2002-2006 - deputy and presidium member of Odessa Regional Council, Chairman of the Committee for Science and Education.

Valentyn Smyntyna is the editor-in-chief of scientific journals "Sensor Electronics and Microsystem Technologies" and "Photoelectronics" recognized as professional ones by Attestation Commission of Ukraine, Editor of "Herald of Odessa University" (1995-2010).

He is successful organizer of many important international conferences, in particular, 1-st national congress "Physics in Ukraine", 1st pan-Ukrainian Conference on Physics of Semiconductors, Congress EUROSENSOR, founder and head the organizing committee of the first five international conferences "Sensor Electronics and Microsystem Technologies ".

Since 1994 he is member of the European Physical Society, the only from Ukraine permanent member of EUROSENSOR steering committee; honorary member of EUROSENSOR and former member of NEXUS program bureau; full member of Optical Society of America, American Physical Society and of other authoritative professional associations, since 1998 he collaborates with the editorial advisory board of Sensors Update publisher, and since 2010 he is member of the council of experts of Danube University Association.

Valentyn Smyntyna has realized his professional development at national research centers in Italy, France, Germany, Finland, South Korea and State Department of the United States and in other countries. Since 1992 he is the coordinator and Ukrainian team leader of series international research projects developed in cooperation with scientists from Italy, France, Portugal, Finland, Sweden, Latvia and Turkey. He collaborates with research and educational institutions of nearly 20 countries. The results of his research are regularly discussed at recognized international scientific conferences, where he made over 100 presentations.

As the University professor Valentyn Smyntyna deliver implemented by him newest special course "Physical and chemical phenomena on the surface of solids" and the fundamental course "Optics", Master course "Photoelectric processes in semiconductors", specialized and review lectures for University students in Italy, Finland, France, Great Britain, the Netherlands and other countries.

Honored Worker of Science of Ukraine, laureate of the State Prize of Ukraine in Science and Technology, Professor Valentyn Smyntyna is marked by over 50 governmental and branch awards and distinctions of Ukraine, Italy, Vatican, USA, France, Great Britain, Bulgaria, China, Finland, and Hungary, by insignia of Orthodox churches of Ukraine and Russia. He is Honorary Senator of Szeged University (Hungary), Honorary Professor of Technical University of Qingdao (China), Kherson National Technical University, Institute of Management and Economics "Galician Academy", Academy of St. Peter and Paul (Vatican), Moscow Humanitarian University, member of the Club of Rectors of Europe, member of the Association of Rectors of European universities, Honorary Citizen of Ochakiv, Honorary member of the Council of Rectors of Odessa region.

The article is received in editorial 15.07.2013

PACS: 07.07.Df, 68.43.-h

A. Tereshchenko, R. Viter, I. Konup, V. Ivanitsa, S. Geveliuk, Yu. Ishkov, V. Smyntyna

Odessa National I. I. Mechnikov University, 42, Pastera str., Odessa, 65023, Ukraine
e-mail: alla_teresc@onu.edu.ua

TiO_2-PORPHYRIN NANOSTRUCTURES FOR AMINO ACID DETECTION

A novel optical sensor based on TiO_2 nanoparticles for Valine (one of the twenty standard amino acids within proteins) detection has been developed. In the presented work, commercial TiO_2nanoparticles (Sigma Aldrich, particle size 32 nm) were used as sensor templates. The sensitive layer was formed by a porphyrin coating on a TiO2 nanostructured surface. As a result, an amorphous layer between the TiO_2 nanostructure and porphyrin was formed. Photoluminescence (PL) spectra were measured in the range of 370-900 nm before and after porphyrin application. Porphyrin adsorption led to a decrease of the main TiO_2 peak at 510 nm and the emergence of an additional peak of high intensity at 700 nm. Absorption spectra (optical density vs. wavelenght, measured from 300 to 800 nm) also showed great changes; absorption edge shift and additional peaks appearing. Adsorption of amino acid resulted in a decrease of the intensity of the PL peak due to porphyrin and an increase of intensity of the TiO_2 main PL peak. The interaction between the sensor surface and the amino acid leads to the formation of new complexes on the surface and results in a reduction of the optical activity of porphyrin. Sensitivity of the sensor with respect to different concentrations of Valine was calculated. The developed sensor can determine the consentration of Valine in the range of 0.04 to 0.16 mg/ml.

1. INTRODUCTION

Amino acids are complex molecules forming building blocks of proteins and involved in metabolism as intermediates. There are twenty amino acids involved in protein construction. Each of them contains a unique functional group, which defines the fundamental properties such as size, shape, charge, capacity for hydrogen bonding, hydrophilicity/hydrophobicity and chemical reactivity. Valine ($C_5H_{11}NO_2$), the one of the most important amino acids, is a branched-chain essential amino acid, hydrophobic and usually localized inside of proteins [1]. It is a stimulating agent which promotes muscle growth and tissue regeneration [2,3]. Valine can be used as food additive [4,5], nutrient and/or dietary supplement in animal drugs, feeds, and related products [6,7]. Because of the above mentioned properties, Valine is often used by bodybuilders (in conjunction with leucine and isoleucine) as stimulating agent. However, high concentrations of Valine can induce a crawling sensation on the skin and hallucinations [8], what is crucial for people with kidney or liver disease. Therefore, the determination of the Valine concentration in human body is an important task in medicine.

Titanium dioxide is chemically stable, nontoxic and a low-cost material which is well known for its good optical, photocatalytic and sensing properties [9-15]. Over the last decade, TiO_2 nanostructures, due to quantum-size effects such as absorption edge shift and the appearance of photoluminescence at room temperature, have been increasingly used as a sensor platform [16-26]. Recently, there has been a growing interest in the development of a new class of hybrid systems - TiO_2 -sensitizers, in which macrocycles such as porphyrins are used to form the sensitive layer [24]. Porphyrins are brightly colored pigments, containing nitrogen, that consist of conjugated multiple-loop systems, based on six-

teen-membered microcycles, composed of four pyrrole molecules and bridges. A porphyrin molecule contains a coordination cavity, bound by four nitrogen atoms, having a radius of about 2Å. This molecule is capable to coordinate with metal ions of different degree of oxidation. As a result, porphyrin-metal complexes, so-called metalloporphyrins, are being formed, that possess unique combinations of structural, physical and chemical features with high biological and catalytic activity.

It is known that porphyrin application enhances photocatalytic activity of the samples. In [27], the role of both metal and macrocycle in the photocatalytic processes have been studied by utilizing TiO_2 samples coated by porphyrins and metalloporphyrins. Significant changes in optical properties of nanoporous glass filled with TiO_2 and TiO_2 /porphyrin nanostructures have previously been found [28]. In this paper we report on the investigation of new optical biosensor based on TiO_2 nanoparticles coated by porhyrin for Valine detection.

2. EXPERIMENTAL

Commercial TiO_2 nanoparticles (Sigma Aldrich, particle size 32 nm) were used as a biosensor template. TiO_2 nanoparticles were dissolved in water to prepare sols. TiO_2 layers were formed on glass substrates by dropping TiO_2 sols on the substrate and drying it at room temperature [21]. Post annealing treatment at 300 0C for 1 hour was performed to remove water from the samples. Structural properties of the obtained samples were studied by SEM.

The fabrication of sensitive layers was performed by dropping of porphyrin "5,15-di(n-nonyl),10,20-di(4-pyridyl) porphynatotin dichloride" (chemical structure is shown in Figure 1) solution in chlorophorm on TiO_2 surface. Photoluminescence (PL) spectra were measured with the setup presented in Figure 2. The samples were excited by a UV laser (LCS-DTL-374QT, L_{ex}=355 nm) and PL spectra were recorded in the wavelength range of 370-800 nm. Absorbance spectra were measured with the use of a UV-VIS spectrophotometer (Shimadzu UV-1700) in the range of 350-1100 nm.

To check the sensitivity of porphyrin to Valine, PL spectra of porphyrin layer before and after interaction with Valine were studied. To study biosensor response, different concentrations of Valine in aqueous solution were deposited on TiO_2-porphyrin surfaces.

The spectra, measured after Valine deposition, showed no drastic changes in the PL intensity and peak position (see Fig.3 in sec.).

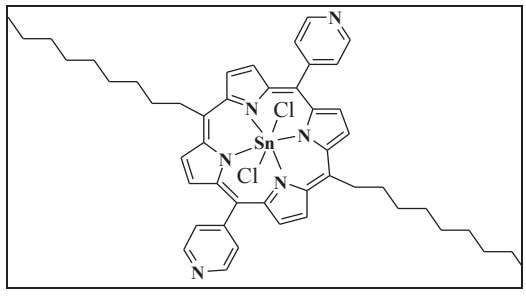

Fig.1. **Chemical structure of porphyrin**

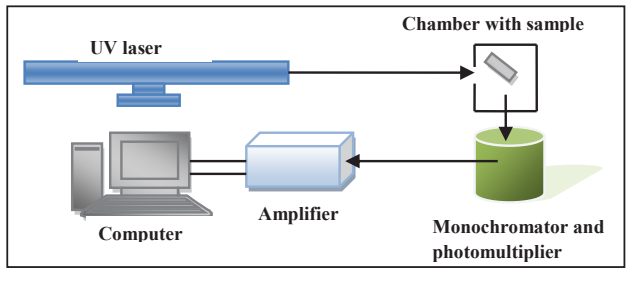

Fig.2. **Experimental setup for photoluminescence measurements**

3. RESULTS AND DISCUSSION

The obtained TiO_2 nanostructures were rough and porous as it is shown in Figure 3. Absorption spectra of initial porphyrin layer and porphyrin coated TiO_2 nanostructure are shown on Figure 4. The porphyrin demonstrated a Sorret band absorption, centered at 424 nm. It was found that after deposition of porhyrin on TiO_2, the Sorret band was shifted toward IR region, matching the interaction TiO_2-porphyrin.

Deposition of porphyrin layer resulted in significant changes in the PL spectrum of TiO_2-porhyrin nanostructure (Figure 4). Initially, TiO_2 emission spectrum showed wide peak, centered at 510 nm and the poprhyrin emission was centered at 693 nm.

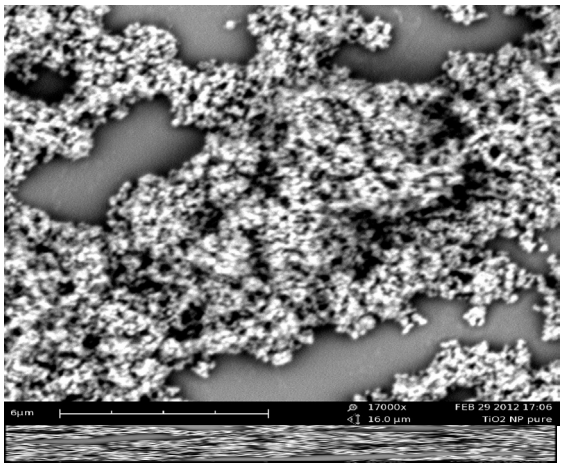

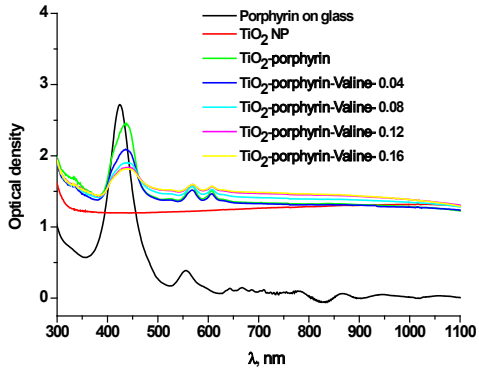

Fig.3. **SEM image of TiO_2 nanostructures**
Fig.4. **Absorption spectra of the studied samples**

The peak, related to pure TiO_2 was quenched by a factor of three, while a peak, related to porphyrin, shifted to 700 nm after the formantion of TiO_2 -porphyrin complex (Fig.5). The obtained PL data confirm the absorption results, matching to the interaction between metal oxide and porphyrin (ADD pure porphyrin spectra in the PL to discuss the changes).

We suggest that the creation of the porphyrin-metal oxide structure was caused by the formation of an amorphous layer as a result of the activation of porphyrin complexes by TiO_2. The optical properties of porphyrin could change due to a special porphyrin complex containing both hydrophobic and hydrophilic parts as well as due to labile chlorine atoms associated with the central tin atom.

Sensor response to Valine is shown in Figures 4, 5. It was found that absorption of TiO_2-porphyrin decreased with increase of Valine concentration (Figure 4).

It was found that initially, the porphyrin showed low sensitivity to Valine (Figure 5, inserted plot). The significant changes of PL intensities and peak positions observed after adsorption of Valine on TiO_2-porphyrin surface (Figure 5). Adsorption of Valine led to a quenching and a blue-shift of the porphyrin emission band. At the same time, an increase of the intensity of TiO_2 emission was observed.

The obtained results point to the irreversible interaction between porphyrin and amino acid, resulted in the formation of new complexes between them and a reduction of optical activity of porphyrin.

The sensor signal was calculated using photoluminescence and absorption data S_{lumin} (and S_{ads}):

$$S = \frac{S_0 - S_{Val}}{S_0}, \qquad (1)$$

where S_0 and S_{Val} are PL (and absorption) signals of TiO_2-porphyrin nanostructure related to porhyrin emission and absorption, measured before and after Valine adsorption, respectively. The sensitivity of the sensor was obtained as the ration of the sensor response S_{lumin} (and S_{ads}) due to (1) to the corresponding concentration of amino acid[26] C.

The sensitivity of the sensor vs Valine concentration is plotted in Figure 6. The obtained TiO_2 based sensor coated by porphyrin can detect Valine in the range of 0.04 to 0.16 mg/ml.

4. CONCLUSIONS

The TiO_2 and porphyrin form stable complex, proofed by the changes of absorption and PL of the porphyrin (IR shift) after deposition on TiO_2, matching to TiO_2 -porphyrin interaction. TiO_2 nanostructure coated by porphyrin showed good properties for Valine detection. The irreversible interaction between TiO_2 -porphyrin complex and Valine was confirmed by PL and absorption quenching after Valine adsorption and UV shift of PL peak position. The obtained results provide a basis for perspective applications of TiO_2 -porphyrin nanostructures for effective detection of Valine.

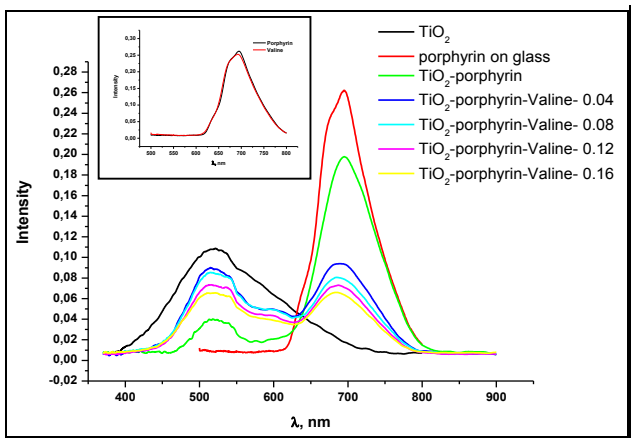

Fig.5. **PL spectra of the TiO_2-porphyrin sensor measured at**

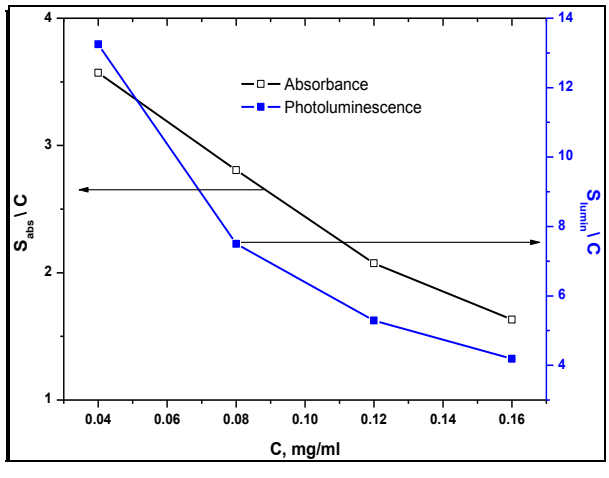

Fig.6. **Response of sensor for different concentrations different concentrations of Valine of Valine**

References

[1] Chawla, S. and Pundir, C. S., "An electrochemical biosensor for fructosylvaline for glycosylated hemoglobin detection based on core-shell magnetic bionanoparticles modified gold electrode," Biosens Bioelectron 26(8), 3438-3443 (2011).

[2] Borsheim, E., Tipton, K. D., Wolf, S. E. and Wolfee, R. R., "Essential amino acids and muscle protein recovery from resistance exercise," Am J Physiol Endocrinol Metab 283, 648–657 (2002).

[3] Volpi, E., Nazemi, R., and Fujita, S., "Muscle tissue changes with aging," Curr Opin Clin Nutr Metab Care.7(4), 405–410 (2004).

[4] Maher T. J. and Wurtmant, R. J., "Possible Neurologic Effects of Aspartame, a Widely Used Food Additive," Environmental Health Perspectives, 75, 53-57 (1987).

[5] Senyuva, H., Gokmen, V., "Interference-free determination of acrylamide in potato and cereal-based foods by a laboratory validated liquid chromatography–mass spectrometry method," Food Chemistry 97, 539–545 (2006).

[6] Fleurence, J., "Seaweed proteins: biochemical, nutritional aspects and potential uses," Trends in Food Science & Technology 10, 25-28 (1999).

[7] Tatsumi, R., "Mechano-biology of skeletal muscle hypertrophy and regeneration: Possible mechanism of stretch-induced activation of resident myogenic stem cells," Animal Science Journal 81, 11–20 (2010).

[8] http://www.anyvitamins.com/valine-info.htm

[9] Notestein, J. M., Iglesia, E. and Katz, A., "Photoluminescence and Charge-Transfer Complexes of Calixarenes Grafted on TiO_2 Nanoparticles," Chem. Mater. 19, 4998-5005 (2007).

[10] Habibi, M. H., Nasr-Esfahani, M. and Egerton, T. A., "Preparation, characterization and photocatalytic activity of TiO_2 Methylcellulose nanocomposite films derived from nanopowder TiO_2 and modified sol–gel titania," J Mater Sci 42, 6027–6035 (2007).

[11] Ding, Y., Zhang, P., Long, Z., Jiang, Y., Xu, F. and Lei, J., "Fabrication and photocatalytic property of TiO_2 nanofibers," J Sol-Gel Sci Technol 46, 176–179 (2008).

[12] Hosseinnia, A., Pazouki, M and Karimian K., "Photocatalytic reaction of aryl amines/alcohols on TiO_2 nanoparticles," Res Chem Intermed 36, 937–945 (2010).

[13] Chan, S. C and Barteau, M. A., "Physico-Chemical Effects on the Scale-Up of Ag Photodeposition on TiO_2 Nanoparticles," Top Catal 54, 378–389 (2011).

[14] Ruiterkamp, G. J., Hempenius, M. A., Wormeester, H. and Vancso, G. J., "Surface functionalization of titanium dioxide nanoparticles with alkanephosphonic acids for transparent nanocomposites," J Nanopart Res 13, 2779–2790 (2011).

[15] Qi, F., Moiseev, A., Deubener, J and Weber, A., "Thermostable photocatalytically active TiO_2

anatase nanoparticles," J Nanopart Res 13, 1325–1334 (2011).
[16] Viticoli, M., Curulli, A., Cusma, A., Kaciulis, S., Nunziante, S., Pandolfi, L., Valentini, F. and Padeletti, G., "Third-generation biosensors based on TiO_2 nanostructured films," Materials Science and Engineering C 26, 947 – 951 (2006).
[17] XiLin, X., LiXia, Y., ManLi, G., ChunFeng, P., QingYun C. and ShouZhuo, Y., " Biocompatibility and in vitro antineoplastic drug-loaded trial of titania nanotubes prepared by anodic oxidation of a pure titanium," Sci China Ser B-Chem 52(12), 2161-2165 (2009).
[18] Tasviri, M., Rafiee-Pour, H.-A., Ghourchian, H. and Gholami, M. R., "Amine functionalized TiO_2 –carbon nanotube composite: synthesis, characterization and application to glucose biosensing," Appl Nanosci 1, 189–195 (2011).
[19] Zhong, H., Yuan, R., Chai, Y., Li, W, Zhang, Y. and Wang, C., "Amperometric biosensor for hydrogen peroxide based on horseradish peroxidase onto gold nanowires and TiO_2 nanoparticles," Bioprocess Biosyst Eng 34, 923–930 (2011).
[20] Memesa, M., Lenz, S., Emmerling, S. G. J., Nett, S., Perlich, J., Müller-Buschbaum, P and Gutmann, J. S., "Morphology and photoluminescence study of titania nanoparticles," Colloid Polym Sci 289, 943–953 (2011).
[21] Viter, R., Smyntyna, V., Starodub, N., Tereshchenko, A., Kusevitch, A., Doycho, I., Geveluk, S., Slishik, N., Buk, J., Duchoslav, J., Lubchuk, J., Konup, I., Ubelis A. and Spigulis, J., "Novel Immune TiO_2 Photoluminescence Biosensors for Leucosis Detection," Procedia Engineering 47, 338 – 341 (2012).
[22] Tereschenko, A., Viter, R., Starodub, N., Ogorodniichuk Y. and Smyntyna, V., "Photoluminescence Immune Biosensor for Salmonella Detection, Based on TiO_2 Nanowires," "Photonics Technologies – Riga 2012" Programme Abstracts 48 (2012).
[23] Drbohlavova, J., Chomoucka, J., Hrdy, R., Prasek, J., Janu, L., Ryvolova, M., Adam, V., Kizek, R., Halasova, T and Hubalek, J., "Effect of Nucleic Acid and Albumin on Luminescence Properties of Deposited TiO_2 Quantum Dots," Int. J. Electrochem. Sci. 7, 1424 – 1432 (2012).
[24] Kharian, S., Teymoori, N., Khalilzadeh and M. A., "Multi-wall carbon nanotubes and TiO_2 as a sensor for electrocatalytic determination of epinephrine in the presence of p-chloranil as a mediator," J Solid State Electrochem 16, 563–568 (2012).
[25] Li, J., Kuang, D., Feng, Y., Zhang, F. and Liu, M., "Glucose biosensor based on glucose oxidase immobilized on a nanofilm composed of mesoporous hydroxyapatite, titanium dioxide, and modified with multi-walled carbon nanotubes," Microchim Acta 176, 73–80 (2012).
[26] Cosnier, S., Gondran, C., Senillou, A., Gratzel, M. and Vlachopoulos, N., "Mesoporous TiO_2 Films: New Catalytic Electrode Materials for Fabricating Amperometric Biosensors Based on Oxidases," Electroanalysis 1997, 9, No. 18 0 WILEY-VCH Verlag GmbH, D-69469 Weinheim, 1387-1392 (1997).
[27] Mele, G., Del Sole, R., Vasapollo, G., Garcia-Lopez, E., Palmisano, L., Jun, L., Slota, R. and Dyrda, G., "TiO_2-based photocatalysts impregnated with metallo-porphyrins employed for degradation of 4-nitrophenol in aqueous solutions: role of metal and macrocycle," Res. Chem. Intermed. 33(3–5), 433–448 (2007).
[28] Viter, R., Geveliuk, S., Smyntyna, V., Doycho, I., Rysiakiewicz-Pasek E. and Buk, J "Investigation of optical properties of nanoporous glass filled with TiO_2 and TiO_2/porphyrin nanostructures," PGL'2011, 32 (2011).
[29] Smyntyna V., [Semiconductor Materials for Gas Sensors], Nova Publishers, New York, 39-91 (2013)

The article is received in editorial 17.07.2013

PACS: 07.07.Df, 68.43.-h

A. Tereshchenko, R. Viter, I. Konup, V. Ivanitsa , S. Geveliuk, Yu. Ishkov, V. Smyntyna

TiO_2-PORPHYRIN NANOSTRUCTURES FOR AMINO ACID DETECTION

Abstract

A novel optical sensor based on TiO_2 nanoparticles for Valine (one of the twenty standard amino acids within proteins) detection has been developed. In the presented work, commercial TiO_2 nanoparticles (Sigma Aldrich, particle size 32 nm) were used as sensor templates. The sensitive layer was formed by a porphyrin coating on a TiO_2 nanostructured surface. As a result, an amorphous layer between the TiO_2 nanostructure and porphyrin was formed. Photoluminescence (PL) spectra were measured in the range of 370-900 nm before and after porphyrin application. Porphyrin adsorption led to a decrease of the main TiO_2 peak at 510 nm and the emergence of an additional peak of high intensity at 700 nm. Absorption spectra (optical density vs. wavelenght, measured from 300 to 800 nm) also showed great changes; absorption edge shift and additional peaks appearing. Adsorption of amino acid resulted in a decrease of the intensity of the PL peak due to porphyrin and an increase of intensity of the TiO_2 main PL peak. The interaction between the sensor surface and the amino acid leads to the formation of new complexes on the surface and results in a reduction of the optical activity of porphyrin. Sensitivity of the sensor with respect to different concentrations of Valine was calculated. The developed sensor can determine the consentration of Valine in the range of 0.04 to 0.16 mg/ml.

Key words Titanium dioxide, nanoparticles, optical sensor, porphyrin, amino acid

PACS: 07.07.Df, 68.43.-h

А. Терещенко, Р. Витер, И. Конуп, В. Иваница, С. Гевелюк, Ю. Ишков, В. Смынтына

НАНОСТРУКТУРА TiO_2-ПОРФИРИН ДЛЯ ОПРЕДЕЛЕНИЯ АМИНОКИСЛОТЫ

Резюме

Разработан новый оптический датчик, основанный на наночастицах TiO_2 для обнаружения валина (одна из двадцати стандартных аминокислот среди белков). В представленной работе наночастицы коммерческого TiO_2 (Sigma Aldrich, размер частиц 32 нм) использовались как образцы датчика. Чувствительный слой был сформирован порфириновым покрытием на наноструктурированную поверхность TiO_2. В результате, между TiO_2 наноструктурой и порфирином был сформирован аморфный слой. Спектр фотолюминесценции (ФЛ) был измерен в диапазоне 370-900 нм до и после нанесения порфирина. Адсорбция порфирина приводила к уменьшению главного пика TiO_2 при 510 нм и появлению дополнительного пика большой интенсивности при 700 нм. Спектры поглощения (зависимость оптической плотности от длины волны измеренная в интервале от 300 до 800 нм) также проявляют большие изменения; сдвиг края поглощения и появление дополнительных пиков. Адсорбция аминокислоты проявилась уменьшением интенсивности пика ФЛ обусловленная порфирином и увеличением интенсивности главного пика ФЛ TiO_2. Взаимодействие между поверхностью датчика и аминокислотой ведет к формированию новых комплексов на поверхности и является результатом уменьшением оптической активности порфирина. Была рассчитана чувствительность датчика относитель-

но различных концентраций валина. Разработанный датчик может определять концентрацию валина в диапазоне 0.04 - 0.16 мг/мл.

Ключевые слова: Диоксид титана, наночастицы, оптический датчик, порфирин, аминокислота

PACS: 07.07.Df, 68.43.-h

А. Терещенко, Р. Вітер, І. Конуп, В. Іваниця, С. Гевелюк, Ю. Ішков, В. Сминтина

НАНОСТРУКТУРА TiO_2-ПОРФІРИН ДЛЯ ВИЗНАЧЕННЯ АМІНОКИСЛОТИ

Резюме

Розроблено новий оптичний датчик, заснований на наночастинках TiO_2 для виявлення валіну (одна з двадцяти стандартних амінокислот серед білків). У представленій роботі наночастинки комерційного TiO_2 (Sigma Aldrich, розмір частинок 32 нм) використовувалися як зразки датчика. Чутливий шар було сформовано порфіриновим покриттям на нано- структуровану поверхню TiO_2. У результаті, між наноструктурою TiO_2 і порфірином було сформовано аморфний шар. Спектр фотолюмінесценції (ФЛ) вимірювався у діапазоні 370-900 нм до і після нанесення порфірина. Адсорбція порфірина призводила до зменшення головного піка TiO_2 при 510 нм і появи додаткового піка великої інтенсивності при 700 нм. Спектри поглинання (залежність оптичної щільності від довжини хвилі вимірювана в інтервалі від 300 до 800 нм) також виявляють великі зміни; зсув краю поглинання і появу додаткових піків. Адсорбція амінокислоти проявилася зменшенням інтенсивності піка ФЛ обумовлена порфірином і збільшенням інтенсивності головного піка ФЛ TiO_2. Взаємодія між поверхнею датчика та амінокислотою веде до формування нових комплексів на поверхні і має результатом зменшенням оптичної активності порфірину. Було розраховано чутливість датчика щодо різних концентрацій валіну. Розроблений датчик може визначати концентрацію валіну в діапазоні 0.04–0.16 мг/мол.

Ключові слова: Діоксид титану, наночастинки, оптичний датчик, порфірин, амінокислота

PACS nambers:65.40.De, 62.25.De
UDC 53.096; 53.092; 539.89

A. G. Kuzmich, D. A. Andrusenko, P. A. Tesel'ko, M. V. Isaiev, R. M. Burbelo

Faculty of Physics, Taras Shevchenko National University of Kyiv, 64/13, Volodymyrs'ka St., 01601 Kyiv, Ukraine, e-mail: kuzmich@univ.kiev.ua

THERMOLELASTIC STRESSES STUDY IN NANOCOMPOSITE SYSTEM "POROUS SILICON – LIQUID"

In the paper the results of thermoelastic properties of nanocomposite system "porous silicon – liquid" study is presenting. Contribution of different mechanisms that lead to such system deformation under its heating was evaluated. Different sources of such deformation – as dynamical, related with thermal induced pressures of liquids in the pores, as stationary, related with forces of different nature that occur at the interface "porous matrix – liquid" – were compared.

1. INTRODUCTION

The main interest for modern material research is provided by multicomponent advanced materials such as composite structures of different nature. Among such system should be marked out the complex composite materials the separated components of which have very different properties. Especially its deals with materials which structure have been designed in vitro from the smallest scale up. This system can behave like any materials that can be found in nature [1].

For this kind of materials nanocomposite structures "porous solid matrix – liquid" may be included. From applied point of view investigations of composite system "porous silicon – liquid" properties [2, 3] are very important because such structures appear in different fields of science and technology (e. g. medicine, chemistry industry, optoelectronics [4], alternative energy craft [5] etc.). Under practical implementations this structures subjected to thermal loads that why investigation of elastic deformations and pressures that occur in such materials is necessary.

The thermal physical properties of such inhomogeneous structures are often investigating by photoacoustic techniques [6] because these methods are noncontact and nondestructive. Such methods give the possibility to exanimate the thermoelastic deformations of porous matrix, thermal induced pressures of liquid in the pore and even taking in consideration liquid' moving in porous media. Let notice that the thermalelasticity properties of complex composite systems "porous matrix – liquid" are ambiguous.

In the paper the results of thermaelasticity stresses investigations in nanocomposite systems "porous silicon –liquid" are presenting.

2. THERMALLY INDUCED DEFORMATIONS

2.1 Thermoelasticity stresses of solid state

Value of elasticity strain that occur in unbounded sample under it heating from the temperature T_0 to T is

$$\varepsilon_{ij} = \alpha_T (T - T_0)\delta_{ij}$$

here a_T – coefficient of thermal expansions, d_{ij} - Kronecker delta.

These strain occur as results of thermoelastic source action, which can be estimate as

$$\Delta\sigma = K\varepsilon = -K\alpha_T \Delta T\,, \qquad (1)$$

here K - elastic modulus, $\Delta T = T - T_0$.

In the paper [7] the formations of photoacoustic response (piezoelectric type formations) in porous silicon on substrate was experimentally measurement. It was shown that expressions described thermoelasticity stresses in porous media but the elasticity modulus and thermal expansions coefficient must be taken in effective media approximation.

2.2 Thermally induced pressures of "porous matrix - liquid" composite system

Under nanocomposite system "porous matrix – liquid" heating beside thermoelastic source the liquid expansions influence on overall sample stresses have been also considered

$$\Delta\sigma = -\left(K\alpha_T + \xi\beta_T/\beta\right)\Delta T, \qquad (2)$$

here x - porosity of porous matrix, β_T - liquid thermal expansions coefficient, β - liquid compressibility. For ethanol the value $\beta_T = 108\times10^{-5}\,\mathrm{K}^{-1}$, $1/\beta = 1275\times10^{6}$ Pa and $\beta_T/\beta = 1{,}3\times10^{6}$ Pa/K respectively.

The expression describes the source of thermal induced pressures (TIP) that appeared in the composite structure under it heating in the case of viscount liquid.

In the [2] was shown that liquid' moving in the pore can influence significantly on TIP distribution in the structures. So in general case

$$\Delta\sigma = -K\alpha_T\Delta T - \xi p, \qquad (3)$$

here p - pressures of liquid in the pores, that included thermal expansions and relaxations (that depend on liquid moving) components.

The expressions (3) do not depend on interactions between the solids matrix and liquids filler. This interaction forces can influence on general structures deformations and will analyzed more details in the next sections.

3. Interections between solid matrix and liquids

It is known [8] that general deformations of structure "Porous matrix – liquid" depend on interactions forces of different nature (such as surface tension and disjoining pressure) between solid matrix and liquid. The pressures that caused by these forces from grand potential (Ω) adjusted

$p_s = \left(\partial\Omega/\partial V\right)_{\mu,T}$, μ – chemical potential.

In this sections we will experimentally estimate the value of these forces and will analyzed its dependence on temperature.

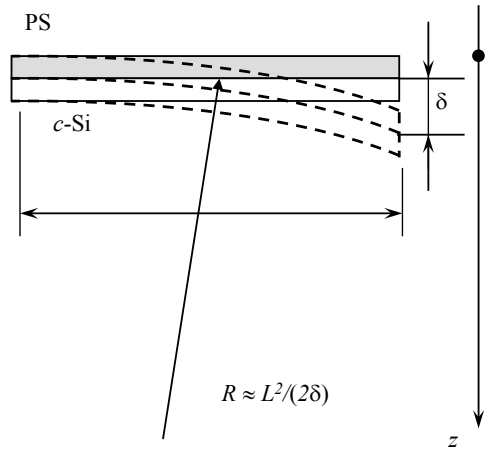

Fig. 1 – **Geometry of the experiment**

3.1 Experiment and results

As sample the plate (50x5x0.53 mm) which consist layer of porous silicon (thickness 0.24 mm, porosity 60%) on monocrystalline Si (thickness 0.29 mm) wafer was chosen. Sample was immersed in a cell with an ethanol under temperature 293 K. Under alcohol in the pores absorption the sample was bended as results of pressures that appeared at development interphase boundary of porous silicon specific surface action [9]. The initial value of this bending (see fig. 1) was δ = 375 μm.

In the cell with the sample the temperature was changed slowly in diapason 285-310 K and sample' bending was measurement. The dependence δ on temperature is presented at the fig.2.

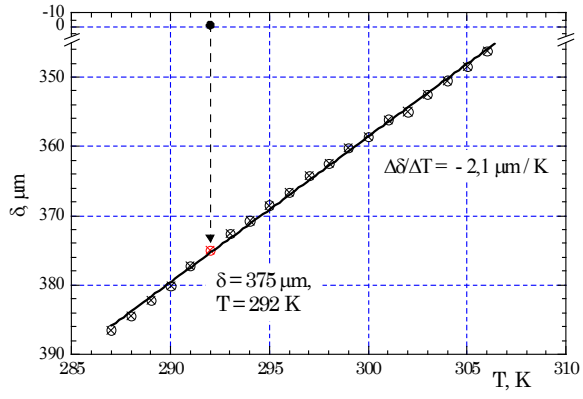

Fig. 2 – **Dependence of the bending composite system "porous silicon – liquid" on temperature. Let us estimate the value of pressures that provide the experimentally observed initially bending of the sample on the basis of balance forces and moment forces:**

$$\int_0^{h_{PS}} (\sigma_{PS} - p_s)dz + \int_{h_{PS}}^{h_{PS}+h_{c-Si}} (\sigma_{c-Si})dz = 0$$

$$\int_0^{h_{PS}} (\sigma_{PS} - p_s)zdz + \int_{h_{PS}}^{h_{PS}+h_{c-Si}} (\sigma_{c-Si})zdz = 0$$

here E_{PS}, E_{c-Si} - Young's modulus; ν_{PS} ν_{c-Si} - Poisson's ratio; h_{PS} h_{c-Si} - the thickness of porous monocrystalline layer respectively; p_s - interface pressures $\sigma_{PS} = E_{PS}/(1-\nu_{PS})\times\varepsilon_{PS} = \hat{E}_{PS}\times\varepsilon_{PS}$, $\sigma_{c-Si} = E_{c-Si}/(1-\nu_{c-Si})\times\varepsilon_{c-Si} = \hat{E}_{c-Si}\times\varepsilon_{c-Si}$ – the thermoelasticity stresses.

According to the linear law of spatial sample strain distribution [10] $\varepsilon = (a - bz)$ and taking in account that $b = 1/R = 2\delta/L^2$ (R – bending radius and L - the sample length) we can obtained

$$\delta = \left[p_s + \hat{E}_{PS}(\alpha_{T\,PS} - \alpha_{T\,c\text{-}Si})\Delta T\right]\times\frac{3L^2}{h_{C\text{-}Si}\hat{E}_{c\text{-}Si}}\times \times\frac{m(m+1)}{m^4n^2 + n(4m^3 + 6m^2 + 4m) + 1} \quad (4)$$

here $n = \hat{E}_{PS}/\hat{E}_{c-Si}$ $m = h_{PS}/h_{c-Si}$.

Using value of Younge' modulus of porous silicon and c-Si and its Poisson' ratio [11] the value of the interface pressures calculated by is

$$p_s = (3.9 \div 4.6)\times 10^6 \text{ Pa}.$$

Experimentally observed changing δ on temperature ($d\delta/dT$) is negative, so the sample extension under heating. The change of pressures value that caused decreasing bending ($\Delta\delta$) can be estimated as

$$\left|p_s + \hat{E}_{PS}(\alpha_{T\,PS} - \alpha_{T\,c\text{-}Si})\Delta T\right|/\Delta T \approx -6\times10^4 \text{ Pa/K} \textbf{ Pa /K.}$$

Using the value of thermal expansions coefficient for porous silicon and c-Si [12] changing of interfaces pressures on temperature can be estimated as

$$dp_s/dT \approx -6\times10^4 \text{ Pa/K} \textbf{ Pa /K}$$

4. Conclusions

In the paper the value of pressures that appeared at interface surface "porous matrix – liquid" was estimate. The dependence of these pressures on temperature was presented. The results of experimental measurement were analyzed in such cases:

The porous matrix was filled by liquid;

The "porous silicon – liquid" was subjected by heating;

The value of the pressures where compared with value of thermally induced pressures obtained by photoacoustic methods.

It was established that the value of thermally induced pressures that appeared in structure under it heating much more than the value of temperature changing pressures of interaction between solid matrix and liquid.

The results of this paper at the 2nd International Conference "Nanomaterial: Applications and Properties" was presented.

References

1. J. Page Metamaterials: Neither solid nor liquid. // *Nature materials*. Nature Pub-

lishing Group. – 2011. – Vol. 10, № 8. – P. 565–566.
2. D. A. Andrusenko, R. M. Burbelo, A. G. Kuzmich Photothermoacoustic conversion in porous matrix-liquid filler systems // *Technical Physics Letters*. –2010. –Vol.36, №12. – P. 1121-1124.
3. D. Andrusenko, M. Isaiev, A. Kuzmich, V. Lysenko, R. Burbelo Photoacoustic effects in nanocomposite structure 'porous silicon-liquid'// *Nanoscale research letters*. –2012. –Vol. 7, № 1. –P.1–5.
4. W. Sun, N. P. Kherani, K. D. Hirschman, L. L. Gadeken, P.M. Fauche. A Three-Dimensional Porous Silicon p-n Diode for Betavoltaics and Photovoltaics // *Advanced Materials*. –2005. –Vol. 17, № 10. –P.1230–1233.
5. K.-L Chu., M. Shannon, R.I.Masel. Porous silicon fuel cells for micro power generation // *Journal of Micromechanics and Microengineering*. –2007. – Vol.17, № 9. – P. S243–S249.
6. R. Burbelo, D. Andrusenko, M. Isaiev, A. Kuzmich. Laser photoacoustic diagnostics of advanced materials with different structure and dimensions // *Archives of Metallurgy And Materials*. –2011. –Vol. 56, №4. –P.1157-1162.
7. S. Alekseev, D. Andrusenko, R. Burbelo, M. Isaiev and A. Kuzmich. Photoacoustic thermal conductivity determination of layered structures PS-Si: piezoelectric detection // *Journal of Physics: Conference Series*. –2011. – Vol. 278. – P. 012003.
8. G. Y. Gor, A.V. Neimark. Adsorption-Induced Deformation of Mesoporous Solids: Macroscopic Approach and Density Functional Theory // *Langmuir*. –2011.–Vol.27, №11. –P.6926-6931.
9. L. T. Canham, and A.J. Groszek. Characterization of microporous Si by flow calorimetry: Comparison with a hydrophobic SiO_2 molecular sieve // *J. Appl. Phy*s. –1999. –Vol.72, №4. –P.1558-1562.
10. W. Nowacki. *Thermoelasticity*. Pergamom Press. Oxford–London–New York–Paris. 1999.
11. Y. Al-Douri, N.M. Ahmed, N. Bouarissa, A. Bouhemadou. Investigated optical and elastic properties of Porous silicon: Theoretical study // *Materials and Design* . – 2011. –Vol.32, №7. –P.4088-4093. C
12. Faivre, D. Bellet, and G. Dolino. X-ray diffraction investigation of the low temperature thermal expansion of porous silicon // *Journal of Applied Physics* . – 2000. – Vol.87, №5. –P.2131-2137.

The article is received in editorial 21.05.2013

UDC 53.096; 53.092; 539.89

A. G. Kuzmich, D. A. Andrusenko, P. A. Tesel'ko, M. V. Isaiev and R. M. Burbelo

THERMOLELASTIC STRESSES STUDY IN NANOCOMPOSITE SYSTEM "POROUS SILICON – LIQUID"

Abstract

In the paper the results of thermoelastic properties of nanocomposite system "porous silicon – liquid" study is presenting. Contribution of different mechanisms that lead to such system deformation under its heating was evaluated. Different sources of such deformation – as dynamical, related with

thermal induced pressures of liquids in the pores, as stationary, related with forces of different nature that occur at the interface “porous matrix – liquid” – were compared.

Keywords: Porous Silicon, Composite System, Thermally Induced Deformations, Thermally Induced pressure.

УДК 53.096; 53.092; 539.89

А. Г. Кузьмич, Д. А. Андрусенко, П. А. Теселько, Н. В. Исаев, Р. М. Бурбело

ТЕМОУПРУГИЕ НАПРЯЖЕНИЯ В НАНОКОМПОЗИТНОЙ СИСТЕМЕ «ПОРИСТЫЙ КРЕМНИЙ – ЖИДКОСТЬ»

Резюме

В роботе представлены результаты исследования термоупругих напряжений, которые возникают в нанокомпозитной системе «пористый кремний – жидкость». Оценен вклад различных механизмов, приводящих к деформациям указанных систем под воздействием теплового возмущения. Проведен сравнительный анализ различных источников таких деформаций: динамических, связанных с термоиндуцированным давлением жидкости в порах, и стационарных, связанных с силами взаимодействия различной природы, которые возникают на интерфейсе «пористая матрица – жидкость».

Ключевые слова: пористый кремний, композит, термоиндуцированные деформации, термоиндуцированное давление.

УДК 53.096; 53.092; 539.89

А. Г. Кузьмич, Д. А. Андрусенко, П. О. Теселько, М. В. Ісаєв, Р. М. Бурбело

ТЕРМОПРУЖНІ НАПРУГИ В НАНОКОМПОЗИТНІЙ СИСТЕМІ «ПОРУВАТИЙ КРЕМНІЙ – РІДИНА»

Резюме

В роботі приведено результати дослідження термопружних напружень, що виникають у нанокомпозитній системі «поруватий кремній – рідина». Оцінено внесок різних механізмів, що призводять до деформацій вказаних систем при термічному збудженні. Проведено порівняльний аналіз різних джерел таких деформацій: динамічних, зумовлених термоіндукованим тиском рідини в порах, та стаціонарних, пов’язаних із силами взаємодії різної природи на інтерфейсі «порувата матриця –рідина».

Ключові слова: поруватий кремній, композит, термоіндуковані деформації, термоіндукований тиск.

UDC 539.184

A. V. Glushkov

Odessa State Environmental University, 15, Lvovskaya str., Odessa, Ukraine
e-mail: dirac13@mail.ru

OPERATOR PERTURBATION THEORY TO HYDROGEN ATOM IN A STRONG DC ELECTRIC FIELD

A consistent uniform quantum approach to the solution of the non-stationary state problems including the DC strong-field Stark effect and also scattering problem is presented. It is based on the operator form of the perturbation theory for the Schrödinger equation. The method includes the physically reasonable distorted-waves approximation in the frame of the formally exact quantum-mechanical procedure. The zero-order Hamiltonian possessing only stationary states is determined only by its spectrum without specifying its explicit form. The method allows calculating the resonance complex energies and widths plus a complete orthogonal complementary of the scattering state functions. The calculation results of the Stark resonance energies and widths for the hydrogen atom are presented and compared with other theoretical data.

1. Introduction

The Stark effect [1] is one of the best known problems in quantum mechanics, but at the same time one of the most difficult (outside the weak-field region) [1-8]. A new interest in this effect has been stimulated in the last two decades. A range of the interesting phenomena to be studied includes: quasi-discrete state mixing; a zoo of the Landau- Zener anticrossings in non-hydrogenic (non-H) atoms; autoionization in non-H atoms; the effects of potential barriers (shape resonances); new kinds of resonances above threshold etc [1-63]. The dielectronic recombination involves highly excited (Rydberg) atomic states, which are very strongly affected by relatively weak fields [3-6]. In fact these states provide the gateway for ion-electron recombination processes. Now it is well known that weak-field effects on Rydberg states can cause the large changes in electron-ion collision cross sections. One subject stands out quite clearly: possible non-perturbative effects of the electric fields on the autoionization states responsible for dielectronic recombination. It is of a great importance for a consistent treating the different processes in a laser plasma, astrophysical environments etc [4-14]. Naturally in the last two decades a great progress has been made on the Stark effect for the hydrogen atom as well as for non-H atoms [2-62].

An external electric field shifts and broadens the bound state atomic levels. The standard quantum -mechanical approach relates complex eigenenergies (EE) $E = E_r + i\Gamma/2$ and complex eigenfunctions (EF) to the shape resonances. The field effects drastically increase upon going from one excited level to another. The highest levels overlap forming a "new continuum" with lowered boundary. The calculation difficulties inherent to the standard quantum mechanical approach are well known. Here one should mention the well-known Dyson phenomenon. The Wentzel-Kramers-Brillouin (WKB) approximation overcomes these difficulties for the states lying far from the " new continuum" boundary. Some modifications of the WKB method [4,8,50,65,66] are introduced in Stebbings and Dunning (1983), Kondratovich and Ostrovsky (1982, 1984), Popov et al (1988, 1990) and Glushkov, Ivanov and Letokhov (1975, 1992), where the first theoretical estimation of the effectiviness of the selective ionization of the Rydberg atom using electric and laser fields has been fulfilled. The usual WKB approximation applicability is substantiated in the case of a relatively weak electric field [2,3]. One can show that the standard form of the WKB method

applicability condition can be reformulated as the requirement that the examined resonances be well separated one from other. The same is so regarding the widespread asymptotic phase method (Damburg and Kolosov 1976), based on the Breit-Wigner parameterization for the asymptotic phase shift dependence on scattering energy and the method by Luc-Koenig and Bachelier, who have used a normalization constant [42,48]. Different calculational procedures are used in the Pade and then Borel summation of the divergent Rayleigh-Schrödinger perturbation theory (PT) series (Franceschini et al 1985, Popov et al 1990) and in the sufficiently exact numerical solution of the difference equations following from expansion of the wave function over finite basis (Benassi ans Grecchi 1980, Maquet et al 1983, Kolosov 1987, Telnov 1989, Anokhin-Ivanov 1994), complex-scaling method [17-55]. It should be noted that the latter has been extensively used to describe the resonance behavior in different atomic and even molecular systems. Its mathematical foundation is linked with the theory of dilatation analyticity [27,28]. Surely, though the Hamiltonian of an atom in a DC electric field is not a dilatational analytic operator, Reinhardt [44] has performed the numerical experiments on the diagonalization of the complex-scaled Stark Hamiltonian for a hydrogen with a real L basis set. The same method has been used by Cerjan et al. [40] to get new data on the ground and low-excited states of a hydrogen atom in a DC and AC fields. Farrelly and Reinhardt [47] have used the complex coordinate rotation method in combination with numerical integration of the separated equation. Ivanov-Ho [54] have applied the method for the Dirac Hamiltonian. Different applications are reviewed in Refs. [53]. Hehenberger, McIntosh and E. Brändas (1974) [21] have applied the Weyl's theory to the Stark effect in the hydrogen atom. They have shown that one of the interesting features of Weyl's theory is that it requires a complex parameter and complex solutions to the differential equations making it a powerful tool for the treatment of resonance states [21]. Rittby, Elander and Brändas (1981) [25] have applied the Weyl's theory and the complex-rotation method to phenomena associated with a continuum spectrum. Brändas and Froelich (1977) [23] have shown that a complex scale transformation of the time–dependent Schrödinger equation leads to a symmetric EE value problem containing both bound states and resonance (complex) EE values as solutions. They have stated the extended virial theorem and developed an original approach to determination of the resonance eigenvalues by means of elementary matrix manipulations. The error estimates for the approximate complex eigenvalues of the dilated Schrödinger operator are derived in Ref. [24], where the calculation data for the resonances of the DC Stark effect in the hydrogen are presented. In the complex-coordinate method a dilation transformation is used to make the resonance EF square integrable. The resonance of nondilation analytic potentials can be obtained numerically by using Simons exterior-scaling procedures within the finite-basis-set approximation [27,28]. The exterior-scaling procedure has been used only with direct numerical integration methods [27-30]. The use of a finite basis set in these calculations will enable one to use numerical techniques developed for bound states in calculating resonance positions and widths for nondilation potentials [27-36]. Rao, Liu and Li (1994) [18]) have studied theoretically the DC strong-field Stark resonances by a complex-scaling plus B-spline approach and shown that the high accuracy is attributed to the good stationarity behavior of eight trajectories with a well-adjusted 8-spline basis. Rao and Li (1995) [19] have also studied the behavior of the resonances of a hydrogen atom in parallel magnetic and electric fields with a complex scaling plus B-spline method too and received a consistent data on the corresponding resonance parameters in dependence upon the ratio of the magnetic-field strength to the electric-field strength. It is worth to remind that the similar approaches have been developed to describe the Zeemane resonances. Namely, for hydrogen atoms in pure magnetic fields, the properties of resonant states were calculated by the complex scaling, the R matrix, the operator PT (OPT) and other methods (look, for example, [4-7]. The generalization of methods to account for the resonance interference, non-H and relativistic effects is still an important problem,

though here a definite progress has been reached too. One should mention such approaches as a model potential method, quantum defect approximation, the OPT, complex scaling plus B-spline method etc [3-19, 64-75]. Regarding the quantum chaos phenomenon in atoms in electromagnetic fields (look, for example, [76-79]) note that this topic should not be considered here. Let us only note that the approach presented below together with the various methods of the theory of chaos in options [79-81] has been effectively used to describe the chaotic behavior

of the hydrogen and non-H atoms in the magnetic and microwave fields.

Here a consistent uniform quantum-mechanical approach to the solution of the non-stationary state problems including the DC strong-field Stark effect and also scattering problem is presented. It allows calculation of complex EE and especially is destined for investigation of the spectral region near the new continuum boundary. The essence of the method is the inclusion of the well known "distorted waves approximation" method in the frame of the formally exact PT. The zero-order Hamiltonian H_0 of this PT possesses only stationary bound and scattering states. To overcome formal difficulties, we define the zero-order Hamiltonian by the set of orthogonal eigenfunctions (EF) and EE without specifying the explicit form of the corresponding zeroth-order potential. To ensure rapid PT convergence, a physically reasonable spectrum (EE and EF) must be chosen as the zero order, similar to the "distorted waves" method [6,56-58]. In a case of the optimal zeroth-order spectrum, the PT smallness parameter is of the order of $\Gamma/\mathring{A}$, where Γ and E are the field width and bound energy of the state level examined. The successive PT corrections can be expressed through the matrix elements of the total Hamiltonian calculated between the zeroth-order basis functions. This method is called the OPT. We will define H_0 so that it coincides with the total Hamiltonian H at $\varepsilon \Rightarrow 0$ (e is the electric field strength.) Let us emphasize that perturbation in our theory does not coincide with the electric field potential though they disappear simultaneously. We also present a generalization of the OPT for calculation of the DC strong field Stark effect in the non-H atoms in an electric field [59-61]. The difference between the atomic and Coulomb field is taken into account by introducing the quantum defects on a parabolic basis. The results of calculation of the Stark resonance energies and widths for the H atom are listed and compared with other theoretical and experimental data.

2 Operator perturbation theory for DC strong-field Stark effect

2.1. DC strong –field Stark effect for the hydrogen atom

The Schrödinger equation for the electron function taking into account the uniform electric field and field of the nucleus (Coulomb units are used: for length, 1 unit is h^2/Ze^2m; for energy 1 unit is mZe^2e^4/h^2) is [6,57]:

$$[-(1 - N/Z) / r+V_m(r) + \varepsilon z -1/2\Delta - E] \Psi = 0, \quad (1)$$

where E is the electron energy, Z is the nucleus charge, N is the number of electrons in the atomic core (for the hydrogen atom: Z=1, N=0), V_m is an model potential (for the hydrogen atom V_m=0). Firstly, we only deal with the Coulomb part of the electron- atomic residue interaction. The non-Coulomb part, as well as relativistic effects, can be approximately accounted for next step. The separation of variables in the parabolic coordinates ($\xi = r + z,\ \eta = r - z,\ \varphi = \tan^{-1}(y/x)$):

$$\Psi(\varepsilon,h,\varphi)=f(\varepsilon)g(h)(\varepsilon\times h)^{|m|/2}\exp(im\varphi)/(2\pi)^{1/2} \quad (2)$$

transforms it to the system of two equations for the functions f, g:

$$f^{II}+\frac{|m|+1}{t}\ f^{I}+[1/2E\ +(\beta_1-N/Z)/t-1/4\varepsilon(t)t]\ f\ =\ 0, \quad (3)$$

$$g^{H}+\frac{|m|+1}{t}\ g^{1}+[1/2E+\beta_2/t+1/4\varepsilon(t)\,t]\,g=0, \quad (4)$$

coupled through the constraint on the separation constants:

$$\beta_1+\beta_2=1 \quad (5)$$

For the uniform electric field $\varepsilon(t) = \varepsilon$. In principle, the more realistic models can be considered in the framework of our approach. Potential energy in equation (4) has the barrier. Two turning points for the classical motion along the η axis, t_1 and t_2, at a given energy E are the solutions of the quadratic equation ($\beta = \beta_1$, $E = E_0$):

$$t_2 = \{[E^2_0 - 4\varepsilon(1\text{-}b)]^{1/2} - E_0\}/\varepsilon, \quad (6)$$

$$t_1 = \{-[E^2_0 - 4\varepsilon(1\text{-}\beta)]^{1/2} - E_0\}/\varepsilon, \quad t_1 < t_2 \quad (7)$$

Here and below t denotes the argument common for the whole equation system. To simplify the calculational procedure, the uniform electric field ε in (3) and (4) should be substituted by the function [57,58]:

$$\varepsilon(t) = \frac{1}{t}\,\varepsilon\left[(t-\tau)\frac{\tau^4}{\tau^4 + t^4} + \tau\right] \quad (8)$$

with sufficiently large r (r=1.5t_2). The function $\varepsilon(t)$ practically coincides with the constant ε in the inner barrier motion region (t<t_2) and disappears at t>>t_2. The minimal acceptable value of t introduced in the spatial dependence of the electric field, which does not influence the final results, can be established experimentally. Thus, the final results do not depend on the parameter t (the further calculation has entirely confirmed this fact). Besides the pure technical convenience, the case of an asymptotically disappearing electric field is more realistic from the physical point of view. Now we deal with the asymptotically free (without electric field) motion of the ejected electron along the h-axis. The corresponding effective wavenumber is:

$$k = (E/2 + \varepsilon t/4)^{1/2}. \quad (9)$$

The scattering states energy spectrum now spreads over the range $\left(-\varepsilon\tau/2, +\infty\right)$, compared with $\left(-\infty, +\infty\right)$ in the uniform field. In contrast to the case of a free atom in scattering states in the presence of the uniform electric field remain quantified at any energy E, i.e. only definite values of β_1 are possible. The latter are determined by the confinement condition for the motion along the h-axis. The same is true in our case, but only for $E \subset \left(-\frac{1}{2}\varepsilon\tau, +\frac{1}{2}\varepsilon\tau\right)$. The motion with larger E is non-quantified, similar to the free atom case.

2.2 Energy and width of the Stark resonance

The total Hamiltonian $H(\varsigma, \nu, \varphi)$ does not possess the bound stationary states. According to OPT [6, 56-58]), one has to define the zero order Hamiltonian H_0, so that its spectrum reproduces qualitatively that of the initial one. In contrast to H, it must have only stationary states. To calculate the width G of the concrete quasistationary state in the lowest PT order one needs only two zeroth–order EF of H_0: bound state function $\Psi_B(\varepsilon, \eta, \varphi)$ and scattering state function $\Psi_E(\varepsilon, \eta, \varphi)$ with the same EE. We solve a more general problem: a construction of the bound state function along with its complete orthogonal complementary of scattering functions Ψ_E with $E \subset \left(-\frac{1}{2}\varepsilon\tau, +\infty\right)$. First, one has to define the EE of the expected bound state. It is the well known problem of states quantification in the case of the penetrable barrier [65,66]. Following [57], we solve the system (3) and (4) with the total Hamiltonian H under the conditions:

$$f(t) \to 0 \text{ at } t \to \infty, \quad (10a)$$

$$\partial x(\beta, E) / \partial E = 0 \quad (10b)$$

with

$$x(b, E) = \lim_{t \to \infty} [\, g^2(t) + \{g^1(t) / k\}^2 \,]\, t^{|m|+1}. \quad (11)$$

The first condition ensures the finiteness of motion along the ς-axis, the second condition minimizes the asymptotic oscillation amplitude for the function describing the motion along the η-axis. These two conditions quantify the bound energy E and separation constant β_1. We elaborated a special numerical procedure for this two-dimensional eigenvalue problem. Our procedure deals repeatedly with the solving of the system of the ordinary differential equations (3) and (4) with probe pairs of E, β_1. The corresponding EF:

$$y_{Eb}(\zeta,\eta,\varphi)=f_{Eb}(\zeta)g_{Eb}(\eta)(\zeta\eta)^{|m|/2}exp(im\varphi)(2\eta)^{-1/2} \quad (12)$$

Here $f_{Б}(t)$ is the solution of (3) (with the just determined E, β_1) at $t\subset(0,\infty)$ and $g_{Eb}(t)$ is the solution of (4) (with the same E, β_1) at $t<t_2$ (inside barrier) and $g(t)=0$ otherwise. These bound state EE, eigenvalue β_1 and EF for the zero-order Hamiltonian H_0 coincide with those for the total Hamiltonian H at $\varepsilon\Rightarrow 0$, where all the states can be classified due to the quantum numbers n, n_1, n_2, m (principal, parabolic, azimuthal) connected with E, β_1, m by the well known expressions. We preserve the n, n_1, m states classification in the non-zero ε case. The scattering state functions:

$$\Psi_{E's}(\zeta,\eta,\varphi)=f_{E's}(z)g_{E\phi's}(\eta)(\zeta\eta)^{|m|/2}exp(im\varphi)(2\pi)^{-1/2} \quad (13)$$

must be orthogonal to the above defined bound state function and to each other. In addition, these functions must describe the motion of the ejected electron, i.e. $g_{E's}$ must satisfy the equation (4) asymptotically. Following the OPT ideology [57], we choose the next form of $g_{E's}$:

$$g_{E\phi's}(t) = g_1(t) - z_2' g_2(t) \quad (14)$$

with $f_{E's}$ and $g_1(t)$ satisfying the differential equations (3) and (4). The function $g_2(t)$ satisfies the non-homogeneous differential equation, which differs from (4) only by the right-hand term, disappearing at $t\Rightarrow\infty$. The total equation system, determining the scattering function, reads

$$f''_{E's}+\frac{|m|+1}{t}f'_{E's}+[1/2E'+(\beta_1'-N/Z)/t-1/4\cdot\varepsilon(t)t]f_{E's}=0, \quad (15a)$$

$$g_1''+\frac{|m|+1}{t}g_1'+[1/2E'+\beta_2'/t+1/4\varepsilon(t)t]g_1=0, \quad (15б)$$

$$g_2''+\frac{|m|+1}{t}g_2'+[1/2E+\beta_2'/t+1/4\varepsilon(t)t]g_2=2g_{Eb} \quad (15c)$$

($\beta_1'+\beta_2'=1$). As mentioned above there remains motion quantification for $Å'\subset\left(-\frac{1}{2}\varepsilon\tau\,,+\frac{1}{2}\varepsilon\tau\right)$. At the given E', the only quantum parameter β_1' is determined by the natural boundary condition: $f_{E's}\to 0$ at $t\to\infty$. Of course: $\beta_1'=\beta_1$, $f_{E's}=f_{Eb}$ at $E'=E$; only this case is needed in the particular problem we deal with here. The coefficient z_2' ensures the orthogonality condition $\langle\Psi_{Eb}|\Psi_{E's}\rangle=0$:

$$z_2' = \{\iint d\zeta d\eta\,(\zeta+\eta)f^2_{Eb}(\zeta)g_{Eb}(\eta)g_1(\eta)\}/\{\iint d\zeta d\eta\,(\zeta+\eta)f^2_{Eb}(\zeta)g_{Eb}(\eta)g_2(\eta)\}. \quad (16)$$

One can check that

$$\langle\psi_{Es'}|\psi_{E''s}\rangle=0 \text{ for } E'\neq E''.$$

The imaginary part of state energy in the lowest PT order is

$$\mathrm{Im}E=\Gamma/2=\pi|<\Psi_{Eb}|H|\Psi_{Es}>|^2 \quad (17)$$

with the total Hamiltonian H. The state functions $\Psi_{Б}$ and $\Psi_{Б}$ are assumed to be normalized to 1 and by the $\delta(k-k')$ condition, accordingly. The action of H on $\Psi_{Б}$ is defined unambiguously by (15):

$$(H-E')\psi_s=2|m|(\zeta\cdot\eta^2)\cdot f_{E's}(\zeta)\,g_{Eb}(\eta)z_2'\,\exp(im\varphi)/[(2\pi)^{1/2}(\zeta+\eta)],$$
$$\langle\psi_{Eb}|H|\psi_{E's}\rangle=\iint d\zeta d\eta\,(\zeta\eta)^{|m|}\eta f^2_{Eb}(\zeta)\,f^2_{E's}(\zeta)g_{Eb}(\eta)\,z_2'. \quad (18)$$

The matrix elements $\langle\Psi_{Б}|H|\Psi_{E's}\rangle$ entering the high-order PT corrections can be determined in the same way. All the two-dimensional integrals in (16)-(18) and the normalization coefficients can be expressed through the next set of one-dimensional integrals:

$$I_2=\int dt\,f_b^2(t)t^{|m|+1},\quad I_3=\int dt\;g_b(t)\,g_1(t)\,t^{|m|},\quad I_4=\int dt\,g_b(t)g_1(t)t^{|m|+1},$$
$$I_5=\int dt\;g_b(t)\,g_2(t)\,t^{|m|},\quad I_6=\int dt\;g_b(t)\,g_2(t)t^{|m|+1},\quad I_7=\int dt\,g_b{}^2(t)\,t^{|m|},\quad I_8=\int dt\,g_b{}^2(t)t^{|m|+1}, \quad (19)$$

calculated with the arbitrary normalized functions f_{Eb}, g_{Eb}, f_2, g_2 and $f_1=f_{Eb}$, $g_1=g_{Eb}$. In

this notation

$$\Gamma = 32\pi z_2^2 N_s^2 I_1^2 I_8^2 /[I_2 I_7 + I_1 I_8],$$
$$z_2 = [I_1 I_4 + I_2 I_3]/[I_1 I_6 + I_2 I_5] \qquad (20)$$

with

$$N^2{}_s = \lim_{t\Rightarrow\infty} X(t)/\{2\pi\eta^{2|m|+1}[\, g^2{}_s(\eta) X^2(t) + g'^2_s(\eta)]\}$$
$$X(t) = \{E/2 + (\beta - N/Z)/t - E\, t/4\}^{1/2} \qquad (21)$$

Remember that arbitrary normalized state functions are assumed in (20) and (21). The whole calculational procedure at known resonance energy E and separation parameter β_1 has been reduced to the solution of one system of the ordinary differential equations. This master system includes the differential equations for the state functions f_{Eb}, g_{Eb}, f_{Es}, g_{Es}, as well as the equations for the integrals $I_1 - I_8$. Thus, our calculational procedure is one-dimensional. The procedure is sufficiently simple and realized as the numerical code with using the fourth-order Runge–Kutta method of solving the differential equations (the atomic code "Superatom-ISAN-Stark").

3 Calculation results and discussion

The calculation results for the Stark resonances energies and widths of the ground state hydrogen atom in the DC electric field with the strength ε=0.04, 0.08, 0.10, 0.80 a.u. are presented in table 1 and 2. The comparison with earlier similar results, obtained within the generalized WKB approximation, summation of divergent PT series, the numerical solution of the differential equations following from expansion of the wave function over finite basis, a complex scaling plus B-spline calculation [15-51] shows quite acceptable agreement. The calculation results of the Stark resonances parameters for the excited state H atom (n=2,5,15) for different strength values are listed in table 3. The comparison with earlier similar results, obtained within the summation of divergent PT series, the numerical solution of the differential equations with using the finite basis expansion of the wave function again shows acceptable agreement.

Table 1. Energies, widths (a.u.)of Stark resonances of ground state H atom (ε=0.04, 0.08 a.u.). Notation: (a1) Mendelson [15], (a2) Alexander [17], (b1) Hehenberger- McIntosh-Brändas [21], (b2) Brändas-Froelich [23], (c) Benassi-Grecchi [46], (d) Cerjan et al. [40], (e) Farrelly-Reinhardt [47], (f) Franceschini-Greechi-Silverstone [45], (g) Reinhardt [43], (h) Maquet-Chu-Reinhardt [41], (i) Kolosov [48], (j) Damburg-Kolosov [42], (k) Anokhin-Ivanov [51], (l) Ivanov-Ho (relativistic and non-relativistic results respectively) [54], (m) Rao- Liu-Li [18], (n) the OPT method (our data), (o) – Filho et al [49].

ε	Method	*E*r, a.u.	Γ/2, a.u.
0.04	a1	-0.5038	-
	a2	-0.5038	0.2×10^{-5}
	b1	-0.5037714	0.195×10^{-5}
	b2	-0.5037715	0.191×10^{-5}
	c	-0.5037716	0.1946×10^{-5}
	f	-0.5037716	0.1946×10^{-5}
	j	-0.5037716	0.195×10^{-5}
	k	-0.5038	0.248×10^{-5}
	l	-0.5037780 -05037716	0.205×10^{-5} 0.195×10^{-5}
	m	-05037716	0.1946×10^{-5}
	n	-05037714	0.1945×10^{-5}
	o	-0503752	-
0.08	a1	-0.5193	-
	a2	-0.5175	0.230×10^{-2}
	b1	-0.51756	0.227×10^{-2}
	c	-0.51756	0.2270×10^{-2}
	f	-0.51756	0.2270×10^{-2}
	g	-0.51756	0.2269×10^{-2}
	h	-0.51756	0.2270×10^{-2}
	j	-0.51749	0.2255×10^{-2}
	k	-0.5176	0.220×10^{-2}
	m	-0.51756	0.2270×10^{-2}
	n	-0.51757	0.2270×10^{-2}
	o	-0.51745	-

Table 2. Energies and widths of the 1s H atom Stark resonances (ε=0.10,0.8a.u.); Notation: (a1) Mendelson [15], (a2) Alexander [17], (b1) Hehenberger-McIntosh-Brändas [21], (b2) Brändas-Froelich [23], (c) Benassi-Grecchi [46], (d) Cerjan et al. [40], (e) Farrelly-Reinhardt [47], (f) Franceschini-Greechi-Silverstone [45], (g) Reinhardt [43], (h) Maquet-Chu-Reinhardt [41], (i) Kolosov [48], (j) Damburg-Kolosov [42], (k) Anokhin- Ivanov [51], (l) Ivanov-Ho [54], (m) Rao, Liu and Li [18], (n) OPT method, (o) – Filho et al [49], (p)- Popov et al [65,66].

ε	Method	Er, a.u.	Γ/2, a.u.
0.10	a1	-0.556	-
	a2	-0.527	0.7500×10^{-2}
	b1	-0.52743	0.7250×10^{-2}
	b2	-0.52742	0.7270×10^{-2}
	c	-0.527418	0.7269×10^{-2}
	d	-0.527417	0.7270×10^{-2}
	f	-0.527418	0.7269×10^{-2}
	g	-0.527425	0.7271×10^{-2}
	h	-0.527418	0.7269×10^{-2}
	i	-0.527418	0.7269×10^{-2}
	j	-0.526905	0.7170×10^{-2}
	l	-0.527423 -0.527418	0.7268×10^{-2} 0.7269×10^{-2}
	m	-0.527418	0.7269×10^{-2}
	n	-0.527419	0.7269×10^{-2}
	o	-0.531090	-
	p	-0.5274	0.727×10^{-2}
0.80	e	-0.6304	0.5023
	i	-0.630415	0.50232
	m	-0.630415	0.50232
	n	-0.630416	0.50232

It is important to compare the theoretical values of the resonance energy and width for the H atom in the field ε = 16.8 kV/cm with experimental data [4]. There is quite good agreement between theory and experiment. Note that our results are obtained in the first PT order, i.e. already the first PT order provides the physically reasonable results. Naturally its accuracy can be increased by an account of the next PT order. The range of validity of the proposed method which uses the Fermi golden rule is quite wide and it is not restricted to resonances lying far from the continuum boundary.

Table 3. The energies and widths of the Stark resonances of the hydrogen atom (n=2,5). Notation: a, OPT calculation; b, Damburg and Kolosov (1976); c, Kolosov (1987); d, Benassi and Grecchi (1980); e, Telnov (1989); f, Popov et al (1990); E_x – experimental data
(from Refs. [4, 42, 46,48,57,58,65,66]).

$(n\ n_1\ n_2\ m)$	ε , a.u.	Method	Er, a.u.	Γ, a.u.
2 0 1 0	0,005	a	0.1426	$0.102\cdot10^{-3}$
		c	0.1426	$0.106\cdot10^{-3}$
		e	0.1426	$0.106\cdot10^{-3}$
	0,01	a	0.1661	$0.108\cdot10^{-1}$
		c	0.1661	$0.109\cdot10^{-1}$
		d	0.1661	$0.109\cdot10^{-1}$
		e	0.1661	$0.109\cdot10^{-1}$
2 0 0 1	0.005	a	0.1272	$0.267\cdot10^{-4}$
		c	0.1272	$0.262\cdot10^{-4}$
		e	0.1272	$0.262\cdot10^{-4}$
	0.01	a	0.1345	$0.637\cdot10^{-2}$
		c	0.1345	$0.628\cdot10^{-2}$
		e	0.1345	$0.628\cdot10^{-1}$
5 2 2 0	$1.8\cdot10^{-4}$	a	0.2062	$0.278\cdot10^{-5}$
		b	0,2062	$0.228\cdot10^{-5}$
		f	0.2062	$0.228\cdot10^{-5}$
		f	0.2062	$0.222\cdot10^{-5}$
15 10 4 0	$3.27\cdot10^{-6}$	a	$1.9098\cdot10^{-3}$	$2.782\cdot10^{-7}$
		f	$1.9095\cdot10^{-3}$	$2.278\cdot10^{-7}$
		E_x	$1.91\cdot10^{-3}$	$2.92\cdot10^{-7}$

4. Conclusions

In this paper we present the basises of a new uniform quantum-mechanical approach to the solution of the non-stationary state problems including the DC strong-field Stark effect and also scattering problem. New OPT method allows sufficiently exact calculating the complex EE and resonance widths and especially is destined for investigation of the spectral region of an atom near the new continuum boundary in a strong field. The essence of the method is the inclusion of the well known “distorted waves approximation” in

the frame of the formally exact PT. The results of the calculation of the Stark resonance energies and widths for the hydrogen atom are presented and in a physically reasonable agreement with the best results of the alternative theoretical methods and experiment. It is noted that the zeroth model approximation, including the potential of a strong external electric field, can be implemented into the general formalism of the formally exact PT for many-electron atom [6,12,59-63,71-75]. The range of validity of the presented method which uses the Fermi golden rule is sufficiently wide and it is not restricted to resonances lying far from the continuum boundary. Let us conclude that the OPT method has been also successfully applied to correct description of the resonances of the Zeeman effect in a strong magnetic field, crossed electric and magnetic fields, the resonances in molecular systems, as well as descriptions of resonant states in nuclear systems such as the resonances of the compound nucleus and the resonances arising from the collision of heavy ions (nuclei), accompanied by electron-positron pairs production (look Refs. [6,79,82-90]).

References

1. J. Stark, Ann.Phys. **43**, 965 (1914).
2. H. A. Bethe and E.E. Salpeter, Quantum mechanics of One- and Two-Electron Atoms (Springer, Berlin, 1957).
3. L. D. Landau and E. M. Lifshitz, Quantum Mechanics (Pergamon, Oxford, 1977).
4. R. F. Stebbings and F. B. Dunning (ed), Rydberg States of Atoms and Molecules (Cambridge Univ. Press, N.-Y., 1983).
5. M.N. Nayfeh and C.W. Clark (ed), Atomic Excitation and Recombination in External Fields (NBS, Gaithersburg, 1984).
6. A. V. Glushkov, Atom in an Electromagnetic Field (KNT, Kiev, 2005), pp.1-450.
7. V. S. Lisitsa, Phys.-Uspekhi **153**, 369 (1987).
8. L. N. Ivanov and V. S. Letokhov, Quantum Electron. **2**, 585 (1975).
9. L. N. Ivanov and E.P.Ivanova, Atom. Data Nucl. Data Tabl. **24**, 95 (1979).
10. A. V. Glushkov and L. N. Ivanov, Phys. Lett. A **170**, 33 (1992).
11. E. P. Ivanova and I. P. Grant, J. Phys.B: At. Mol. Opt. Phys. **31**, 2871 (1998).
12. A. V. Glushkov, in: Advances in the Theory of Quantum Systems in Chemistry and Physics. Series: Frontiers in Theoretical Physics and Chemistry, vol.**26**, ed. by K.Nishikawa, J. Maruani, E.Brändas, G.Delgado-Barrio, P.Piecuch (Berlin, Springer, 2012), pp.231-254.
13. N. B. Delone and M.V. Fedorov, Phys.-Uspekhi. **158**, 215 (1989).
14. A. J. F Siegert, Phys.Rev. **56**, 750 (1939).
15. L. B. Mendelson, Phys. Rev. **176**, 90 (1968).
16. A. D. Dolgov and A.V. Turbiner, Phys. Lett. A**77**, 15 (1977).
17. M. H. Alexander, Phys. Rev. **178,** 34 (1969).
18. J. Rao, W. Liu and B. Li, Phys. Rev. A **50**, 1916 (1994).
19. J. Rao and B. Li, Phys. Rev. A **51**, 4526 (1995).
20. H.-Y. Meng, Y.-X. Zhang, S. Kang, T.-Y. Shi and M.-S. Zhan J. Phys. B: At. Mol. Opt. Phys. **41**, 155003 (2008).
21. M. Hehenberger, H.V. McIntosh and E. Brändas, Phys. Rev. A **10**, 1494 (1974).
22. M. Hehenberger, H. V. McIntosh and E. Brändas, Phys. Rev. A **12**, 1 (1975).
23. E. Brändas and P. Froelich, Phys. Rev. A **16**, 2207 (1977).
24. E. Brändas, M. Hehenberger and H. V. McIntosh, Int. J.Quant.Chem. **9**, 103 (1975).
25. M. Rittby, N. Elander and E. Brändas, Phys. Rev. A **24**, 1636 (1981).
26. P. Froelich, E. R. Davidson, E. Brändas, Phys. Rev. A **28**, 2641 (1983).
27. N. Lipkin, N. Moiseyev and E. Brändas, Phys. Rev. A **40**, 549 (1989).
28. M. Rittby, N. Elander and E. Brändas, Int. J.Quant.Chem. **23**, 865 (1983).
29. B. Simon, Phys.Lett. A 7**1**, 211 (1979).
30. C.A. Nicolaides and D.R. Beck, Phys. Lett. A **65**, 11 (1978).
31. E. Brändas, P. Froelich, C. H. Obcemea,

N. Elander, M. Rittby, Phys. Rev. A **26**, 3656 (1982).
32. E. Engdahl, E. Brändas, M. Rittby, N. Elander, J. Math. Phys. **27**, 2629 (1986)
33. E. Engdahl, E. Brändas, M. Rittby and N. Elander, Phys. Rev. A**37**, 3777 (1988).
34. Resonances. The Unifying Route Towards the Formulation of Dynamical Processes - Foundations and Applications in Nuclear, Atomic and Molecular Physics, Series: Lecture Notes in Physics, vol. **325**, ed. by E. Brändas,N. Elander (Springer, Berlin, 1989), pp.1-564.
35. A. Scrinzi and N. Elander, J. Chem. Phys. **98**, 3866 (1993)
36. V. N. Ostrovsky and N. Elander, Phys. Rev. A**71**, 052707 (2005)
37. J. M. Sigal, Commun. Math. Phys. **119**, 287 (1988).
38. I.W. Herbst and B. Simon, Phys. Rev. Lett. **41**, 67 (1978).
39. H. J. Silverstone, B. G. Adams, J. Cizek and P.Otto, Phys. Rev. Lett. **43**, 1498 (1979).
40. C. Cerjan, R. Hedges, C. Holt, W. P. Reinhardt, K. Scheibner and J. J. Wendoloski, Int.J.Quant.Chem. **14**, 393 (1978).
41. Maquet, S. I. Chu and W. P. Reinhardt, Phys. Rev. A **27**, 2946 (1983).
42. R. J. Damburg. and V.V. Kolosov, J. Phys.B: At. Mol. Phys. **9**, 3149 (1976).
43. E. Luc-Koenig and A. Bachelier, J. Phys.B: At. Mol. Phys. **13**, 1743 (1980).
44. W. P. Reinhardt, Int.J.Quant.Chem. **21**, 133 (1982).
45. V. Franceschini, V. Grecchi and H.J. Silverstone, Phys. Rev. A **32**, 1338 (1985).
46. L. Benassi and V. Grecchi, J. Phys. B: At. Mol. Phys. **13**, 911-24 (1980).
47. D. Farrelly and W.P. Reinhardt, J. Phys. B: At. Mol. Phys. **16**, 2103 (1983).
48. V. V. Kolosov, J. Phys. B.: At. Mol. Phys. **20**, 2359 (1987).
49. Filho, A. Fonseca, H. Nazareno and P. Guimarães, Phys. Rev. A **42**, 4008 (1990).
50. V. D. Kondratovich and V. N. Ostrovsky, J. Phys. B.: At. Mol. Phys. **17**, 2011 (1984).
51. S. B. Anokhin and M. V. Ivanov, Opt. Spectr. **59**, 499 (1984).
52. D. A. Telnov, J. Phys. B.: At.Mol. Opt. Phys. **22**, 1399-403 (1989).
53. Y.-K. Ho, Phys.Rep. **99,** 3 (1983).
54. I. A. Ivanov, and Y.-K. Ho, Phys.Rev. A **69**, 023407 (2004).
55. R. González-Férez and W. Schweizer, in Quantum Systems in Chemistry and Physics, Series: Progress in Theoretical Chemistry and Physics, vol. **2/3**, ed. by A. Hernández-Laguna, J. Maruani, R. McWeeny, S.Wilson (Springer, Berlin, 2000), p. 17.
56. A. V. Glushkov and L. N. Ivanov, Proc. of 3rd Symposium on Atomic Spectroscopy (Moscow-Chernogolovka, 1992).
57. A. V. Glushkov and L. N. Ivanov, J. Phys.B: At. Mol. Phys. **26**, L379 (1993).
58. A. V. Glushkov, S. V. Malinovskaya, S. V. Ambrosov, I. M. Shpinareva, O. V. Troitskaya, J. Techn. Phys. **38**, 215 (1997).
59. A. V. Glushkov, S. V. Ambrosov, A. V. Ignatenko, D.A. Korchevsky, Int.J.Quant. Chem. **99,** 936 (2004).
60. A. V. Glushkov and A. V. Loboda, J. Appl.Spectr. (Springer) **74**, 305 (2007).
61. A. V. Glushkov, O. Yu. Khetselius, A. V. Loboda, A.A. Svinarenko, in Frontiers in Quantum Systems in Chemistry and Physics, Series: Progress in Theoretical Chemistry and Physics, vol. **18**, ed. by S. Wilson, P.J. Grout., J. Maruani, G. Delgado-Barrio, P. Piecuch (Springer, Berlin, 2008), pp.523-588;
62. A. V. Glushkov, O. Khetselius, S. Malinovskaya, Europ.Phys. Journ. T**160**, 195 (2008).
63. A. V. Glushkov, O. Yu. Khetselius, A. A. Svinarenko and G.P.Prepelitsa, in: Coherence and Ultrashort Pulsed Emission, ed. F.J. Duarte. (Intech, Vienna, 2011), pp.159-186.
64. M. L. Zimmerman, M.G. Littman, M.M. Kash, D. Kleppner, Phys. Rev. **A20**, 2251 (1979).
65. D.A. Harmin, Phys.Rev. A **26**, 2656 (1982).
66. V. Popov, V. Mur, A. Sergeev and

V. Weinberg, Phys.Lett.A **149**, 418, 425 (1990).
67. M. Grutter, O.Zehnder, T.Softley, F.Merkt, J.Phys.B: At. Mol. Opt. Phys. **41,** 115001 (2008).
68. E. Stambulchik and Y. Maron, J. Phys. B: At. Mol. Opt. Phys. 41, 095703 (2008).
69. F. B. Dunning, J. J. Mestayer, C. O. Reinhold, S. Yoshida and J Burgdörfer, J. Phys. B: At. Mol. Opt. Phys. **42**, 022001 (2009).
70. H. C. Bryant, D. A.Clark, K. B. Butterfield et al, Phys.Rev.A **27,** 2889 (1983).
71. A. V. Glushkov, S. Ambrosov, O. Yu. Khetselius, A. V. Loboda, E. Gurnitskaya, in: Recent Advances in Theoretical Physics and Chemistry Systems, Series: Progress in Theoretical Chemistry and Physics, vol. 15, ed. by J.-P. Julien, J. Maruani, D. Mayou, S. Wilson, G. Delgado-Barrio (Springer, Berlin, 2006), pp. 285-300.
72. Yu. Khetselius, J. Phys.: Conf.Ser. **397**, 012012 (2012); Int.J.Quant.Chem. **109**, 3330 (2009).
73. O. Yu. Khetselius, T. Florko, A. Svinarenko and T. Tkach, Phys.Scr.**T153**, 01437 (2013).
74. E. P. Ivanova, L. N. Ivanov, A. V. Glushkov and A.E. Kramida, Phys. Scr. **32**, 512 (1985).
75. E. P. Ivanova and A. V. Glushkov, J.Quant. Spectr. Rad. Tr. **36**, 127 (1986).
76. F. Benvenuto, G. Casati and D.L. Shepelyansky, Z.Phys.B. **94**, 481 (1994).
77. A. Buchleitner and D. Delande, Phys. Rev.A. **55**, 1585 (1997).
78. T.F. Gallagher, M. Noel and M.W. Griffith, Phys. Rev. A. **62**, 063401 (2000).
79. A. V. Glushkov and S. V. Ambrosov, J. Techn. Phys. **37,** 347 (1996).
80. A.V. Glushkov, V. Khokhlov and I. Tsenenko, Nonlin. Proc. Geophys.**11,** 285 (2004).
81. A. V. Glushkov, V. Khohlov, N. Loboda and Yu. Bunyakova, Atm.Env. **42**, 7284 (2008).
82. A. V. Glushkov, O. Yu. Khetselius, S. V. Malinovskaya, Molec.Phys. **106**, 1257 (2008).
83. A. V. Glushkov, V. D. Rusov, S. V. Ambrosov, A. V. Loboda, in New Projects and New Lines of Research in Nuclear Physics, ed. by G. Fazio, F. Hanappe (World Sci., Singapore, 2003), pp. 126-142.
84. A. V. Glushkov, in: Low Energy Antiproton Physics, vol.**796**, ed. by D. Grzonka, R. Czyzykiewicz, W. Oelert, T. Rozek and P. Winter (AIP, N.-Y., 2005), pp. 206-210.
85. A. V. Glushkov, in Meson-Nucleon Physics and the Structure of the Nucleon, vol.**2**, ed. by S. Krewald, H. Machner (IKP, Juelich, Germany), SLAC eConf C070910 (Menlo Park, CA, USA, 2007), pp.111-117.
86. A. V. Glushkov, O. Yu. Khetselius, A. V. Loboda and S.V. Malinovskaya, in Meson-Nucleon Physics and the Structure of the Nucleon, vol.**2**, ed. by S. Krewald, H. Machner (IKP, Juelich, Germany), SLAC eConf C070910 (Menlo Park, CA, USA, 2007), pp.118-122.
87. A. V. Glushkov, O. Yu. Khetselius, L. Lovett, E. P. Gurnitskaya, Yu. V. Dubrovskaya, A. V. Loboda, Int.J. Mod. Phys. A: Particles and Fields, Nucl. Phys. **24**, 611 (2009).
88. A. V. Glushkov O. Yu. Khetselius, L. Lovett, in: Advances in the Theory of Atomic and Molecular Systems: Dynamics, Spectroscopy, Clusters, and Nanostructures. Series: Progress in Theoretical Chemistry and Physics, vol. **20**, ed. by P.Piecuch, J. Maruani, G. Delgado-Barrio and S. Wilson (Springer, Berlin, 2010), pp.125-151.
89. A. V. Glushkov, O. Yu. Khetselius, A. A. Svinarenko, in: Advances in the Theory of Quantum Systems in Chemistry and Physics. Series: Progress in Theoretical Chemistry and Physics, vol. **22**, ed. by P. Hoggan, E. Brändas, J. Maruani, G. Delgado-Barrio and P. Piecuch (Springer, Berlin, 2012), pp.51-70.
90. A. V Glushkov, Relativistic Quantum Theory. Quantum Mechanics of Atomic Systems (Astroprint, Odessa, 2008), pp.1-704.

The article is received in editorial 21.05.2013

UDC 539.184

A. V. Glushkov

OPERATOR PERTURBATION THEORY TO HYDROGEN ATOM IN A STRONG DC ELECTRIC FIELD

Abstract.

A consistent uniform quantum approach to the solution of the non-stationary state problems including the DC (Direct Current) strong-field Stark effect and also scattering problem is presented. It is based on the operator form of the perturbation theory for the Schrödinger equation. The method allows calculating the resonance complex energies and widths plus a complete orthogonal complementary of the scattering state functions. The calculation results of the Stark resonance energies and widths for the hydrogen atom are presented and compared with other theoretical data.

Key words: Stark effect, hydrogen atom, DC electric field, operator perturbation theory

УДК 539.184

А. В. Глушков

ОПЕРАТОРНАЯ ТЕОРИЯ ВОЗМУЩЕНИЙ ДЛЯ ОПИСАНИЯ АТОМА ВОДОРОДА В ПОСТОЯННОС ЭЛЕКТРИЧЕСКОМ ПОЛЕ

Резюме.

Представлен новый, последовательный квантовый подход к решению проблемы нестационарных состояний, включая эффект Штарка для сильных полей, а также задачи рассеяния. Подход основан на операторной теории возмущений для уравнения Шредингера. Метод позволяет рассчитать комплексные энергии и ширины резонансов, а также полный ортогональный набор функций состояний рассеяния. Приведены результаты расчета энергий и ширин штарковских резонансов для атома водорода и проведено сравнение с другими теоретическими данными.

Ключевые слова: эффект Штарка, атом водорода, электрическое поле, операторная теория возмущений

УДК 539.184

О. В. Глушков

ОПЕРАТОРНА ТЕОРІЯ ЗБУРЕНЬ ДЛЯ ОПИСУ АТОМУ ВОДНЮ У СТАЛОМУ ЕЛЕКТРИЧНОМУ ПОЛІ

Резюме.

Представлено новий послідовний квантовий підхід до вирішення проблеми нестаціонарних станів, включаючи ефект Штарка для сильних полів, а також задачі розсіювання. Підхід заснований на операторній теорії збурень для рівняння Шредінгера. Метод дозволяє розрахувати комплексні енергії та ширини резонансів плюс повний ортогональний набір функцій станів розсіювання. Приведені результати розрахунку енергій та ширин штарківських резонансів для

UDC 681.322

O. Yu. Khetselius

I. Mechnikov Odessa National University, 2, Dvoryanskaya str., Odessa, Ukraine
Odessa State Environmental University, 15, Lvovskaya str., Odessa, Ukraine
e-mail: nuckhet@mail.ru

NEW GEOMETRIC ATTRACTOR AND NEURAL NETWORKS APPROACH TO STUDYING CHAOTIC PROCESSES IN PHOTOELECTRONICS SYSTEMS

Nonlinear modelling of chaotic processes in systems and devices, including quantum electronics and photo may be based on the concept of compact geometric attractors. We present a new approach to analyze and predict the nonlinear dynamics of chaotic systems based on the concept of geometric attractors, chaos theory methods and algorithms for neural network simulation. Using information on the phase space evolution of the physical process in time and AI simulation of neural network modelling techniques can be considered as one of the fundamentally new approaches in the construction of global nonlinear models of the most effective and accurate description of the structure of the corresponding attractor.

1. Introduction

It is very well known now that multiple quantum-and photoelectronics systems and devices could demonstrate the typical chaotic behaviour [1-2]. One could remind here laser and different quantum generators, radio-technical devices, multi-element semiconductors etc. To date, the obvious is the fact that the overwhelming number of physical and technical systems are formally very complex, and this feature is manifested at different spatial and temporal scale levels [1-11]. Naturally, the task list for studying the dynamics of complex systems is not limited to the above examples. It is not difficult to understand that examples of such systems are the chemical systems, biological populations, and finally, cybernetical (neurocybernetical) and communication system and its subsystems.

Most important, the fundamental issue in the description of the dynamics of the system is its ability to forecast its future evolution, i.e. predictability of behavior. Recently, the theory of dynamical systems is intensively developed, and, in particular, speech is about the application of methods of the theory to the analysis of complex systems that provide description of their evolutionary dynamics by means solving system of differential equations. If the studied system is more complicated then the greater the equations is necessary for its adequate description. Meanwhile, examples of the systems described by a small amount of equations, are known nevertheless, theses systems exhibit a complicated behavior. Probably the best-known examples of such systems are the Lorenz system, the Sinai billiard, etc. They are described, for example, three equations (i.e., in consideration included three independent variables), but the dynamics of their behavior over time shows elements of chaos (so-called "deterministic chaos"). In particular, Lorentz was able to identify the cause of the chaotic behavior of the system associated with a difference in the initial conditions. Even microscopic deviation between the two systems at the beginning of the process of evolution leads to an exponential accumulation of errors and, accordingly, their stochastic divergence. During the analysis of the observed dynamics of some characteristic parameters of the systems over time it is difficult to say to what class belongs to the system and what will be its evolution in the future. Many interesting examples can be reminded in the modern sstatistical physics, physics of non-ordered semiconductors etc.

In recent years for the analysis of time series of fundamental dynamic parameters there are with varying degrees of success developed and implemented a variety of methods, in particular, the nonlinear spectral and trend analysis , the study of Markov chains, wavelet and multifractal analysis, the formalism of the matrix memory and the method of evolution propagators etc. Most of the cited approaches are defined as the methods of a chaos theory. In the theory of dynamical systems methods have been developed that allow for the recording of time series of one of the parameters to recover some dynamic characteristics of the system. In recent years a considerable number of works, including an analysis from the perspective of the theory of dynamical systems and chaos, fractal sets, is devoted to time series analysis of dynamical characteristics of physics and other systems [1-11]. In a series of papers [12-15] the authors have attempted to apply some of these methods in a variety of the physical, geophysical, hydrodynamic problems. In connection with this, there is an extremely important task on development of new, more effective approaches to the nonlinear modelling and prediction of chaotic processes in physical, (in particular, quantum- and photo-electronics) systems. In this work we present an advanced approach to analysis and forecasting nonlinear dynamics of chaotic systems, based on conceptions of a geometric attractor and neural networks modelling [11,16].

2. New approach to analysis of chaotic processes

The basic idea of the construction of our approach to prediction of chaotic properties of complex systems is in the use of the traditional concept of a compact geometric attractor in which evolves the measurement data, plus the implementation of neural network algorithms. The existing so far in the theory of chaos prediction models are based on the concept of an attractor, and are described in a number of papers (e.g. [1-10]). The meaning of the concept is in fact a study of the evolution of the attractor in the phase space of the system and, in a sense, modelling ("guessing") time-variable evolution..

From a mathematical point of view, it is a fact that in the phase space of the system an orbit continuously rolled on itself due to the action of dissipative forces and the nonlinear part of the dynamics, so it is possible to stay in the neighborhood of any point of the orbit *y (n)* other points of the orbit y^r *(n), r = 1, 2, ...,* N_B, which come in the neighborhood *y (n)* in a completely different times than *n*. Of course, then one could try to build different types of interpolation functions that take into account all the neighborhoods of the phase space and at the same time explain how the neighborhood evolve from *y (n)* to a whole family of points about *y (n+1)*. Use of the information about the phase space in the simulation of the evolution of some physical (geophysical etc.) process in time can be regarded as a fundamental element in the simulation of random processes.

In terms of the modern theory of neural systems, and neuro-informatics (e.g. [11]), the process of modelling the evolution of the system can be generalized to describe some evolutionary dynamic neuro-equations (miemo-dynamic equations). Imitating the further evolution of a complex system as the evolution of a neural network with the corresponding elements of the self-study, self- adaptation, etc., it becomes possible to significantly improve the prediction of evolutionary dynamics of a chaotic system. Considering the neural network (in this case, the appropriate term "geophysical" neural network) with a certain number of neurons, as usual, we can introduce the operators S_{ij} synaptic neuron to neuron u_i u_j, while the corresponding synaptic matrix is reduced to a numerical matrix strength of synaptic connections: $W = ||\, w_{ij} \,||$. The operator is described by the standard activation neuro-equation determining the evolution of a neural network in time:

$$s_i^{'} = sign(\sum_{j=1}^{N} w_{ij} s_j - \theta_i), \qquad (1)$$

where $1<i<N$.

Of course, there can be more complicated versions of the equations of evolution of a neural network. Here it is important for us another proven fact related to information behavior neuro-dynamical system. From the point of view of

the theory of chaotic dynamical systems, the state of the neuron (the chaos-geometric interpretation of the forces of synaptic interactions, etc.) can be represented by currents in the phase space of the system and its the topological structure is obviously determined by the number and position of attractors. To determine the asymptotic behavior of the system it becomes crucial information aspect of the problem, namely, the fact of being the initial state to the basin of attraction of a particular attractor.

Modelling each physical attractor by a record in memory, the process of the evolution of neural network, transition from the initial state to the (following) the final state is a model for the reconstruction of the full record of distorted information, or an associative model of pattern recognition is implemented. The domain of attraction of attractors are separated by separatrices or certain surfaces in the phase space. Their structure, of course, is quite complex, but mimics the chaotic properties of the studied object. Then, as usual, the next step is a natural construction parameterized nonlinear function ***F*** *(x,* ***a)***, which transforms:

$$\mathbf{y}(n) \rightarrow \mathbf{y}(n+1) = \mathbf{F}(\mathbf{y}(n), \mathbf{a}),$$

and then to use the different (including neural network) criteria for determining the parameters a (see below). The easiest way to implement this program is in considering the original local neighborhood, enter the model(s) of the process occurring in the neighborhood, at the neighborhood and by combining together these local models, designing on a global nonlinear model. The latter describes most of the structure of the attractor.

Although, according to a classical theorem by Kolmogorov-Arnold -Moser, the dynamics evolves in a multidimensional space, the size and the structure of which is predetermined by the initial conditions, this, however, does not indicate a functional choice of model elements in full compliance with the source of random data. One of the most common forms of the local model is the model of the Schreiber type [3] (see also [10]).

3. Construction of the model prediction

Nonlinear modelling of chaotic processes is based on the concept of a compact geometric attractor, which evolve with measurements. Since the orbit is continually folded back on itself by the dissipative forces and the non-linear part of the dynamics, some orbit points $\mathbf{y}^r(k)$, $r = 1, 2, \ldots, N_B$ can be found in the neighbourhood of any orbit point $\mathbf{y}(k)$, at that the points $\mathbf{y}^r(k)$ arrive in the neighbourhood of $\mathbf{y}(k)$ at quite different times than k. Then one could build the different types of interpolation functions that take into account all the neighborhoods of the phase space, and explain how these neighborhoods evolve from y (n) to a whole family of points about y (n + 1). Use of the information about the phase space in modelling the evolution of the physical process in time can be regarded as a major innovation in the modelling of chaotic processes.

This concept can be achieved by constructing a parameterized nonlinear function F(x, a), which transform y(n) to y(n+1)=F(y(n), a), and then using different criteria for determining the parameters a. Further, since there is the notion of local neighborhoods, one could create a model of the process occurring in the neighborhood, at the neighborhood and by combining together these local models to construct a global nonlinear model that describes most of the structure of the attractor.

Indeed, in some ways the most important deviation from the linear model is to realize that the dynamics evolve in a multidimensional space, the size and the structure of which is dictated by the data. However, the data do not provide “hints” as to which model to select the source to match the random data. And the most simple polynomial models, and a very complex integrated models can lead to the asymptotic time orbits of strange attractors, so for part of the simulation is connected with physics. Therefore, physics is “reduced” to fit the algorithmic data without any interpretation of the data. There is an opinion that there is no algorithmic solutions on how to choose a model for a mere data.

As shown Schreiber [3], the most common form of the local model is very simple :

$$s(n+\Delta n) = a_0^{(n)} + \sum_{j=1}^{d_A} a_j^{(n)} s(n-(j-1)\tau) \quad (2)$$

where Δ n - the time period for which a forecast.

The coefficients $a_j^{(k)}$, may be determined by a least-squares procedure, involving only points $s(k)$ within a small neighbourhood around the reference point. Thus, the coefficients will vary throughout phase space. The fit procedure amounts to solving (d_A + 1) linear equations for the (d_A + 1) unknowns.

When fitting the parameters *a*, several problems are encountered that seem purely technical in the first place but are related to the nonlinear properties of the system. If the system is low-dimensional, the data that can be used for fitting will locally not span all the available dimensions but only a subspace, typically. Therefore, the linear system of equations to be solved for the fit will be ill conditioned. However, in the presence of noise the equations are not formally ill-conditioned but still the part of the solution that relates the noise directions to the future point is meaningless . Note that the method presented here is not only because, as noted above, the choice of fitting requires no knowledge of physics of the process itself. Other modelling techniques are described, for example, in [3,10].

Assume the functional form of the display is selected, wherein the polynomials used or other basic functions. Now, we define a characteristic which is a measure of the quality of the curve fit to the data and determines how accurately match y (k + 1) with F (y (k), a), calling it by a local deterministic error:

$$\varepsilon_D(k) = \mathbf{y}(k+1) - \mathbf{F}(\mathbf{y}(k), \mathbf{a}). \quad (3)$$

The cost function for this error is called W (ε). If the mapping F (y, a), constructed by us, is local, then one has for each adjacent to y (k) point, y $^{(r)}$ (k) (r = 1, 2, ..., N_B),

$$\varepsilon_D^{(r)}(k) = \mathbf{y}(r, k+1) - \mathbf{F}(\mathbf{y}^{(r)}(k), \mathbf{a}), \quad (4)$$

where y (r, k + 1) - a point in the phase space which evolves y (r, k). To measure the quality of the curve fit to the data, the local cost function is given by

$$W(\varepsilon, k) = \frac{\sum_{r=1}^{N_B} \left|\varepsilon_D^{(r)}(k)\right|^2}{\sum_{r=1}^{N_B} \left[\mathbf{y}(k) - \left\langle \mathbf{y}(r,k) \right\rangle\right]^2} \quad (5)$$

and the parameters identified by minimizing W (ε, k), will depend on a.

Furthermore, formally the neural network algorithm is launched, in particular, in order to make training the neural network system equivalent to the reconstruction and interim forecast the state of the neural network (respectively, adjusting the values of the coefficients). The starting point is a formal knowledge of the time series of the main dynamic parameters of a chaotic system, and then to identify the state vector of the matrix of the synaptic interactions $||w_{ij}||$ etc. Of course, the main difficulty here lies in the implementation of the process of learning neural network to simulate the complete process of change in the topological structure of the phase space of the system and use the output results of the neural network to adjust the coefficients of the function display. The complexity of the local task, but obviously much less than the complexity of predicting the original chaotic processes in physical or other dynamic systems.

4. Conclusions

Here we have considered an new approach to nonlinear modelling and prediction of chaotic processes in physical and other systems which is based on two key functional elements. Besides using other elements of starting chaos theory method the proposed approach includes the application of the concept of a compact geometric attractor, and one of the neural network algorithms, or, in a more general definition of a model of artificial intelligence. The meaning of the latter is precisely the application of neural network to simulate the evolution of the attractor in phase space, and training most neural network to predict (or rather, correct) the necessary coefficients of the parametric form of functional display.

References

1. Lichtenberg A., Liebermann A., Regular and chaotic dynamics.-N.-Y.: Springer.-1992.
2. Abarbanel H., Analysis of observed chaotic data.- N.-Y.: Springer.-1996.
3. Schreiber T., Interdisciplinary application of nonlinear time series methods// Phys. Rep. 1999.-Vol.308(1).-P.1-64.
4. Sivakumar B., Chaos theory in geophysics: past, present and future // Chaos, Solitons & Fractals.-2004.-Vol.19.-P.441-462.
5. Kennel M. B., Brown R., Abarbanel H., Determining embedding dimension for phase-space reconstruction using a geometrical construction // Physical Review A.-1992.-Vol.45.- P.3403-3411.
6. Turcotte D. L., Fractals and chaos in geology and geophysics.-Cambridge: Cambridge University Press, 1997.
7. Hastings A. M., Hom C., Ellner S, Turchin P., Godfray Y., Chaos in ecology: is Mother Nature a strange attractor?// Ann. Rev. Ecol. Syst.-1993.-Vol.24.-P.1-33.
8. May R. M., Necessity and chance: deterministic chaos in ecology and evolution // Bull. Amer. Math. Soc.-1995.-Vol.32.-P.291-308.
9. Grassberger P., Procaccia I., Measuring the strangeness of strange attractors// Physica D.-1983.-Vol.9.-P.189–208.
10. Glushkov A. V., Methods of a chaos theory.- Odessa: OSENU, 2012.
11. Glushkov A. V., Svinarenko A. A., Loboda A. V., Theory of neural networks on basis of photon echo and its program realization.-Odessa: TEC.- 2004.
12. Glushkov A. V., Loboda N. S., Khokhlov V. N., Using meteorological data for reconstruction of annual runoff series: Orthogonal functions approach// Atmospheric Research (Elsevier).-2005.-Vol.77.-P.100-113.
13. Glushkov A. V., Khokhlov V. N., Tsenenko I. A.: Atmospheric teleconnection patterns: wavelet analysis //Nonlinear Processes in Geophysics.-2004.-Vol.11(3).-P.285-293.
14. Khokhlov V. N., Glushkov A. V., Loboda N. S, Bunyakova Yu. Ya., Short-range forecast of atmospheric pollutants using non-linear prediction method// Atmospheric Environment (Elsevier).-2008.-Vol.42.-P.1213-1220.
15. Glushkov A. V., Kuzakon' V. M., Khetselius O. Yu., Prepelitsa G. P., Svinarenko A. A., Zaichko P. A.: Geometry of Chaos: Theoretical basis's of a consistent combined approach to treating chaotic dynamical systems and their parameters determination // Proceedings of International Geometry Center.-2013.-Vol.6(1).-P.43-48.
16. Khetselius O. Yu., Forecasting evolutionary dynamics of chaotic systems using advanced non-linear prediction method // Dynamical Systems - Theory and Applications.-2013.-Vol.1.-P. LIF142 (11p.).

The article is received in editorial 05.05.2013

UDC 681.322

O. Yu. Khetselius

GEOMETRIC ATTRACTOR AND NEURAL NETWORKS APPROACH TO STUDYING CHAOTIC PROCESSES IN PHOTOELECTRONICS SYSTEMS

Abstract

Nonlinear modelling of chaotic processes in systems and devices, including quantum electronics and photo may be based on the concept of compact geometric attractors. We present a new approach to analyze and predict the nonlinear dynamics of chaotic systems based on the concept of geometric attractors, chaos theory methods and algorithms for neural network simulation. Using information on the phase space evolution of the physical process in time and simulation of neural network modelling techniques can be considered as one of the fundamentally new approaches in the construction of global nonlinear models of the most effective and accurate description of the structure of the corresponding attractor.

Key words: electronics systems, chaotic processes, the geometric attractor neural network approach

УДК 681.322

О. Ю. Хецелиус

НОВЫЙ ПОДХОД К ИЗУЧЕНИЮ ХАОТИЧЕСКИХ ПРОЦЕССОВ В СИСТЕМАХ ФОТОЭЛЕКТРОНИКИ НА ОСНОВЕ КОНЦЕПЦИИ ГЕОМЕТРИЧЕСКИХ АТТРАКТОРОВ И НЕЙРОННО-СЕТЕВОГО МОДЕЛИРОВАНИЯ

Резюме

Нелинейное моделирование хаотических процессов в системах и устройствах, в частности, квантовой- и фотоэлектроники, может быть основано на концепции компактных геометрических аттракторов. Мы представляем новый подход к анализу и прогнозированию нелинейной динамики хаотических систем, основанный на концепции геометрических аттракторов, методах теории хаоса и алгоритмах нейросетевого моделирования. Использование информации о фазовом пространстве эволюции физического процесса во времени и ее имитация методами нейросетевого моделирования может рассматриваться в качестве одной из принципиально новых идей при построении глобальной нелинейной модели наиболее эффективного и точного описания структуры соответствующего аттрактора физического процесса.

Ключевые слова: системы электроники, хаотические процессы, геометрический аттрактор, нейросетевой подход

УДК 681.322

О. Ю. Хецелиус

НОВИЙ ПІДХІД ДО ВИВЧЕННЯ ХАОТИЧНИХ ПРОЦЕСІВ В СИСТЕМАХ ФОТОЕЛЕКТРОНІКИ НА ОСНОВІ КОНЦЕПЦІЇ ГЕОМЕТРИЧНИХ АТРАКТОРІВ І НЕЙРОННО- МЕРЕЖЕВОГО МОДЕЛЮВАННЯ

Резюме

Нелінійне моделювання хаотичних процесів в системах та приладах, зокрема, квантової- та фото електроніки, може бути засновано на концепції компактних геометричних атракторів. Ми представляємо новий підхід до аналізу та прогнозування нелінійної динаміки хаотичних систем, заснованих на концепції геометричних атракторів, методах теорії хаосу та алгоритмах нейромережевого моделювання. Використання інформації про фазовий простір еволюції фізичного процесу у часі та її імітація методами нейромережевого моделювання може розглядатися в якості однієї з принципово нових ідей при побудові глобальної нелінійної моделі найбільш ефективного та точного опису структури відповідного аттрактора.

Ключові слова: системи електроніки, хаотичні процеси, геометричний атрактор, нейромережевий підхід

PACS: 73.20.Hb, 73.25.+I; UDC 621.315.592

O. O. Ptashchenko[1], F. O. Ptashchenko[2], V, R.Gilmutdinova[1]

TUNNEL SURFACE CURRENT IN GaAs P-N JUNCTIONS INDUCED BY AMMONIA MOLECULES ADSORPTION

1I. I. Mechnikov National University of Odessa, Dvoryanska St., 2, Odessa, 65026, Ukraine
2Odessa National Maritime Academy, Odessa, Didrikhsona St., 8, Odessa, 65029, Ukraine

The effect of a treatment in concentrated wet ammonia vapors on I-V characteristics of GaAs p-n junctions, measured in air and in ammonia vapors, was studied. Such a treatment strongly enhances the sensitivity of the surface current to the water- and ammonia vapors. In ammonia vapors of high enough partial pressure, a maximum in the forward branch of I-V characteristic appeared. The treated p-n junctions have higher gas sensitivity at reverse bias than at forward bias. This suggests that ammonia molecules adsorption, under sufficiently high NH3 partial pressure, forms in the p-n junction a surface conducting channel with degenerated electrons. And the observed maximum in the I-V characteristic is explained by tunnel injection of electrons from the conducting channel to the degenerated p+ region.

1. INTRODUCTION

P-n junctions as gas-sensitive devices [1, 2] have some advantages in comparison with structures, based on oxide polycrystalline films [3, 4] and Shottky diodes [5, 6]. P-n junctions have high potential barriers for current carriers, which results in low background currents. Sensors on p-n junctions [1, 2] have crystal structure, high sensitivity at room temperature

In previous papers the gas sensitivity of p-n structures on GaAs and GaAs–AlGaAs [1, 2], GaP [7], InGaN [8], and Si [9, 10] was investigated. It was shown that the gas sensitivity of all these p-n junctions is due to forming of a surface conducting channel in the electric field induced by the ammonia ions adsorbed on the surface of the natural oxide layer.

The mostly interest for gas sensors on p-n junction are Si and GaAs. The Si p-n junctions can be combined in a transistor, which has much higher gas sensitivity than a single junction [11]. They can be easy integrated into microelectronic circuits. And GaAs p-n junctions can have very high gas sensitivity [12].

Some tunnel effects on *I-V* characteristics of the surface current, due to ammonia molecules adsorption, were observed on AlGaAs-GaAs p-n junctions under high, of 4 kPa ammonia partial pressure [13]. The threshold ammonia vapors partial pressure of 5 Pa for GaAs–AlGaAs p-n junctions is caused by filling up the surface states at the middle of band gap. And the treated GaAs p-n junctions have a threshold ammonia vapors partial pressure of 0,1 Pa [12]. Therefore the tunnel effects must be observed on these junctions under lower NH_3 pressures.

The aim of this work is a study of the influence of ammonia vapors on the forward and reverse currents in a GaAs p-n structures after a treatment in wet ammonia vapors of high partial pressure.

2. EXPERIMENT

The measurements were carried out on GaAs p-n structures, described in the previous paper [12]. The junctions were treated by durable exposure in wet ammonia vapors under an NH_3 partial pressure of 12 kPa. *I-V* characteristics of the forward and reverse currents were measured in air with various concentrations of ammonia vapors.

Fig.1 represents *I–V* characteristics a p-n structure, measured in air and in air with wet ammonia vapors of various partial pressures. The forward and reverse currents increased with enhanced NH_3 concentration. At an ammonia pressure of *P*=100Pa a pronounced peak in the *I-V* curve was observed, witch can be ascribed to electron tunneling between the c–band in the surface conducting channel and the v– band in the degenerated p^+ region at the contact. It is seen that the reverse current is greater than forward one at the same ammonia pressure. It is characteristic for tunnel currents in tunnel- and inverted diodes.

3. DISCUSSION

The experimental results can be explained with the model, depicted in fig. 2. Ionized ammonia molecules 2 are located on the natural oxide surface. Their electric field bend the depletion layer 3 and forms a n- conducting channel 4. The forward current consists of two components. Arrow *a* corresponds to the through component I_t of the current in the channel. And arrow *b* represents the current component I_i due to electron injection from the channel into the p^+ layer at the contact. The *I-V* curves, measured under ammonia pressures *P*<100 Pa, are monotonous and correspond to the case of

$$I_t > I_i. \qquad (1)$$

At $P \geq 100$ Pa a clear maximum in the *I-V* curve apiers. And, at low enough voltages, the forward and reverse currents are equal. This is characteristic for tunnel current in p-n junction.

It is remarkable, that the current in the minimum of the *I-V* curve, measured at *P*=100 Pa, is lower than currents, meaeured at the same voltage under *P*= 50 Pa and *P*=20 Pa. It can be explained as a result of the quantization of electron energy in the channel [14].

There is a triangular potential well for the electrons in the channel. For the electron energy levels in this well one can write [14]

$$E_n = \left[\frac{3}{2}\pi\left(n-\frac{1}{4}\right)\right]^{2/3}\left(\frac{e^2F^2\hbar^2}{2m^*}\right)^{1/3}, \qquad (2)$$

where *F* is the slope of the wall; *m** is the electron effective mass; *n*=1, 2, ... Electrons in the cannel are located on the lowest level of the triangular well and, at corresponding voltages, resonantly tunnel to the empty states in the p^+ layer. And the lateral mobility of the electrons on this level is lower than without quantization. Therefore the current in the minimum in the *I-V* curve at *P*=100 Pa is lower than current, measured at *P*=20 Pa.

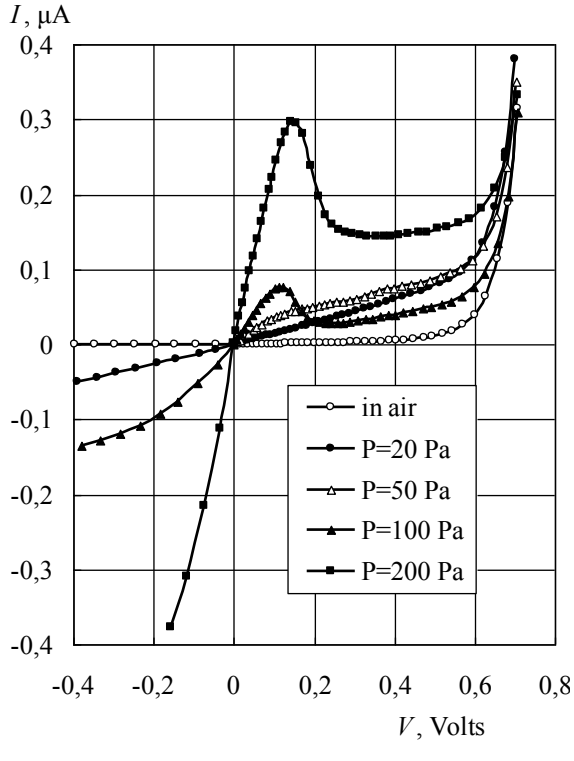

Fig. 1. *I–V* characteristics of a p-n structure in ammonia vapors of various pressures *P*.

4. CONCLUSIONS

Ammonia molecules adsorption, under sufficiently high NH_3 partial pressure, forms in p-n GaAs a surface conducting channel with degenerated electrons. *I–V* curve of the p-n junction with such channel, having a pronounced peak, is char-

acteristic of a tunnel diode. The electron energy in the channel is quantized.

P-n junctions with degenerated p^+ region have higher gas sensitivity at reverse bias than at forward bias. This effect is due to tunnel injection of electrons into the channel from the degenerated p^+ region at a reverse bias.

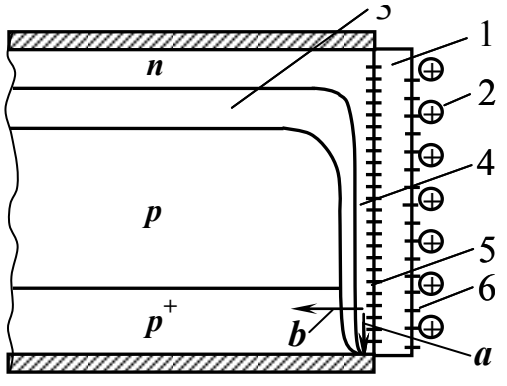

Fig 2. Schematic of a *p-n* structure, placed in a donor gas: 1 – oxide layer; 2 – ions; 3 – depletion layer; 4 – conducting channel; 5 – surface (fast) centers; 6 – states on the oxide surface (slow centers). Arrows: *a* – direction of the electron movement along the channel; b – tunneling from the channel into the p^+ region.

The threshold ammonia vapors partial pressure of 0,1 Pa for GaAs junctions is caused by filling up the surface states at the middle of band gap during the treatment.

REFERENCES

1. Ptashchenko O. O., Artemenko O. S., Ptashchenko F. O. Vliyanie gazovoi sredy na poverhnostnyi tok v p-n geterostrukturakh na osnove GaAs-AlGaAs // Fisika i khimiya tverdogo tila. – 2001. – V. 2, № 3. – P. 481 – 485.
2. Ptashchenko O. O., Artemenko O. S., Ptashchenko F. O. Vplyv pariv amiaku na poverkhnevyi strum v p-n perekhodakh na osnovi napivprovidnykiv A^3B^5 // Journal of physical studies. – 2003. – V. 7, №4. – P. 419 – 425.
3. Bugayova M. E., Koval V. M., Lazarenko B. I. et al. Gazovi sensory na osnovi oksydu tsynku (oglyad) // Sensorna electronika i mikrosystemni tehnologii. – 2005. - №3. – P. 34 – 42.
4. Russhikh D.V., Rembeza S. I., Shironkin S. Yu. et al. Vysokochuvstvitel'nyi poluprovodnikovyi datchik gazovych sred // Sensors & Systems. 2008. – № 8. – P. 14 – 16.
5. Bomk O. I., Il'chenko L. G., Il'chenko V. V. et al. Pro pryrodu chutlyvosti do amiaku gazovykh sensoriv na osnovi struktur nadtonka tytanova plivka – kremniy // Ukr. fiz. journ. – 1999. – V. 44, №9. – P. 759 – 763.
6. Baluba V. I., Gritsyk V. Y., Davydova T. A. et al. Sensory ammiaka na osnove diodov Pd-n-Si // Fizika i tekhnika poluprovodnikov. – 2005. – V. 39, № 2. P. 285 – 288.
7. Ptashchenko O. O., Artemenko O. S., Dmytruk M. L. et al. Effect of ammonia vapors on the surface morphology and surface current in p-n junctions on GaP. // Photoelectronics. – 2005. – No. 14. – P. 97 – 100.
8. Ptashchenko F. O. Effect of ammonia vapors on surface currents in InGaN p-n junctions. // Photoelectronics. – 2007. – No. 17. – P. 113 – 116.
9. Ptashchenko F. O. Vplyv pariv amiaku na poverkhnevyi strum u kremniyevykh p-n perekhodakh // Ptashchenko F. O. Visnyk ONU, ser. Fizyka.– 2006. – V. 11, №. 7. – P. 116 – 119.
10. Ptashchenko O. O., Ptashchenko F. O., Yemets O. V. Effect of ammonia vapors on the surface current in silicon p-n junctions. // Photoelectronics. – 2006. – No. 16. – P. 89 – 93.
11. Ptashchenko F. O. Characteristics of silicon transistors as gas sensors. // Photoelectronics. – 2010. – No. 19. – P. 18 – 21.
12. Ptashchenko O. O., Ptashchenko F. O., Gilmutdinova V. R. Vplyv poverkhnevogo leguvannya na charakterystyky p-n perekhodiv na osnovi GaAs yak gazovykh sensoriv // Sensorna elektronika i mikrosystemni tekhnologiyi– 2013

– V. 10, № 1. – P. 114 – 123.
13. Ptashchenko O. O., Ptashchenko F. O., Shugarova V. V. Tunnel surface current in GaAs–AlGaAs p-n junctions, due to ammonia molecules adsorption // Photoelectronics. – 2009. – No. 18. – P. 95 – 98.
14. Martinez-Duart J.M., Martin-Palma R.J., Agullo-Rueda F. Nanotekhnologiya dlya mikro- i optoelektroniki. M.: Tekhnosfera, 2007. – 368 p.

The article is received in editorial 21.07.2013

PACS: 73.20.Hb, 73.25.+I; UDC 621.315.592

O. O. Ptashchenko, F. O. Ptashchenko, V. R.Gilmutdinova

TUNNEL SURFACE CURRENT IN GaAs P-N JUNCTIONS INDUCED BY AMMONIA MOLECULES ADSORPTION

Abstract

The effect of a treatment in concentrated wet ammonia vapors on *I-V* characteristics of GaAs p-n junctions, measured in air and in ammonia vapors, was studied. Such a treatment strongly enhances the sensitivity of the surface current to the water- and ammonia vapors. In ammonia vapors of high enough partial pressure, a maximum in the forward branch of *I-V* characteristic appeared. The treated p-n junctions have higher gas sensitivity at reverse bias than at forward bias. This suggests that ammonia molecules adsorption, under sufficiently high NH_3 partial pressure, forms in the p-n junction a surface conducting channel with degenerated electrons. And the observed maximum in the *I-V* characteristic is explained by tunnel injection of electrons from the conducting channel to the degenerated p^+ region.

Key words: p-n junction, gas sensor, surface current; conducting channel, tunneling.

PACS: 73.20.Hb, 73.25.+I; UDC 621.315.592

О. О. Птащенко, Ф. О. Птащенко , В. Р. Гільмутдінова

ТУНЕЛЬНИЙ ПОВЕРХНЕВИЙ СТРУМ В P-N ПЕРЕХОДАХ НА ОСНОВІ GaAs, ІНДУКОВАНИЙ АДСОРБЦІЄЮ МОЛЕКУЛ АМІАКУ

Резюме

Досліджено вплив обробки у концентрованих вологих парах аміаку на ВАХ p-n переходів на основі GaAs, виміряних у повітрі та в парах аміаку. Така обробка різко підвищує чутливість поверхневого струму до парів води та аміаку. В парах аміаку достатньо високого парціального тиску з’являється максимум на ВАХ. Оброблені p-n переходи мають більш високу газову чутливість при зворотному зміщенні, ніж при прямому зміщенні. Це свідчить, що адсорбція молекул аміаку , при достатньо високих значеннях парціального тиску NH_3, створює в p-n переході поверхневий провідний канал з виродженими електронами. І наявність спостереженого максимуму на ВАХ пояснюється тунельною інжекцією електронів із провідного каналу у вироджену p^+ область.

Ключові слова: p-n перехід, газовий сенсор, поверхневий струм, провідний канал, тунелювання.

PACS: 73.20.Hb, 73.25.+I; UDC 621.315.592

А. А. Птащенко, Ф. А. Птащенко, В. Р. Гильмутдинова

ТУННЕЛЬНЫЙ ПОВЕРХНОСТНЫЙ ТОК В P-N ПЕРЕХОДАХ НА ОСНОВЕ GaAs, ИНДУЦИРОВАННЫЙ АДСОРБЦИЕЙ МОЛЕКУЛ АММИАКА

Резюме

Исследовано влияние обработки в концентрированных влажных парах аммиака на ВАХ p-n переходов на основе GaAs, измеренных в воздухе и в парах аммиака. Такая обработка резко повышает чувствительность поверхностного тока к парам воды и аммиака. В парах аммиака с достаточно высоким парциальным давлением появляется максимум на ВАХ. Обработанные p-n переходы имеют более высокую газовую чувствительность при обратном смещении, чем при прямом смещении. Это свидетельствует, что адсорбция молекул аммиака , при достаточно высоких значениях парциального давления NH_3, создает в p-n переходе поверхностный проводящий канал с вырожденными электронами. И появление максимума на ВАХ объясняется туннельной инжекцией электронов из проводящего канала в вырожденную p^+ область.

Ключевые слова: p-n переход, газовый сенсор, поверхностный ток, проводящий канал, туннелирование.

UDC 539.182

A. A. Svinarenko

Odessa National Polytechnical University, 1, Shevchenko av., Odessa, Ukraine
Odessa State Environmental University, 15, Lvovskaya str., Odessa, Ukraine
e-mail: quantsvi@mail.ru

SPECTROSCOPY OF AUTOIONIZATION STATES IN SPECTRA OF HELIUM, BARIUM AND LEAD ATOMS: NEW SPECTRAL DATA AND CHAOS EFFECT

We applied a generalized energy approach (Gell-Mann and Low S-matrix formalism) combined with the relativistic multi-quasiparticle (QP) perturbation theory (PT) with the Dirac-Kohn-Sham zeroth approximation to studying excites states and autoionization resonances (AR) in complex atoms and ions, in particular, energies and widths for the He and He-like ion, barium and lead atoms, with accounting for the exchange-correlation, relativistic corrections and the weak chaos effect.

1. Introduction

Traditionally an investigation of spectra, spectral, radiative and autoionization characteristics for heavy and superheavy elements atoms and multicharged ions is of a great interest for further development atomic and nuclear theories and different applications in the plasma chemistry, astrophysics, laser physics, etc. (look Refs. [1–10]). Theoretical methods of calculation of the spectroscopic characteristics for heavy atoms and ions may be divided into a few main groups [1-6]. First, the well known, classical multi-configuration Hartree-Fock method (as a rule, the relativistic effects are taken into account in the Pauli approximation or Breit hamiltonian etc.) allowed to get a great number of the useful spectral information about light and not heavy atomic systems, but in fact it provides only qualitative description of spectra of the heavy and superheavy ions. Second, the multi-configuration Dirac-Fock (MCDF) method is the most reliable version of calculation for multielectron systems with a large nuclear charge. In these calculations the one- and two-particle relativistic effects are taken into account practically precisely. In this essence it should be given special attention to two very general and important computer systems for relativistic and QED calculations of atomic and molecular properties developed in the Oxford group and known as GRASP ("GRASP", "Dirac"; "BERTHA", "QED") (look [1-5] and refs. therein). In particular, the BERTHA program embodies a new formulation of relativistic molecular structure theory within the framework of relativistic QED. This leads to a simple and transparent formulation of Dirac-Hartree-Fock-Breit (DHFB) self-consistent field equations along with algorithms for molecular properties, electron correlation, and higher order QED effects. The DHFB equations are solved by a direct method based on a relativistic generalization of the McMurchie-Davidson algorithm [4]. In this paper we applied a new relativistic approach [11-15] to relativistic studying the excites states spectra and autoionization states for the He and He-like ion, barium and lead atoms. New approach in optics and spectroscopy of heavy atomic systems is the combined the generalized energy approach and the gauge-invariant QED many-QP PT with the Dirac-Kohn-Sham (DKS) "0" approximation (optimized 1QP representation) and an accurate accounting for relativistic, correlation, nuclear, radiative effects. [17-20].

2. Method

The generalized gauge-invariant version of the energy approach has been further developed in Refs. [12,13]. In relativistic case the Gell-Mann and Low formula expressed an energy shift DE through the QED scattering matrix including the interaction with as the photon vacuum field as the laser field. The first case is corresponding to definition of the traditional radiative and autoionization characteristics of multielectron atom. The wave function zeroth basis is found from the Dirac-Kohn-Sham equation with a potential, which includes the ab initio (the optimized model potential or DF potentials, electric and polarization potentials of a nucleus; the Gaussian or Fermi forms of the charge distribution in a nucleus are usually used) [5]. Generally speaking, the majority of complex atomic systems possess a dense energy spectrum of interacting states with essentially relativistic properties. Further one should realize a field procedure for calculating the energy shifts DE of degenerate states, which is connected with the secular matrix *M* diagonalization [8-12]. The secular matrix elements are already complex in the second order of the PT. Their imaginary parts are connected with a decay possibility. A total energy shift of the state is presented in the standard form:

$$\Delta \mathrm{E} = \mathrm{Re}\,\Delta E + i\,\mathrm{Im}\,\Delta E \qquad \mathrm{Im}\,\Delta E = -\Gamma/2\,, \tag{1}$$

where Γ is interpreted as the level width, and the decay possibility $\mathrm{P} = \Gamma$. The whole calculation of the energies and decay probabilities of a non-degenerate excited state is reduced to the calculation and diagonalization of the *M*. The *jj*-coupling scheme is usually used. The complex secular matrix *M* is represented in the form [9,10]:

$$M = M^{(0)} + M^{(1)} + M^{(2)} + M^{(3)}. \tag{2}$$

where $M^{(0)}$ is the contribution of the vacuum diagrams of all order of PT, and $M^{(1)}$, $M^{(2)}$, $M^{(3)}$ those of the one-, two- and three-QP diagrams respectively. $M^{(0)}$ is a real matrix, proportional to the unit matrix. It determines only the general level shift. We have assumed $M^{(0)} = 0$. The diagonal matrix $M^{(1)}$ can be presented as a sum of the independent 1QP contributions. For simple systems (such as alkali atoms and ions) the 1QP energies can be taken from the experiment. Substituting these quantities into (2) one could have summarized all the contributions of the 1QP diagrams of all orders of the formally exact QED PT. However, the necessary experimental quantities are not often available. So, the optimized 1-QP representation is the best one to determine the zeroth approximation. The correlation corrections of the PT high orders are taken into account within the Green functions method (with the use of the Feynman diagram's technique). All correlation corrections of the second order and dominated classes of the higher orders diagrams (electrons screening, polarization, particle-hole interaction, mass operator iterations) are taken into account [10-14]. In the second order, there are two important kinds of diagrams: polarization and ladder ones. Some of the ladder diagram contributions as well as some of the 3QP diagram contributions in all PT orders have the same angular symmetry as the 2QP diagram contributions of the first order [10-12]. These contributions have been summarized by a modification of the central potential, which must now include the screening (anti-screening) of the core potential of each particle by two others. The additional potential modifies the 1QP orbitals and energies. Then the secular matrix is : $M \simeq \tilde{M}^{(1)} + \tilde{M}^{(2)}$, where $\tilde{M}^{(1)}$ is the modified 1QP matrix (diagonal), and $\tilde{M}^{(2)}$ the modified 2QP one. $\tilde{M}^{(1)}$ is calculated by substituting the modified 1QP energies), and $\tilde{M}^{(2)}$ by means of the first PT order formulae for $M^{(2)}$, putting the modified radial functions of the 1QP states in the interaction radial integrals. Let us remind that in the QED theory, the photon propagator D(12) plays the role of this interaction. Naturally, an analytical form of D depends on the gauge, in which the electrodynamic potentials are written. In general, the results of all approximate calculations depended on the gauge. Naturally the correct result must be gauge invariant. The gauge dependence of the amplitudes of the

photoprocesses in the approximate calculations is a well known fact and is in details investigated by Grant, Armstrong, Aymar-Luc-Koenig, Glushkov-Ivanov [1,2,5,9]. Grant has investigated the gauge connection with the limiting non-relativistic form of the transition operator and has formulated the conditions for approximate functions of the states, in which the amplitudes are gauge invariant. These results remain true in an energy approach as the final formulae for the probabilities coincide in both approaches. In ref. [16] it has been developed a new version of the approach to conserve gauge invariance. Here we applied it to get the gauge-invariant procedure for generating the relativistic DKS orbital bases (abbreviator of our method: GIRPT). The autoionization width is defined by the square of interaction matrix element [9]:

$$V^{\omega}_{1234} = [(j_1)(j_2)(j_3)(j_4)]^{1/2} \sum_{\lambda\mu} (-1)^{\mu} \begin{pmatrix} j_1 j_3 & \lambda \\ m_1 - m_3 & \mu \end{pmatrix} \times \times \mathrm{Re}\, Q_{\lambda}(1234) \tag{3}$$

The real part of the interaction matrix element can be expanded in terms of Bessel functions [5,8]:

$$\frac{\cos|\omega|r_{12}}{r_{12}} = \frac{\pi}{2\sqrt{r_1 r_2}} \sum_{\lambda=0} (\lambda) J_{\lambda+1/2}(|\omega|r_<) J_{-\lambda-1/2}(|\omega|r_>) P_{\lambda}(\cos \mathbf{r}_1 \mathbf{r}_2) \tag{4}$$

The Coulomb part $Q^{\mathrm{Qul}}_{\lambda}$ is expressed in the radial integrals R_l, angular coefficients S_l as follows:

$$\mathrm{Re}\, Q^{\mathrm{Qul}}_{\lambda} \sim \mathrm{Re}\{R_l(1243) S_{\lambda}(1243) + R_{\lambda}(\tilde{1}24\tilde{3}) S_{\lambda}(\tilde{1}24\tilde{3}) + R_{\lambda}(1\tilde{2}4\tilde{3}) S_{\lambda}(1\tilde{2}4\tilde{3}) + R_{\lambda}(\tilde{1}\tilde{2}4\tilde{3}) S_{\lambda}(\tilde{1}\tilde{2}4\tilde{3})\} \tag{5}$$

where $\mathrm{Re}Q_l(1243)$ is as follows:

$$\mathbf{Re}\, R_{\lambda}(1243) = \iint dr_1 r_1^2 r_2^2 f_1(r_1) f_3(r_1) f_2(r_2) f_4(r_2) Z^{(1)}_{\lambda}(r_<) Z^{(1)}_{\lambda}(r_>) \tag{6}$$

where f is the large component of radial part of the 1QP state Dirac function and function Z is :

$$Z^{(1)}_{\lambda} = [2/|\omega_{13}|\alpha Z]^{\lambda+1/2} J_{\lambda+1/2}(\alpha|\omega_{13}|r) / [r^{\lambda} \Gamma(\lambda + 3/2)]. \tag{7}$$

The angular coefficient is defined by standard way as above [3]. The calculation of radial integrals $\mathbf{Re}R_l(1243)$ is reduced to the solution of a system of differential equations:

$$\left.\begin{aligned} y_1' &= f_1 f_3 Z^{(1)}_{\lambda}(\alpha|\omega|r) r^{2+\lambda}, \\ y_2' &= f_2 f_4 Z^{(1)}_{\lambda}(\alpha|\omega|r) r^{2+\lambda}, \\ y_3' &= [y_1 f_2 f_4 + y_2 f_1 f_3] Z^{(2)}_{\lambda}(\alpha|\omega|r) r^{1-\lambda}. \end{aligned}\right\} \tag{8}$$

In addition, $y_3(\infty)=\mathbf{Re}R_{\lambda}(1243)$, $y_1(\infty)=X_{\lambda}(13)$. The system of differential equations includes also equations for functions $f/r^{|æ|-1}$, $g/r^{|æ|-1}$, $Z^{(1)}_{\lambda}$, $Z^{(2)}_{\lambda}$. The formulas for the autoionization (Auger) decay probability include the radial integrals $R_a(akgb)$, where one of the functions describes electron in the continuum state. When calculating this integral, the correct normalization of the function Ψ_k is a problem. The correctly normalized function should have the following asymptotic at $r \to 0$:

$$\left.\begin{matrix} f \\ g \end{matrix}\right\} \to (\lambda\omega)^{-1/2} \begin{cases} [\omega + (\alpha Z)^{-2}]^{-1/2} \sin(kr + \delta), \\ [\omega - (\alpha Z)^{-2}]^{-1/2} \cos(kr + \delta). \end{cases} \tag{9}$$

When integrating the master system, the function is calculated simultaneously:

$$N(r) = \{\pi\omega_k [f_k^2 [\omega_k + (\alpha Z)^{-2}] + g_k^2 [\omega_k + (\alpha Z^{-2})]]\}^{-1/2} \tag{10}$$

It can be shown that at r®¥, $N(r)$®N_k, where N_k is the normalization of functions f_k, g_k of continuous spectrum satisfying the condition (9). Other details can be found in refs.[10-13,16-20].

3. Results and conclusions

In Table 1 we present the results of our calculating energies of levels in Pb: experimental data and the results of the calculation method in the framework of the relativistic Hartree-Fock (RHF) (see [21] and references therein) and our theory. Our data are in quite good agreement with the experimental data.

Table 2 shows our calculated result for transition probabilities corresponding to the line 1278.9 nm in the spectrum of Pb, together with the results of alternative theories, in particular, the data obtained on the basis of the calculation in the many approximation DF using, respectively, the theoretical and experimental values of the DF

transition energy (MCDF: theor.E; exp.E), in the many relativistic random phase approximation (MCRRPA), in the relativistic Hartree-Fock (RHF), in the intermediate-coupling approximation (ICC) and finally, the method of empirical MP (EMP) [22].

Table.1.

The energies of the levels of the np2, npn's (n = 6, n '= 7) lead (see text)

		Exp.	RHF	RPT
np^2	$^3P_0$	59821	59960	59862
	$^3P_1$	52002	51996	52005
	$^3P_2$	49171	49174	49172
	$^1D_2$	38363	38301	38352
	$^1S_0$	30354	30282	30332
npn's	$^3P_0$	24861	25163	24924
	$^3P_1$	24534	25721	24598

Table 2.

Probability (s^{-1}) of transition corresponding to the line 1278.9 nm in Pb

RPT-EA (our data)	6.95
MCDF (exp.E); Horodecki et al	7.27
MCDF (theor.E); Horodecki et al	4.29
EMP; Horodecki et al	7.50
RHF (Biemont-Quinat)	7.85
MCRRPA (Chou-Huang)	7.00
RHF (Dzuba et al)	7.08
ICC (Garstang)	7.14
Laser absorption	6.1±1.5

In the next table 3 we present the measured and calculated autoionization width (cm^{-1}) for 5d5g levels of the Ba atom with angular momentum J <6: (3) Experiment (4) Theory: HF method with a partial view of the correlations (Van Leeuwen et al; (5) R-matrix method without into account the effect of the polarization shells basis: 6snl +5 dnl (Luc-Koenig et al); (6) R-matrix method taking into account the polarization of the c shell and without dielectronic polarization interaction (Luc-Koenig et al); (7) R-matrix method taking into account the effect of the polarization of shells and dielectronic polarization interaction (Luc-Koenig et al); (8) - our theory, taking full account of correlations. As indicated in Ref. [23]. The experimental studying of the spectrum considered had been performed in the remarkable work [24].

Analyzing shown in Table 3 the data on measured and calculated widths for 5d5g levels of the Ba atom with momentum J = 6, we note that to reach a physically reasonable agreement between theory and experiment it is necessary to carry put a precise account of the polarization and dielectronic interaction effects. This has been accurately done in the framework of our theory and the R-matrix method Luc-Koenig et al [24]. In the last paper the known polarization potentials have used with such a parameter as static dipole polarizability. In our theory we have used the multiparticle polarization functionals [12], which have been obtained by summation of the PT polarization diagrams sequence in the Thoams –Fermi approximation.

Another interesting feature of the auto resonances spectra in barium is connected with elements of the weak chaos. In ref. [25] we have treated a problem of a chaos manifestation in dynamical systems from the geometrical and spectral points point of view. There3 we have presented the theoretical basis's of a consistent chaos-geometrical approach to treating of chaotic dynamical systems which combines together the non-linear analysis methods to dynamics, such as the wavelet analysis, multi-fractal formalism, mutual information approach, correlation integral analysis, false nearest neighbour algorithm, Lyapunov exponent's analysis, surrogate data method etc. Application of this approach to studying dense and very complicated spectrum of barium (there are taken into account more 400 levels and resonances, including the Rydberg, twice excited Autoionization resonances etc)) has shown that one could find the elements of the weak chaos (the first two spectral Lyapunov's exponents have positive and a little negative values).

The next system to be studied is the systems of the autoionization resonances in helium, which includes states with double excited electrons. Table 4 shows the data of our theory for the energy and width of the Autoionization resonance 3s3p

$^1P_0$, along with those of other theories (see details in [27] and references therein). In the next table 5 we present some of the theoretical and experimental data on the energy and the width of the resonance 3s3p $^1P_0$, (theoretical): our theory, the method of complex rotation method diagonalization MHF R-matrix method; Experiment: NIST (NBS 2SO-MeV electron synchrotron storage ring (SURF-II)), Wisconsin laboratory (Wisconsin Tantalus storage ring), Stanford Synchrotron Radiation Laboratory (SSRL), Berlin electron storage ring (BESSY), Daresbury Synchrotron Radiation Source (DSRS) [27]. With regard to the data of different methods it should be noted that these data are different theories degree of agreement with the experimental data. Surely, the value of of any theory is determined by not only the studying the helium atom, but also of other atoms, as well as the level of complexity of the computational procedure. In this sense, the method of complex rotation stand, MHF, R-matrix approach is now actively used in different tasks.

The results of our theory is physically reasonable, fairly good agreement with the experimental data obtained in a number of well-known laboratories.

Table 3. The measured and calculated autoionization width (cm^{-1}) for 5d5g levels of the Ba atom with angular momentum J <6:
(3) Experiment (4) Theory: HF method (5) R-matrix method without account of polarization; (6) R-matrix method with account polarization and without dielectronic interaction; (7) R-matrix method with account of polarization of and dielectronic interaction; (8) - our theory

1:j	K	J	2: εl	(3)	(4)	(5)
$5d_{3/2}$	5/2	2	εd	0.062(4)	0.0074	0.077
$5d_{3/2}$	5/2	3	εd	0.056(5)	0.0074	0.048
$5d_{3/2}$	7/2	3	εg	0.34(3)	1.96	2.34
$5d_{3/2}$	7/2	4	εg	0.34(3)	1.96	2.41
$5d_{3/2}$	9/2	4	εg	0.18(2)	1.00	1.11
$5d_{3/2}$	9/2	5	εg	0.18(2)	1.00	1.19
$5d_{3/2}$	11/2	5	εi	-	2.90	3.19
$5d_{3/2}$	11/2	6	εi	-	2.90	3.20
$5d_{5/2}$	3/2	1	εd	0.046(3)	0.012	0.038
$5d_{5/2}$	3/2	2	εd	0.057(4)	0.012	0.077
$5d_{5/2}$	5/2	2	εd	0.0107(15)	0.0041	0.025
$5d_{5/2}$	5/2	3	εd	0.0174(23)	0.0041	0.017
$5d_{5/2}$	7/2	3	εg	0.29(3)	1.43	1.61
$5d_{5/2}$	7/2	4	εg	0.29(3)	1.43	1.73
$5d_{5/2}$	9/2	4	εg	0.43(4)	2.29	2.57
$5d_{5/2}$	9/2	5	εg	0.43(4)	2.29	2.71
$5d_{5/2}$	11/2	5	εi	0.28(3)	0.45	0.56
$5d_{5/2}$	11/2	6	εi	0.32(3)	0.45	0.55
$5d_{5/2}$	13/2	6	εi	-	3.37	3.95
1:j	K	J	2: εl	(6)	(7)	(8)
5d3/2	5/2	2	εd	0.072	0.018	0.058
5d3/2	5/2	3	εd	0.046	0.025	0.055
5d3/2	7/2	3	εg	0.12	0.34	0.34
5d3/2	7/2	4	εg	0.12	0.33	0.33
5d3/2	9/2	4	εg	0.11	0.23	0.20
5d3/2	9/2	5	εg	0.11	0.23	0.19
5d3/2	11/2	5	εi	1.44	1.74	1.52
5d3/2	11/2	6	εi	1.44	1.73	1.51
5d5/2	3/2	1	εd	0.066	0.041	0.044
5d5/2	3/2	2	εd	0.061	0.025	0.053
5d5/2	5/2	2	εd	0.023	0.008	0.009
5d5/2	5/2	3	εd	0.021	0.013	0.015
5d5/2	7/2	3	εg	0.13	0.29	0.28
5d5/2	7/2	4	εg	0.13	0.31	0.30
5d5/2	9/2	4	εg	0.22	0.48	0.45
5d5/2	9/2	5	εg	0.22	0.48	0.46
5d5/2	11/2	5	εi	0.25	0.30	0.28
5d5/2	11/2	6	εi	0.25	0.30	0.29
5d5/2	13/2	6	εi	1.83	2.15	2.17

Table 4. Energy and width of the resonance 3s3p $^1P_0$ (theoretical): our theory, the method of complex rotation (MCR), the algebraic close coupling (ACC), a method of diagonalization (DM), multiconf. HF, R-matrix method, the adiabatic potential curves method (APC), L^2 technique with using the Sturmian expansions, Feshbach method (FM), K -matrix (KM)

Method		E_r (Ry)	Γ/2 (Ry)
PT-EA	This	-0.668802	0.006814
MCR	Ho	-0.671252	0.007024
ACC	Wakid etaa	-0.670	0.00695
MD	Senashenko	-0.6685	0.00548
MHF	Nicolaides	-0.671388	-
R-matr	Hayes-Scott	-0.6707	0.00660
APC	Koyoma et al	-0.6758	-
APC	Sadeghpour	-0.67558	-
L^2 tech.	Gershacher	-0.67114	0.00704
FM	Wu et al	-0.669 27	0.00420
KM	Moccia et al	-0.670 766	0.00676

Table 5. Theoretical and experimental data on the energy and the width of the resonance 3s3p $^1P_0$, (theoretical): our theory, the method of complex rotation method diagonalization MHF R-matrix method; Experiment: NIST (NBS), Wisconsin (Wisconsin storage ring), Stanford - SSRL; Berlin-BESSY; Daresbury-DSRS.

	E_r (eV)	Γ/2 (eV)
This	69.9055	0.1854
MCR	69.8722	0.1911
MHF	69.8703	-
R-matr.	69.8797	0.1796
NBS	69.919±0.007	0.132±0.014
Wisconsin	69.917±0.012	0.178±0.012
SSRL	69.917±0.012	0.178±0.012
BESSY	69.914±0.015	0.200±0.020
DSRS	69.880±0.022	0.180±0.015

References

1. Grant I. P., Relativistic Quantum Theory of Atoms and Molecules.-Oxford, 2008.-650P.
2. Wilson S., Handbook on Molecular Physics & Quantum Chemistry.-Wiley, 2003.-680P.
3. Quiney H., Relativistic Quantum Mechanics of Atoms and Molecules//New Trends in Quantum Systems in Chemistry and Physics (Springer).-2002.-Vol.6.-P.135–173.
4. Bell K. L., Berrington K., Crothers D., Hibbert A., Taylor K.T., BERTHA: 4-Component Relativistic Molecular Quantum Mechanics// Supercomputing, Collision Processes, and Application, Series: Physics of Atoms and Molecules (Springer).-2002.-P.213–224.
5. Glushkov A.V., Relativistic Quantum Theory. Quantum, mechanics of Atomic Systems.-Odessa: Astroprint, 2008.-900P.
6. Safronova U. I., Safronova M. S., Third-order relativistic many-body calculations of energies, transition rates, hyperfine constants, and blackbody radiation shift in $^{171}Yb^+$//Phys. Rev. A.-2009.-Vol.79.-P.022512.
7. Bieron J, Froese-Fischer C., Fritzsche S., Pachucki K., Lifetime and hyperfine structure of $^3D_2$ state of radium // J.Phys.B:At.Mol.Opt.Phys.-2004.-Vol.37.-P.L305-311.
8. Ivanov L. N., Ivanova E. P., Extrapolation of atomic ion energies by model potential method: Na-like spectra/ // Atom.Data Nucl .Data Tab.-1979.-Vol.24.-P.95-121.
9. Bekov G. I., Vidolova-Angelova E., Ivanov L. N., Letokhov V. S., Mishin V. I., Laser spectroscopy of low excited autoionization states of the ytterbium atom //JETP.-1981.-Vol.80.-P.866-878.
10. Vidolova-Angelova E., Ivanov L. N., Autoionizing Rydberg states of thulium. Re-orientation decay due to monopole interaction// J.Phys.B:At.Mol.Opt.Phys.-1991.-Vol.24.-P.4147-4158
11. Ivanov L. N., Letokhov V. S. Spectroscopy of autoionization resonances in heavy elements atoms // Com.Mod.Phys.D.:At.Mol.Phys.-1985.-Vol.4.-P.169-184.

12. Glushkov A.V ., Ivanov L. N., Ivanova E. P., Radiation decay of atomic states. Generalized energy approach// Autoionization Phenomena in Atoms.-M.: Moscow State Univ.-1986.
13. Glushkov A. V., Ivanov L. N. Radiation decay of atomic states: atomic residue and gauge non-invariant contributions // Phys. Lett.A.-1992.-Vol.170.-P.33-38.
14. Glushkov A. V., Ivanov L. N. DC Strong-Field Stark-Effect: consistent quantum-mechanical approach // J.Phys.B: At. Mol. Opt. Phys.-1993.-Vol.26.- P.L379-386.
15. Glushkov A. V., Khetselius O. Yu., Svinarenko A. A., Relativistic theory of cooperative muon-gamma-nuclear processes: Negative muon capture and metastable nucleus discharge // Advances in the Theory of Quantum Systems in Chemistry and Physics (Springer).-2012.-Vol.22.-P.51-70.
16. Glushkov A. V., Khetselius O. Yu., Loboda A. V., Svinarenko A. A., QED approach to atoms in a laser field: Multiphoton resonances and above threshold ionization//Frontiers in Quantum Systems in Chemistry and Physics (Springer).-2008.-Vol.18.-P.541-558.
17. Glushkov A. V., Svinarenko A. A., Ignatenko A. V., Spectroscopy of autoionization resonances in spectra of lanthanides atoms// Photoelectronics.-2011.-Vol.20.-P.90-94**.**
18. Svinarenko A. A., Nikola L. V., Prepelitsa G. P., Tkach T., Mischenko E., The Auger (autoionization) decay of excited states in spectra of multicharged ions: Relativistic theory // Spectral Lines Shape.-2010.-Vol.16.-P.94-98
19. Malinovskaya S. V., Glushkov A. V., Khetselius O. Yu., Svinarenko A., Bakunina E., Florko T., Optimized perturbation theory scheme for calculating interatomic potentials and hyperfine lines shift for heavy atoms in buffer inert gas // Int. Journ. Quant. Chem.-2009.-Vol.109.-P.3325-3329.
20. Svinarenko A. A., Mischenko E. V., Loboda A. V., Dubrovskaya Yu. V., Quantum measure of frequency and sensing the collisional shift of the ytterbium hyperfine lines in medium of helium gas// Sensor Electronics and Microsystem Techn.-2009.-N1.-P.25-29.
21. Dzuba V. A., Flambaum V. V., Silvestrov P. G., Sushkov D. E.Many-body perturbation theory calculations in atoms with open shells//Phys.Rev.A-1991.-Vol.44.-P.2828-2831.
22. Vadla C., Horvatic V., Niemax K., Oscillator strength of the strongly forbidden Pb $6p^2\ ^3P_0$ - $6p^2\ ^3P_1$ transition at 1278.9 nm//Eur. Phys. J. D.-2001.-Vol.14.-P. 23-25.
23. Van Leuwen R., Ubachs W., Hogervorst W.,Autoionization of low-lying 5dng states in barium//J.Phys.B.: Atom.Mol. Opt.Phys.-1994.-Vol.27.-P.3891-3904.
24. Luc Koenig E., Aymar M., Van Leeuwen R., Ubachs W., Hogervorst W., Polarization effects in Autoionization processes: The 5d5g states in barium// Phys.Rev.A.-1995.-Vol.52.-P.208-215.
25. Wesdorp C., Noordam L.D., Robicheaux F., Dynamics of forced autoionization// Phys. Rev.A.-1999.-Vol.60.-P.R3377-R3380..
26. Glushkov A. V., Kuzakon' V. M., Khetselius O. Yu., Prepelitsa G. P., Svinarenko A. A., Geometry of Chaos: Theoretical basis's of a consistent combined approach to treating chaotic dynamical systems and their parameters determination//Proceedings of International Geometry Center.-2013.-Vol.6, N1.-P.43-48
27. Ho Y. K., Autoionizing $^1P^0$ states of He between the N=2 and 3 threshold of He^+//Phys.Rev.A.1991/-Vol/44.-P. 4154-4161.

The article is received in editorial 27.07.2013

UDC 539.183

A. A. Svinarenko

SPECTROSCOPY OF AUTOIONIZATION RESONANCES IN SPECTRA OF HE-LIKE IONS AND ALKALI-EARTH ATOMS: NEW SPECTRAL DATA AND CHAOS EFFECT

Abstract

We applied a generalized energy approach (Gell-Mann and Low S-matrix formalism) combined with the relativistic multi-quasiparticle (QP) perturbation theory (PT) with the Dirac-Kohn-Sham zeroth approximation to studying excites states and autoionization resonances (AR) in complex atoms and ions, in particular, energies and widths for the He and He-like ion, barium and lead atoms, with accounting for the exchange-correlation, relativistic corrections and a chaos effect.

Key words: spectroscopy of autoionization resonances, relativistic energy approach

УДК 539.183

А. А. Свинаренко

СПЕКТРОСКОПИЯ АВТОИОНИЗАЦИОННЫХ РЕЗОНАНСОВ В СПЕКТРАХ He-ПОДОБНЫХ ИОНОВ И ЩЕЛОЧНО-ЗЕМЕЛЬНЫХ АТОМОВ: НОВЫЕ СПЕКТРАЛЬНЫЕ ДАННЫЕ И ЭФФЕКТ ХАОСА

Резюме

Обобщенный энергетический подход (S-матричный формализм Гелл-Мана и Лоу) и релятивистская теория возмущений с дирак-кон-шэмовским нулевым приближением применены к изучению спектра возбужденных состояний и автоионизационных резонансов в сложных атомах, в частности, энергий и ширин автоионизационных резонансов в гелии, барии и свинце, с учетом обменно-корреляционных и релятивистских поправок и эффекта хаоса.

Ключевые слова: спектроскопия автоионизационных резонансов, релятивистский энергетический подход

УДК 539.183

А. А. Свинаренко

СПЕКТРОСКОПІЯ АВТОІОНІЗАЦІЙНИХ РЕЗОНАНСІВ В СПЕКТРАХ He- ПОДІБНИХ ІОНІВ ТА ЛУЖНО-ЗЕМЕЛЬНИХ АТОМІВ: НОВІ СПЕКТРАЛЬНІ ДАНІ ТА ЕФЕКТ ХАОСУ

Резюме

Узагальнений енергетичний підхід (S-матричний формалізм Гелл-Мана та Лоу) и релятивістська теорія збурень з дірак-кон-шемівським нульовим наближенням застосовані до вивчення збуджених спектрів збуджених станів та автоіонізаційних резонансів у складних атомах, зокрема, енергій та ширин автоіонізаційних резонансів у гелію, барії та свинцу з урахуванням обмінно-кореляційних і релятивістських поправок та ефекту хаосу.

Ключові слова: спектроскопія автоіонізаційних резонансів, релятивістський енергетичний

UDC541.47

G. P. Prepelitsa

Odessa State Environmental University, 15, Lvovskaya str., Odessa, Ukraine
e-mail: quantpre@mail.ru

NON-LINEAR OPTICS AND SPECTROSCOPY OF ATOMIC AND LASER SYSTEMS WITH ELEMENTS OF A CHAOS

The whole class of modern problems of the nonlinear optics and spectroscopy of the atomic and laser systems is considered from the point of view of a chaos theory. An advanced techniques of using the non-linear analysis methods and chaos theory such as the wavelet analysis, multi-fractal formalism, mutual information approach, correlation integral analysis, false nearest neighbour algorithm, Lyapunov exponent's analysis, and surrogate data method are used in studying the cited problems.

1. Introduction

As it is well known in the modern quantum electronics, photoelectronics etc there are many physical systems (multielement semiconductors and gas lasers, different radiotechnical devices etc), which should be considered in the first approximation as set of autogenerators, coupled by different way (c.f.[1,2]). The typical schemes of different autogenerators (semiconductor quantum generators, coupled by means optical waveguide etc) are presented in refs. [1,2]. The key aspect of studying the dynamics of these systems is analysis of the temporal set for characteristic signals. In refs.[1-4] it has been numerically studied a regular and chaotic dynamics of the system of the Van-der-Poll autogenerators with account of finiteness of the signals propagation time between them and also with special kind of inter-oscillators interaction forces. Chaos theory establishes that apparently complex irregular behaviour could be the outcome of a simple deterministic system with a few dominant nonlinear interdependent variables. The past decade has witnessed a large number of studies employing the ideas gained from the science of chaos to characterize, model, and predict the dynamics of various systems phenomena (c.f.[1-25]). The outcomes of such studies are very encouraging, as they not only revealed that the dynamics of the apparently irregular phenomena could be understood from a chaotic deterministic point of view but also reported very good predictions using such an approach for different systems. Here we consider some problems of the nonlinear optics and spectroscopy of the atomic and laser systems from the point of view of a chaos theory, namely we consider the hydrogen atom and laser with absorbing cell. An advanced techniques of using the non-linear analysis methods and chaos theory such as the wavelet analysis, multi-fractal formalism, mutual information approach, correlation integral analysis, false nearest neighbour algorithm, Lyapunov exponent's analysis, and surrogate data method are applied to these systems.

2. Advanced technique of a chaos theory in optics and spectroscopy

In this section we briefly present an advanced technique of nonlinear analysis methods and chaos theory following to the Refs. [2-4,24,25]. Let us consider scalar measurements $s(n) = s(t_0 + n\Delta t) = s(n)$, where t_0 is the start time, Δt is the time step, and is n the number of the measurements. In a general case, $s(n)$ is any time series, particularly the amplitude level of any optical or spectroscopic characteristics. Since processes resulting in the chaotic behaviour are fundamentally multivariate, it is necessary to re-

construct phase space using as well as possible information contained in the $s(n)$. Such a reconstruction results in a certain set of d-dimensional vectors $\mathbf{y}(n)$ replacing the scalar measurements. Packard et al. [7] introduced the method of using time-delay coordinates to reconstruct the phase space of an observed dynamical system. The direct use of the lagged variables $s(n + t)$, where t is some integer to be determined, results in a coordinate system in which the structure of orbits in phase space can be captured. Then using a collection of time lags to create a vector in d dimensions,

$$\mathbf{y}(n) = [s(n), s(n + t), s(n + 2t), \ldots, s(n + (d\text{-}1)t)], \quad (1)$$

the required coordinates are provided. In a nonlinear system, the $s(n + jt)$ are some unknown nonlinear combination of the actual physical variables that comprise the source of the measurements. The dimension d is called the embedding dimension, d_E. Example of the Lorenz attractor given by Abarbanel et al. [5,6] is a good choice to illustrate the efficiency of the method.

According to Mañé [13] and Takens [12], any time lag will be acceptable is not terribly useful for extracting physics from data. If t is chosen too small, then the coordinates s(n + jt) and s(n + (j + 1)t) are so close to each other in numerical value that they cannot be distinguished from each other. Similarly, if t is too large, then s(n + jt) and s(n + (j + 1)t) are completely independent of each other in a statistical sense. Also, if t is too small or too large, then the correlation dimension of attractor can be under- or overestimated respectively [8,18]. It is therefore necessary to choose some intermediate (and more appropriate) position between above cases. First approach is to compute the linear autocorrelation function

$$C_L(\delta) = \frac{\frac{1}{N}\sum_{m=1}^{N}[s(m+\delta) - \bar{s}][s(m) - \bar{s}]}{\frac{1}{N}\sum_{m=1}^{N}[s(m) - \bar{s}]^2}, \quad (2)$$

where $\bar{s} = \frac{1}{N}\sum_{m=1}^{N} s(m)$, and to look for that time lag where C_L(d) first passes through zero (see [18]). This gives a good hint of choice for t at that $s(n + jt)$ and $s(n + (j + 1)t)$ are linearly independent. However, a linear independence of two variables does not mean that these variables are nonlinearly independent since a nonlinear relationship can differs from linear one. It is therefore preferably to utilize approach with a nonlinear concept of independence, e.g. the average mutual information. Briefly, the concept of mutual information can be described as follows. Let there are two systems, A and B, with measurements a_i and b_k. The amount one learns in bits about a measurement of a_i from a measurement of b_k is given by the arguments of information theory [9] as

$$I_{AB}(a_i, b_k) = \log_2\left(\frac{P_{AB}(a_i, b_k)}{P_A(a_i)P_B(b_k)}\right), \quad (3)$$

where the probability of observing a out of the set of all A is $P_A(a_i)$, and the probability of finding b in a measurement B is $P_B(b_i)$, and the joint probability of the measurement of a and b is $P_{AB}(a_i, b_k)$. The mutual information I of two measurements a_i and b_k is symmetric and non-negative, and equals to zero if only the systems are independent. The average mutual information between any value a_i from system A and b_k from B is the average over all possible measurements of $I_{AB}(a_i, b_k)$,

$$I_{AB}(\tau) = \sum_{a_i, b_k} P_{AB}(a_i, b_k) I_{AB}(a_i, b_k) \quad (4)$$

To place this definition to a context of observations from a certain physical system, let us think of the sets of measurements $s(n)$ as the A and of the measurements a time lag t later, $s(n + t)$, as B set. The average mutual information between observations at n and $n + t$ is then

$$I_{AB}(\tau) = \sum_{a_i, b_k} P_{AB}(a_i, b_k) I_{AB}(a_i, b_k). \quad (5)$$

Now we have to decide what property of I(t) we should select, in order to establish which among the various values of t we should use in making the data vectors $\mathbf{y}(n)$. In ref. [11] it has been suggested, as a prescription, that it is necessary to choose that t where the first minimum of I(t) occurs. On the other hand, the autocorrelation coefficient failed to achieve zero, i.e. the autocorrelation function analysis not provides us

with any value of t. Such an analysis can be certainly extended to values exceeding 1000, but it is known [15] that an attractor cannot be adequately reconstructed for very large values of t. The mutual information function usually [4] exhibits an initial rapid decay (up to a lag time of about 10) followed more slow decrease before attaining near-saturation at the first minimum.

One could remind that the autocorrelation function and average mutual information can be considered as analogues of the linear redundancy and general redundancy, respectively, which was applied in the test for nonlinearity. If a time series under consideration have an *n*-dimensional Gaussian distribution, these statistics are theoretically equivalent as it is shown by Paluš (see [15]). The general redundancies detect all dependences in the time series, while the linear redundancies are sensitive only to linear structures. Further, a possible nonlinear nature of process resulting in the vibrations amplitude level variations can be concluded.

The goal of the embedding dimension determination is to reconstruct a Euclidean space R^d large enough so that the set of points d_A can be unfolded without ambiguity. In accordance with the embedding theorem, the embedding dimension, d_E, must be greater, or at least equal, than a dimension of attractor, d_A, i.e. $d_E > d_A$. In other words, we can choose a fortiori large dimension d_E, e.g. 10 or 15, since the previous analysis provides us prospects that the dynamics of our system is probably chaotic. However, two problems arise with working in dimensions larger than really required by the data and time-delay embedding [5,6,18].

First, many of computations for extracting interesting properties from the data require searches and other operations in R^d whose computational cost rises exponentially with *d*. Second, but more significant from the physical point of view, in the presence of noise or other high dimensional contamination of the observations, the extra dimensions are not populated by dynamics, already captured by a smaller dimension, but entirely by the contaminating signal. In too large an embedding space one is unnecessarily spending time working around aspects of a bad representation of the observations which are solely filled with noise. It is therefore necessary to determine the dimension d_A.

There are several standard approaches to reconstruct the attractor dimension (see, e.g., [5,6,15]), but let us consider in this study two methods only. The correlation integral analysis is one of the widely used techniques to investigate the signatures of chaos in a time series. The analysis uses the correlation integral, $C(r)$, to distinguish between chaotic and stochastic systems. To compute the correlation integral, the algorithm of Grassberger and Procaccia [10] is the most commonly used approach. According to this algorithm, the correlation integral is

$$C(r) = \lim_{N\to\infty} \frac{2}{N(n-1)} \sum_{\substack{i,j \\ (1\le i<j\le N)}} H\left(r - |\ \mathbf{y}_i - \mathbf{y}_j\ |\right), \tag{6}$$

where H is the Heaviside step function with $H(u) = 1$ for $u > 0$ and $H(u) = 0$ for $u \le 0$, r is the radius of sphere centered on $\mathbf{y}_i$ or $\mathbf{y}_j$, and N is the number of data measurements. If the time series is characterized by an attractor, then the integral $C(r)$ is related to the radius r given by

$$d = \lim_{\substack{r\to 0 \\ N\to\infty}} \frac{\log C(r)}{\log r}, \tag{7}$$

where d is correlation exponent that can be determined as the slop of line in the coordinates log $C(r)$ versus log r by a least-squares fit of a straight line over a certain range of r, called the scaling region. If the correlation exponent attains saturation with an increase in the embedding dimension, then the system is generally considered to exhibit chaotic dynamics. The saturation value of the correlation exponent is defined as the correlation dimension (d_2) of the attractor. The nearest integer above the saturation value provides the minimum or optimum embedding dimension for reconstructing the phase-space or the number of variables necessary to model the dynamics of the system. On the other hand, if the correlation exponent increases without bound with increase in the embedding dimension, the system under investigation is generally considered stochastic.

There are certain important limitations in the use of the correlation integral analysis in the search for chaos. For instance, the selection of inappropriate values for the parameters involved

in the method may result in an underestimation (or overestimation) of the attractor dimension [8]. Consequently, finite and low correlation dimensions could be observed even for a stochastic process [18]. To verify the results obtained by the correlation integral analysis, we use surrogate data method.

The method of surrogate data [16] is an approach that makes use of the substitute data generated in accordance to the probabilistic structure underlying the original data. This means that the surrogate data possess some of the properties, such as the mean, the standard deviation, the cumulative distribution function, the power spectrum, etc., but are otherwise postulated as random, generated according to a specific null hypothesis. Here, the null hypothesis consists of a candidate linear process, and the goal is to reject the hypothesis that the original data have come from a linear stochastic process. One reasonable statistics suggested by Theiler et al. [16] is obtained as follows.

If we denote Q_{orig} as the statistic computed for the original time series and Q_{si} for the *i*th surrogate series generated under the null hypothesis and let m_s and s_s denote, respectively, the mean and standard deviation of the distribution of Q_s, then the measure of significance *S* is given by

$$S = \frac{|Q_{orig} - \mu_s|}{\sigma_s} \tag{8}$$

An *S* value of ~2 cannot be considered very significant, whereas an *S* value of ~10 is highly significant [16]. The details on the null hypothesis and surrogate data generation are described in ref. [18]. To detect nonlinearity in the amplitude level data, the one hundred realizations of surrogate data sets were generated according to a null hypothesis in accordance to the probabilistic structure underlying the original data. The correlation integrals and the correlation exponents, for embedding dimension values from 1 to 20, were computed for each of the surrogate data sets using the Grassberger-Procaccia algorithm as explained earlier.

Often, a significant difference in the estimates of the correlation exponents, between the original and surrogate data sets, can be observed. In the case of the original data, a saturation of the correlation exponent is observed after a certain embedding dimension value (i.e., 6), whereas the correlation exponents computed for the surrogate data sets continue increasing with the increasing embedding dimension. The high significance values of the statistic indicate that the null hypothesis (the data arise from a linear stochastic process) can be rejected and hence the original data might have come from a nonlinear process.

It is worth consider another method for determining d_E, namely, a method of false nearest neighbours. In practice, the percentage of false nearest neighbours is determined for each dimension *d*. A value at which the percentage is almost equal to zero can be considered as the embedding dimension. In ref. [4] under studying the chaotic dynamics of the quantum generat0rs was shown that the percentage of false neighbours drops to almost zero at 4 or 5, i.e. a four or five-dimensional phase-space is necessary to represent the dynamics (or unfold the attractor) of the amplitude level series. From the other hand, the mean percentage of false nearest neighbours computed for the surrogate data sets decreases steadily but at 20 is about 35%. Such a result seems to be in close agreement with that was obtained from the correlation integral analysis, providing further support to the observation made earlier regarding the presence of low-dimensional chaotic dynamics in the amplitude level variations.

The Lyapunov exponents are the dynamical invariants of the nonlinear system. In a general case, the orbits of chaotic attractors are unpredictable, but there is the limited predictability of chaotic physical system, which is defined by the global and local Lyapunov exponents. A negative exponent indicates a local average rate of contraction while a positive value indicates a local average rate of expansion. In the chaos theory, the spectrum of Lyapunov exponents is considered a measure of the effect of perturbing the initial conditions of a dynamical system. Note that both positive and negative Lyapunov exponents can coexist in a dissipative system, which is then chaotic. Since the Lyapunov exponents are defined as asymptotic average rates, they are independent of the initial conditions, and

therefore they do comprise an invariant measure of attractor. In fact, if one manages to derive the whole spectrum of Lyapunov exponents, other invariants of the system, i.e. Kolmogorov entropy and attractor's dimension can be found. The Kolmogorov entropy, *K*, measures the average rate at which information about the state is lost with time. An estimate of this measure is the sum of the positive Lyapunov exponents. The inverse of the Kolmogorov entropy is equal to the average predictability. The estimate of the dimension of the attractor is provided by the Kaplan and Yorke conjecture (see [15,18]). There are several approaches to computing the Lyapunov exponents (see, e.g., [5,6,18]). One of them [18] is in computing the whole spectrum and based on the Jacobin matrix of the system function [14]. To calculate the spectrum of Lyapunov exponents from the amplitude level data, one could determine the time delay t and embed the data in the four-dimensional space. In this point it is very important to determine the Kaplan-Yorke dimension and compare it with the correlation dimension, defined by the Grassberger-Procaccia algorithm. The estimations of the Kolmogorov entropy and average predictability can further show a limit, up to which the amplitude level data can be on average predicted. Surely, the important moment is a check of the statistical significance of results.

3. Atomic system in electromagnetic field and Laser with absorbing cell: Chaotic dynamics

One of actual problem of modern optics and spectroscopy of atomic systems is their behaviour in an external field. The classical task is studying a dynamics of a hydrogen atom in an external microwave field. This problem has been in details studied in Refs. [6-8] from the point of view of classical mechanics. Here we apply the above presented method to it. As the first example of chaotic atomic systems, in figures 1,2 we present the characteristic behaviour of the ionization probability for the hydrogen atom in the microwave electromagnetic field and correlation dimension results for chaotic dynamics (the relationship between the correlation exponent and embedding dimension values).

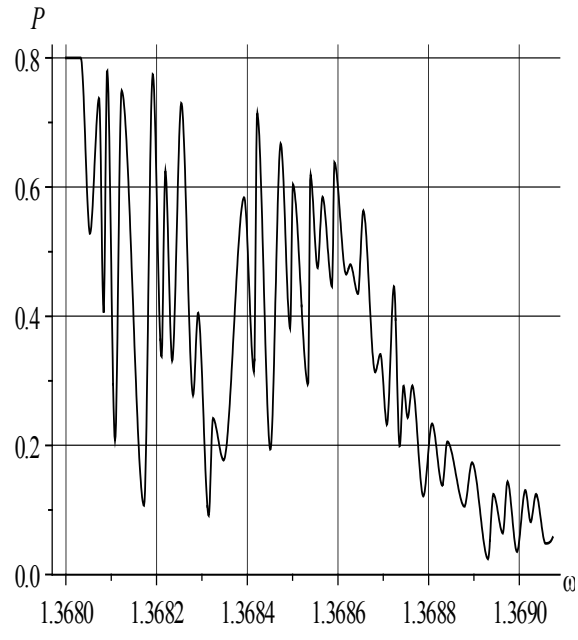

Fig.1. **Characteristic behaviour of the ionization probability for the hydrogen atom in the microwave electromagnetic field [25]**

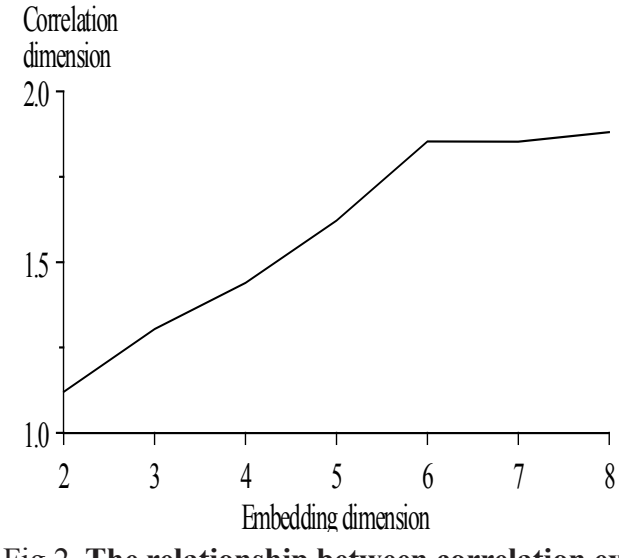

Fig.2. **The relationship between correlation exponent and embedding dimension values the hydrogen atom in the microwave electromagnetic field)**

As it can be seen, the correlation exponent value increases with embedding dimension up to a certain value, and then saturates beyond that value. The saturation of the correlation exponent beyond a certain embedding dimension is an indication of the existence of deterministic dynamics. The saturation value of the correlation exponent, i.e. correlation dimension of attractor, for the amplitude level series is about 1.8 and occurs

at the embedding dimension value of 6.The low, non-integer correlation dimension value indicates the existence of low-dimensional chaos in the dynamics of the hydrogen atom in the microwave electromagnetic field . the same picture has been found for the vibrations dynamics of the autogenerators [4]. The nearest integer above the correlation dimension value can be considered equal to the minimum dimension of the phase-space essential to embed the attractor. The value of the embedding dimension at which the saturation of the correlation dimension occurs is considered to provide the upper bound on the dimension of the phase-space sufficient to describe the motion of the attractor. Furthermore, the dimension of the embedding phase-space is equal to the number of variables present in the evolution of the system dynamics. The results of such studying can indicate that to model the dynamics of process resulting in the amplitude level variations the minimum number of variables essential is equal to 4 and the number of variables sufficient is equal to 6. Therefore, the amplitude level attractor should be embedded at least in a four-dimensional phase-space. The results can indicate also that the upper bound on the dimension of the phase-space sufficient to describe the motion of the attractor, and hence the number of variables sufficient to model the dynamics of process resulting in the level variations is equal to 6.

We performed a calculation of the energies and widths of the resonances in the hydrogen atom for the parameters of the external magnetic field corresponding to Kleppnera experiments and calculations using the models of the IWC and TMM [7,37,52]. The classical dynamics of the system depends on the scaled energy : $e=Eg^{-2/3}$ and is completely chaotic at $e>-0.12$. Detected resonances correspond in the experiments Kleppner etal. (look the review in [24]) are related to the already chaotic regime in the dynamics of the system. Examined several ranges of values of the magnetic field and, in particular, the value of B 6T. There are analyzed fully convergent series of resonances in the energy ranges: [(n-0.5)g, (n-0.3g] for n=1,2,3,4. Rydberg series of resonances are converging to the Landau ionization limit: $E_{ion}(n_r) = (n_r+1/2)\,g$. At each interval there is studied the distribution of levels and widths. For the energy interval between the first and second outside ionization (n_r=0, only one channel is open), the ratio of average width to average levels interval is equal [25]: G_{av}/DE_{av} =0.22±0.01 , that is agreed with results, obtained on the basis of the complex coordinates method (CCM): G_{av}/DE_{av} =0,23±0,01. Respectively, it can be written for the n opened channels: G_{av}/DE_{av} =0,23n (in the CCM), G_{av}/DE_{av} =0,22n (on the operator perturbation theory=OPT). To identify the statistical properties of the resonance it has been normalized the levels and widths interval with respect to the mean. The above determined value G_{av}/DE_{av} =0.22±0.01 is used used to scan the distribution of widths. Figure 3 shows the integral distribution of the energy levels: $N(s)=\int_0^s P(x)dx$,calculated within the random matrix theory (RMT), advanced OPT model (look [24,25]). Each system in Figure 3 corresponds to a fixed number of open channels intervals: a, b, c, d correspond to the number of open channels 1,2,3,4. The notations are used as follows: dotted line-prediction models RMT, the line points - CCM model and our model [25], solid line - model 2D-OPT. As can be seen between the results of calculations within all three models have a fairly good agreement.

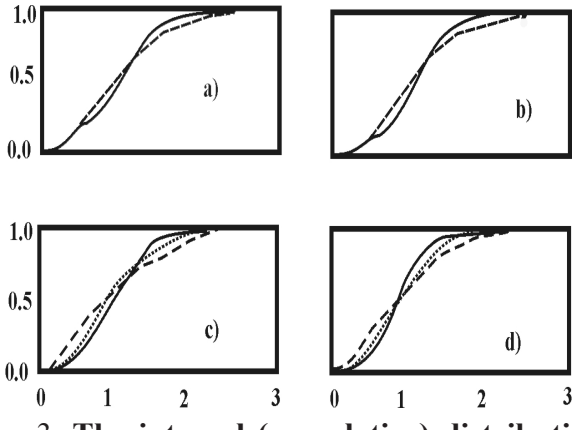

Fig. 3. **The integral (cumulative) distribution of the energy intervals for the resonances in the hydrogen atom in a magnetic field 6T.**

It is important to note that for n=1 all distributions are satisfying to the Porter-Thomas distribution:

$$P_n(\Gamma) = \{1/(2\Gamma_{av})^{n/2}\Gamma(n/2)\}\,\Gamma^{(n/2)-1}\exp[-\Gamma/2\Gamma_{av}] \quad (9)$$

where n-number of open channels, Γ(n/2) is the gamma function (not to be confused with a width Γ). The density of states in the middle of the each Landau channel is: to our data ~ 33 resonances at cm^{-1}, according to the CMM model ~ 40 cm^{-1}, that is in good agreement with the experimental value of 30 resonances cm^{-1} . The average width of the resonance is, to our data, 0.0055 cm^{-1}, which is also consistent with the experiment Kleppner et al.: 0.004-0.006 cm^{-1} , the OPT result: 0.005 cm^{-1} [24,25]. In the energy range [25,30 cm^{-1}], the average width of the resonance in our data is 0,034 cm^{-1}, which is in agreement with the experimental value of 0.03 cm^{-1} and in the evaluation of the CCM model 0.04 cm^{-1} and OPT model: 0,035 cm^{-1}. From a physical point of view, the presence in the spectrum of the hydrogen atom in a magnetic field, many resonances with anomalously small widths explained quite naturally. Their appearance is obviously not due to some hidden symmetry or the phenomenon of localization, and is due to interference effects and random fluctuations inherent in general to all chaotic systems. The numerical calculation of the Lyapunov exponents for the hydrogen atom in a magnetic field (6T) gives the following results: l_1=0.484; l_2 =0.195, that confirms the conclusion regarding the chaotic behaviour of the system.

Further we consider a chaotic dynamics of a laser system with absorbing cell. It is known that for a single-mode laser, described by the equations of the Lorentz needed to return to the region of chaotic generation combination of parameters is difficult to achieve. The results of study [23] indicate that the laser with a nonlinear absorption cell may be more convenient physical system for the experimental observation of dynamic chaos. We consider a theoretical model of a single-mode laser resonator in which the reinforcement is placed along with a nonlinear absorbing medium. Each of the environments consists of identical two-level atoms. The gain and absorption lines are uniformly broadened and their centers align and coincide with one of the frequencies of the cavity. Such a model can describe the real system of five differential equations [23]:

$$
\begin{aligned}
d_e/d\tau &= -e + p_1 + p_2,\\
dp_1/d\tau &= -\delta_1(p_1 + em_1),\\
dp_2/d\tau &= -\delta_2(p_2 + em_2),\\
dp_2/d\tau &= -\delta_2(p_2 + em_2),\\
dm_1/d\tau &= -\rho_1(m_1 - m_{01} - ep_1),\\
dm_2/d\tau &= -\rho_2(m_2 - m_{02} - \beta ep_2).
\end{aligned}
\qquad (10)
$$

Here, the index 1 refers to intensify, and the index of 2 - to an absorbing medium; e, p_1p_1, p_2p_2, m_1m_1 и m_2m_2- the dimensionless variables, e - the amplitude of the laser of the field, p_kp_k- polarization in the environment, m_km_k- the difference between the populations of the working levels; p_k and d_k - respectively the longitudinal and transverse relaxation rate, related to the half-width of the resonator $\delta\omega_p/2\delta\omega_p/2$, k=1,2; $m_{0k}m_{0k}$- the difference between the populations of the working levels in the absence of generation $(m_{01} < 0,\ m_{02} > 0)$;$(m_{01} < 0,\ m_{02} > 0)$; β β-the ratio of the coefficients of saturation of the absorbing and amplifying media; $\tau = t\,\delta\omega_p/2$ $\tau = t\,\delta\omega_p/2$ is the dimensionless time. According to ref. [23], the system (10) is invariant under the substitution $e\rightarrow$-e, $p_kp_k\rightarrow$ -$p_k(k = 1,2)$ $p_k(k = 1,2)$. Attractor of the system can be as invariant with respect to this change (let's call this attractor «symmetrical») and non-invariant («asymmetric»). In the latter case certainly, there are two attractor into each other after this change. In fig. 3 we list present the results of numerical simulation for the system (10) [23]. Strange attractors occur as a result of sequence of bifurcations of solutions (1), the first of which is Hopf bifurcation of stationary solutions with zero intensity of the laser field. This bifurcation occurs $\eta = \delta_2[1 + (\delta_2)(1 + \delta_1 + m_{02})/\delta_1(1 + \delta_1)]$ $\eta = \delta_2[1 + (\delta_2)(1 + \delta_1 + m_{02})/\delta_1(1 + \delta_1)]$, if $\eta < m_{02}\eta < m_{02}$. According to data [23]

and our analysis the Hopf bifurcation occurs at moderate values $\eta\eta$, if the relative width of the absorption line $\delta_2\delta_2$ is quite small, and the relative width of the gain lineδ_1 is quite large. The numerical calculation shows that in order to get the chaotic lasing it is necessary the following: to saturate the absorber should be saturated stronger than the amplifier ($\beta > 1$). At low β the limit cycles generated from the stationary solutions with the zeroth intensity is stable up to very large values of ŋ. . In table 1 we list the numerical parameters of the chaotic regime for the laser system with absorbing

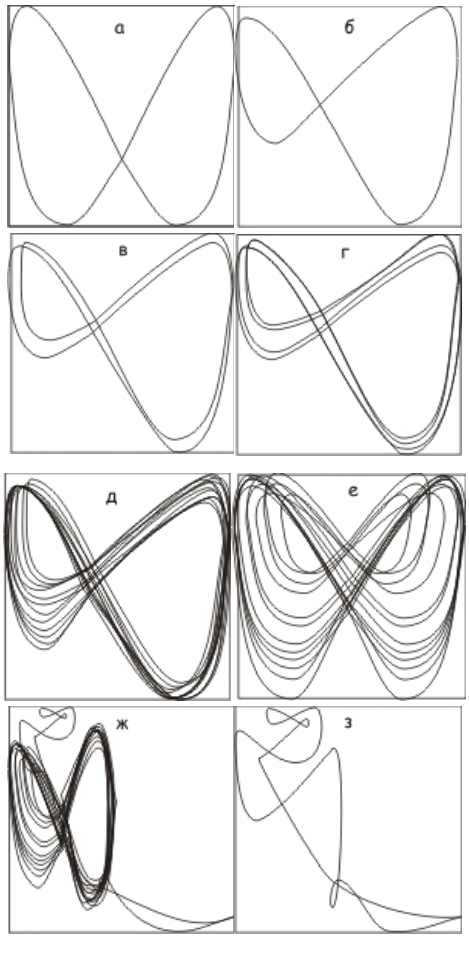

Figure 3. **Projections of the phase trajectories for different values of the parameter ŋ.**
ŋ: а - 1.7000, б - 1.8200, в - 1.8350, г - 1.8385, е - 1.8500, ж - 1.8800, з - 1.9000

cell: l_1-l_6 are the Lyapunov exponents in descending order, *K* - Kolmogorov entropy

Table 1. **Parameters of chaotic regimes in the laser system: l_1-l_6 are the Lyapunov exponents in descending order (our results)**

Regime	λ_1	λ_2	λ_3
Weak chaos	0.175	-0.0001	-0.0003
Strong chaos	0.542	0.203	-0.0001
	λ_4	λ_5	λ_6
Weak chaos	–0.244	–	–
Strong chaos	–0.0004	–0.067	–0.188

The main conclusion of this work is that application of the different chaos theory and nonlinear analysis methods and algorithms to studying chaotic elements in dynamics of the different atomic and laser systems is very useful. In particular, their using allows to study and confirm an existence of chaotic behaviour for the H atom in a microwave and magnetic field and laser with absorbing cell.

References

1. Vedenov A. A., Ezhov A. A., Levchenko E. B., Non-linear systems with memory and functions of neuron ensambles, In: Non-linear waves. Structure and bi-furcations Eds Gaponov-Grekhov A.V., Rabinovich M.I., pp.53-69, Nauka, Moscow (1987).
2. Glushkov A. V., Khetselius O.Y u., Svinarenko A. A., Prepelitsa G. P., Energy approach to atoms in a Laser Field and Quantum Dynamics with Laser Pulses of Different Shape//In: Coherence and Ultrashort Pulsed Emission, Ed. Duarte, F. – Vienna : InTech.-2011.-P.101-130.
3. Prepelitsa G. P., Kuzakon V. M., Buyadzhi V., Solyanikova E., Karpenko A., Korchevsky D., Nonlinear stochastic dynamics governing for quantum systems in external field: Chaos theory and recurrence spectra analysis// Photoelectronics.-2012.-N21.-P.33-36
4. Glushkov A. V., Prepelitsa G. P., Svinarenko A. A., Khetselius O. Yu., Kuzakon V. M., Solyanikova E. P., Modeling of interaction of the nonlinear vibrational systems on the basis

of temporal series analyses (application to semiconductor quantum generators)// Dynamical Systems - Theory and Applications.-2011.-Vol.1.- BIF110.
5. Abarbanel H., Brown R., Sidorowich J., Tsimring L., The analysis of observed chaotic data in physical systems//Rev Mod. Phys.-1993.-Vol.65.-P.1331–1392.
6. Kennel M., Brown R., Abarbanel H., Determining embedding dimension for phase-space reconstruction using geometrical construction//Phys. Rev.A.-1992.-Vol.45.-P.3403–3411.
7. Packard N., Crutchfield J., Farmer J., Shaw R., Geometry from time series// Phys.Rev.Lett-1988.-Vol.45.-P.712–716.
8. Havstad J., Ehlers C., Attractor dimension of nonstationary dynamical systems from small data sets//Phys Rev A.-1989.-Vol.39.-P.845–853.
9. Gallager R.G., Information theory and reliable communication, Wiley, New York.-1986.
10. Grassberger P., Procaccia I., Measuring the strangeness of strange attractors// Physica D.-1983.-Vol.9.-P.189–208.
11. Fraser A., Swinney H., Independent coordinates for strange attractors from mutual information// Phys Rev A.-1986.-Vol.33.-P.1134–1140.
12. Takens F (1981) Detecting strange attractors in turbulence. In: Rand DA, Young LS (eds) Dynamical systems and turbulence, Warwick 1980. (Lecture notes in mathematics No 898). Springer, Berlin-New York.-P.366–381.
13. Mañé R (1981) On the dimensions of the compact invariant sets of certain non-linear maps. In: Rand DA, Young LS (eds) Dynamical systems and turbulence, Warwick 1980. (Lecture notes in mathematics No 898). Springer, Berlin Heidelberg N.-Y.-P. 230–242
14. Sano M, Sawada Y (1985) Measurement of the Lyapunov spectrum from a chaotic time series//Phys Rev.Lett.-1995.-Vol.55.-P.1082–1085
15. Sivakumar B., Chaos theory in geophysics: past, present and future// Chaos, Solitons, Fractals.-2004.-Vol.19.-P.441–462.
16. Theiler J., Eubank S., Longtin A., Galdrikian B., Farmer J., Testing for nonlinearity in time series: The method of surrogate data// Physica D.-1992.-Vol.58.-P.77–94.
17. Glushkov A. V., Khokhlov V. N., Tsenenko I.Atmospheric teleconnection patterns:wavelet analysis//Nonlin. Proc. in Geophys.-2004.-V.11,N3.-P.285-293.
18. Khokhlov V. N., Glushkov A. V., Loboda N. S., Serbov N. G., Zhurbenko K., Signatures of low-dimensional chaos in hourly water level measurements at coastal site// Stoch. Environ. Res. Risk Ass.(Springer).-2008.-Vol.22.-P.777-788
19. Bunyakova Yu. Ya., Glushkov A. V., Fedchuk A. P., Serbov N. G., Svinarenko A. A., Tsenenko I. A., Sensing non-linear chaotic features in dynamics of system of couled autogenerators: standard multifractal analysis// Sensor Electr. and Microsyst. Techn.-2007.-N1.-P.14-17.
20. Glushkov A. V., Khokhlov V. N., Loboda N. S., Bunyakova Yu. Ya., Short-range forecast of atmospheric pollutants using non-linear prediction method // Atmospheric Environment (Elsevier).-2008.-Vol.42.-P. 7284–7292.
21. Gutzwiller M., Chaos in Classical and Quantum Mechanics.-N.-Y.:Springer-Verlag, 1990.-720p.
22. Ott E. Chaos in dynamical systems. Cambridge: Cambridge Univ.Press, 2002.-490p.
23. Vladimirov A. G., Fradkin E. E., Regime of dynamical chaos in generation of laser with absorption cell // Optics and Spectr.-1989.-Vol.67.-P.219-222.
24. Glushkov A. V., Relativistic Quantum Theory. Quantum Mechanics of Atomic Systems.-Odessa:Astroprint, 2008.-704p.
25. Glushkov A. V., Prepelitsa G. P., Dan'kov S. V., Polischuk V. N., Efimov A. V. QED theory of non-linear interaction of the complex atomic systems with laser field. Multi-photon resonances//Journal of Technical Physics.-1997.-Vol.38.- P. 219-225.

The article is received in editorial 09.07.2013

UDC 541.47

G. P. Prepelitsa

NON-LINEAR OPTICS AND SPECTROSCOPY OF ATOMIC AND LASER SYSTEMS WITH ELEMENTS OF A CHAOS

Abstract

The whole class of modern problems of the nonlinear optics and spectroscopy of the atomic and laser systems is considered from the point of view of a chaos theory. An advanced techniques of using the non-linear analysis methods and chaos theory such as the wavelet analysis, multi-fractal formalism, mutual information approach, correlation integral analysis, false nearest neighbour algorithm, Lyapunov exponent's analysis, and surrogate data method are used in studying the cited problems.

Key words: optics and spectroscopy, atomic and laser systems, nonlinear analysis methods and chaos theory

УДК541.47

Г. П. Препелица

НЕЛИНЕЙНАЯ ОПТИКА И СПЕКТРОСКОПИЯ АТОМНЫХ И ЛАЗЕРНЫХ СИСТЕМ С ЭЛЕМЕНТАМИ ХАОСА

Резюме

Класс современных задач нелинейной оптики и спектроскопии атомных и лазерных систем рассматривается с точки зрения теории хаоса. Для решения искомых задач применены усовершенствованные нелинейные методы анализа и теории хаоса, в частности, вэйвлет-анализ, мультифрактальный формализм, метод взаимной информации, метод корреляционного интеграла, алгоритм ложных ближайших соседей, анализ показателей Ляпунова, метод сурогатных данных.

Ключевые слова: оптика и спектроскопия, атомные и лазерные системы, нелинейные методы, теория хаоса

УДК541.47

Г. П. Препелица

НЕЛІНІЙНА ОПТИКА І СПЕКТРОСКОПІЯ АТОМНИХ І ЛАЗЕРНИХ СИСТЕМ З ЕЛЕМЕНТАМИ ХАОСА

Резюме

Клас сучасних задач нелінійної оптики і спектроскопії атомних і лазерних систем розглядається з точки зору теорії хаосу. Для вирішення шуканих завдань застосовані вдосконалені нелінійні методи аналізу та теорії хаосу, зокрема, вейвлет-аналіз, мультіфрактальний формалізм, метод взаємної інформації, метод кореляційного інтеграла, алгоритм помилкових найближчих сусідів, аналіз показників Ляпунова, метод сурогатних даних.

Ключові слова: оптика і спектроскопія, атомні, лазерні системи, нелінійні методи, теорія хаосу

UDC 681.320

V. V. Buyadzhi, S. V. Brusentseva, P. A. Zaichko

Odessa National Maritime Academy, Odessa, Ukraine, 4, Didrikhsona, Odessa, Ukraine

Odessa State Environmental University, 15, Lvovskaya str., Odessa, Ukraine
e-mail: vbuayad@mail.ru

STUDYING ENSEMBLES OF INTERVALS OF THE PARKINSONIAN TREMOR AND LOCAL POTENTIAL FLUCTUATIONS ON THE BASIS OF THE THEORY OF CHAOS

The work is devoted to the use of methods of chaos theory to characterize the nonlinear dynamics of neurophysiological systems and identify the presence of chaotic elements. The data of the studying the Parkinsonian tremor interval ensembles and the corresponding fluctuations of the local potential are presented.

1. Introduction

The task of studying the dynamics of chaotic dynamical systems arises in many areas of science and technology. We are talking about a class of problems of identifying and estimating the parameters of interaction between the sources of complex (chaotic) oscillations of the time series of experimentally observed values. Such problems arise in physics, biology, medicine, neuroscience, geophysics, engineering, etc. Many studies in the cited and other fields of science and technique have appeared, where a chaos theory was applied to a great number of dynamical systems [1-12]. These studies show that chaos theory methodology can be applied and the short-range forecast by the non-linear prediction method can be satisfactory. Time series of the dynamical variables are however not always chaotic, and chaotic behaviour must be examined for each time series. In series of papers it has been developed an effective version of using a chaos theory method and non-linear prediction approach to studying chaotic behaviour of the different dynamical systems. In our opinion, using these methods has very attractive perspectives in medicine and physiology (neuro- physiology). As example, let us underline that an ability to provide interaction between the different areas of the brain by using a multi-channel electroentselophalograms helps determine the location of the foci of abnormal activity in brain of patients with epilepsy. Many diseases of the brain, including epilepsy, Parkinson's disease, are associated with abnormal synchronization large groups of neurons in the brain. Particular attention is paid to a non-linear signals as obvious is a typicality of a chaotic behavior of nonlinear systems.

This paper is devoted to an employing a variety of techniques for characterizing dynamics of the nonlinear neuro-physiological systems identifying the presence of chaotic elements. To analyze measured time histories of the neurophysiological system responses the phase space of these systems was reconstructed by delay embedding. Here we also present the numerical results regarding the Parkinsonian tremor interval ensembles of a few patients and the corresponding fluctuations of the local potential. To implement this program, we follow the procedure set out in detail in [10-12].

2. Method: Testing for chaos in time series

2.1. Data

Many diseases of the nervous system, including epilepsy and Parkinson's disease associated with abnormal synchronization large groups of neurons in the brain. A sign of Parkinson's disease is the synchronization of neurons in the ranks of the thalamus and basal ganglia. However, the functional role of synchronization in the generation of Parkinsonian tremor (involuntary limb regular oscillations with frequencies ranging from 3 to 6 Hz) remains a matter of debate (see [9]). Standard therapy with no effect of medication - it's a deep electrical deep brain stimulation (DEBS) at high frequencies (above 100 Hz). Standard DEBS has been found empirically, the mechanism of its effect has not yet been elucidated, and it has restrictions, such as those associated with side effects. Confirmation that the tremor caused synchronous neuronal activity in nuclei of the thalamus and basal ganglia, would presumably result in a softer therapies with fewer side effects. In this connection of the relevance of the problem of determining the nature of the links between different areas of the brain and the muscles of patients.

The ensembles intervals of spontaneous Parkinsonian tremor three patients have been investigated in ref. [9]. Fluctuations in the limbs were presented accelerometer signals recorded at the sampling rate of 200 Hz and 1 kHz. Information about the activity of the brain was presented recordings of local potentials (LP) of the four deep electrodes implanted in the thalamus and basal ganglia. The data were obtained at the Department of Stereotactic and Functional Neurosurgery, University of Cologne and the Institute of Neurosciences and Biophysics, Research Center Juelich (Germany). Accelerometer signals and the LP with one of the electrodes during heavy Parkinsonian tremor are shown in Fig. 1

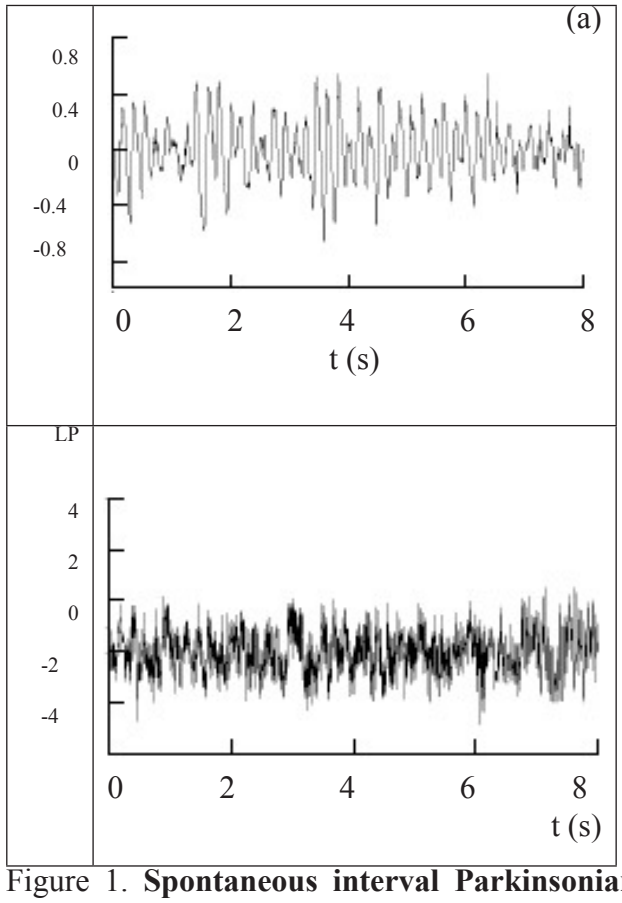

Figure 1. **Spontaneous interval Parkinsonian tremor (total duration 0.1x800) (a, b) and the accelerometer signal LP with one of the electrodes in arbitrary units (only first 8 s shown);**

According to [9], the main conclusion is as the tests also showed that linear techniques do not reveal the activity of the thalamus and basal ganglia on the limb. Besides, it has been found that there are the fluctuations in the accelerometer signal, which correspond to a distinct peak in the power spectrum at a frequency of 5 Hz. The statistical significance of the findings [9] has been confirmed by tests on surrogate data.

2.2. Testing for chaos in time series

In order to make testing for chaos in time series, we use the methodology [10-12]. As usually, let us consider scalar measurements $s(n)=s(t_0+n\Delta t)=s(n)$, where t_0 is a start time, Δt is time step, and n is number of the measurements. In a general case, $s(n)$ is any time series (f.e. atmospheric pollutants concentration). As processes resulting in a chaotic behaviour are fundamentally multivariate, one needs to reconstruct phase space using as well as possible information contained in $s(n)$.

Such reconstruction results in set of d-dimensional vectors $\mathbf{y}(n)$ replacing scalar measurements. The main idea is that direct use of lagged variables $s(n+t)$, where t is some integer to be defined, results in a coordinate system where a structure of orbits in phase space can be captured. Using a collection of time lags to create a vector in d dimensions, $\mathbf{y}(n)=[s(n),s(n+t),s(n+2t),..,s(n+(d-1)t)]$, the required coordinates are provided. In a nonlinear system, $s(n+jt)$ are some unknown nonlinear combination of the actual physical variables. The dimension d is the embedding dimension, d_E.

2.3. Time lag

The choice of proper time lag is important for the subsequent reconstruction of phase space. If t is chosen too small, then the coordinates $s(n+jt)$, $s(n+(j+1)t)$ are so close to each other in numerical value that they cannot be distinguished from each other. If t is too large, then $s(n+jt)$, $s(n+(j+1)t)$ are completely independent of each other in a statistical sense. If t is too small or too large, then the correlation dimension of attractor can be under-or overestimated. One needs to choose some intermediate position between above cases. First approach is to compute the linear autocorrelation function $C_L(d)$ and to look for that time lag where $C_L(d)$ first passes through 0. This gives a good hint of choice for t at that $s(n+jt)$ and $s(n+(j+1)t)$ are linearly independent. It's better to use approach with a nonlinear concept of independence, e.g. an average mutual information. The mutual information I of two measurements a_i and b_k is symmetric and non-negative, and equals to 0 if only the systems are independent. The average mutual information between any value a_i from system A and b_k from B is the average over all possible measurements of $I_{AB}(a_i, b_k)$. Usually it is necessary to choose that t where the first minimum of $I(t)$ occurs.

2.4. Embedding dimension

The goal of the embedding dimension determination is to reconstruct a Euclidean space R^d large enough so that the set of points d_A can be unfolded without ambiguity. The embedding dimension, d_E, must be greater, or at least equal, than a dimension of attractor, d_A, i.e. $d_E > d_A$. In other words, we can choose a fortiori large dimension d_E, e.g. 10 or 15, since the previous analysis provides us prospects that the dynamics of our system is probably chaotic. The correlation integral analysis is one of the widely used techniques to investigate the signatures of chaos in a time series. The analysis uses the correlation integral, $C(r)$, to distinguish between chaotic and stochastic systems. According to [8], it is computed the correlation integral $C(r)$. If the time series is characterized by an attractor, then the correlation integral $C(r)$ is related to the radius r as $d = \lim_{\substack{r\to 0 \\ N\to\infty}} \frac{\log C(r)}{\log r}$, where d is correlation exponent. If the correlation exponent attains saturation with an increase in the embedding dimension, then the system is generally considered to exhibit chaotic dynamics. The saturation value of correlation exponent is defined as the correlation dimension (d_2) of the attractor (see details in refs. [10-12]).

2.5. Nonlinear prediction model

As usually, the predictability can be estimated by the Kolmogorov entropy, which is proportional to a sum of positive Lyapunov exponents (LE) . The spectrum of LE is one of dynamical invariants for non-linear system with chaotic behaviour. The limited predictability of the chaos is quantified by the local and global LE, which can be determined from measurements. The LE are related to the eigenvalues of the linearized dynamics across the attractor. Negative values show stable behaviour while positive values show local unstable behaviour. For chaotic systems, being both stable and unstable, LE indicate the complexity of the dynamics. The largest positive value determines some average prediction limit. Since the LE are defined as asymptotic average rates, they are independent of the initial conditions, and hence the choice of trajectory, and they do comprise an invariant measure of the attractor. An estimate of this measure is a sum of the positive LE. The estimate of the attractor dimension is provided by the conjecture d_L and the LE are taken in descending order. The dimension d_L gives values close to the dimension estimates discussed earlier and is preferable when estimating high dimensions. To compute LE, we use a method with linear fitted map, although the maps with higher order polynomials can be used too

3. Results and conclusions

In our studying, we have analyzed the time series of of the LP signal using methodology from chaos theory. Table 1 summarizes our preliminary results for the time lag calculated for first 800 values of time series of the LP signal. The values, where the autocorrelation function first crosses 0.1, can be chosen as t, as an attractor cannot be adequately reconstructed for very large values of t.

Table 1. **Time lag (t), correlation dimension (d_2), embedding dimension (d_E),Kaplan- Yorke dimension (d_L), average limit of predictability (Pr_{max}), Gottwald-Melbourne chaos availability parameter K**

τ	d_2	d_E	λ_1	λ_2	d_L	Pr	K
9	5.61	6	0.0143	0.0039	4,07	8	0,63

Let us note that the Kaplan-Yorke dimensions, which are also the attractor dimensions, are smaller than the dimensions obtained by the algorithm of false nearest neighbours. Our results show that the time series is resulted from the low-dimensional chaos. The embedding dimension for the time series is $d_N = 6$. Also, the correlation dimensions were calculated using the algorithm of Grassberger and Procaccia. It is noteworthy that the nearest integer above the saturation value provides the minimum or optimum embedding dimension for reconstructing the phase-space or the number of variables necessary to model the dynamics of the system. This concept can be applied, since the embedding dimension determined by both the correlation dimension method and the algorithm of false nearest neighbours are identical. In this case, the number of variables necessary to model the dynamics of the system equals six (preliminary estimate). From the other hand, the analysis of correlation dimension provides only the number of variables, but not their physical meaning. At last, let us comment regarding the Lyapunov exponents. Fistly, our data show that the Kaplan-Yorke dimensions, which are also the attractor dimensions, are smaller than the dimensions obtained by the algorithm of false nearest neighbours.

There are the two positive l_i for the time series under consideration. Since the Lyapunov exponents determine conversion rate from a sphere into an ellipsoid, then the smaller sum of positive exponents results in the more stable dynamical system and, correspondingly, the higher predictability. The further work in application of the chaos theory methods to neuro-physiological problems requires the availability of reliable empirical data and the corresponding time series of measured values.

References

1. Tsonis A. A., Chaos: from theory to application.-NY: Plenum Press.- 1992.
2. Schuster H.G.,Deterministic chaos: an introduction.Weinheim: Verlagsgesellsch. -1989.
3. Grassberger P., Procaccia I., Measuring the strangeness of strange attractors// Physica D.-1983.-Vol.9.-P.189–208
4. Gallager R., Information theory & reliable communication.-N-Y.: Wiley.-1986.
5. Fraser A. M., Swinney H. L.: Independent coordinates for strange attractors from mutual information // Phys. Rev. A. 33(2), 1986, 1134-1140.
6. Kennel M. B., Brown R., Abarbanel H., Determining embedding dimension for phase-space reconstruction using a geometrical construction // Phy. Rev.A.-1992.-Vol.45.- P.3403-3411.
7. Schreiber T.: Interdisciplinary application of nonlinear time series methods// Phys. Rep.-1999.-Vol.308(1).-P.1-64.
8. Grassberger P, Schreiber T.,Schaffrath C, Non-linear time sequence analysis// Int. J. Bifurcat. Chaos.-1991.-Vol.1.-P.521-547.
9. Bezruchko B., Ponomarenko V., Prokhorov M., Smirnov D., Tass P.A., Modeling and diagnostics of nonlinear oscillatory systems using chaotic time series analysis (applications in neurophy-
siology) // Phys.Usp.-2008.-Vol.178.-P.323-328.
10. Glushkov A. V., Methods of a chaos theory. Odessa: OSENU, 2012.
11. Glushkov A. V., Khokhlov V. N.,

Tsenenko I., Atmospheric teleconnection patterns:wavelet analysis//Nonlinear Proc. in Geophysics.-2004.-Vol.11.-P.285-293.
12. Glushkov A. V., Kuzakon' V. M., et al, Geometry of Chaos: Theoretical basis's of consistent combined approach to treating chaotic dynamical systems and their parameters determination // Proc. of Int. Geometry Center.-2013.-Vol.6.-P.43-48.

The article is received in editorial 09.05.2013

UDC 681.322

V. V . Buyadzhi, S. V. Brusentseva, P. A. Zaichko

STUDYING ENSEMBLES OF INTERVALS OF THE PARKINSONIAN TREMOR AND LOCAL POTENTIAL FLUCTUATIONS ON THE BASIS OF THE THEORY OF CHAOS

Abstract

The work is devoted to the use of methods of chaos theory to characterize the nonlinear dynamics of neurophysiological systems and identify the presence of chaotic elements. The data of the studying Parkinsonian tremor interval ensembles and the corresponding fluctuations of the local potential are presented.

Key words: chaos theory, Parkinsonian tremor interval ensembles, fluctuations of the local potential

УДК 681.320

В. В. Буяджи, С. В. Брусенцева, П. А. Заичко

ИЗУЧЕНИЕ АНСАМБЛЕЙ ИНТЕРВАЛОВ ПАРКИНСОНОВСКОГО ТРЕМОРА И ФЛУКТУАЦИЙ ЛОКАЛЬНОГО ПОТЕНЦИАЛА НА ОСНОВЕ МЕТОДОВ ТЕОРИИ ХАОСА

Резюме

Работа посвящена использованию методов теории хаоса для характеристики динамики нелинейных нейрофизиологических систем и идентификации наличия элементов хаоса в систем.. Приведены данные изучения ансамблей интервалов паркинсоновского тремора и соответствующих флуктуаций локального потенциала.

Ключевые слова: теория хаоса, ансамбли интервалов паркинсоновского тремора, флуктуации локального потенциала

УДК 681.320

В. В. Буяджи, С. В. Брусенцева, П. А. Заїчко

ВИВЧЕННЯ АНСАМБЛІВ ІНТЕРВАЛІВ ПАРКІНСОНОВСКОГО ТРЕМОРУ І ФЛУКТУАЦІЙ ЛОКАЛЬНОГО ПОТЕНЦІАЛУ НА ОСНОВІ МЕТОДІВ ТЕОРІЇ ХАОСУ

Резюме

Робота присвячена використанню методів теорії хаосу для характеристики динаміки нелінійних нейрофізіологічних систем та ідентифікації наявності елементів хаосу. Наведені дані вивчення ансамблів інтервалів паркінсонівського тремору та відповідних флуктуацій локального потенціалу.

Ключові слова: теорія хаосу, ансамблі інтервалів паркінсонівського тремору, флуктуації локального потенціалу

PACS: 07.07.Df, 68.43.-h

Iatsunskyi I. R., Smyntyna V. A., Pavlenko M. M.

Department of Experimental Physics, Odessa I. I.Mechnikov National University,
Pastera Street 42, Odessa 65023, Ukraine, yatsunskiy@gmail.com

DETECTION OF AMMONIA MOLECULES USING OPTICAL REFLECTANCE FROM NANOSTRUCTURED SILICON SURFACE

The reflectance properties of various porous silicon structures after ammonia adsorption were investigated. It was shown that increasing of ammonia concentration in the measurement chamber leads to an increase of the optical reflectance. The most sensitive structures for ammonia detection are porous silicon having approximately size of pores – 10-15 μm.

1. INTRODUCTION

Porous silicon (PS) technologies have many applications in semiconductor technology, optoelectronics, chemical, biological sensors and other fields of science [1-3]. Changes in electrical and optical properties of the porous silicon under gas adsorptions are well-known and it is still under attentive investigation [4-8]. Porous silicon exhibits a great potential in optical sensor applications due to the possibility to change its reflectance index and luminescence properties after adsorption of molecules. The sensitivity of an optical sensor depends on the adsorption properties of the measured substances and the interaction of the specific analyte with the porous silicon, which can be adjusted and improved by proper fabrication parameters.

Porous silicon, obtained conventionally by anodisation of crystalline p-type silicon (electrochemical method), is a potential platform for high efficiency gas sensors mainly due to its very large surface to volume ratio, which enhances adsorption of the sensing gas, a primary step for gas sensor. Also the high chemical reactivity of PS with the environment and the possibility of porosity control by the variation of the formation parameters further create an interest in sensing applications. Recently, a new method, termed metal-assisted chemical etching, has been developed, which is relatively simple compared to the electrochemical method. The method does not need an external bias and enables a formation of uniform PS layers more rapidly than the conventional methods. Thin metallic films or particles (Au, Pt, Al, Pd, etc.) are generally deposited directly on a silicon surface prior to immersion in an etchant composed of HF and an oxidizing agent [9, 10]. Metal-assisted chemical etching is essentially a wet etching method yet produces anisotropic high aspect ratio semiconductor micro and nanostructures without incurring lattice damage.

In present paper, we report on the formation of porous p-type silicon using H_2O_2 as an oxidizing agent and silver (Ag) as deposited metal. We discuss the reflectance properties of obtained PS layers after adsorption of NH_3 molecules.

2. EXPERIMENTAL

Metal-assisted chemical etching (MaCE) is fundamentally a wet etch technique. MaCE was first used as an electroless etching technique to produce porous Si and porous III–V compound semiconductor by Li et. al. in 2000 and 2002, respectively [11,12], in contrast to the conventional anodic etching method for porous semiconductor formation. Details on the MaCE mechanism and development can be found elsewhere [13].

The metal-assisted chemical etching processes were applied to p-type Si wafers Czochralski-grown (100) 1-4 Ohm·cm. After standard RCA cleaning the wafers were cleaned with acetone and deionized water via ultrasonic cleaning. A thin oxide layer was formed and the surface became hydrophilic. This oxide layer was removed by dipping the samples into a dilute HF solution. The silver particles, which act as catalysts to assist the etching of silicon, were deposited on Si samples by immersion in 0.23 M HF and 5×10^{-5} M $AgNO_3$ (samples series No 1) and in 0.23 M HF and 10^{-3} M $AgNO_3$ (samples series No 2) metallization aqueous solutions. The time of immersion was varied between 0.5 to 30 minutes. After the electroless metallization, the wafers were etched in aqueous solutions containing HF (40%), H_2O_2 (30%) and ultra-pure H_2O at different concentration ratios and for etching times varied from 1 to 30 minutes. After etching, the samples were rinsed with deionized water. The etching and immersion procedures were performed at room temperature. Structural properties of porous silicon prepared by metal-assisted chemical etching have been investigated by Atomic Force Microscope (AFM) NT-206. AFM studies were done at atmospheric conditions. Using AFM we could characterize the shape and sizes of isolated particles, their distribution depending of the chemicals conditions.

Reflectance measurement system

Instead of a conventional spectrum analyzer which is expensive and hard to miniaturize a cost-effective and transportable evaluation system was developed. In the proposed system the light sources are three different LEDs (red, green and blue). The total reflection is detected by a photodiode. Fig. 1 shows the schematic setup of a simple optical system. The implementation of the developed system and determination of the suitable application areas with the corresponding resolutions is actually in evaluation.

3. RESULTS AND DISCUSSIONS

3.1 AFM studies of porous silicon

During the experiment, we obtained samples with different surface morphology. Fig. 2 displays an AFM image of the porous silicon surface (samples series No 1). At a low concentration of oxidizing agent - H_2O_2 ($H_2O_2/H_2O/HF=10/80/40$), as seen from this image, there were pores that had a conical form, like a crater, having approximately the same size and uniformly distributed over its surface. The approximate diameter of pores ranged from 1 to 1.6 um in diameter.

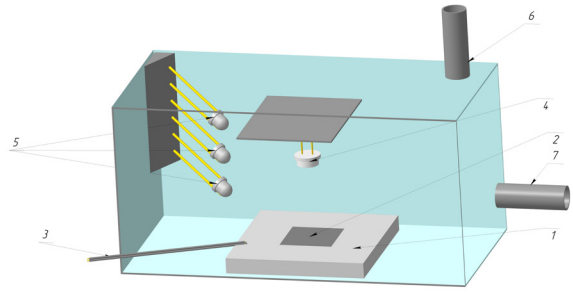

Figure 1. Experimental setup: 1 – Peltier Module; 2 – Sample; 3 – Thermoresistor; 4 – Photodiode; 5 – LED's; 6, 7 – Inlet/Outlet gas

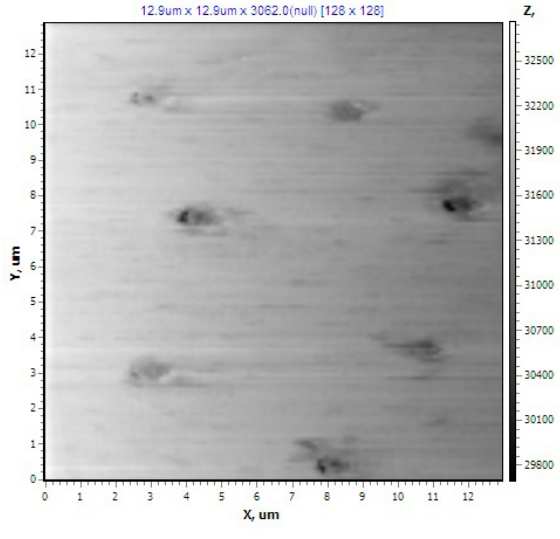

Figure 2. AFM image of Si(100) with a resistivity of 100 Ohm cm after 10 minutes etching in solution—$H_2O_2/H_2O/HF$ = 10/80/40. Ag particles were deposited before etching in solution 0.23 M HF and 5×10^{-5} M $AgNO_3$ within 15 min

The next step was to figure out how the increasing of oxidant concentration affects surface morphology. The increase of oxidant concentration ($H_2O_2/H_2O/HF$ = 25/80/40) leads to a change in the surface structure of silicon from microporous to highly porous structure. We have observed highly porous structure with the dimensions of the pores having an approximate size of 50–200 nm depending on the deposition time (Fig. 3). For both concentrations of H_2O_2, the prolonged etching time induces an increase of pore depth. The changing

of surface morphology due to increasing of H_2O_2 concentration could be explained by the theory proposed by Chartier et al. [14]. Charties et al. have shown that as the composition varies from high to low HF/H_2O_2 ratio, mesopores, cone-shaped macropores, craters could be obtained. This change occurred because of fast dissolving of the silicon surface.

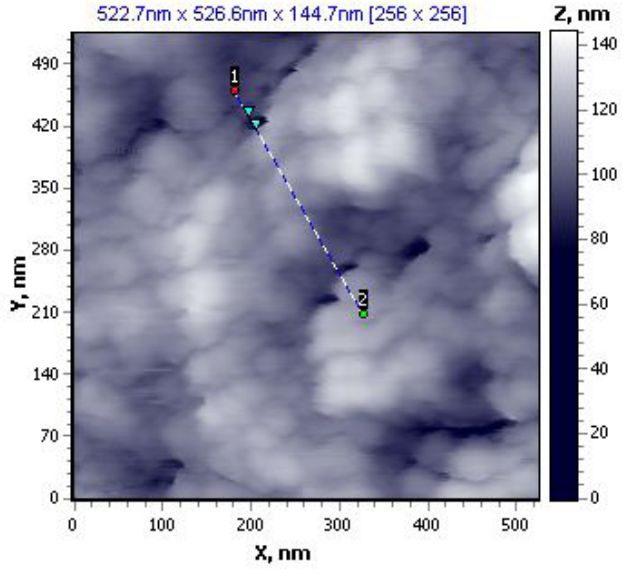

Figure 3. AFM image of Si(100) with a resistivity of 4 Ohm cm after 10 minutes etching in solution—$H_2O_2/H_2O/HF$ = 25/80/40. Ag particles were deposited before etching in solution 0.23M HF and 5×10^{-5}M $AgNO_3$ within 15min

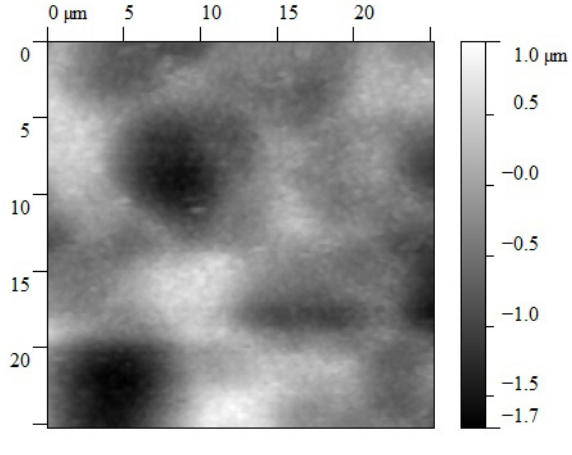

Figure 4. AFM image of Si(100) with a resistivity of 4 Ohm cm after 10 minutes etching in solution—$H_2O_2/H2O/HF$ = 15/80/40. Ag particles were deposited before etching in solution 0.23M HF and 10^{-3}M $AgNO_3$ within 5min

For samples series no. 2, that had higher concentration of $AgNO_3$ in immersion solution (10^{-3} M), we have obtained more remarkable experimental results. The color of the silicon surface after etching has been almost black (1–15 minutes of immersion time) or light brown (15–30 minutes of immersion time) depending on the immersion time. First, we supposed that it is similar to "black" silicon having a needle-shaped surface structure where needles are made of single-crystal silicon and have a height above 10 microns and diameter less than 1 micron [15]. However, AFM investigation showed an absolutely other morphology (Fig.4) having macropores.

3.2 Reflectance of porous silicon after NH_3 adsorption

Reflectance measurements were conducted with the optical system mentioned above (fig.1). Figures 5 and 6 show reflectance spectrum at different concentrations of ammonia in the chamber. Figures demonstrate a shift in the reflectance before and after ammonia exposure for different concentration of ammonia. An increase of ammonia concentration in the measurement chamber leads to an increase of the reflectance for all samples. Notice that samples No 2 (macro porous structures) are most sensitive to ammonia exposure compared to samples No 1 for all wavelengths. Adsorption of ammonia in porous silicon layer affected the reflectance magnitudes appreciably. The reflectance is changing after removal of the ammonia molecules to ever decreasing reflectance values.

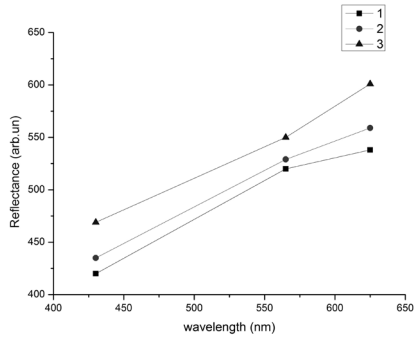

Figure 5. Dependences of maximal magnitudes of reflectance for samples No 1 under nitrogen (curve 1) and different concentrations of ammonia (curve 2 – 20 ppm, curve 3 – 60 ppm).

A possible explanation for this behavior is the change in surface area due to the rough textured surface of the porous silicon. The results seem to indicate that ammonia molecules are diffusing further and further into the pore cavities changing the reflectance index. On the other hand, it is possible that ammonia molecules are adsorbed mainly on surface of wires and in the pore cavities. Adsorption of ammonia molecules creates new surface levels. A re-charging of levels and electrical micro fields close to polar ammonia molecules can affect on recombination rates of electron-hole pairs changing the charge concentration and thus changing the local dielectric constant of the medium (ε) and refractive index ($n = \sqrt{\varepsilon}$).

Next we looked at how porous structure evolves in time. The reflectance after ammonia exposure is shown in fig.7. Here, the reflectance after NH_3 exposure is observed to slowly increase with time. Saturation occurs after about 3-5 minutes for all samples. Research has shown that increase in concentration of ammonia increases the saturation time. Such fast response of porous silicon on the adsorption of ammonia molecules may be used for development of new sensor's structures.

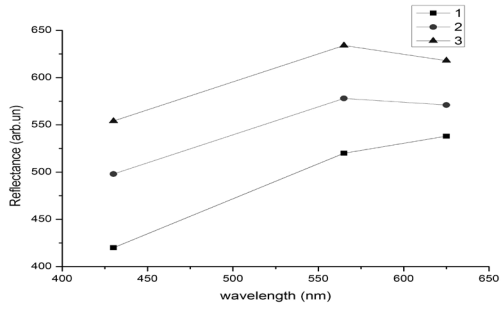

Figure 6. Dependences of maximal magnitudes of reflectance for samples No 2 under nitrogen (curve 1) and different concentrations of ammonia (curve 2 – 20 ppm, 3 – 60 ppm).

4. CONCLUSION

Reflectance and surface morphologies of porous silicon prepared by metal-assisted chemical etching using H_2O_2 as an oxidizing agent have been studied. Depending on the metal-assisted chemical etching conditions, the macro- or microporous structures could be formed. The optical reflectance changes significantly when exposed to ammonia gas. The PS is most sensitive for pores having approximately size 10-15 μm. A fast response of porous silicon on the adsorption of ammonia molecules may be used for development of new sensors. This is an interesting result and an area for further investigation.

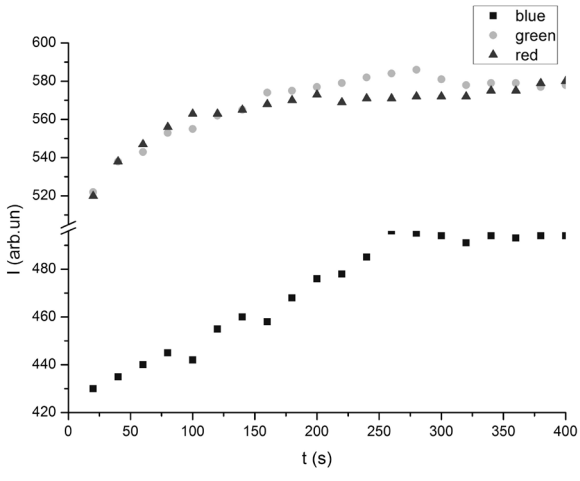

Figure 7. The reflection after ammonia exposure of samples No 1; ammonia concentration 20 ppm.

References

[1] Bisi, O.; Ossicini, S.; Pavesi, L., "Porous silicon: A quantum sponge structure for silicon based optoelectronics," Surf. Sci. Rep. 38, 1-126 (2000).

[2] Pavesi, L.; Turan, R., [Silicon Nanocrystals. Fundamentals, Synthesis and Applications], Wiley-VCH: Weinheim, Germany, 349-394 (2010).

[3] Kilian, K. A.; Bocking, T.; Lai, et al., "Organic modification of mesoporous silicon rugate filters: The influence of nanoarchitecture on optical behavior,". Int. J. Nanotechnol. 5, 170-178 (2008).

[4] Igor Iatsunskyi, Valentin Smyntyna, Nykolai Pavlenko, and Olga Sviridova, "Peculiarities of Photoluminescence in Porous Silicon Prepared by Metal-Assisted Chemical Etching," ISRN Optics, Article ID 958412, 6 pages (2012).

[5] Ben-Chorin, M.; Kux, A., "Adsorbate effects on photoluminescence and electrical conductivity of porous silicon," Appl. Phys. Lett. 64, 481-483 (1994).

[6] Galeazzo, E.; Peres, H.E.M.; Santos, G.; et al., "Gas sensitive porous silicon devices: Responses to organic vapors," Sens. Actuat. B 93, 384-390 (2003).
[7] Barillaro, G.; Diligenti, A.; Nannini, A.; Strambini, L.; Comini, E.; Sberveglieri, G,."Low-concentration NO_2 detection with an adsorption porous silicon FET," IEEE Sensors J. 6, 19-23 (2006).
[8] V. A. Smyntyna, I. Iatsunskyi, O. Sviridova, and N. Pavlenko, "Photoluminescence Properties of Nanostructured Silicon Fabricated by Metal-assisted Chemical Etching," in *Frontiers in Optics Conference*, OSA Technical Digest (online) (Optical Society of America, 2012), paper FTu1A.6.
[9] K. Balasundaram, J. S. Sadhu, J. C. Shin, et al., "Porosity control in metal-assisted chemical etching of degenerately doped silicon nanowires," Nanotechnology, vol. 23, no. 30, Article ID 305304 (2012).
[10] Y. Harada, X. Li, P. W. Bohn, and R. G. Nuzzo, "Catalytic amplification of the soft lithographic patterning of Si. Nonelectrochemical orthogonal fabrication of photoluminescent porous Si pixel arrays," Journal of the American Chemical Society, vol. 123, no. 36, 8709–8717 (2001).
[11] X. Li and P. W. Bohn, "Metal-assisted chemical etching in HF/H_2O_2 produces porous silicon," Applied Physics Letters, vol. 77, Article ID 2572 (2000).
[12] X. Li, Y. W. Kim, P. W. Bohn, and I. Adesida, "In-plane bandgap control in porous GaN through electroless wet chemical etching," Applied Physics Letters, vol. 80, no. 6, 980 (2002).
[13] Z. Huang, N. Geyer, P. Werner, J. De Boor, and U. Gösele, "Metal-assisted chemical etching of silicon: a review," Advanced Materials, vol. 23, no. 2, 285–308 (2011).
[14] C. Chartier, S. Bastide, and C. Lévy-Clément, "Metal-assisted chemical etching of silicon in $HF-H_2O_2$," Electrochimica Acta, vol. 53, no. 17, 5509–5516 (2008).
[15] S. Koynov, M. S. Brandt, and M. Stutzmann, "Black nonreflecting silicon surfaces for solar cells," Applied Physics Letters, vol. 88, Article ID 203107 (2006).

The article is received in editorial 05.06.2013

PACS: 07.07.Df, 68.43.-h

Iatsunskyi I. R., Smyntyna V. A., Pavlenko M. M.

DETECTION OF AMMONIA MOLECULES USING OPTICAL REFLECTANCE FROM NANOSTRUCTURED SILICON SURFACE

Abstract

The reflectance properties of various porous silicon structures after ammonia adsorption were investigated. It was shown that increasing of ammonia concentration in the measurement chamber leads to an increase of the optical reflectance. The most sensitive structures for ammonia detection are porous silicon having approximately size of pores - 10-15 μm.

Key words: porous silicon, adsorption, reflectance, ammonia

PACS: 07.07.Df, 68.43.-h

Яцунский И. Р., Смынтына В. А., Павленко Н. Н.

ДЕТЕКТИРОВАНИЕ АММИАКА МЕТОДОМ ОПТИЧЕСКОГО ОТРАЖЕНИЯ НАНОСТРУКТУРИРОВАННОЙ ПОВЕРХНОСТЬЮ КРЕМНИЯ

Резюме

Было исследовано оптическое отражение различных пористых структур кремния после адсорбции аммиака. Показано, что повышение концентрации аммиака приводит к увеличению оптического отражения. Наиболее чувствительными структурами для детектирования аммиака является пористый кремний, имеющий размер пор - 10-15 мкм.

Ключевые слова: пористый кремний, адсорбция, оптическое отражение, аммиак

PACS: 07.07.Df, 68.43.-h

Яцунський І. Р., Сминтина В. А., Павленко М. М.

ДЕТЕКТУВАННЯ АМІАКУ МЕТОДОМ ОПТИЧНОГО ВІДБИТТЯ НАНОСТРУКТУРОВАНОЮ ПОВЕРХНЕЮ КРЕМНІЮ

Резюме

Було досліджено оптичне відбиття різних поруватих структур кремнію після адсорбції аміаку. Показано, що підвищення концентрації аміаку призводить до збільшення оптичного відбиття. Найбільш чутливими структурами для детектування аміаку є поруватий кремній, що має розмір пор - 10-15 мкм.

Ключові слова: поруватий кремній, адсорбція, оптичне відбиття, аміак

UDC 539.185

A. P. Fedchuk, A. V. Glushkov, Ya. I. Lepikh, L. Lovett, A. V. Ignatenko

I. Mechnikov Odessa National University, 2, Dvoryanskaya str., Odessa, Ukraine
Odessa State Environmental University, 15, Lvovskaya str., Odessa, Ukraine
UK National Academy of Sciences and Bookdata Co., London SW1Y 5AG, The United Kingdom
e-mail: dirac13@mail.ru

STARK EFFECT AND RESONANCES IN THE IONIZATION CONTINUUM FOR EXCITONS IN QUANTUM DOTS AND ATOMS IN AN ELECRIC FIELD

The Stark effect for non- hydrogenic atom of the rubidium and excitons in semiconductor in an external uniform electric field is theoretically studied within the operator perturbation theory method (J.Phys.B26, L379 (1993)). The Stark resonance energies in the rubidium atom and te excitons in the Cu_20 semiconductor and in the GaAs quantum dots in the external uniform electric field are listed.

1. Introduction

This work goes on our investigations of the multi-electron atomic systems and excitons in semiconductrs in an external electric field (the Stark effect) [1-17]. The remarkable Stark effect has a long history and until recently it was believed that the Stark effect is fully understood and fundamental problems remained. However, an observation of the Stark effect in a constant (DC) electric field near threshold in hydrogen and alkali atoms led to the discovery of resonances extending into the ionization continuum by Glab et al and Freeman et al (c.f.[1]). Calculation of the characteristics of these resonances as well as the Stark resonances in the strong electric field remains very important problem of modern atomic physics.

It should be noted that the same class of problems has been arisen in a physics of semiconductors (c.f.[14-17]). It is well known that the availability of excitons in semiconductors resulted experimentally in the special form of the main absorption band edge and appearance of discrete levels structure (f.e. hydrogen-like spectrum in Cu_2O). Beginning from known papers of Gross-Zaharchenya, Thomas and Hopfield et al (c.f.[14-17]), a calculation procedure of the Stark effect for exciton spectrum attracts a deep interest permanently. Very interesting physics occurs in a case of the excitons in quantum dots, wires etc, where the other geometry and energetics in comparison with the bulk semiconductor makes the field effect more intrigues. The exciton states in the quantum dots have been studied in a number of papers and have been observed by photoluminescence experiments (c.f. [14-17]). Naturally, the electronic states in quantum dots (wires) depends on either the confining potential and the interacting force between the particles. Now the electric field effect on the electron-hole states and on the confined excitonic states is often referred to the quantum confined Stark effect. Now it is represented an interest to study an influence of quantum well concentration profile and width on Stark shifts in case of such a system as system GaAs-AlGaAs etc. In this paper we study the Stark effect for non-H atom of rubidium and for excitons in an external uniform electric field within the operator perturbation theory method. The Stark resonance energies in rubidium and the Stark shift for the n=2 state of the Wannier-Mott excitons in the Cu_20 semiconductor and excitons in the parabolic quantum dot (GaAs) in the electric field are listed.

2. Stark effect for atomic systems: Operator perturbation theory

Regarding the operator perturbation theory approach, let us note that this method, originally proposed Ref. [2], is in details presented in [1] and used in many papers. So, here we are limited

only by the key aspects. According to [1,2], the essence of operator perturbation theory approach is the inclusion of the well known method of "distorted waves approximation" in the frame of the formally exact perturbation theory [11]. The zeroth order Hamiltonian H_0 of this PT possesses only stationary bound and scattering states. In order to overcome the formal difficulties, the zeroth order Hamiltonian was defined using the set of the orthogonal EF and EE without specifying the explicit form of the corresponding zeroth order potential. In the case of the optimal zeroth order spectrum , the PT smallness parameter is of the order of G/*E*, where G and *E* are the field width and bound energy of the state level. It is true that G/*E* £ 1/n even in the vicinity of the "new continuum" boundary (where n is the principal quantum number). An influence of the corresponding electric potential model function choice on the values of the Stark resonances energies and bandwidths does not significantly change the final results for the resonances shifts and widths [1].

According to [3], the Schrödinger equation for the electronic eigen-function taking into account the uniform DC electric field (the field strength is *F*)and the field of the nucleus (Coulomb units are used: a unit is $h^2/Ze^2 m$ and a unit of $mZ^2 e^4/h^2$ for energy) looks like:

$$[-(1 - N/Z) / r + F z - 0{,}5D - E] y = 0 \qquad (1)$$

where *E* is the electronic energy, *Z* — charge of nucleus, *N* — the number of electrons in atomic core. Our approach allow to use more adequate forms for the core potential (c.f.[25-27]), including the most consistent quantum electrodynamics procedure for construction of the optimized one-quasi-electron representation and *ab initio* core potential , providing a needed spectroscopic accuracy. For multielectron atom one may introduce the ion core charge z^*. According to standard quantum defect theory (c.f.[3]), relation between quantum defect value m_l, electron energy *E* and principal quantum number *n* is: $m_l=n-z^*(-2E)^{-1/2}$. As it is known, in an electric field all the electron states can be classified due to quantum numbers: n, n_1, n_2, m (principal, parabolic, azimuthal: $n=n_1+n_2+m+1$). Then the quantum defect in the parabolic co-ordinates $d(n_1n_2m)$ is connected with the quantum defect value of the free ($F=0$) atom by the following relation [3]:

$$d(n_1n_2m)=(1/n)\sum_{l=m}^{n-1}(2l+1\ \ C^{JM}_{J,M-m;lm})^2\mu_l$$

$$J=(n-1)/2,\ \ M=(n_1-n_2+m)/2;$$

Naturally, it is possible to use more complicated forms for the ion core potential (c.f.[1]). After separation of variables, equation (1) in parabolic co-ordinates could be transformed to the system of two equations for the functions *f and g*:

$$f'' + \frac{|m|+1}{t} f' + [0{,}5E + (\beta_1 - N/Z) / t - 0{,}25\times$$
$$\times F(t)\, t\,] f = 0 \qquad (2)$$

$$g'' + \frac{|m|+1}{t} g' + [0{,}5E + \beta_2/t + 0{,}25\, F(t)\, t] g = 0 \qquad (3)$$

coupled through the constraint on the separation constants:

$$b_1 + b_2 = 1.$$

For the uniform electric field $F(t) = F$. In ref. [11], the uniform electric field *e* in (3) and (4) was substituted by model function *F*(t) with parameter t (t = 1.5 t_2) . Here we use similar function, which satisfies to necessary asymptotic conditions (c.f.[11,12]) :

$$F(t) = \frac{1}{t}\, F\left[(t-\tau)\frac{\tau^2}{\tau^2 + t^2} + \tau\right] \qquad (4)$$

Potential energy in equation (4) has the barrier. Two turning points for the classical motion along the *h* axis, t_1 and t_2 , at a given energy *E* are the solutions of the quadratic equation ($b = b_1$, $E = E_0$). It should be mentioned that the final results do not depend on the parameter t . It is necessary to know two zeroth order EF of the H_0: bound state function Y_{Eb} (e, n, j) and scattering state function Y_{Es} (e, h, j) with the same EE in order to calculate the width G of the concrete quasi-stationary state in the lowest PT order. Firstly, one would have to define the EE of the expected bound state. It is the well known problem of states quantification in the case of the penetrable barrier. We solve the (2, 3) system here with the total Hamiltonian *H* using the conditions [11]:

$$f(t) \to 0 \text{ at } t \Rightarrow \infty \qquad (5)$$
$$\partial x(\beta, E) / \partial E = 0$$

with

$$x(b, E) = \lim_{t \Rightarrow \infty} [\, g^2(t) + \{g'(t) / k\}^2 \,]\, t^{|m|+1}.$$

These two conditions quantify the bounding energy E, with separation constant b_1 . The further procedure for this two-dimensional eigenvalue problem results in solving of the system of the ordinary differential equations(2, 3) with probe pairs of E, b_1. The bound state EE, eigenvalue b_1 and EF for the zero order Hamiltonian H_0 coincide with those for the total Hamiltonian H at e Þ 0, where all the states can be classified due to quantum numbers: n, n_1, l , m (principal, parabolic, azimuthal) that are connected with E, b_1, m by the well known expressions. We preserve the n, n_1 ,m states-classification in the e¹0 case . The scattering states' functions must be orthogonal to the above defined bound state functions and to each other. According to the OPT ideology [11,12], the following form of $g_{E\acute{e}s}$:is possible:

$$g_{E\acute{}s}(t) = g_1(t) - z_2' \, g_2(t) \tag{6}$$

with $f_{E\acute{e}s}$, and $g_1(t)$ satisfying the differential equations (2) and (3). The function g_2(t) satisfies the non-homogeneous differential equation, which differs from (3) only by the right hand term, disappearing at $t \to \infty$.

3. Stark effect for exciton

The above analogous method can be formulated for description of the Stark effect for the Wannier-Mott excitons in the bulk semiconductors [4]. Really, the Schrödinger equation for the Wannier-Mott exciton looks as follows:

$$[-\hbar^2\nabla_e^2 / 2m_e^* - \hbar^2\nabla_h^2 / 2m_h^* - e^2 / \varepsilon r_{eh} + \\ + eFr_e - eFr_h]\Psi = E\Psi \tag{7}$$

where m^*_e(m^*_h) are the effective-mass for the electron (hole), e is the background dielectric constant. Introducing the relative coordinates: $r = r_e - r_h$ and the corresponding momenta p with reduced mass $p = m^*_e m^*_h / M$ (the momenta P with the total-mass M= $m^*_e + m^*_h$,) and center-of-mass coordinate

$$\rho = (m_e^* r_e + m_h^* r_h)(\, m_e^* + m_h^*)' ,$$

one could rewrite (7) as:

$$[-\hbar^2\nabla^2 / 2\mu - e^2 / \varepsilon r - \hbar / 2 \cdot (1/m_h^* - 1/m_e^*)K \cdot p - \\ - eFr]\Psi F = [E - \hbar^2 K^2 / 8\mu]\Psi \tag{8}$$

This equation then could be solved by the method, described above. The other details can be found in Refs. [1,4].

A problem of the Stark effect for quantum dots requires more detailed consideration. For definiteness, below we study the Stark effect in the parabolic quantum dot. Within the effective-mass approximation and neglecting the band-structure effects , the Hamiltonian of an exciton in a parabolic quantum dot with the same quantization energy $\hbar\Omega$ (for the electron and hole), nd subjected to an external electric field , can be expressed as :

$$H = -\hbar^2\nabla_e^2 / 2m_e^* + (1/2)(\, m_e^*)\Omega^2 r_e^2 - \hbar^2\nabla_h^2 / \\ / 2m_h^* + (1/2)(\, m_h^*)\Omega^2 r_h^2 - e^2 / \varepsilon r_{eh} + eFr_e - eFr_h \tag{9}$$

where all notations are defined above. Further, as above, using the relative coordinate, the momenta with reduced mass and center-of-mass coordinate and the momenta with the total-mass M, the Hamiltonian H (7) can be represented as :

$$H = P^2 / 2M + (1/2)M\Omega^2\rho^2 + p^2 / 2\mu + \\ + (1/2)\mu\Omega^2 r^2 - e^2 / \varepsilon r + eFz \,. \tag{10}$$

Further let us note that the part which depends only on the center-of-mass coordinate in Eq.(10) is corresponding to the Hamiltonian of a well-known 3D harmonic oscillator and the exciton properties is essentially determined by the relative Hamiltonian H_r.

The field term added to the z-direction confinement describes a displaced harmonic oscillator centred in $z_0 = eF/mW^2$ with the frequency W_r inferior to W. Besides, as usually [17], in order to solve the Hamiltonian H_r , one should introduce an interaction potential which obeys to the known Hooke's force with the parameter l by adding and substracting the potential:

$$V(r) = \lambda[(1/2)\mu\Omega^2 r^2 - \hbar\Omega] \,.$$

Surely then the Hamiltonian H is splitted into two terms with the one term being exactly solvable while the other can be treated as a perturbation. Such a scheme is corresponding to method by Jaziri-Bastard-Bennaceur [17]. Our approach is in he direct numerical solving the problem. Let us remind that the introduced potential is similar to the interaction potential between electron-electron used by Johnson-Payne and it can hardly

be considered as the correct potential for the all electron-hole separation. Nevertheless, here one could adjust the interaction parameter *l* so in order to provide the best fit of the true interaction which is the Coulomb interaction, and for the dominant range of separation *r* [17]. The attraction potential *V*(*r*) will have negative value with positive *l* , and it yields a physically reasonable fit to the exact interaction for electron-hole separation $r<(2)^{1/2}R_0$ (here R_0 is the quantum dot radius defined as $\sqrt{\hbar/\mu\Omega}$. As usually, the total energy corresponding to exciton ground state is obtained as :

$$E_T = (3/2)\hbar\Omega + (3/2)\hbar\Omega_r - \lambda\hbar\Omega - (e^2F^2)(2\mu\Omega^2)$$

where $\Omega_r = \Omega\sqrt{1+\lambda}$. The field-induced energy shifts can be expressed as: $DE = E_T(F=O)-E_T(F)$, where E(*F*=0)is the corresponding energy in the free (i.e. zero-field) state. The main aim is to determine the exciton binding energy defined by $E_B = E_e+E_h-E_T$, where E_e,E_h are the energies corresponding to the one-particle Hamiltonian.

4. Results and conclusions

The calculation results for Stark resonances energies in the rubidium atom for the electric field strength *e*=2.189 kV/cm are presented in Table 1. For comparison we have also presented the experimental data [13], the results of calculation within the *1/n*-expansion method by Popov etal [12]. For the most long-living Stark resonances with quantum numbers $n_2 = 0$, m = 0, a width of energy level is significantly less than a distance between them. These states are mostly effectively populated by p-polarized light under transitions from states with (n_1-n_2) = max, m = 0. As a result, the sharp isolated resonances (their positions under E>0 are determined by energies of quasi-stationary states with $n_2=0$, m=0) are appeared under photo ionization from these states in a case of p-polarization

In ref. [4] there are listed the preliminary estimates of the Stark shifts of the n=2 state of excitons in the Cu_20 semiconductor (yellow series) at the electric field strength 600 V/cm results and indicated on the physically reasonable agreement with the known results by Thomas and Hopfield (TH) [14].

Table 1. The energies (cm^{-1})of the Stark resonances for the Rb atom (*ε = 3,59 kV/cm)*:
A-experimental data ; B- Popov et al; C- OPT approach.

n_1n_2m	*d*	A	B		C
23,0,0	0,656	133,1	132,8	132,9	133,0
22,0,0	0,681	157,0	157,1	157,2	157,1
21,1,0	0,517	161,1	159,5	160,6	160,9
20,2,0	0,400	163,9	163,2	163,7	163,9
21,0,0	0,708	185,2	184,2	184,8	185,1
20,1,0	0,531	186,3	185,4	185,8	186,2
20,0,0	0,737	217,2	214,6	214,9	216,9
18,1,0	0,561	248,4	247,2	247,3	248,2
16,2,0	0,428	-	-	-	285,5
18,0,0	0,802	-	-		289,3

Our final value for the Stark shift of the n=2 state excitons in the Cu_20 semiconductor (yellow series) at the electric field strength 600 V/cm results in – 0,308 meV in a good agreement with experimental data of Gross et al.[28]. Under increasing the electric field strength changing a potential on a small enough distance (the orbits diameter) will become comparable with the bond energy of particle on this orbit. According to our data and data by Gross et al., the corresponding electric field is ~ 9×10^3 V/cm. we have tried to discover the chaotic behavior of the exciton dynamics in an electric field, however near ionization boundary exciton does not demonstrate behaviour of quantum chaotic system, which is similar to hydrogen or on-H atom dynamics in a strong field and manifested as unusual features in a photoionization spectra (alkali atoms) [5,14]. Further we list some data on the Stark shifts excitons in a GaAs semiconductor quantum dot (table 2).

Table 2. The Stark shifts (meV) for exciton in the GaAS quantum dot: A- Jaziri-Bastard-Bennaceur method; B- OPT approach

F (kV/cm)	*R* (A)	A	B
50	50	3.9	4.0
50	80	14	14.1
50	120	45	45.2
100	50	13	13.1
100	80	56	56.6
100	120	158	159.8

Comparison of the presented preliminary data shows that the different results are in the physically reasonable agreement. The corresponding accuracy is of the order of 1%, however, is should be noted [17] that though the method [17] is much simpler in comparison with the direct variational approach, but it cannot enviseaged for any strength electric field and/nor any quantum dot size. The important feature of the operator perturbation theory formalism is that it can be applied for any strength electric field.

References

1. Glushkov A. V., Atom in electromagnetic field.-Kiev: KNT, 2005.-400P.
2. Glushkov A. V.,Ivanov L.N. DC Strong-Field Stark-Effect: Consistent Quantum-mechanical Approach // J. Phys. B: At. Mol. Opt. Phys.-1993.-Vol.26,N16.-P.L379-L386.
3. Glushkov A. V., Ambrosov S. V., Ignatenko A. V., Korchevsky D.A., DC Strong Field Stark effect for non-hydrogenic atoms: consistent quantum mechanical approach // Int.Journ.Quant. Chem.-2004.-Vol.99,N5.-P.936-949.
4. Glushkov A. V., Lepikh Ya.I., Khetselius O. Yu.,Fedchuk A. P., Ambrosov S. V , Ignatenko A. V., Wannier-mott excitons and atoms in a DC elecric field: photoionization, Stark effect, resonances in the ionization continuum// Sensor Electr. and Microsyst. Techn.-2008.-N4.-P.5-11.
5. Ambrosov S. V., Khetselius O. Yu., Ignatenko A. V., Wannier-mott exciton and H, Rb atom in a dc elecric field: Stark effect // Photoelectronics.-2008.-N17.-P.82-85.
6. Matter in super-intense laser fields. Eds. D. Batani and C.J.Joachain.-AIP Serie.-2006;
7. Superintense Laser Atoms Physics.Eds. C.A Ullrich., S Erhard., E.K.Gross.-N-Y: Kluwer,2005.
8. Lisitsa V. S. New in Stark and Zeemane effects for Hydrogen Atom// Usp.Fiz. Nauk.- 1987.-Vol.153,N3.- P.379-422.
9. Harmin D. A. Theory of the Non hydrogenic Stark Effect // Phys.Rev. Lett.-1982.-Vol.49,N2.-P.128-131.
10. Krajewska K, Kaminski J.Z., Potvliege R.M., Stabilization of Resonance States in Crossed Magnetic and Laser Fields in a Parabolic Quantum Well// Laser Physics.-2005.-Vol.15,N2.-P.238-244.
11. Glushkov A. V., Malinovskaya S. V., Chernyakova Yu.G., Svinarenko A. A., Cooperative Laser-Electron-Nuclear Processes: QED Calculation of Electron Satellites Spectra for Multi-Charged Ion in Laser Field// Int.Journ.Quant.Chem.-2004.-Vol.99, №5.-P.889-894.
12. Popov V. S., Mur V. D., Sergeev A. V., Weinberg V. M., Strong field Stark effect: perturbation theory and 1/n expansion / // Phys.Lett.A.-1990.-V.149.-P.418-424.
13. Zimmerman M., Littman M., Kash M., Kleppner D., Stark and Zeemane structure of Rydberg states of alkali-metal atoms/ // Phys.Rev.A.-1979.-V.20,N6.-P.2251-2275.
14. Electron-Hole Drops in Semiconductors. Eds. Jeffriss K.D., Keldysh L.V. (Moscow, 1988).
15. Singh S. Physics of Semiconductors and Heterostructures.-Singapore: Mc-Graw-Hill Book Co., 1993.
16. Nguyen Ba A., Hartmut Haug, Theory of the excitonic optical Stark effect in quasi-one-dimensional semiconductor quantum weires//Phys.Rev.A..-1992.-Vol.46(15).-P.9569-9576.
17. Jaziri S., Bastard G., Bennaceur R., Stark effect in parabolic quantum dot// J. de Physique.IV. Colloque C.5.-1993.-Vol.11(3).-P.367-374.

The article is received in editorial 05.05.2013

UDC 539.185

O. P. Fedchuk, A. V. Glushkov , Ya. I. Lepikh, L. Lovett, A. V. Ignatenko

STARK EFFECT, RESONANCES IN THE IONIZATION CONTINUUM FOR EXCITONS INQUANTUM DOTS AND ATOMS IN AN ELECRIC FIELD

Abstract

The Stark effect for non-H atom of rubidium and exciton in semiconductor in an external uniform electric field is studied within the operator perturbation theory method. The Stark resonance energies in rubidium and excitons in the Cu_20 semiconductor and in the GaAs quantum dots in the electric field are listed.

Key words: atom, exciton, Stark effect

УДК 539.185

О. П. Федчук, О. В. Глушков, Я. І. Лепіх, L. Lovett, Г. В. Інгатенко

ШТАРК ЕФЕКТ ТА РЕЗОНАНСИ У ІОНІЗАЦІЙНОМУ КОНТИНУУМІ ДЛЯ ЕКСІТОНІВ І АТОМІВ У ЕЛЕКТРИЧНОМУ ПОЛІ

Резюме

На підставі методу операторної теорії збурень виконано дослідження Штарк-ефекту для атому рубідію та ексітонів в напівпровідниках у зовнішньому однорідному електричному полі. Надані дані щодо енергій штарківських резонансів для атому рубідію та ексітонів у Cu_20 та GaAs напівпровідників в електричному полі.

Ключові слова: атом, ексітон, Штарк-ефект

УДК 539.185

А. П. Федчук, А. В. Глушков, Я. И. Лепих, L. Lovett, А. В. Игнатенко

ШТАРК ЭФФЕКТ И РЕЗОНАНСЫ В ИОНИЗАЦИОННОМ КОНТИНУУМЕ ДЛЯ ЭКСИТОНОВ И АТОМОВ В ЭЛЕКТРИЧЕСКОМ ПОЛЕ

А. В. Глушков, Я. И. Лепих, С. В. Амбросов, А. П. Федчук, О. Ю. Хецелиус, А. В. Игнатенко

Резюме

На основе метода операторной теории возмущений выполнено исследование Штарк-эффекта для атома рубидия и экситонов в полупроводниках во внешнем однородном электрическом поле. Получены данные по энергиям штарковских резонансов для атома рубидия и экситонов в полупроводниках Cu_20 и GaAs в электрическом поле.

Ключевые слова: атом, экситон, Штарк-эффект

UDC 621.315.592

Yu. F. Vaksman, Yu. A. Nitsuk, Yu. N. Purtov, A. S. Nasibov, P. V. Shapkin**

I. I. Mechnikov Odessa National University
*P. N. Lebedev Physical Institute, Russian Academy of Sciences,
e-mail: nitsuk@onu.edu.ua

OBTAINING AND OPTICAL PROPERTIES OF ZnS:Ti CRYSTALS

ZnS:Ti single crystals obtained by diffusion doping are investigated. The spectra of optical density in the energy range 0.4-3.8 eV are investigated. On absorption edge shift of investigated crystals the titan concentration is calculated. Nature of optical transitions determining optical properties of ZnS:Ti single crystals in the visible and IR-region of spectrum is identified.

The diffusion profile of the Ti dopant is determined via measurement of the relative optical density of the crystals in the visible spectral region. The Ti diffusivities in the ZnS crystals at 1270-1370 K are calculated. The Ti diffusivity at 1270 K equals 10-10 cm^2/s.

INTRODUCTION

The zinc sulphide single crystals, doped with transitional metals ions can be used as active media for the lasers of mid-infrared (IR) spectral region. In particular, the effective laser generation in the spectral region of 2.35 mkm were fabricated based on the ZnS:Cr crystals [1]. In the work [2] it was reported about creation of impulsive laser based on ZnS:Fe crystal with continuous tuning of the laser wavelength within the range of 3.49-4.65 mkm. At the same time, essentially nothing is known about possibility of infrared laser radiation realization using ZnS:Ti crystals.

The ZnS crystal doping during the growing process is difficult because the transitional metal evaporation temperatures exceed considerably than of zinc sulphide sublimation. In [3], we have described the procedure of ZnS crystals doping with nickel. A method for diffusion doping of ZnS single crystals with titanium is offered in this work that provides crystals with known titanium impurity concentration. The structure of the optical absorption spectra for the ZnS:Ti crystals has been studied and identified in the visible and infrared regions. The analysis of the profile of the relative optical density allowed us to determine the diffusivity of Ti in the ZnS crystals.

The goals of this study are development of a procedure of diffusion doping of the ZnS crystals with Ti, identification of the optical absorption spectra, and determination of diffusivity of Ti in ZnS crystals.

EXPERIMENTAL

The samples under study are obtained by diffusion doping with Ti of starting pure ZnS single crystals in P.N. Lebedev physical institute of Russian Academy of Sciences. A detailed description of this growth method and main characteristics of the ZnS crystals are presented in [4].

The crystals doping was carried out by impurity diffusion from a metal Ti layer deposited on the crystal surface. A titanium is deposited on one of the large surfaces of the crystalline plate (10×5×1mm) cut out parallel to the plane (111). The nickel layer thickness made the order 10μm. Crystals were annealed in He+Ar atmosphere at the temperatures of 1270-1370 K. The diffusion process was 5h long. After annealing, the ZnS:Ti crystals were characterized by the presence of diffusion profile with a thickness increasing with the annealing temperature elevation. The profile color varied from light yellow to dark yellow

as the temperature increases, in contrast with colourless undoped crystals.

Diffusion of Ti was performed under conditions in which the impurity concentration in the source remained virtually constant. In this case, the solution of Fick's diffusion equation for the one-dimensional diffusion has the form

$$\tilde{N}(x,t) = C_0\left(1 - erf\frac{x}{\sqrt{4Dt}}\right), \qquad (1)$$

where C_0 is the activator concentration at the surface and the symbol "*erf*" denotes the error function (the Gaussian function).The optical density D^* spectra were measured using a MDR-6 monochromator with 1200, 600, and 325 grooves/mm diffraction grates. The first grate was used to analyze the absorption spectra in the 3.8-1.6 eV photon energy range, the second, in the 1.6-0.6 eV one, and third, in the 0.6-0.4 eV one. A FEU-100 photomultiplier was used as a light flow receiver in the visible spectral region, while FR-1P photoresistor working in the alternating current mode in the IR region. The optical density spectra were measured at 77 and 300 K.

When measuring the diffusion profile of the Ti impurity, a thin plate of the crystal (0.2–0.4 mm) was cleaved in the plane parallel to the direction of the diffusion flux. The measurement of the profile of optical density of the Ti-doped crystals was performed using an MF-2 microphotometer. This device allowed us to measure the magnitude of optical density with a step of 10 μm in the direction of the diffusion flux. In this case, the integrated optical density was measured in the spectral range of 2.8–2.4 eV.

ANALYSIS OF OPTICAL DENSITY SPECTRA

The spectra of optical density of undoped ZnS crystals at 77K are feature an absorption edge with energy of 3.75 eV (Fig. 1, curve 1). In the range 0.40-3.6 eV, no features of the absorption spectra of undoped crystals are found.

Doping of crystals with titanium leads in the absorption edge shift towards lower energies (Fig. 1, curves 2-3). The shift value increases with annealing temperature and is due to the interimpurity Coulomb interaction. The band gap width variation ΔE_g (in meV) as a function of impurity concentration depending on concentration of introduced impurities is determined in [5] by the

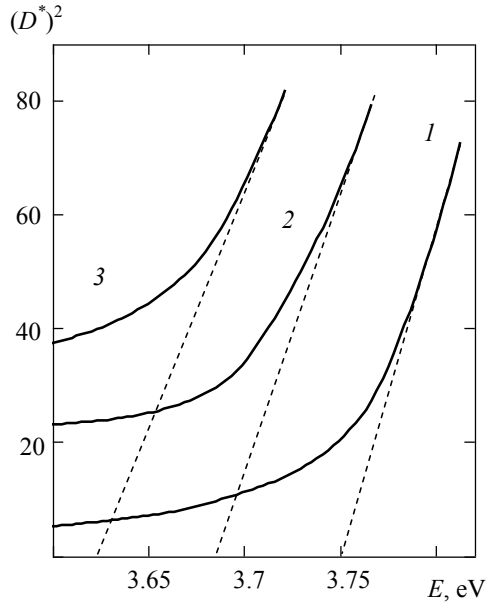

Fig. 1. **Spectra of optical density of ZnS (1) and ZnS:Ti samples 3 (2) and 4 (3)**

Table 1.

Optical characteristics of ZnS:Ti crystals in the absorption edge region

Sample No	Type of the crystal	E_g, eV	ΔE_g, meV	N, cm^{-3}
1	ZnS starting	3.75	---	---
2	ZnS:Ti, annealing 1270 K	3.69	60	$5\cdot10^{18}$
3	ZnS:Ti, annealing 1320 K	3.65	100	$2\cdot10^{19}$
4	ZnS:Ti, annealing 1370 K	3.62	130	$5\cdot10^{19}$

relation:

$$\Delta E_g = 2\cdot10^5\left(\frac{3}{\pi}\right)^{1/3}\frac{eN^{1/3}}{4\pi\varepsilon_0\varepsilon_s}, \qquad (2)$$

where e is electron charge, N, impurity concentration in cm^{-3}, e_s = 8.3 is ZnS dielectric constant, e_0, electric constant. The titanium concentration in the studied crystals was calculated from band gap width changing (see Table 1). The maximum Ti concentration ($5\cdot10^{19}$ cm^{-3}) for the crystals annealed at 1370 K.

In the visible spectral region, the spectra of the optical density of the ZnS:Ti crystals involve a series of poorly resolved lines (Fig. 2). The absorption of the light in this region increases as the titanium concentration. In the absorption spectrum of the lightly-doped ZnS:Ti crystals obtained at 1270 K, nine absorption lines can be distinguished, namely, at 1.58, 1.72, 2.0, 2.13, 2.37, 2.52, 2.75, 2.85 and 3.26 eV(Fig. 2, curve 1).

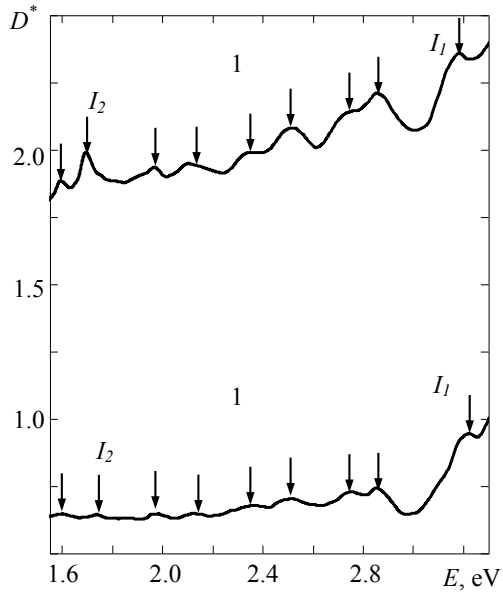

Fig. 2. **Spectra of optical density of ZnS:Ti crystals in the visible region. Samples (1) 2 and (2) 3**

As the doping level increased, the location of the lines at 1.58, 2.0, 2.13, 2.37, 2.52, 2.75, 2.85 eV remained unchanged (Fig. 2, curve 2). Studies of optical density in the temperature range 77-300 K showed that the location of these lines remained unchanged. Such conduct is characteristic for the absorption lines conditioned by the optical transitions of electrons within the impurity ion limits [6]. In the Table 2, the energies of optical transitions in the limits of the Ti^{2+} ion and their identification are given. This table is constructed based on our experimental results and our calculations of the Ti^{2+} ion energy states in ZnS lattice performed on the Tanabe-Sugano diagrams [7]. It is achieved the best accordance of experiment and theory at the parameters of the crystalline field of Δ=3800 cm^{-1} and B=770 cm^{-1}. Values of Δ and B parameters correspond with the results of the calculations performed in [8].

Table 2.

Optical transitions in the limits of Ti^{2+} ion

Line no.	E_{exp}, eV	E_{calc}, eV	Transition
1.	3.26	---	$^3A_2(F)+h\nu\rightarrow {}^2E(D)+e_{c.b.}$
2.	2.85	2.87	$^3A_2(F)\rightarrow {}^1T_2(G)$
3.	2.75	2.76	$^3A_2(F)\rightarrow {}^1E(G)$
4.	2.52	2.55	$^3A_2(F)\rightarrow {}^1T_2(G)$
5.	2.37	2.39	$^3A_2(F)\rightarrow {}^1A_1(G)$
6.	2.13	2.10	$^3A_2(F)\rightarrow {}^3T_1(P)$
7.	2.0	1.98	$^3A_2(F)\rightarrow {}^1T_2(D)$
8.	1.72	1.72[8]	$^2E(D)+h\nu\rightarrow {}^3A_2(F)+e^+_{v.b}$
9.	1.58	1.55	$^3A_2(F)\rightarrow {}^1E(D)$
10.	0.78	0.77	$^3A_2(F)\rightarrow {}^3T_1(F)$
11.	0.48	0.47	$^3A_2(F)\rightarrow {}^3T_2(F)$

It is established that the 3.26 eV line (I_1-line) change their position under variations in the Ti concentration. I_1-line shift towards lower energies at 40 meV with the increase of titan concentration from $5\cdot10^{18}$ cm^{-3} to $2\cdot10^{19}$ cm^{-3} (Fig 2, curve 2). Such shift corresponds to the concentration change of zinc sulfide band gap width by titan doping (see Table 1). At the increase of crystals temperature from 77 to 300 K I_1-line shift towards lower energies at 110 meV. Such shift corresponds to the temperature change of zinc sulfide band gap. Thus, the I_1-line absorption can be conditioned by Ti^{2+} ion photoionization

$$Ti^{2+}+h\nu\rightarrow Ti^{3+}+e^-_{c.b.} \qquad (3)$$

This is also confirmed by a photoconductivity presence in this region.

The behavior of the absorption line at 1.72 eV (I_2-line) is identical to the behavior of the I_1-line. I_2-line also shift towards lower energies at 40 meV with the increase of titan concentration from $5\cdot10^{18}$ cm^{-3} to $2\cdot10^{19}$ cm^{-3} (Fig. 2, curve 2). At the increase of crystals temperature from 77 to 300 K I_2-line shift towards lower energies at 110

meV. The corresponding absorption process can be represented as

$$Ti^{+} + h\nu \rightarrow Ti^{2+} + e^{+}_{v.b.} \qquad (4)$$

In the IR-region the spectra of optical density of ZnS:Ti crystals are characterized by the broad absorption bands at 0.48 and 0.78 eV. The optical density of the crystals increased with titanium concentration growth. The location of this band was unchanged under the temperature varying from 77 to 300 K and titanium concentration varying. These absorption lines were observed before in [8]. According to our calculations (see Table 2), the absorption band at 0.48 eV can be explained by $^3A_2(F) \rightarrow {}^3T_1(F)$ transitions occurring in the limits of Ti^{2+} ion. The absorption band at 0.78 eV is due to the $^3A_2(F) \rightarrow {}^3T_2(F)$ intracenter transitions. At excitation by light corresponding to the high-energy intrinsic absorption region of Ti^{2+} ions intracenter emission $^3T_1(F) \rightarrow {}^3A_2(F)$ transitions were observed.

It should be noted that, as the doping level of the crystals increased, the absorption bands broadened. A similar broadening of the structure of the lines takes place in the absorption spectra in the visible spectral region. This is apparently associated with manifestation of the impurity–impurity interaction of the Ti^{2+} ions.

DETERMINATION OF THE TITANIUM DIFFUSIVITY IN THE ZnS CRYSTALS

The presence of characteristic titanium-absorption lines in the visible region of the spectrum indicates that it is possible to determine the impurity-diffusion profile by measuring the relative optical density (Δ^*). This quantity is a function of the coordinate x in the direction of the diffusion flux and is defined by the expression

$$\Delta^* = \frac{D^*(x) - D^*(\infty)}{D^*(0) - D^*(\infty)}, \qquad (5)$$

where $D^*(x)$ is the crystal's optical density as a function of the coordinate x, $D^*(0)$ is the optical density of the crystal in the surface layer with the coordinate $x = 0$, and D^*(¥) is the optical density of the crystal in the region, where the titanium concentration is negligible (the crystal is not doped). The chosen definition of relative optical density makes it possible to compare the dependence $\Delta^*(x)$ with the impurity concentration profile $C(x)/C_0$ calculated by formula (1). By choosing the value of the diffusivity in Eq. (1), we managed to obtain good agreement between the relative optical density and titanium concentration profiles in the crystals (Fig. 3).

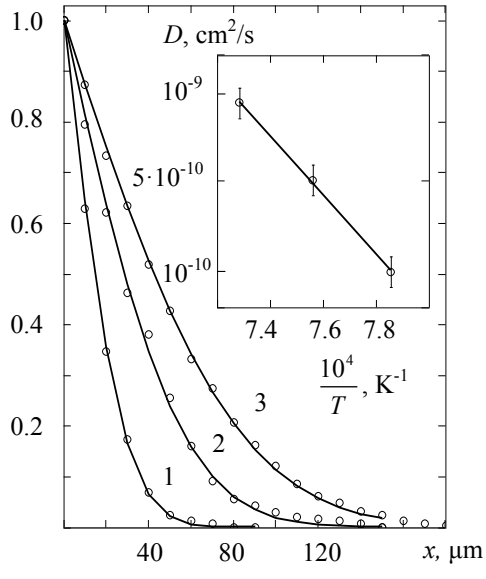

Fig. 3. **Profiles of relative optical density (points in the curve) and diffusion profiles of Ti (solid lines) of ZnS:Ti crystals, samples (1) 3 and (2) 4. The temperature dependence of the Ti diffusivity in ZnS crystals is in the inset.**

The diffusivities of Ti in ZnS crystals at temperature 1270-1370 K were calculated similarly. The temperature dependence of diffusivity $D(T)$, presented in inset to Fig. 3, is described by Arrhenius equation

$$D(T) = D_0 \exp\left(-\frac{E}{kT}\right), \qquad (6)$$

where the factor $D_0 = 2.2 \cdot 10^3$ cm²/s, while the activation energy of diffusion $E = 2.33$ eV. At the crystals annealing temperature of 1270 K the diffusivities of titanium is 10^{-10} cm²/c. This value is the same order that iron diffusivity in ZnS crystals, which we determined according to the procedure described in [9].

CONCLUSIONS

The study allows a number of conclusions. These are as follows:

1. The method of titanium diffusion doping of ZnS single crystals was developed. The maximum concentration of titanium impurity determined by the shift of the absorption edge in ZnS:Ti crystals was $5 \cdot 10^{19}$ cm^{-3}.
2. The nature of absorption lines of ZnS:Ti crystals in the visible and IR regions of the spectrum was identified.
3. The diffusivities of titanium in ZnS crystals in the temperature range 1270-1370 K were calculated for the first time. Analysis of the temperature dependence *D(T)* allowed us to determine the coefficients in Arrhenius equation: $D_0 = 2.2 \cdot 10^3$ cm^2/s and $E = 2.33$ eV. At 1270 K the diffusivity of Ti is 10^{-10} cm^2/s.

REFERENCES

1. 1. *Sorokina I.T., Sorokin E., Mirov S., et. al.* Broadly tunable compact continuous-wave Cr2+:ZnS laser //Optics letters – 2002. – V. 27, N.12. – P. 1040-1042.
2. 2. *Kozlovskii V. I., Korostelin Yu. V., Landman A. I., et. al.* Pulsed Fe^{2+}:ZnS laser continuously tunable in the wavelength range of 3.49 — 4.65 μm//Quantum Electronics.–2011.- V. 41. - P.1-3.
3. 3. *Vaksman Yu. F., Nitsuk Yu. A., Yatsun V. V., Purtov Yu. N., Nasibov A. S., Shapkin P.V.* Optical Properties of ZnS:Ni Crystals Obtained by Diffusion Doping // Functional Materials. – 2010. – V. 17. –N. 1. – P. 75-79.
4. 4. *Korostelin Yu. V., Kozlovsky V. I., Nasibov A. S., Shapkin P. V.* Vapour growth of II-VI solid solution single crystals // J. Cryst. Growth. – 1996. – V. 159. - P. 181-185.
5. 5. *Ukhanov Yu. I.* Optical Properties of Semiconductors. – Moscow: Nauka. – 1997. – 366 p.
6. 6. *Агекян В. Ф.* Внутрицентровые переходы ионов группы железа в полупроводниковых матрицах типа A_2B_6 (Обзор) // ФТТ. – 2002. – Т. 44, №. 11. – С. 1921-1939.
7. 7. *Huheey J. E.* Inorganic chemistry, New York: Harper & Row - .1990 - 190. – 696 p.
8. 8. *Dziesiaty J., Lehr M. U., Peka P., Klimakow A., Muller S., and Schulz H.-J.* Optical and paramagnetic properties of titanium centres in ZnS // Eur. Phys. J., B – 1998. - V.4, P. 269-277.
9. 9. *Nitsuk Yu. A., Vaksman Yu. F., Yatsun V. V., Purtov Yu. N.* Optical absorption and diffusion of iron in ZnS single crystals // Functional Materials. – 2012. – V. 19. –N. 2. – P. 75-79.

The article is received in editorial 29.07.2013

UDC 621.315.592

Yu. F. Vaksman, Yu. A. Nitsuk, Yu. N. Purtov, A. S. Nasibov, P. V. Shapkin

OBTAINING AND OPTICAL PROPERTIES OF ZnS:Ti CRYSTALS

Abstract

ZnS:Ti single crystals obtained by diffusion doping are investigated. The spectra of optical density in the energy range 0.4-3.8 eV are investigated. On absorption edge shift of investigated crystals the titanium concentration is calculated. Nature of optical transitions determining optical properties of ZnS:Ti single crystals in the visible and IR-region of spectrum is identified.

The diffusion profile of the Ti dopant is determined via measurement of the relative optical density of the crystals in the visible spectral region. The Ti diffusivities in the ZnS crystals at 1270-1370 K are calculated. The Ti diffusivity at 1270 K equals 10^{-10} cm^2/s.

Key words: zinc sulfide, diffusion doping, titanium impurity, optical density, diffusivity.

УДК 621.315.592

Ю. Ф. Ваксман, Ю. А. Ницук, Ю. Н. Пуров, А. С. Насибов, П. В. Шапкин

ПОЛУЧЕНИЕ И ОПТИЧЕСКИЕ СВОЙСТВА КРИСТАЛЛОВ ZnS:Ti

Резюме

Исследованы монокристаллы ZnS:Ti, полученные методом диффузионного легирования. Исследованы спектры оптической плотности в области энергий 0.4-3.8 эВ. По величине смещения края поглощения определена концентрация титана в исследуемых кристаллах. Идентифицирована природа оптических переходов, определяющих оптические свойства монокристаллов ZnS:Ti в видимой и ИК-области спектра.

Диффузионный профиль примеси титана определен путем измерения относительной оптической плотности кристаллов в видимой области спектра. Рассчитаны коэффициенты диффузии титана в кристаллах ZnS при температурах 1270-1370 К. При 1270 К коэффициент диффузии титана составляет 10^{-10}см^2/с.

Ключевые слова: сульфид цинка, диффузионное легирование, примесь титана, оптическая плотность, коэффициент диффузии.

УДК 621.315.592

Ю. Ф. Ваксман, Ю. А. Ніцук, Ю. Н. Пуров, А. С. Насібов, П. В. Шапкін

ОТРИМАННЯ І ОПТИЧНІ ВЛАСТИВОСТІ КРИСТАЛІВ ZnS:Ti

Резюме

Методом дифузійного легування отримані монокристали ZnS:Ti. Досліджено спектри оптичної густини в області енергій 0.4-3.8 еВ. За величиною зсуву краю поглинання визначена концентрація титану в досліджуваних кристалах. Ідентифіковані оптичні переходи, що визначають спектр поглинання монокристалів ZnS:Ti в видимій та ІЧ області спектру.

Дифузійний профіль домішки Ti визначався за вимірюваннями відносної оптичної густини кристалів у видимій області спектру. Вперше розраховано коефіцієнти дифузії титану в кристалах ZnS при температурах 1270-1370 К. При 1270 К коефіцієнт дифузії титану становить 10^{-10} см^2/с.

Ключові слова: сульфід цинку, дифузійне легування, домішка титану, оптична густина, коефіцієнт дифузії.

UDC 539.184

N. Serga

Odessa State Environmental University, 15, Lvovskaya str., Odessa, Ukraine
e-mail: nucserga@mail.ru

RELATIVISTIC THEORY OF SPECTRA OF PIONIC ATOMS WITH ACCOUNT OF THE RADIATIVE AND NUCLEAR CORRECTIONS

A new theoretical approach to the description of spectral parameters pionic atoms in the excited states with precise accounting relativistic, radiation, nuclear, electron screening effects on the basis of the relativistic Klein-Gordon-Fock equation and QED perturbation theory formalism is developed. A consistent relativistic theory of hyperfine structure of spectra for the pionic atoms is presented. Numerical data on the electromagnetic contributions to the transition energies in spectra of different pionic atoms are listed.

1. Introduction

Our work is devoted to the development of a new theoretical approach to the description of spectral parameters pionic atoms in the excited states with precise accouting relativistic, radiation, nuclear, electron screening effects on the basis of Klein-Gordon-Fock equation and a development of a consistent relativistic theory of hyperfine structure of spectra. There are calculated energies of X-ray np-1s (n=2-4) transitions in the pionic hydrogen spectrum, 5g-4f, 5f-4d, transitions, hyperfine structure levels energies and probabilities in pionic nitrogen, 6h-5g, 6g-5f transitions for pionic Ne, transitions energies in the spectra of middle and heavy pionic atoms (scuh as ^{133}Ss, ^{175}Lu, ^{181}Ta, ^{205}Tl, ^{202}Pb, ^{238}U) with precise accouting radiation (vacuum polarization), nuclear, electron screening effects. As introduction let us remind that at present time studying the exotic hadronic atomic systems such as pionic atoms is of a great interest for further development of atomic and nuclear theories as well as new tools for sensing the nuclear structure and fundamental pion-nucleus strong interactions. In the last few years transition energies in pionic atoms [1] have been measured with an unprecedented precision. Besides, light pionic atoms can additionally be used as a new low-energy X-ray standards [1]. More over, their spectra studying allows to determine the pion mass using the highest accuracy in comparison with other methods. TO nowadays, new advanced experiments are been preparing in order to make sensing the electromagnetic and strong interaction effects in different pionic atoms.

The most popular theoretical models are naturally (pion is the Boson with spin 0, mass m_{π^-} =139.57018 МэВ, r_{p^-}=0.672±0.08 fm) based on the using the Klein-Gordon-Fock equation, but there are many important problems connected with accurate accounting for as pion-nuclear strong interaction effects as QED radiative corrections (firstly, the vacuum polarization effect etc.). This topic has been a subject of intensive theoretical and experimental interest (see [1-14]). The perturbation theory expansion on the physical; parameter aZ is usually used to take into account the radiative QED corrections, first of all, effect of the polarization of electron-positron vacuum etc. This approximation is sufficiently correct and comprehensive in a case of the light pionic atoms, however it becomes incorrect in a case of the heavy atoms with large charge of a nucleus Z. So, there is a high necessity to develop non- perturbative methods in order to account the QED effects. Besides, let us underline that more correct accounting of the finite nuclear size and electron-screening effects for heavy pionic atoms is also very serious and actual problem. At last, a development of the comprehensive theory of

hyperfine structure is of a great interest and importance in a modern theory of the pionic atom spectra.

2. New relativistic theory of pionic atoms with accounting the radiative, nuclear, electron-screening and hyperfine structure effects

As usually, the relativistic dynamic of a spinless boson particle should be described on the basis of the Klein-Gordon-Fock (KGF) equation. The electromagnetic interaction between a negatively charged pion and the atomic nucleus can be taken into account introducing the nuclear potential $A_\nu$in the KG equation via the minimal coupling $p_\nu \rightarrow p_\nu - qA_\nu$. The wave functions of the zeroth approximation for pionic atoms are determined from the KGF equation [1]:

$$m^2c^2\Psi(x) = \{\frac{1}{c^2}[i\hbar\partial_t + eV_0(r)]^2 + \hbar^2\nabla^2\}\Psi(x) \quad (1)$$

where *h* is the Planck constant, c the velocity of the light and the scalar wavefunction $\Psi_0(x)$ depends on the space-time coordinate x = (ct,r). Here it is considered a case of a central Coulomb potential (V_0(r), 0). Here we consider the stationary solution of (1) and represent the wave function as follows:

$$\Psi\,(x) = \exp(-iEt/\hbar)\,\varphi(x)\,. \quad (2)$$

Resulting master equation looks as:

$$\{\frac{1}{c^2}[E + eV_0(r)]^2 + \hbar^2\nabla^2 - m^2c^2\}\varphi(x) = 0 \quad (3)$$

where E is the total energy of the system (sum of the mass energy mc^2 and binding energy e_0). In principle, the central potential V_0 should include the central Coulomb potential, the radiative (in particular, vacuum-polarization) potential as well as the electron-screening potential in the atomic-optical (electromagnetic) sector. Surely, the full solution of the pionic atom energy especially for the low-excited state requires an inclusion the pion-nuclear strong interaction potential. However, if a pion is on the high orbit of the atom, the strong interaction effects can not be accounted because of the negligible value.

The solution of the Eq. (3) can be resulted in system of the differential equations as follows:

$$\frac{d}{dr}p = q\,, \quad (4)$$

$$\frac{d}{dr}q = \left[\mu c^2 + \frac{l(l+1)}{r^2} - \alpha^2\left(V_c - E\right)^2\right]p \quad (5)$$

where p is the radial part of the pion wave function.

The important nuclear effect is the finite size one (the Breit-Rosenthal-Crawford-Schawlow effect). We will use the widespread Gaussian model for nuclear charge distribution. This is the smooth function, and as result it has a advantage in comparison with usually used model of a uniformly charged sphere [2-5]. It is obvious that it simplifies the calculation procedure and permits to perform a flexible simulation of the real distribution of the charge in a nucleus. Another variant for the nuclear charge distribution function is given by the known Fermi model. Within this model the charge distribution in the nucleus $\rho(r)$ is defined as (c.f.[15]):

$$\rho(r) = \rho_0\,/\{1 + \exp[(r-c)/a)]\} \quad (6)$$

where the parameter *a=0.523* fm, the parameter *c* is chosen by such a way that it is true the following condition for average-squared radius:

$$<r^2>^{1/2}=(0.836\times A^{1/3}+0.5700)\text{fm}.$$

The Gauss model is determined as follows:

$$\rho(r|R) = \left(4\gamma^{3/2}/\sqrt{\pi}\right)\exp\left(-\gamma r^2\right), \quad (7)$$

where $\gamma = 4\pi/R^2$, R is an effective radius of a nucleus.

Further let us present the formulas for the finite size nuclear potential (its derivatives on the nuclear radius). If the point-like nucleus has the central potential *W(R),* then a transition to the finite size nuclear potential is realized by exchanging *W(r)* by the potential [16]:

$$W(r|R) = W(r)\int_0^r dr\, r^2 \rho(r|R) + \int_r^\infty dr\, r^2 W(r)\rho(r|R)\cdot \quad (8)$$

We assume it as some zeroth approximation. Further the derivatives of various characteristics on R are calculated. They describe the interaction of the nucleus with outer electron; this permits recalculation of results, when R varies within reasonable limits. The Coulomb potential for the spherically symmetric density $\rho(r|R)$ is:

$$V_{FS}(r|R) = -((1/r)\int_0^r dr' r'^2 \rho(r'|R) + \int_r^\infty dr' r' \rho(r'|R) \quad (9)$$

It is determined by the following system of differential equations (for the Fermi model) [16]:

$$V'_{FS}(r,R) = (1/r^2)\int_0^r dr' r'^2 \rho(r',R) \equiv (1/r^2) y(r,R)$$

$$y'(r,R) = r^2 \rho(r,R) \quad (10)$$

$$\rho'(r) = (\rho_0/a)\exp[(r-c)/a] \bullet$$
$$\cdot \{1+\exp[(r-c)/a)]\}^2$$

with the corresponding boundary conditions.

The next important topic is connected with a correct accounting the radiation QED corrections and, first of all, the vacuum polarization correction. We firstly introduce into the theory the Flambaum-Ginges radiative potential. In includes the standard Ueling-Serber potential and electric and magnetic form-factors plus potentials for accounting of the high order QED corrections such as [15]

$$\Phi_{rad}(r) = \Phi_U(r) + \Phi_g(r) + \Phi_f(r) +$$
$$+ \Phi_l(r) + \frac{2}{3}\Phi_U^{high-order}(r) \quad . \quad (11)$$

where

$$\Phi_U^{high-order}(r) = -\frac{2\alpha}{3\pi}\Phi(r)\frac{0.092Z^2\alpha^2}{1+(1.62r/r_C)^4} \cdot \quad (12)$$

$$\Phi_l(r) = -\frac{B(Z)}{e} Z^4 \alpha^5 mc^2 e^{-Zr/a_B} \quad (13)$$

Here e – a proton charge and universal function $B(Z)$ is defined by expression: $B(Z)$=0.074+0.35Za. The corresponding Ueling-Serber potential in Eq. (11) can be written as follows:

$$\Phi_U(r) = -\frac{2\alpha}{3\pi r}\int_1^\infty dt \exp(-2rt/\alpha Z)\cdot$$
$$(1+1/2t^2)\frac{\sqrt{t^2-1}}{t^2} \equiv -\frac{2\alpha}{3\pi r} C(x) \quad (14)$$

where $x = r/\alpha Z$ .The quite complex expressions for determination of the electric and magnetic form-factors are given in ref. [15]. An account of the finite nuclear size effect changes (12) as follows [13,16]:

$$\Phi_U^{FS}(r) = -\frac{2\alpha^2}{3\pi}\int d^3r' \int_m^\infty dt \exp(-2t|r-r'|/\alpha Z)\cdot$$
$$\cdot\left(1+\frac{1}{2t^2}\right)\frac{\sqrt{t^2-1}}{t^2}\frac{\rho(r')}{|r-r'|}, \quad (15)$$

The next step is an account of the electron screening effect. It should be noted that the electron shells are not survived in the light pionic atoms during the cascade processes accompanying the formation of a pionic atom. However, in a case of the heave systems, the internal electron shells survive and this fact should be reflected in a precise theory. Our procedure for accounting this effect is a standard one and includes addition to the total interaction potential SCF potential of the electrons, which can be determined within the Dirac-Fock method by solution of the standard relativistic Dirac equations. To realize this step, we have used the QED perturbation theory formalism for relativistic many-electron atom. Further in order to calculate probabilities of the Radiative transitions between energy level of the pionic atoms we have used the relativistic energy approach [16].

The final topic of the theory is calculation of the hyperfine structure parameters. Here one could use the standard theory of hyperfine structure of the usual multi-electron atom. As usually, the hyperfine structure is arisen because of the interaction of the orbital pion with a magnetic di-

pole moment m and quadruple electric moment Q of a nucleus. Hitherto, only magnetic contribution has been studied. The quadruple interaction is not treated hitherto. One could consider energy of the hyperfine interaction, which looks as:

$$W = W_\mu + W_Q = -\mu \cdot H(0) + \\ + \frac{1}{6} e \sum_{\alpha\beta} Q_{\alpha\beta} \frac{\partial^2 \varphi}{\partial x_\alpha \partial x_\beta} \qquad (15)$$

Here H and j are defined as, respectively, the magnetic field and electrostatic potential produced by an electron (pion) in the position of the nucleus. Following to the standard procedure, after multiple transformations the final expression for the energy of the hyperfine splitting (magnetic part of) the energy levels of the atom in the pion:

$$E_1^{nlF} = \frac{\mu_I \mu_N e \mu_0 \hbar c^2}{4\pi\left(E_0^{nl} - \langle nl|V_0(r)|nl\rangle\right)} \times \\ \left[\frac{F(F+1) - I(I+1) - l(l+1)}{2I}\right] \langle nl|r^{-3}|nl\rangle \qquad (16)$$

Here

$$\mu_N = e\hbar / 2m_p c$$

and other notations are standard.

In a consistent precise theory it is important allowance for the contribution to the energy of the hyperfine splitting of the levels in the spectrum of the pion atom due to the interaction of the orbital momentum of the pion with the quadrupole moment of the atomic nucleus. The corresponding part looks as follows:

$$< LIFM|W_Q|LIFM \geq \Delta + \mathrm{BC}\ (C+1) \qquad (17)$$

where

$$C=F(F+1)-L(L+1)-I(I+1), \qquad (18)$$

$$B = -\frac{3}{4} \frac{e^2 Q}{I(2I-1)} \frac{(\gamma \cdot L \| \eta_2 \| \gamma \cdot L)}{\sqrt{L(L+1)(2L-1)(2L+1)(2L+3)}}, \qquad (19)$$

$$\Delta = \frac{e^2 Q(I+1)}{(2I-1)} \frac{(\gamma \cdot L \| \mu_2 \| \gamma \cdot L) L(L+1)}{\sqrt{L(L+1)(2L-1)(2L+1)(2L+3)}}. \qquad (20)$$

Here L – is orbital moment of pion, F is a total moment of an atom.

3. Results and conclusions

Table 1 and Figure 1 shows the experimental data by Schröder etal, Gotta etal («Pionic hydrogen & pion mass collaboration»; Inst-PSI, Switzerland) and theoretical results: our data and data from other theories (KGF theory with analytical formula for the pionic H atom taking into account QED account within expansions in aZ by Schlesser-Indelicato, Schröder etal, two-channel theory considering the Uehling-Serber correction and the finite size of the nucleus by Sigg etal [4-12]. Besides, the QED contributions to the energy of the ground state pionic hydrogen are listed.

Table 1. **Theoretical (T), experimental (Exp) energies (eV) for the np-1s (n = 2-4) transitions in p-H and QED contributions to the ground state energy**

Data/ Transition	QED (meV)	2p-1s	3p-1s	4p-1s
T.:Schlesser-Indelicato	3238.287	2429.547	2878.844	3036.098
T.:Sigg etal	-	-	2878.808	3036.073
T.: Schroder etal	3238.264	-	2878.809	-
T.: Lyubovitski-Rusetsky	3238.250	-	-	-

Our theory: ΔE_{EM}	3238.282	2429.546	2878.839	3036.098
Exp. (Schröder etal)	-	-	2885.916	-
Exp. (Gotta etal)	-	-	2885.929	-

Overall, between different theories is a good agreement that, in principle, due apparently

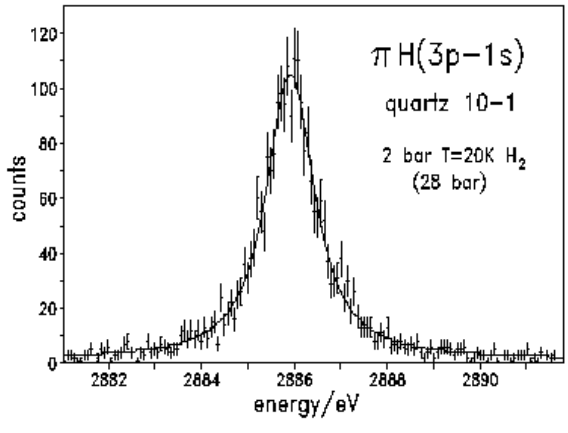

Fig 1. **X-ray 3-1 transition in the spectrum of pionic H (Gotta etal); (narrow structure inside line indicates resolution spectrometer**

negligible contribution to QED, nuclear and others corrections for little Z (here Z=1, aZ<1).

The pion-nuclear strong shift of the 1s level in pionic hydrogen DE_{1s} can be calculated as a difference between the experimental energy and exact electromagnetic value.

The corresponding results are listed below [4-12]: in the theory Schlesser-Indelicato etal with using the experimental data by Schröder etal: DE_{1s} = -7.072 ± 0.013 (stat.) ± 0.034 (syst.) eV, with experimental data by Gotta etal: DE_{1s} = -7.085 ± 0.011 (stat.) ± 0.026 (syst.); the result by Sigg etal: DE_{1s} = -7.108 ± 0.013 (stat.) ± 0.034 (syst.); the result by Gotta etal DE_{1s} = 7.120 ± 0.014eV; the theory of quantum defect by Mitroy-Ivallov gives the value: DE_{1s} = 7.108 ± 0.047 eV.

Our relativistic theory provides such results: DE_{1s} = 7.077 ± ± 0.013 (stat.) ± 0.034 (syst.) with using the experimental data by Schröder etal and DE_{1s} = 7.090эV ± 0.011 (stat.) ± 0.026 (syst.) with the data by Gotta etal.

In table 2 we present our data on the hyperfine splitting energies of the 9p level (F=1/2,3/2) for a number of the light, medium, heavy pionic atoms. The data by Trassinelli-Indelicato [6] are presented for comparison too.

Table 2. **Hyperfine splitting energies of the 9p level (F=1/2,3/2) for a number of the light, medium, heavy pionic atoms: Theory I - Trassinelli-Indelicato ; Theory II – our data;**

Atom	Z	T.I	T.II
^{1}H	1	0.0001	0.0001
^{13}C	6	0.0060	0.0058
^{14}N	7	-	0.0296
^{15}N	7	-0.0039	-0.0033
^{17}O	8	-	0.0531
^{19}F	9	0.0767	0.0764
^{20}Ne	10	-	0.1003
^{43}Ca	20	-	-0.1256
^{57}Fe	26	0.0643	0.0639
^{129}Xe	**54**	-4.1295	-4.1620
^{133}Cs	55	-	1.0569
^{175}Lu	71	-	1.2304
^{181}Ta	73	-	1.2521
^{205}Tl	81	-	7.0407
^{202}Pb	82	-7.8662	-7.7954
^{235}U	92	-	9.2074

In table 3 we present our data on the different contributions to the 5f - 4d energy in pionic nitrogen (our data).

Table 3. **Different contributions to the 5f - 4d energy (eV)in pionic nitrogen (our data)**

Contribution	5f-4d
Coulomb	4054.7160
Finite size of a nucleus	0.0000
Self-energy	-0.0003
Vacuum polarization- Uehling-Serber	2.9462
Vacuum polarization- Wichman-Kroll	-0.0012
Vacuum polarization- Kallen-Sabry	0.0271
Relativistic recoil effect	0.0028
Other	-0.0020
Total energy	4057.6886

It is interesting to compare the results of our theory for the nitrogen atom with similar data in the theory of Trassinelli-Indelicato for the 5g-4f transition. The Radiative vacuum polarization corrections in our theory are as follows: the Uehling-Serber contribution -1.2478 eV; the total vacuum polarization one is 1.2618 eV; the total polarization contribution in the theory by Trassinelli-Indelicato: 1.2602 eV [6]. There is a very good agreement between two theories for sufficiently light atom of nitrogen. This is regarding the 5g-4f transition energies: our theory - 4055.3791eV, theory by Trassinelli-Indelicato: 4055.3801eV.

We have carried out the calculating the parameters (table 4) of a number of the X-ray transitions (5g-4f, 4f-3d) spectra of medium and heavy pionic atoms (^{43}Ca, ^{133}Cs, ^{175}Lu,^{181}Ta, ^{205}Tl etc) with precise accounting of the relativistic, QED (corrections of the Uehling-Serber, Källen-Sabry, Wichmann-Kroll etc.), nuclear (finite size of the nucleus within the Fermi and Gauss models), electron screening (availability of the internal electronic shells) effects.

Table 4. **The 4f-3d, 5g-4f transition energies (keV) in spectra of some atoms (see text)**

Atom	nl-n'l'	E_{EXP} Berkley	E_{EXP} CERN	$E_{KGF+\alpha Z}$	E_{EM}	E_N^1	E_N^2
^{43}Ca	4f-3d	72.352 ± 0,009	-	72.361	72.356	-	-
^{133}Cs	4f-3d	560.5 ± 1.1	562.0 ± 1.5	556.45	556. 484	561.47	562.12
^{205}Tl	4f-3d	-	-	-	963.920	-	-
^{175}Lu	5g-4f	-	-	-	427.313	-	-
^{205}Tl	5g-4f	-	561.67 ± 0.25	559.65	559.681	560.93	561.63
^{202}Pb	5g-4f	-	575.56 ± 0.25	573.83	573.862	575.21	575.78
^{238}U	5g-4f	731.4 ± 1.1	732.0 ± 0.4	725.52	725.574	729.80	730.52

Note:E_{EXP}(Virginia)^{238}U (5g-f)=730.88± 0.75

Our new data (E_{EM}) for a number of pionic atoms are listed in Table 4, where for comparison there are presented other experimental data (E_{EXP}; Berkley, CERN, Virginia laboratories) and theoretical data: the KGF alternative theory of the use of model of the uniformly charged ball and aZ QED expansion decay (E_{KGF+aZ}) [1-13]. Besides, we also list the corresponding data , obtained within different nuclear model calculations with the standard (E_N^1) and generalized (E_N^2) potentials [3-5,13].

Table 5 gives very interesting illustration of the electron screening contributions to the energy transitions 5g-4f, 4f-3d for the pion lead atom due to the presence of 2 [He], 4 [Be] and 10 [Ne] electrons, as well as (for Be-like configuration) contribution due to electron correlations.

Table 5. **Contribution to the energy (eV) of the transition to a pion atom Pb, due tothe presence of 2 [He], 4 [Be] and 10 [Ne] electron (our theory)**

Transition	[He]	[Be]	[Be] + correlations	[Ne]
4-3	-56.15	-65.24	-65.16	-68.12
5-4	-63.08	-72.17	-72.08	-75.64

Our main conclusion is that an accounting of the Radiative, nuclear and electron-screening effects is very important in a precise relativistic theory of spectra of the pionic atoms. As example let us give the corresponding values of corrections: corrections to the energy, in particular, for the 5g-4f transition of atoms ^{43}Ca, ^{133}Cs, ^{175}Lu (5g-4f, 4f-3d), ^{181}Ta, ^{205}Tl (4f-3d), ^{202}Pb, ^{238}U, due to the radiative effects ate ~2-4.6keV, the nuclear effects - up to 0.2 keV and electron-screening effect, for example, for the 5g-4f, 4f-3d in the pionic Pb and others to availability of the 2[He]-10[Ne] electrons - ~0.05-0.08 keV. Using these measurements in the laboratories of CERN, Berkley, Virginia, one could obtained the pion-nuclear strong interaction shift (the difference between the experimental value and the "exact" electromagnetic energy(, which are for the studied atoms lying in the limits ~~ 0.1-6.4 keV.

References

1. Deloff A., Fundamentals in Hadronic Atom Theory, Singapore: World Scientific, 2003.-352P.
2. Serga I. N., Electromagnetic and strong interactions effects in X-ray spectroscopy of pionic atoms// Photoelectronics.-2011.-Vol.20.-P. 109-112.
3. Deslattes R., Kessler E., Indelicato P., de Billy L., Lindroth E. , Anton J., Exotic atoms//Rev. Mod. Phys. -2003.-Vol.75.-P.35-70.
4. Backenstoss G., Pionic atoms // Ann. Rev.Nucl.Sci.-1970.-Vol.20.-P.467-510.
5. Menshikov L I and Evseev M K, Some questions of physics of exotic atoms// Phys. Uspekhi.2001-Vol. 171.-P.150-184.
6. Indelicato P., Trassinelli M., From heavy ions to exotic atoms// arXiv:physics.-2005.-V1-0510126v1.-16P.
7. Mitroy J., Ivallov I.A., Quantum defect theory for the study of hadronic atoms// J. Phys. G: Nucl. Part. Phys.-2001.-Vol.27.-P.1421–1433
8. Lyubovitskij V., Rusetsky A., πp atom in ChPT: Strong energy-level shift// Phys. Lett.B.-2000.-Vol.494.-P.9-13.
9. Schlesser S., Le Bigot E.-O., Indelicato P., Pachucki K., Quantum-electrodynamics corrections in pionic hydrogen// Phys.Rev.C.-2011.-Vol.84.-P.015211 (8p.).
10. Sigg D., Badertscher A., Bogdan M. et al, The strong interaction shift and width of the ground state of pionic hydrogen// Nucl. Phys. A.-1996.-Vol.609.-P.269-309.
11. Gotta D., Amaro F., Anagnostopoulos D., Conclusions from recent pionic–atom experiments // Cold Antimatter Plasmas and Application to Fundamental Physics, ed. Y.Kania and Y.Yamazaki (AIP).-2008.-Vol.CP1037.-P.162-177.
12. Gotta D., Amaro F., Anagnostopoulos D., Pionic Hydrogen//Precision Physics of Simple Atoms and Molecules, Ser. Lecture Notes in Physics (Springer, Berlin / Heidelberg).-2008.-Vol.745.-P.165-186
13. Serga I. N., Dubrovskaya Yu. V., Kvasikova A. S., Shakhman A. N., Sukharev D. E., Spectroscopy of hadronic atoms: Energy shifts// Journal of Physics: C Ser.-2012.- Vol.397.-P.012013.
14. Pavlovich V. N., Serga I. N., Zelentsova T. N., Tarasov V. A., Mudraya N. V., Interplay of the hyperfine, electroweak and strong interactions in heavy hadron-atomic systems and x-ray standards status// Sensor Electronics and Microsyst.

Techn.-2010.-N2.-P.20-26.
15. Flambaum V. V., Ginges J. S. M., Radiative potential and calculation of QED radiative corrections to energy levels and electromagnetic amplitudes in many-electron atoms // Phys.Rev.-2005.-Vol.72.-P.052115 (16p).
16. Glushkov A. V., Relativistic quantum theory. Quantum mechanics of atomic systems,Odessa:Astroprint,2008.-700P.

The article is received in editorial 01.07.2013

UDC 539.184

I. N. Serga

RELATIVISTIC THEORY OF SPECTRA OF PIONIC ATOMS WITH ACCOUNT OF THE RADIATIVE AND NUCLEAR CORRECTIONS

Abstract

A new theoretical approach to the description of spectral parameters pionic atoms in the excited states with precise accounting relativistic, radiation, nuclear, electron screening effects on the basis of the relativistic Klein-Gordon-Fock equation and QED perturbation theory formalism is developed. A consistent relativistic theory of hyperfine structure of spectra for the pionic atoms is presented. Numerical data on the electromagnetic contributions to the transition energies in spectra of different pionic atoms are listed.

Keywords: relativistic theory, hyperfine structure, pionic atoms

УДК 539.184

И. Н. Серга

РЕЛЯТИВИСТСКАЯ ТЕОРИЯ СПЕКТРОВ ПИОННЫХ АТОМОВ С УЧЕТОМ РАДИАЦИОННЫХ И ЯДЕРНЫХ ПОПРАВОК

Резюме

Предложен новый теоретический подход к описанию спектральных параметров пионных атомов в возбужденном состоянии с прецизионным учетом релятивистских, радиационных, ядерных и электронно-экранировочных эффектов на основе уравнения Клейна-Гордона-Фока и КЭД теории возмущений. Развита последовательная релятивистская теория сверхтонкой структуры пионных атомов. Приведены численные данные по электромагнитным вкладам в энергии переходов в спектрах различных пионные атомов.

Ключевые слова: релятивистская теория, сверхтонкая структура, пионные атомы

УДК 539.184

І. М. Сєрга

РЕЛЯТИВІСТСЬКА ТЕОРІЯ СПЕКТРІВ ПІОННИХ АТОМІВ З УРАХУВАННЯМ РАДІАЦІЙНИХ ТА ЯДЕРНИХ ПОПРАВОК

Резюме

Запропоновано новий теоретичний підхід до опису спектральних параметрів піонних атомів у збудженому стані з точною деталлю урахуванням релятивістських, радіаційних, ядерних та електронно-екраніровочних ефектів на основі рівняння Клейна-Гордона-Фока і КЕД теорії збурень. Розвинена послідовна релятивістська теорія надтонкої структури піонних атомів. Наведені чисельні дані по електромагнітним внескам в енергії переходів у спектрах різних піонних атомів.

Ключові слова: релятивістська теорія, надтонка структура, піонні атоми

UDC 539.182

A. N. Shakhman

Kherson Department, Odessa National Polytechnical University, 1, Shevchenko pr., Ukraine
e-mail: quantsha@mail.ru

STRONG π NUCLEAT INTERACTION EFFECTS IN SPECTROSCOPY OF HADRONIC ATOMS

New New relativistic method on the basis of the Klein-Gordon-Fock equation with a generalized pion-nuclear potential is used to determine the strong interaction effects in spectroscopy of pionic atoms. The numerical data on 2p-1s, 3d-2p, 4f-3d,5g-4f transition energies on the basis of the Klein-Gordon-Fock theory with the pion-nucleus potential, the Klein-Gordon-Fock theory with account of the radiative and the finite nuclear size corrections are presented for in some middle and heavy pionic atoms. It is performed comparison between theoretical data and results of measurements in the Berkley, CERN and Virginia laboratories.

1. Introduction

In this paper we goes on our studying on spectroscopy of pionic atoms and quantitative estimate of the strong pion-nucleon interactions contributions to the transitions energies in the X-ray spectra of pionic atomic systems. Let us note that the spectroscopy of hadron atoms has been used as a tool for the study of particles andfundamental properties for a long time. Exotic atoms are also interesting objects as they enable to probe aspects of atomic and nuclear structure that are quantitatively different from what can be studied in electronic or "normal" atoms. As it is known, one of the fundamental questions in the modern hadron's physics is that the hadron masses being much higher than the mass of their quark content. The current mass of the up (u) and down (d) quarks is two orders of magnitude smaller than a typical hadron's mass of about 1 GeV. This extraordinary phenomenon is proposed to originate from spontaneous breaking of chiral symmetry of massless quarks in strong interaction physics [1-5]. At present time one of the most sensitive tests for the chiral symmetry breaking scenario in the modern hadron's physics is provided by studying the exotic hadron-atomic systems. Nowadays the transition energies in pionic (kaonic, muonic etc.) atoms are measured with an unprecedented precision and from studying spectra of the hadronic atoms it is possible to investigate the strong interaction at low energies measuring the energy and natural width of the ground level with a precision of few meV [1-10].

The mechanism of creation of the hadronic atoms is well known now (e.g. [1,2]). Really, such an atom is formed when a negative pion enters a medium, looses its kinetic energy through ionization and excitation of the atoms and molecules and eventually is captured, replacing the electron, in an excited atomic orbit. The further de-excitation scenario includes the different cascade processes such as the Auger transitions, Coulomb de-excitation, scattering etc. When a pion reaches a low-n state with the little angular momentum, strong interaction with the nucleus causes its absorption. The strong interaction is the reason for a shift in the energies of the low-lying levels from the purely electromagnetic values and the finite lifetime of the state corresponds to an increase in the observed level width. The possible energy shifts caused by the pion-induced fluorescence X-rays were checked in the measurement of the pion beams at PSI in Switzerland. For a long time the similar experimental investigations have been carried out in the laboratories of Berkley, Virginia (USA), CERN (Switzerland).

The most known theoretical models to treating the hadronic (pionic, kaonic, muonic, antiprotonic etc.) atomic systems are presented in refs. [1-5,7,8]. The most difficult aspects of the theo-

retical modeling are reduced to the correct description of pion-nuclear strong interaction [1-3] as the electromagnetic part of the problem is reasonably accounted for. Besides, quite new aspect is linked with the possible, obviously, very tiny electroweak and hyperfine interactions.

2. Relativistic approach to pionic atoms spectra

All available theoretical models to treating the hadronic (kaonic, pionic) atoms are naturally based on the using the Klein-Gordon-Fock equation [2,5], which can be written as follows :

$$m^2c^2\Psi(x)=\{\frac{1}{c^2}[i\hbar\partial_t+eV_0(r)]^2+\hbar^2\nabla^2\}\Psi(x) \quad (1)$$

where c is a speed of the light, *h* is the Planck constant, and Ψ_0(x) is the scalar wave function of the space-temporal coordinates. Usually one considers the central potential [V_0(r), 0] approximation with the stationary solution:

$$\Psi\,(\mathrm{x})=\exp(-\mathrm{iE}t/\hbar)\,\varphi(x)\,, \quad (2)$$

where $\varphi(x)$ is the solution of the stationary equation:

$$\{\frac{1}{c^2}[E+eV_0(r)]^2+\hbar^2\nabla^2-m^2c^2\}\varphi(x)=0 \quad (3)$$

Here E is the total energy of the system (sum of the mass energy mc^2 and binding energy e_0). In principle, the central potential V_0 naturally includes the central Coulomb potential, the vacuum-polarization potential, the strong interaction potential.

The most direct approach to treating the strong interaction is provided by the well known optical potential model (c.g. [2]). Practically in all papers the central potential V_0 is the sum of the following potentials. The nuclear potential for the spherically symmetric density $\rho(r|R)$ is [6,13]:

$$V_{nucl}(r|R)=-((1/r)\int_0^r dr'r'^2\rho(r'|R)+\int_r^\infty dr'r'\rho(r'|R) \quad (4)$$

The most popular Fermi-model approximation the charge distribution in the nucleus $\rho(r)$ (c.f.[12]) is as follows:

$$\tilde{n}(r)=\tilde{n}_0/\{1+\exp[(r-c)/a)]\}, \quad (5)$$

where the parameter *a=0.*523 fm, the parameter *c* is chosen by such a way that it is true the following condition for average-squared radius:

$$<r^2>^{1/2}=(0.836\times A^{1/3}+0.5700)\mathrm{fm}.$$

The effective algorithm for its definition is used in refs. [12] and reduced to solution of the following system of the differential equations:

$$V'nucl(r,R)=(1/r^2)\int_0^r dr'r'^2\rho(r',R)\equiv(1/r^2)y(r,R) \quad (6)$$

$$y'(r,R)=r^2\rho(r,R), \quad (7)$$

$$\tilde{n}'(r)=(\tilde{n}_0/a)\exp[(r-c)/a]\{1+\exp[(r-c)/a)]\}^2 \quad (8)$$

with the corresponding boundary conditions. Another, probably, more consistent approach is in using the relativistic mean-field (RMF) model, which been designed as a renormalizable meson-field theory for nuclear matter and finite nuclei [13].To take into account the radiation corrections, namely, the effect of the vacuum polarization we have used the generalized Ueling-Serber potential with modification to take into account the high-order radiative corrections [5,12]. The most difficult aspect is an adequate account for the strong interaction. In the pion-nucleon state interaction one should use the following pulse approximation expression for scattering amplitude of a pion on the "i" nucleon [2,3]:

$$f_i(r)=\{b_0'+b_1'(t\tau)+[c_0'+c_1'(t\tau)]kk'\}\delta(r-r_i); \quad (9)$$

where t and τ are the isospines of pion and nucleon. The nucleon spin proportional terms of the kind $\sigma[kk']$ are omitted. The constants in (9) can be expressed through usual s-wave (α_{2T}) and p-wave $(\alpha_{2T,2J})$ scattering length (T and J -isospin and spin of he system πN. The corresponding parameters in the Compton wave length $\lambda\!\!\!^{-}_{\pi}$ terms are as follows:

$$b_0' = (\alpha_1 + 2\alpha_3)/3 = -0.0017\,\lambda_\pi.$$

$$b_0' = (\alpha_3 - \alpha_1)/3 = -0.086\,\lambda_\pi.$$

$$c_0' = (4\alpha_{33} + 2\alpha_{13} + 2\alpha_{31} + \alpha_{11})/3 = -0.208(\lambda_\pi)^3.$$

$$c_1' = (2\alpha_{33} - 2\alpha_{13} + \alpha_{31} - \alpha_{11})/3 = -0.184(\lambda_\pi)^3. \quad (10)$$

The scattering amplitude for pion on a nucleus can be further received as a coherent sum of the πN -scattering lengths. рассеяния. In approximation of the only s-wave interaction the corresponding potential can be written in the Dezer form:

$$V_N(r) = -2\pi\hbar^2\mu_\pi^{-1}\left[ZA^{-1}a_p + (A-Z)A^{-1}a_n\right]\rho(r). \quad (11)$$

The s-wave lengths of the $\pi^{-1}p$ -scattering $a_p = (2\alpha_1 + \alpha_3)/3$ и $\pi^{-1}n$ - scattering $a_n = \alpha_3$; scattering are introduced to Eq. (11). Because of the equality between $a_n = b_0' + b_1'$ and $a_p = b_0' - b_1'$ (with an opposite sign) the theoretical shift of the s-level with $T = 0\ (A = 2Z)$ from Eq. (12) is much less than the observed shift. So, the more correct approximation must take into account the effects of the higher orders.

In whole the energy of the hadronic atom is represented as the sum:

$$E \approx E_{KG} + E_{FS} + E_{VP} + E_N; \quad (12)$$

Here E_{KG} -is the energy of a pion in a nucleus (Z, A) with the point-like charge (dominative contribution in (12)), E_{FS} is the contribution due to the nucleus finite size effect, E_{VP} is the radiation correction due to the vacuum-polarization effect, E_N is the energy shift due to the strong interaction V_N .The last contribution can be defined from the experimental energy values as:

$$E_N = E - (E_{KG} + E_{FS} + E_{VP}) \quad (13)$$

From the other side the strong pion-nucleus interaction contribution can be found from the solution of the Klein-Gordon equation with the corresponding meson-nucleon potential. In this case, this contribution E_N is the function of the potentials (8)-(11) parameters.

3. Results and conclusions

In table 1 we present the data on the transition energies in some pionic atoms (from. Refs. [1-4]): the measured values form the Berkley, CERN and Virginia laboratories, the theoretical values for the *2p-1s, 3d-2p, 4f-3d,5g-4f* pionic transitions ($E_{\hbar 1}^N$ - values from the Klein-Gordon-Fock equation with the pion-nucleus potential [2]; E_{KGF}- values from the Klein-Gordon-Fock equation with account of radiative corrections (our data); E_{KS} – RMF finite nuclear size contribution (our data), $E_{\hbar 2}^N$ - values from the Klein-Gordon-Fock equation with the generalized pion-nuclear potential [5] (our data).

Table 1. **Transition energies (keV) in the spectra of some pionic atoms (see text)**

Atom	E_{EXP} Berkley	E_{EXP} CERN	E_{KGF}	E_{FS}	$E_{\hbar 1}^N$	$E_{\hbar 2}^N$
Transition 4f-3d						
Ca^{40}	72,352 ± 0,009		72,357	0,00	72,361	72,362
I^{127}	519,1 ± 1,1	520,8 ± 0,8	516,50	-0,22	520,25	520,68
Cs^{133}	560,5 ± 1,1	562,0 ± 1,5	556,80	-0,33	561,47	562.12
La^{139}	603,6 ± 0,9	604,9 ± 2,0	597,88	-0,45	604,56	604,84
Transition 5g-4f						
Ta^{181}	453,1 ± 0,4	453,90 ± 0,20	450,67	-0.01	453,56	453,56
Au^{197}	532,5 ± 0,5	533,16 ± 0,20	531,99	-0,025	532,87	532,87
Hg^{201}	-	547,14 ± 0,25	545,730	- 0,036	546,85	547,22
Bi^{209}	589,8 ± 0,9	590,06 ± 0,30	588,24	-0,05	589,75	590,16
Th^{232}	698,0 ± 0,6	698,4 ± 0,4	693,88	-0,17	697,20	698,25
U^{238}	731,4 ± 1,1	732,0 ± 0,4	725,78	-0,23	729,80	730,52

Note: E_{EXP} (Virginia): Ta^{181}(5g-4f)=453.4±0.3; U^{238}(5g-4f)=730.88±0.75;

It is easily to understand that when there is the close agreement between theoretical and experimental shifts, the corresponding energy levels are not significantly sensitive to strong pion-nuclear interaction, i.e the electromagnetic contribution is dominative. In the opposite situation the strong-interaction effect is very significant. The analysis of the presented data indicate on the necessity of the further more exact experimental investigations and further improvement of the pion-nuclear potential modelling. One can see that the contributions provided by the finite size effect should be accounted in a precise theory. Really, under availability of the "exact" values of the transitions energies one can perform the comparison of the theoretically and experimentally defined transition energies in the X-ray spectra in order to make a redefinition of the pion-nucleon model potential parameters using Eqs. (9)-(11). Taking into account the increasing accuracy of the X-ray pionic atom spectroscopy experiments, one can conclude that the such a way will make more clear the true values for parameters of the pion-nuclear potentials and correct the disadvantage of widely used parameterization of the potentials (9)-(11).

References

1. Deslattes R., Kessler E., Indelicato P., de Billy L., Lindroth E. , Anton J., Exotic atoms // Rev. Mod. Phys. -2003.-Vol.75.-P.35-70.
2. Backenstoss G., Pionic atoms//Ann.Rev. Nucl.Sci.-1970.-Vol.20.-P.467-510.
3. Menshikov L I and Evseev M K, Some questions of physics of exotic atoms // Phys. Uspekhi.2001-Vol. 171.-P.150-184.
4. Deloff A., Fundamentals in Hadronic Atom Theory.- Singapore: World Sci., 2003.-352P.
5. Serga I. N., Dubrovskaya Yu. V., Kvasikova A. S., Shakhman A. N., Sukharev D. E., Spectroscopy of hadronic atoms: Energy shifts // J.of Physics: C Ser.(IOP).-2012.-Vol.397.-P.012013 (5p)
6. Scherer S., Introduction to Chiral Perturbation Theory//Advances in Nuclear Physics, Eds. J. W. Negele and E. W. Vogt (Berlin, Springer).-2003.-Vol.27.-P.5-50.
7. Schroder H., Badertscher A., Goudsmit P., Janousch M., Leisi H., Matsinos E., Sigg D., Zhao Z., Chatellard D., Egger J., Gabathuler K., Hauser P., Simons L., Rusi El Hassani A., The pion-nucleon scattering lengths from pionic hydrogen and deuterium//Eur.Phys.J.-2001.-Vol. C21.-P.473
8. Lyubovitskij V., Rusetsky A., πp atom in ChPT: Strong energy-level shift/ // Phys. Lett.B.-2000.-Vol.494.-P.9-13.
9. Anagnostopoulos D., Biri S., Boisbourdain V., Demeter M., Borchert G. et al-PSI, Low-energy X-ray standards from pionic atoms/ //Nucl. Inst. Meth.B.-2003.-Vol.205.-P.9-18.
10. Batty C. J., Eckhause M., Gall K. P., et al, Strong interaction effects in high Z-K^- atoms//Phys. Rev. C.-1989.-Vol.40.-P.2154-2160.
11. Kuznetsova A. A., Kvasikova A. S., Shakhman A. N., Vitavetskaya L. A., Calculating radiative vacuum polarization contribution to the energy shift of 2p-2s transition in m-hydrogen// Photoelec-tronics .- 2012.-N21.-P.66-67.
12. Glushkov A. V., Gauge-invariant QED perturbation theory approach to calculating nuclear electric quadrupole moments, hyperfine structure constants for heavy atoms and ions/ Glushkov A.V., Khetselius O.Yu., Sukharev D.E., Gurnitskaya E.P., Loboda A.V., Florko T.A., Lovett L.// Frontiers in Quantum Systems in Chemistry and Physics (Berlin, Springer).-2008.-Vol.18.- P.505-522.
13. Serot B. D., Advances in Nuclear Physics Vol. 16: The Relativistic Nuclear Many Body Problem / Serot B. D., Walecka J. D.-Plenum Press, New York, 1986.

The article is received in editorial 03.07.2013

UDC 539.182

A. N. Shakhman

STRONG p-NUCLEAT INTERACTION EFFECTS IN SPECTROSCOPY OF HADRONIC ATOMS

Abstract

New relativistic method on the basis of the Klein-Gordon-Fock equation with a generalized pion-nuclear potential is used to determine the strong interaction effects in spectroscopy of pionic atoms. The numerical data on 2p-1s, 3d-2p, 4f-3d,5g-4f transition energies on the basis of the Klein-Gordon-Fock theory with the pion-nucleus potential and account of radiative and finite size nuclear corrections are presented for some middle and heavy pionic atoms. It is performed comparison between theoretical data and results of measurements in the Berkley, CERN and Virginia laboratories.

Key words: strong interaction, hadronic atom, relativistic theory

УДК 539.182

А. Н. Шахман

ЭФФЕКТЫ СИЛЬНОГО ВЗАИМОДЕЙСТВИЯ В СПЕКТРОСКОПИИ АДРОННЫХ АТОМОВ

Резюме

Новый релятивистский метод на основе уравнения Клейна-Гордона-Фока с обобщенными пион-ядерным потенциалом применен для изучения эффектов сильного взаимодействия в спектроскопии пионных атомов. Представлены данные по энергиям 2p-1s, 3d-2p, 4f-3d,5g-4f переходов для некоторых средних и тяжелых пионных атомов, полученные на основе уравнения Клейна-Гордона-Фока с пион-ядерным потенциалом с учетом радиационных и конечно-размерных ядерных поправок. Проведено сравнение теоретических данных с данными измерений в лабораториях Беркли, ЦЕРН и Вирджиния.

Ключевые слова: сильное взаимодействие, адронный атом, релятивистская теория

УДК 539.182

А. М. Шахман

ЕФЕКТИ СИЛЬНОЇ ВЗАЄМОДІЇ В СПЕКТРОСКОПІЇ АДРОННИХ АТОМІВ

Резюме

Новий релятивістський метод на основі рівняння Клейна-Гордона-Фока із узагальненим піон-ядерним потенціалом застосовано до опису ефектів сильної взаємодії в спектроскопії піонних атомів. Отримані чисельні дані про 2p-1s, 3d-2p, 4f-3d,5g-4f енергії переходів для деяких середніх і важких піонних атомів, отримані на основі рівняння Клейна-Гордона-Фока з піон-ядерним потенціалом та урахуванням радіаційних та скінченно-розмірних ядерних поправок. Проведено порівняння теоретичних даних та результатів вимірювань в лабораторіях Берклі, ЦЕРН і Вірджинія.

Ключові слова: сильна взаємодія, адронний атом, релятивістська теорія

PACS 73.40.Gk, Lq; 73.61.Ga

V. A. Borschak., V. A. Smyntyna, IE. V. Brytavskyi, S. V. Zubritskiy, M. I. Kutalova, Ya. I. Lepikh

Odessa I. I. Mechnikov National University,
2, Dvoryanskaya str., Odessa, 65082, Ukraine
Phone: +380(48)7266356, Fax: +380(48)7233461, e-mail: borschak_va@mail.ru

MICROSTRUCTURAL FEATURES AND COMPONENTIAL ANALYSIS OF THIN FILM CdS-Cu_2S PHOTOSENSING STRUCTURES AS ELEMENT OF IMAGE SENSOR

The mechanisms of signal relaxation, associated with the removal processes of nonequilibrium charge from the space charge region of the image sensor on the basis of non-ideal heterojunction were investigated. The mechanism of the observed two-stage process was determined. Microscopic techniques (AFM, SEM) were used to estimate heterojunction properties (grain size, roughness) and their relations with heterojunction processing parameters. Novel results concerning CdS-Cu2S heterojunction surface morphology and impurities depth distribution were obtained. In particular, the question of observed variation of surface photosensitivity and components interdiffusion on heteroborder were clarified. Also the comparison of samples formed by two different methodics (electrodynamical spraying and vacuum evaporation techniques) was made. X-Ray diffraction (XRD) was performed in order to detect Cu–S compounds at CdS – Cu2S heterojunctions, fabricated by the vacuum deposition of CdS on a glass substrate and Cu2S layer, formed in substitution mode. The distribution of several stoichiometric phases of copper (I) sulfide was obtained as main result.

Heterojunction (HJ) structures can serve as basic material of photodetectors for use in optical communication applications [1]. HJ structure between p-type Cu_2S and n-type CdS is a rather complicated system because of the interface between two materials with different band gaps and crystal structure. Nonideality of considered CdS-Cu_2S structure causes the effect of photon induced modulation of HJ potential barrier, that can be used in opto-sensorics and X-ray imaging applications [2, 3]. High spatial resolution, signal storage and large working surface are reported as main advantages of obtained sensor.

The mechanisms of signal relaxation, associated with the removal processes of nonequilibrium charge from the space charge region of the image sensor on the basis of non-ideal heterojunction were investigated. The mechanism of the observed two-stage process was determined: phase of slow relaxation - implementation of the thermal emission of localized charge, that depends on temperature; phase of rapid relaxation - the result of tunneling mechanism of ejection.

CdS- Cu_2S is considered as an interesting compound for photovoltaic applications. Thin film CdS- Cu_2S sells are reported to have conversion efficiency of more than 9%, low cost and easy fabrication [4].

However, the heterojunction structure between p-type Cu_2S and n-type CdS is a rather complicated system because of the interface between two materials with different electron affinities, band gaps and crystal structures. The lattice mismatch and interdiffusion of components cause defect states at or near the interface that strongly affect the junction properties. In particular, there is Cu diffusion into the CdS adjacent to the interface, which leads to stoichiometry changing of CuxS layer and may cause shunting effect in CdS layer. But this process can be used also in positive way.

In [5] the possibility of controlling the phase structure, composition, and stoichiometry of Cu_xS

films is discussed. This enables changing certain optoelectronic properties of studied material for the fabrication of devices such as nanoscale switches, sensors, and solar cells.

The research of current transfer processes in nonideal geteropare CdS-Cu_2S allowed developing image sensor in the X-rays and optical range with high sensitivity and possibility of signal accumulation [3, 6].

The data-storage time and sensitivity of the sensor are determined by relaxation time of nonequilibrium positive charge. Possible ways of captured by traps holes removing from the barrier of non-ideal heterojunction were considered: the thermal holes emission to the CdS valence band; direct holes tunneling from trapping centers to the Cu_2S valence band; two-stage free-electron tunneling from CdS quasi-neutral region to the space charge region and subsequent recombination with nonequilibrium hole; tunnel-hopping recombination.

Relaxation curves of short-circuit current at different points of the sensor were obtained experimentally. The relaxation curve has two well-marked area: rapid initial photocurrent drop and then its relatively slow decay. At different points signal showed decrease with the same characteristic relaxation time, but very different in magnitude. This suggests, that sensor heterogeneity on the photosensitivity is caused by a substantial change of trapping centers concentration along the surface, that determine the thermal emission probability.

To clarify mechanisms implemented by charge release, sensor signal relaxation characteristics at different temperatures were studied. The time constants of later relaxation stage decrease with temperature increasing. This shows the implementation of thermal mechanism, which determines relaxation kinetics at this region. Relaxation time constants derived from experimental data and theoretical calculations are in good agreement and demonstrate the same temperature dependence. Thus, the current relaxation in considered part of current dependence is determined exceptionally by thermal charge emission from the deep hole traps.

The magnitude and the slope of initial part of the photocurrent decay don't depend on temperature. This demonstrates the implementation of photocurrent relaxation mechanism in this region, which isn't due to the thermal release and has apparently, tunneling character. Assessing the contribution of tunneling mechanisms in trapped charge relaxation was carried out by calculating the barriers tunneling transparency for the corresponding transitions. Calculations were made taking into account the changes of potential barrier shape under illumination [7]. The lack of temperature dependence of relaxation curve is due to the fact, that the values of barriers tunneling transparency don't depend on temperature. Account of tunneling processes leads to characteristics harmonization of the short-circuit current relaxation curves obtained experimentally and theoretically.

Experimentally observed phenomenon of investigated sensor signals relaxation considered and analyzed theoretically within the model of relaxation processes in the heterojunction CdS-Cu_2S.

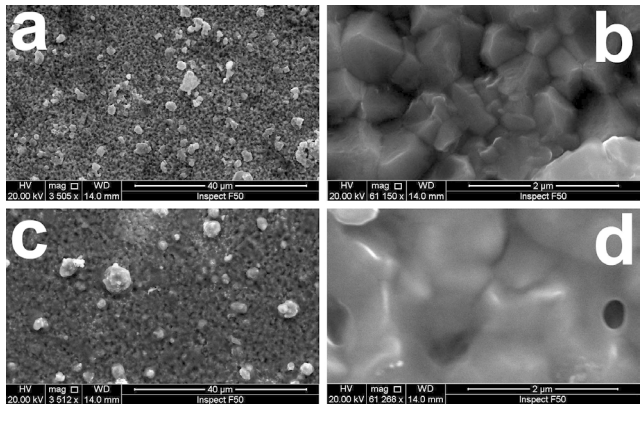

Fig. 1. **SEM scanning results for surface of sample, obtained by electro-hydrodynamic spraying methodics: CdS surface (a, b), Cu_2S surface (c, d) under 3500^x (a, c) and $60\ 000^x$ (b, d) zooming**

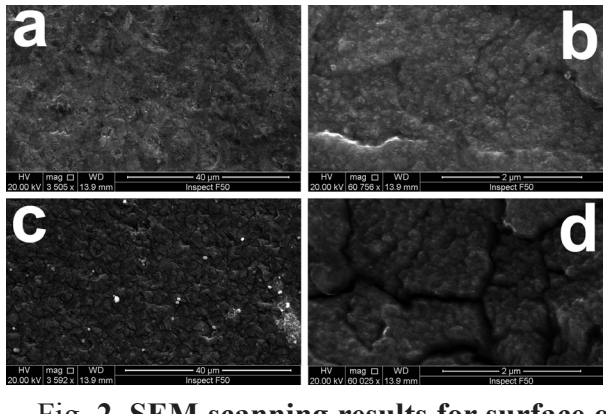

Fig. **2. SEM scanning results for surface of sample, obtained by vacuum evaporation methodics: CdS surface (a, b), Cu_2S surface (c, d) under 3500^x (a, c) and $60\ 000^x$ (b, d) zooming**

Obtained results enable to understand better the features of HJ layers forming procedure, the junction components surface interaction and influence of external environment on sensor samples surface characteristics.

Also, various microscopic techniques (AFM, SEM) were used to estimate HJ properties (grain size, roughness, luminescence depth distribution) and their relations with HJ processing parameters

The revealed differences in doping and traps densities, which lead to significant variations of electrical characteristics of junctions, can be ascribed to layer deposition regimes, to layer thicknesses and chemical combination of present compounds.

Main parameters – substrate temperature and deposition time were varied during films forming process. Thickness of base layer defines its resistivity and size of formed microctystalls.

X-Ray diffraction (XRD) was performed in order to detect Cu–S compounds at CdS – Cu_2S heterojunctions, fabricated by the vacuum deposition of CdS on a glass substrate and Cu_2S layer, formed in substitution mode.

Also phase composition of the deposits was examined by an X-ray diffractometer D8 Advance (Bruker AXS) with Cu K_α radiation (λ=1.54183 Å, U_a= 40 kV, I_a= 40 mA) separated by a curved multilayer monochromator mounted on the primary beam.

Fig. 3. XRD pattern of CdS-Cu_xS HJ sample (t_{dep} = 8 min, T_{sb} = 220º C)

Symmetrical Θ/2Θ geometry and grazing incidence (GIXRD) techniques were used and in the latter case the incidence angle (Θ angle) was 0.5°. The XRD patterns were measured in 2Θ range from 20 to 70° in a step scan mode: a step size (Δ2Θ) 0.04°, counting duration 5 s.

The diffraction angles some of main peaks corresponded to those of hexagonal CdS, and their relative peak intensities were also similar to those of the CdS (Fig. 3).

In XRD investigations of considered samples stoichiometry changing in copper sulphide layer was observed. Figure 3 show the diffraction angles and relative intensities of the XRD peaks of the CdS-Cu_xS films measured experimentally in this study. Each arrow shows the peak that correspond to possible written compounds (diffraction angles taken from JCPDS cards).

$Cu_{1.96}S$, $Cu_{1.92}S$, $Cu_{1.81}S$ and other modifications together with Cu_2S were detected (Table. 1). So in this case copper atoms diffuse from the Cu_xS layer to base CdS layer during the fabrication process and later with time. These impurities can create acceptor centres, which compensate or even overcompensate for the initially existent donors in CdS [8].

Table. 1.

Number of XRD peaks for different compounds in CdS-Cu_xS HJ

Cu_xS compound	Number of peaks
monoclinic Cu_2S (chalcocite)	5
tetragonal $Cu_{1.96}S$	2
monoclinic $Cu_{31}S_{16}$ (djurleite)	3
hexagonal $Cu_{1.92}S$	3
tetragonal $Cu_{1.81}S$	3
hexagonal Cu_9S_5 (digenite)	0
monoclinic Cu_7S_4 (roxbyite)	10
orthorombic Cu_7S_4 (anilite)	1
hexagonal CuS (covellite).	0

Also Cu diffusion between grain borders of CdS microcrystalls can cause shunting effect. Changing of Cu diffusion conditions (and as a result variations in electrical characterisitics) is directly connected with deposition time t_{dep} and substrate temperature T_{sb}. This initial thermal treatment defines first level of diffusion intensity and depth. It's seen, that more Cu_xS phases in samples are observed (Fig. 3). For these samples t_{dep} and T_{sb} were maximised.

Diffusion process may continue and later, at room temperature. That is confirmed by observed degradation of samples photoelectric properties with the time.

Reference

[1] A. S. Gilmore, J. Bangs, A. Gerrish, J. Electron. Mater. 34, 913 (2005).
[2] D. L. Vasilevski, M. S. Vinogradov, V. A. Borschak, Appl. Surf. Sci. 103, (1996).
[3] V. A. Smyntyna, V. A. Borschak, M. I. Kutalo-

va, N. P. Zatovskaya, A. P. Balaban, Semiconductor Physics, Quantum Electronics & Optoelectronics. V.7, No 2, (2004).
[4] Bragagnolo J. A. et al., IEEE Trans.Electron. Dev. ED-27, 645–651 (1980).
[5] Manisha Kundu, Tsuyoshi Hasegawa, Kazuya Terabe, Kazuhiro Yamamoto, Masakazu Aono, Sci. Technol. Adv. Mater. No 9. (2008).
[6] V. A. Borschak, Ie.V. Brytavskyi, V. A. Smyntyna, Ya. I. Lepikh, A. P. Balaban, N. P. Zatovskaya, Semiconductor Physics, Quantum Electronics & Optoelectronics, V. 15, N 1, pp. 41–43 (2012)
[7] V. A. Borschak, V. A. Smyntyna, Ie. V. Brytavskyi, A. A. Karpenko, and N. P. Zatovskaya, Semiconductors, Vol. 47, No. 6, pp. 838–843 (2013).
[8] A. Goldenblum and A. Oprea, J. Phys, D Appl. Phys. 27, pp. 582–586 (1994)

The article is received in editorial 15.05.2013

PACS 73.40.Gk, Lq; 73.61.Ga

V. A. Borschak, V. A. Smyntyna, S. V. Zubritskiy, Ie.V. Brytavskyi, M. I. Kutalova, Ya. I. Lepikh

MICROSTRUCTURAL FEATURES AND COMPONENTIAL ANALYSIS OF THIN FILM CdS-Cu_2S PHOTOSENSING STRUCTURES AS ELEMENT OF IMAGE SENSOR

Abstract

The mechanisms of signal relaxation, associated with the removal processes of nonequilibrium charge from the space charge region of the image sensor on the basis of non-ideal heterojunction were investigated. The mechanism of the observed two-stage process was determined. Microscopic techniques (AFM, SEM) were used to estimate HJ properties (grain size, roughness) and their relations with HJ processing parameters. Novel results concerning CdS-Cu_2S HJ surface morphology and impurities depth distribution were obtained. In particular, the question of observed variation of surface photosensitivity and components interdiffusion on heteroborder were clarified. Also the comparison of samples formed by two different methodics (electrodynamical spraying and vacuum evaporation techniques) was made. X-Ray diffraction (XRD) was performed in order to detect Cu–S compounds at CdS – Cu_2S heterojunctions, fabricated by the vacuum deposition of CdS on a glass substrate and Cu_2S layer, formed in substitution mode. The distribution of several stoichiometric phases of copper (I) sulfide was obtained as main result.

Key words: heterojunction, image sensor, surface morphology, XRD analysis

PACS 73.40.Gk, Lq; 73.61.Ga

В. А. Борщак, В. А. Смынтына, С. В. Зубрицкий, Е. В. Бритавский, М. И. Куталова, Я. И. Лепих

МИКРОСТРУКТУРНЫЕ ОСОБЕННОСТИ И КОМПОНЕНТНЫЙ АНАЛИЗ ТОНКОПЛЁНОЧНЫХ ФОТОЧУВСТВИТЕЛЬНЫХ ЭЛЕМЕНТОВ CdS-Cu_2S

Резюме

В работе были исследованы механизмы релаксации сигнала, связанные с процессами удаления неравновесного заряда из области пространственного заряда сенсора изображения на основе неидеального гетероперехода и их связь со структурными особенностями и компонентным

составом образцов. Были использована комбинация микроскопических методик (АСМ, РЭМ) для оценки морфологических свойств поверхности (размер зерна, шероховатость) и их отношений с технологическими параметрами при получении гетероструктур. Были получены новые результаты, касающиеся морфологии поверхности и глубины распределения примесей. В частности, были уточнены вопросы о наблюдаемом изменении фоточувствительности поверхности и взаимной диффузии компонентов на гетерогранице. Кроме того, проведено сравнение образцов, полученных двумя различными методиками (электродинамическое распыление раствора методы вакуумного испарения). Также применялся рентгеноструктурный анализ с целью выявления различных фаз Cu-S в гетеропереходах, изготовленных вакуумным напылением на стеклянной подложке. В качестве основного результата получено распределение стехиометрических фаз сульфида меди (I) в исследуемых сенсорных структурах.

Ключевые слова: гетеропереход, сенсор изображения, релаксация сигнала, морфология поверхности, рентгеноструктурный анализ

PACS 73.40.Gk, Lq; 73.61.Ga

В. А. Борщак, В. А. Сминтина, С. В. Зубрицький, Є. В. Бритавський, М. І. Куталова, Я. І. Лепіх

МІКРОСТРУКТУРНІ ОСОБЛИВОСТІ ТА КОМПОНЕНТНИЙ АНАЛІЗ ТОНКОПЛІВКОВИХ ФОТОЧУТЛИВИХ ЕЛЕМЕНТІВ CdS-Cu_2S

Резюме

У роботі були досліджені механізми релаксації сигналу, пов’язані з процесами видалення нерівноважного заряду з області просторового заряду сенсора зображення на основі неідеального гетероперехода та їх зв’язок із структурними особливостями і компонентним складом зразків . Була використана комбінація мікроскопічних методик (АСМ , РЕМ) для оцінки морфологічних особливостей поверхні (розмір зерна , шорсткість) та їх зв’язку з технологічними параметрами при формуванні гетероструктур. Були отримані нові результати, що стосуються морфології поверхні і глибини розподілу домішок . Зокрема , були уточнені питання про спостережувану зміну фоточутливості поверхні і взаємну дифузію компонентів на гетерограниці. Крім того, проведено порівняння зразків, отриманих двома різними методиками (електродинамічне розпилювання розчину та метод вакуумного випаровування). Також застосовувався рентгеноструктурний аналіз з метою виявлення різних фаз сполуки Cu-S у гетеропереходах, виготовлених вакуумним напиленням на скляній підкладці. В якості основного результату отримано розподіл стехіометричних фаз сульфіду міді (I) в досліджуваних сенсорних структурах.

Ключові слова: гетеропереход, сенсор зображення, релаксація сигналу, морфологія поверхні, рентгеноструктурний аналіз

UDC 517.9

G. P. Prepelitsa, V. V. Buyadzhi, V. B. Ternovsky

International Humanitarian University, Fontanskaya dor.33, Odessa, Ukraine
Odessa State Environmental University, 15, Lvovskaya str., Odessa, Ukraine
Odessa National Polytechnical University, 1, Shevchenko av., Odessa Ukraine
e-mail: quantpre@mail.ru

NON-LINEAR ANALYSIS OF CHAOTIC SELF-OSCILLATIONS IN BACKWARD-WAVE TUBE

The analysis techniques including multi-fractal approach, methods of correlation integral, false nearest neighbour, Lyapunov exponent's, surrogate data, is applied analysis of numerical parameters of chaotic self-oscillations in the backward-wave tube. There are presented the numerical data on the Lyapunov exponents' for two self-oscillations regimes in the backward-wave tube: i). the weak chaos (normalized length: L=4.24); ii) developed chaos (L=6.1).

As it is well known in the modern electronics, photoelectronics etc there are many physical systems (the backward-wave tubes, multielement semiconductors and gas lasers, different radiotechnical devices etc), which can manifest the elements of chaos and hyperchaos in their dynamics (c.f.[1-4]). The key aspect of studying the dynamics of these systems is analysis of the dynamical characteristics. Chaos theory establishes that apparently complex irregular behaviour could be the outcome of a simple deterministic system with a few dominant nonlinear interdependent variables. The past decade has witnessed a large number of studies employing the ideas gained from the science of chaos to characterize, model, and predict the dynamics of various systems phenomena (c.f.[1-20]). The outcomes of such studies are very encouraging, as they not only revealed that the dynamics of the apparently irregular phenomena could be understood from a chaotic deterministic point of view but also reported very good predictions using such an approach for different systems.

The backward-wave tube is an electronic device for generating electromagnetic vibrations of the superhigh frequencies range. In ref.[2] there have been presented the temporal dependences of the output signal amplitude, phase portraits, statistical quantifiers for a weak chaos arising via period-doubling cascade of self-modulation and for developed chaos at large values of the dimensionless length parameter. The authors of [2] have solved the equations of nonstationary nonlinear theory for the O type backward-wave tubes without account of the spatial charge, relativistic effects, energy losses etc. It has been shown that the finite-dimension strange attractor is responsible for chaotic regimes in the backward-wave tube. In our work in order to study the chaotic self-oscillations regimes in the backward-wave tube we have used earlier developed and adapted techniques of the non-linear analysis, such as the multi-fractal formalism, methods of correlation integral, false nearest neighbour, Lyapunov exponent's, surrogate data (code "Geomath"). As the key ideas of our technique for nonlinear analysis of chaotic systems have been in details presented in refs. [3,4,17-21], here we are limited only by brief representation.. Since processes resulting in the chaotic behaviour are fundamentally multivariate, it is necessary to reconstruct phase space using as well as possible information contained in the dynamical parameter $s(n)$, where n the number of the measurements. Such a reconstruction

results in a certain set of d-dimensional vectors $\mathbf{y}(n)$ replacing the scalar measurements. Packard et al. [7] introduced the method of using time-delay coordinates to reconstruct the phase space of an observed dynamical system. The direct use of the lagged variables $s(n + t)$, where t is some integer to be determined, results in a coordinate system in which the structure of orbits in phase space can be captured. Then using a collection of time lags to create a vector in d dimensions,

$$\mathbf{y}(n) = [s(n), s(n+t), s(n+2t), \ldots, s(n+(d\text{-}1)t)], \quad (1)$$

the required coordinates are provided.

In a nonlinear system, the $s(n + jt)$ are some unknown nonlinear combination of the actual physical variables that comprise the source of the measurements. The dimension d is called the embedding dimension, d_E. According to Mañé [13] and Takens [12], any time lag will be acceptable is not terribly useful for extracting physics from data. If t is chosen too small, then the coordinates s(n + jt) and s(n + (j + 1)t) are so close to each other in numerical value that they cannot be distinguished from each other. Similarly, if t is too large, then s(n + jt) and s(n + (j + 1)t) are completely independent of each other in a statistical sense. Also, if t is too small or too large, then the correlation dimension of attractor can be under- or overestimated respectively [8,18]. The autocorrelation function and average mutual information can be applied here. The first approach is to compute the linear autocorrelation function:

$$C_L(\delta) = \frac{\frac{1}{N}\sum_{m=1}^{N}[s(m+\delta)-\bar{s}][s(m)-\bar{s}]}{\frac{1}{N}\sum_{m=1}^{N}[s(m)-\bar{s}]^2},$$

$$\bar{s} = \frac{1}{N}\sum_{m=1}^{N} s(m) \quad (2)$$

and to look for that time lag where C_L(d) first passes through zero (see [18]). This gives a good hint of choice for t at that $s(n + jt)$ and $s(n + (j + 1)t)$ are linearly independent. a time series under consideration have an n-dimensional Gaussian distribution, these statistics are theoretically equivalent as it is shown by Paluš (see [15]). The general redundancies detect all dependences in the time series, while the linear redundancies are sensitive only to linear structures. Further, a possible nonlinear nature of process resulting in the vibrations amplitude level variations can be concluded.

The goal of the embedding dimension determination is to reconstruct a Euclidean space R^d large enough so that the set of points d_A can be unfolded without ambiguity. In accordance with the embedding theorem, the embedding dimension, d_E, must be greater, or at least equal, than a dimension of attractor, d_A, i.e. $d_E > d_A$.

In other words, we can choose a fortiori large dimension d_E, e.g. 10 or 15, since the previous analysis provides us prospects that the dynamics of our system is probably chaotic. However, two problems arise with working in dimensions larger than really required by the data and time-delay embedding [5,6,18].

First, many of computations for extracting interesting properties from the data require searches and other operations in R^d whose computational cost rises exponentially with d. Second, but more significant from the physical point of view, in the presence of noise or other high dimensional contamination of the observations, the extra dimensions are not populated by dynamics, already captured by a smaller dimension, but entirely by the contaminating signal.

In the large an embedding space there is no necessity spending time working around aspects of a bad representation of the observations which are solely filled with noise. It is therefore necessary to determine the dimension d_A.

There are several standard approaches to reconstruct the attractor dimension (see, e.g., [3-6,15]). The correlation integral analysis is one of the widely used techniques to investigate the signatures of chaos in a time series. The analysis uses the correlation integral, $C(r)$, to distinguish between chaotic and stochastic systems.

To compute the correlation integral, the algorithm of Grassberger and Procaccia [10] is the most commonly used approach. If the time series is characterized by an attractor, then the integral $C(r)$ is related to the radius r given by

$$d = \lim_{\substack{r\to 0 \\ N\to\infty}} \frac{\log C(r)}{\log r}, \quad (3)$$

where d is correlation exponent that can be determined as the slop of line in the coordinates log $C(r)$ versus log r by a least-squares fit of a straight line over a certain range of r, called the scaling region. If the correlation exponent attains saturation with an increase in the embedding dimension, the system is generally considered to exhibit chaotic dynamics. The saturation value of correlation exponent is defined as the correlation dimension (d_2) of attractor.

Lyapunov exponents are the dynamical invariants of the nonlinear system. In a general case, the orbits of chaotic attractors are unpredictable, but there is the limited predictability of chaotic physical system, which is defined by the global and local Lyapunov exponents. A negative exponent indicates a local average rate of contraction while a positive value indicates a local average rate of expansion. In the chaos theory, the spectrum of Lyapunov exponents is considered a measure of the effect of perturbing the initial conditions of a dynamical system. Since the Lyapunov exponents are defined as asymptotic average rates, they are independent of the initial conditions, and therefore they do comprise an invariant measure of attractor. In fact, if one manages to derive the whole spectrum of Lyapunov exponents, other invariants of the system, i.e. Kolmogorov entropy and attractor's dimension can be found. The Kolmogorov entropy, K, measures the average rate at which information about the state is lost with time. An estimate of this measure is the sum of the positive Lyapunov exponents. The inverse of the Kolmogorov entropy is equal to the average predictability. There are several approaches to computing the Lyapunov exponents (see, e.g., [5,6,18]). One of them [18] is in computing the whole spectrum and based on the Jacobin matrix of the system function [14].

In table 1 we present the data on the Lyapunov exponents' for two self-oscillations regimes in the backward-wave tube: i). the weak chaos (normalized length: L=4.24); ii) developed chaos (L=6.1). The correlations dimensions are respectively as 2.9 and 6.2. Our analysis is in very good agreement with the similar data [2] and confirms a conclusion about realization of the chaotic features in dynamics of the backward-wave tube.

Table 1. **numerical parameters of the chaotic self-oscillations in the backward-wave tube: l_1-l_6 are the Lyapunov exponents in descending order, K is the Kolmogorov entropy**

Regime	λ_1	λ_2	λ_3	K
Weak chaos L=4.24	0.261	-0.0001	–0.0004	0.261
Hyper chaos L=6.1	0.514	0.228	0.0000	0.742
Regime	λ_4	λ_5	λ_6	K
Weak chaos L=4.24	–0.528	–	–	0.261
Hyper chaos L=6.1	–0.0002	–0.084	–0.396	0.742

References

1. Ott E. Chaos in dynamical systems. Cambridge: Cambridge Univ.Press, 2002.-490p.
2. Kuznetsov S. P., Trubetskov D. I., Chaos and hyperchaos in the backward-wave tube// Izv.Vuzov. Ser. Radiophys.-2004.Vol.XLVII.-P.1-17.
3. Glushkov A. V., Prepelitsa G. P., Khetselius O. Yu., Kuzakon V. M., Solyanikova E. P., Svinarenko A. A., Modeling of interaction of non-linear vibrational systems on basis of temporal series analyses (application to semiconductor quantum generators) // Dynamical Systems - Theory and Applications.-2011.-P.BIF-110 (8p.).
4. Serbov N. G., Kuzakon V. M., Khetselius O. Yu., Prepelitsa G. P., Solyanikova E. P., Non-linear analysis methods of signal temporal series in modeling interactions in the vibrational systems of the quantum generators type // Photoelectronics.-2011.-Vol.20.-P.117-123.

5. Abarbanel H., Brown R., Sidorowich J., Tsimring L., The analysis of observed chaotic data in physical systems// Rev Modern Phys.-1993.-Vol.65.-P.1331–1392.
6. Kennel M., Brown R., Abarbanel H., Determining embedding dimension for phase-space reconstruction using geometrical construction//Phys. Rev.A.-1992.-Vol.45.-P.3403–3411.
7. Packard N., Crutchfield J., Farmer J., Shaw R., Geometry from a time series // Phys. Rev.Lett.-1988.-Vol.45.-P.712–716.
8. Havstad J., Ehlers C., Attractor dimension of nonstationary dynamical systems from small data sets//Phys Rev A.-1989.-Vol.39.-P.845–853.
9. Gallager R. G., Information theory and reliable communication, Wiley, New York.-1986.
10. Grassberger P., Procaccia I., Measuring the strangeness of strange attractors// Physica D.-1983.-Vol.9.-P.189–208.
11. Fraser A., Swinney H., Independent coordinates for strange attractors from mutual information// Phys Rev A.-1986.-Vol.33.-P.1134–1140.
12. Takens F., Detecting strange attractors in turbulence // Lecture notes in mathematics (Springer).-1981.-N.898.-P.366–381
13. Mañé R., On the dimensions of the compact invariant sets of certain non-linear maps// Lecture notes in mathematics (Springer).-1981.-N898.-P.230–242
14. Sano M., Sawada Y., Measurement of Lyapunov spectrum from a chaotic time series // Phys. Rev.Lett.-1985.-Vol.55.-P.1082–1085
15. Sivakumar B., Chaos theory in geophysics: past, present and future // Chaos, Solitons & Fractals.-2004.-Vol.19.-P.441–462.
16. Theiler J., Eubank S., Longtin A., Galdrikian B., Farmer J., Testing for nonlinearity in time series: The method of surrogate data// Physica D.-1992.-Vol.58.-P.77–94.
17. Glushkov A. V., Khokhlov V. N., Tsenenko I. A. Atmospheric teleconnection patterns: wavelet analysis// Nonlin. Proc.in Geophys.-2004.-V.11.-P.285-293.
18. Glushkov A.V., Khokhlov V.N., Svinarenko A.A., Bunyakova Yu.Ya., Prepelitsa G.P., Wavelet analysis and sensing the total ozone content in the Earth atmosphere: MST “Geomath”// Sensor Electr. and Microsyst.Techn.-2005.-N3.-P.43-48.
19. Glushkov A. V., Khokhlov V. N., Loboda N. S., Bunyakova Yu. Ya., Short-range forecast of atmospheric pollutants using non-linear prediction method // Atm. Environment (Elsevier).-2008.-Vol.42.-P. 7284–7292.
20. Rusov V. D., Glushkov A. V., Prepelitsa G. P., et al, On possible genesis of fractal dimensions in turbulent pulsations of cosmic plasma- galactic-origin rays-turbulent pulsation in planetary atmosphere system//Adv. Space Res.-2008.-Vol42.-P.1614-1617.

The article is received in editorial 25.05.2013

UDC 517.9

G. P. Prepelitsa, V. V. Buyadzhi, V. B. Ternovsky

NON-LINEAR ANALYSIS OF CHAOTIC SELF-OSCILLATIONS IN BACKWARD-WAVE TUBE

Abstract

The analysis techniques including multi-fractal approach, methods of correlation integral, false nearest neighbour, Lyapunov exponent's, surrogate data, is applied analysis of numerical parameters of chaotic self-oscillations in the backward-wave tube. There are presented the numerical data on the Lyapunov exponents' for two self-oscillations regimes in the backward-wave tube: i). the weak chaos (normalized length: L=4.24); ii) developed chaos (L=6.1).

Key words: backward-wave tube, chaos, non-linear methods

УДК 517.9

Г. П. Препелица, В. В. Буяджи, В. Б. Терновский

НЕЛИНЕЙНЫЙ АНАЛИЗ ХАОТИЧЕСКИХ АВТОКОЛЕБАТЕЛЬНЫХ РЕЖИМОВ В ЛАМПЕ ОБРАТНОЙ ВОЛНЫ

Резюме

Техника анализа, включающая мультифрактальный подход, методы корреляционных интегралов, ложных ближайших соседей, экспонент Ляпунова, суррогатных данных, использована для изучения числовых параметров хаотических автоколебательных режимов лампы обратной волны. Представлены данные о численных показателях Ляпунова для двух автоколебательных режимов лампы обратной волны: i).слабого хаоса (нормированная длина: L = 4.24); ii) развитого хаоса (L = 6.1).

Ключевые слова: лампа обратной волны, хаос, нелинейные методы

УДК 517.9

Г. П. Препелица, В. В. Буяджи, В. Б. Терновський

НЕЛІНІЙНИЙ АНАЛІЗ ХАОТИЧНИХ АВТОКОЛИВАЛЬНИХ РЕЖИМІВ У ЛАМПІ ЗВЕРНЕНОЇ ХВИЛІ

Резюме.

Техніка нелінійного аналізу, яка включає мультіфрактальний підхід, методи кореляційних інтегралів, хибних найближчих сусідів, експонент Ляпунова, сурогатних даних, використана для аналізу чисельних параметрів хаотичних автоколивальних режимів лампи зверненої хвилі. Наведені дані по чисельних показниках Ляпунова для двох автоколивальних режимів лампи зворотної хвилі: і). слабкого хаосу (нормована довжина: L = 4.24); ii) розвиненого хаосу (L = 6.1).

Ключові слова: лампа зверненої хвилі, хаос, нелінійні методи

UDC 539.184

A. A. Kuznetsova, L. A.Vitavetskaya, Yu. G. Chernyakova, D. A. Korchevsky

Odessa National Maritime Academy, Odessa, 4, Didrikhsona str., Odessa, Ukraine
Odessa State Environmental University, 15, Lvovskaya str., Odessa, Ukraine
Odessa Computer Academy, 3, Osipova str., Odessa, Ukraine
e-mail: nucvita@mail.ru

CALCULATING THE RADIATIVE VACUUM POLARIZATION CONTRIBUTION TO THE ENERGY SHIFT OF 2P-2S TRANSITION IN PIONIC DEUTERIUM

Calculating the radiative contribution due to the vacuum polarization effect to energy value for the 3p-1s transition in pionic deuterium has been carried out using the modified generalized Uehling-Serber potential which includes effectively the higher order vacuum polarization corrections. Comparison with analogous theoretical data by Indelicato is performed.

Due to the significant progress in the modern experimental technologies now a great interest attracts studying spectra of heavy and super heavy elements atoms, exotic atomic systems, including hadronic and leptonic atoms [1-15]. Especial problem is connected with précised calculating the radiative corrections to the transition energies of the low-Z exotic (pionic, kaonic, muonic) atoms, namely, hydrogen and deuterium. Naturally, it is provided by necessity of further developing the modern as atomic and as nuclear theories. From the other side, detailed information about spectra of the exotic atomic systems (kaonic, pionic, muonic atoms) can be very useful under construction of the new X-ray standards. One could remind a great importance of the muonic chemistry, muonic spectroscopy. Very attractive perspective of the thermonuclear fission through the mechanism of the muonic catalysis is still interesting and widely studied.

The standard Dirac approach is traditionally used as starting basis in calculations of the heavy ions [2]. The problem of accounting the radiative corrections, in particular, self-energy part of the Lamb shift and vacuum polarization contribution is mostly treated with using the expansions on the natural physical parameters *1/Z, aZ* (*a* is fine structure constant) [5,10]. It permits evaluations of the relative contributions of different expansion energy terms: non-relativistic, relativistic ones, as functions of Z. For high Z (Z is a nuclear charge) it should be necessary to account for the high-order QED corrections and the nuclear finite size correction etc [1-3,10-12,16]. Further improvement of this method in a case of the heavy ions is linked with using gauge invariant procedures of generating relativistic orbital basises and more correct treating nuclear and QED effects [1-3]. In a case of the low-Z exotic atomic systems such as an exotic hydrogen (deuterium) a great interest attracts estimation of the radiative, in particular, vacuum polarization, correction. In refs. [17-19] it has been proposed a precise scheme to calculating spectra of heavy systems with account of nuclear and radiative effects, based on the relativistic many-body perturbation theory (see also [3]) and advanced effective procedures for accounting the radiative corrections.

In this paper we present the results of calculating the contribution due to the vacuum polarization effect to energy shift for 3p-1s transition in pionic deuterium. The obtained result is compared with calculation data by Indelicato [19]. The calculation of the radiative vacuum polarization shift in the pionic deuterium should be performed using the Dirac approximation as a zeroth one. Further, the expectation value of the radiative vacuum polarization operator gives the corresponding correction. The total electromagnetic interaction potential:

$$V(r)=V_n(r)+U(r). \qquad (1)$$

includes the electrical V_n and polarization U(r) potentials of a nucleus with accounting the finite

size correction. As usually, the Coulomb potential for spherically symmetric density $\rho(r|R)$ can be written as follows:

$$V_n(r|R) = -\left((1/r)\int_0^r dr' r'^2 \rho(r'|R) + \int_r^\infty dr' r' \rho(r'|R)\right). \quad (2)$$

The details of the determination of this potential can be , for example, found in ref. [21,22]. The vacuum polarization part is usually accounted in the first PT order by using the Uehling potential [1,8,16,17]:

$$U(r) = -\frac{2\alpha}{3\pi r}\int_1^\infty dt \exp(-2rt/\alpha Z)(1+1/2t^2)\bullet$$

$$\bullet \frac{\sqrt{t^2-1}}{t^2} \equiv -\frac{2\alpha}{3\pi r} C(g)$$

$$g = \frac{r}{\alpha Z}. \quad (3)$$

The corresponding expectation value of this operator gives the corresponding vacuum polarization correction. In the scheme [12] this potential is approximated by quite precise analytical function (see details in refs. [3,16,17]).

The most advanced version of the such potential ($C \to \tilde{\tilde{C}}$) is presented by Khetselius [12] and written as follows:

$$\tilde{\tilde{C}}(g) = \tilde{C}_1(g)\tilde{\tilde{C}}_2(g)/\left(\tilde{C}_1(g) + \tilde{\tilde{C}}_2(g)\right),$$
$$\tilde{\tilde{C}}_2(g) = \tilde{C}_2(g) f(g),$$

$$\tilde{C}_2(g) = -1.8801 \exp(-g)/g^{3/2}$$

$$\tilde{C}_1(g) = \text{h}(g/2) + 1.410545 - 1.037837 g,$$

$$f(g) = \left((1.1024/g - 1.3361)/g + 0.8027\right) \quad (4)$$

The using this formula permits one to decrease the calculation errors for this term down to ~0.1%. Error of usual calculation scheme is~10%. We carried out the calculation of the vacuum polarization contribution to the energy shift for 3p-1s transition in pionic deuterium. It should be noted that the energy levels of exotic (pionic) muonic atoms are very sensitive to effects of QED, nuclear structure and recoil since the pion is heavier than the electron. As usually the fundamental constants from the CODATA 1998 are used in the numerical calculations. The most QED effect for pionic atoms is the virtual production and annihilation of a single e^+e^- pair (the Uehling-Serber contribution).

We have evaluated the modified Uehling-Serber potential expectation values and obtained the value for the vacuum-polarization correction: 3.73940 eV. It is interesting to compare this result with the result by Indelicato, namely, the total vacuum polarization contribution: 3.74844 eV. Further, using data by Indelicato [24] for the main Coulomb contribution (3074.1597 eV), the self-energy and finite size correction (-0.0022 eV), the relativistic recoil correction is -0.00029 eV (recoil 1 correction: 0.00293 eV) we can evaluate the pure electromagnetic 3p-1s transition energy in the pionic deuterium E_{QED}=3077.8995 eV. The corresponding value, presented by Indelicato is 3077.90858 eV. The physically reasonable agreement between the theories can be easily explained by the fact that pionic deuterium is the low-Z atomic system and in this case the expansion on the parameter *aZ* works sufficiently well. From the other side, the approach used by us is not perturbative one and can be applied to the non low-Z atomic systems.

References

1. Botham C., Martensson A.M., Sanders P.G. Relativistic effects in atoms and mo-lecules.-Vancouver:Elseiver,2001.-550p.
2. Grant I.P., Relativistic Quantum Theory of Atoms and Molecules.-Oxford, 2008.-650P.
3. Glushkov A.V., Relativistic quantum theory. Quantum mechanics of atomic systems, Odessa: Astroprint, 2008.-700P.
4. Hayano R.S., Hori M., Horvath D., Widman E., Antiprotonic helium and CPT invariance // Rep. Prog. Phys.-2007.-Vol.70.-P.1995-2065.
5. Schlesser S., Le Bigot E.-O., Indelicato P., Pachucki K., Quantum-electro-dynamics corrections in pionic hydrogen// Phys.Rev.C.-2011.-Vol.84.-P.015211 (8p.).

6. Gotta D., Amaro F., Anagnostopoulos D., Pionic Hydrogen//Precision Physics of Simple Atoms and Molecules, Ser. Lecture Notes in Physics (Springer, Berlin / Heidelberg).-2008.-Vol.745.-P.165-186.
7. Mitroy J., Quantum defect theory for the study of hadronic atoms/ Mitroy J., Ivallov I.A.// J. Phys. G: Nucl. Part. Phys.-2001.-Vol.27.-P.1421–1433
8. Deslattes R., Kessler E., Indelicato P., de Billy L., Lindroth E. , Anton J., Exotic atoms // Rev. Mod. Phys. -2003.-Vol.75.-P.35-70.
9. Borie E., Lamb shift in muonic hydrogen // Phys.Rev. A.-2005.-Vol.71.-P.032508-1-8.
10. Mohr P. J. Quantum Electrodynamics Calculations in few-Electron Systems // Phys. Scripta.-1993.-Vol.46,N1.-P.44-52.
11. Klaft I.,Borneis S., Engel T., Fricke B., Grieser R., Huber G., Kuhl T., Marx D., Neumann R., Schroder S., Seelig P., Volker L. Precision laser spectroscopy of ground state hyperfine splitting of H-like $^{209}Bi^{82+}$// Phys.Rev.Lett.-1994.-Vol.73.-P.2425-2427
12. Khetselius O. Yu., Relativistic perturbation theory calculation of the hyperfine structure parameters for some heavy-element isotopes // Int. Journ. of Quantum Chemistry.- 2009.- Vol.109.- N14.- P. 3330-3335.
13. Serga I. N., Electromagnetic and strong interactions effects in X-ray spectroscopy of pionic atoms // Photoelectronics.-2011.-Vol.20.-P.109-112.
14. Backenstoss G., Pionic atoms//Ann.Rev. Nucl.Sci.-1970.-Vol.20.-P.467-510.
15. Menshikov L I and Evseev M K, Some questions of physics of exotic atoms // Phys. Uspekhi.2001-Vol. 171.-P.150-184.
16. Ivanova E. P., Ivanov L. N., Aglitsky E. V., Modern trends in spectroscopy of multicharged ions // Phys.Rep.-1991.-Vol.166.-P.315-390.
17. Glushkov A. V., Ambrosov S., Loboda A., Chernyakova Y. G., Khetselius O., Svinarenko A., QED theory of the superheavy elements ions: energy levels, radiative corrections, and hyperfine structure for different nuclear models // Nuclear Phys.A-2004.-Vol. 734.-P.21-28.
18. Glushkov A. V., Khetselius O. Yu., Gurnitskaya E. P., Loboda A. V., Florko T. A., Sukharev D. E., Lovett L., Gauge-invariant QED perturbation theory approach to calculating nuclear electric quadrupole moments, hfs structure constants for heavy atoms and ions// Frontiers in Quantum Systems in Chem. and Physics (Berlin: Springer).-2008.-Vol.18.- P.505-522.
19. Vitavetskaya L.A., Malinovskaya S.V., Dubrovskaya Yu., Advanced quantum calculation of beta decay probabilities// Low Energy Antiproton Phys.-2005.-Vol.796.- P.201-205.
20. Gurnitskaya E. P., Khetselius O. Yu., Loboda A. V., Vitavetskaya L. A., Consistent quantum approach to quarkony energy spectrum and semiconductor superatom and in external electric field // Photoelectronics.-2008.-N17.-P.127-130.
21. Kvasikova A. S., Ignatenko A. V., Florko T. A., Sukharev D. E., Chernyakova Yu. G., Photoeffect and spectroscopy of the hydrogen atom in the crossed dc electric and magnetic field // Photoelectronics.-2011.-Vol.20.-P.71-75.
22. Kuznetsova A. A., Kvasikova A. S., Shakhman A. N., Vitavetskaya L. A., Calculating the radiative vacuum polarization contribution to the energy shift of 2p-2s transition in m-hydrogen // Photoelectronics.-2012.-N21.-P.66-67.
23. Strauch Th., High-precision measurements of strong-interaction effects in pionic deuterium.-Forschungszentrum, Julich, 2009.
24. Indelicato P., Pionic deuterium // Private communication.

The article is received in editorial 18.06.2013

UDC 539.184

A. A. Kuznetsova, L. A. Vitavetskaya, Yu. G. Chernyakova, D. A. Korchevsky

CALCULATING THE RADIATIVE VACUUM POLARIZATION CONTRIBUTION TO THE ENERGY SHIFT OF 3P-1S TRANSITION IN PIONIC DEUTERIUM

Abstract

Calculating the radiative contribution due to the vacuum polarization effect to energy value for the 3p-1s transition in pionic deuterium has been carried out using the modified generalized Uehling-Serber potential which includes effectively the higher order vacuum polarization corrections. Comparison with analogous theoretical data by Indelicato is performed.

Key words: pionic deuterium, radiative corrections

УДК 539.184

А. А. Кузнецова, Л. А. Витавецкая, Ю. Г. Чернякова, Д. А. Корчевский

РАСЧЕТ РАДИАЦИОННОГО ВКЛАДА ЗА СЧЕТ ЭФФЕКТА ПОЛЯРИЗАЦИИ ВАКУУМА В СДВИГ ЭНЕРГИИ 3P-1S ПЕРЕХОДА В ПИОННОМ ДЕЙТЕРИИ

Резюме

Проведен расчет радиационного вклада за счет эффекта поляризации вакуума в величину энергии 3p-1s перехода в пионом дейтерии с использованием модифицированного потенциала Юлинга-Сербера, эффективно учитывающего вакуум - поляризационные поправки высших порядков. Проведено сравнение с аналогичными данными теории Indelicato.

Ключевые слова: пионный дейтерий, радиационные поправки

УДК 539.184

Г. О. Кузнецова, Л. А. Вітавецька, Ю. Г. Чернякова, Д. О. Корчевський

РОЗРАХУНОК РАДІАЦІЙНОГО ВНЕСКУ ЗА РАХУНОК ЕФЕКТУ ПОЛЯРИЗАЦІЇ ВАКУУМУ У ЗСУВ ЕНЕРГІЇ 3P-1S ПЕРЕХОДУ У ПІОННОМУ ДЕЙТЕРІЇ

Резюме

Виконано розрахунок радіаційного внеску за рахунок ефекту поляризації вакууму у величину енергії 3p-1s переходу у піонному дейтерії з використанням модифікованого потенціалу Юлінга-Сербера який ефективно враховує вакуум - поляризаційні поправки вищих порядків. Проведено порівняння з аналогічними даними теорії Indelicato**.**

Ключові слова: піонний дейтерій, радіаційні поправки

UDC 54.03, PACS 81.70.Pg

V. A. Smyntyna, L. M. Filevska, O. V. Sviridova,*

I. I. Mechnikov Odessa National University, Ukraine
*Odessa National Polytechnic University, Ukraine

TOPOLOGICAL FEATURES OF TIN DIOXIDE FILMS OBTAINED FROM THE BIS(ACETYLACETONATO)DICHLOROTIN COMPLEXES

The paper presents the surface morphology studies of tin dioxide nanoscale films produced from Bis(acetylacetonato)dichlorotin complexes of different concentrations. The films are agglomerates of several nanoscale grains. The film's grain size dependence on the number of Bis(acetylacetonato)dichlorotin in the initial solution is established. Dependencies for each type of precursors differ from each other..

Introduction

Thin films of oxide materials with nanoscale grain are widely used as sensors and as transparent electrodes in solar cells and optoelectronic devices. As catalysts for oxidation processes they are used in modern gas analytical industry, besides they are used in device engineering and in electronics [1 – 3]. Liquid phase chemical methods such as a sol-gel method, chemical vapor deposition from a solution, etc. [4, 5] are successfully applied along with the known methods for physical delivery of tin dioxide nanoscale thin film. As far as the decomposition of thermally unstable compounds of tin is the basic process of these methods, the important step is the selection of a suitable precursor.

The preparation method of thin tin dioxide films with nano-sized grains was proposed in our previous works [6, 7]. Aiming to structure the films we used a polymer in the sol-gel process, Bis(acetylacetonato)dichlorotin studied by the authors in [8, 9], which served as the precursor of tin dioxide. Such compounds have been used as precursors, for example, in the preparation of thin films of zirconium dioxide [10]. Complexes of In^{3+}, Sn^{4+} and Sn^{4+}, Sb^{3+} with acetylacetone were used in [11] as a precursor of oxide films. The sizes of surface irregularities due to morphological studies results are 42 – 125 nm for SnO_2:Sb films and 205 – 520 nm for In_2O_3:Sn films. According to X-ray diffractometry data these inhomogenities consist of crystallites with an average size of 25 ± 5 nm for SnO_2:Sb films, and 10 ± 5 nm for In_2O_3:Sn films, correspondingly. Properties and structure of studied films are predefined by features of film-forming solutions.

The surface morphology studies of nanoscale tin dioxide films produced of Bis(acetylacetonato) dichlorotin complexes of different concentrations is presented in this paper.

Films' preparation technique and research methods

The film preparation procedure is given in [4]. Bis (acetylacetonato)dichlorotin (BADCT) was used as a tin dioxide precursor [6]. Three complexes of precursor were used in this work. Two of them are based on stannic(IV) chloride ($SnCl_4$) [7]: the air-dried one is Complex BADCT (IV) N1, and vacuum-dried is Complex BADCT (IV) N2. Besides those we used complex № 3 (BADCT (II)) obtained from stannous chloride dehydrate ($SnCl_2 \cdot 2H_2O$) [8], which was air-dried.

The sample preparation procedure consisted of several stages: preparation of the polymer solution in acetone, obtaining the precursor solution in acetone, the combination of solutions, film coating, pre-drying at a temperature ~ 60°C, annealing of layers at a temperature 500 – 600°C.

Films were prepared from several solutions with different concentrations of precursors: the complex № 1 – 1, 5, 10% of precursor in the coat-

ing solution, the complex № 2 – 0.5, 1, 2, 4, and 5% of precursor in the coating solution, the complex № 3 – 1, 5, 10% of precursor in the coating solution.

The surface morphology of tin dioxide layers was investigated by the industrial Atomic Force Microscope (AFM) Nano Scope 111 a (Digital instruments, USA). The measurements were fulfilled by siliceous probe with a nominal radius ~10 nm (NT-MDT, Russia) in semi-contact mode (Tapping Mode – TM). The investigated surface area was from 500x500 nm up to 50x50 mkm. AFM NT-206 (Belarus) with Micromasch cantelevers (Germany) was used for Contact Mode measurements.

Experimental results and discussion

Fig.1 presents three dimensional AFM image of tin dioxide films derived of film-forming solutions with different concentrations of complex № 1 precursor (air-dried BADCT(IV)), and the corresponding profiles of the film surface.

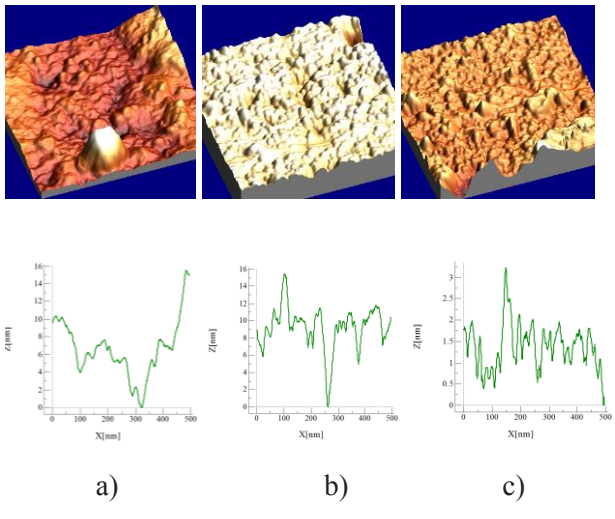

Fig.1. **3-D AFM image of tin dioxide film surface: a) 1%, b) 5% and c) 10% of the complex № 1 in the coating solution (500x500 nm) and the corresponding surface profiles of the samples**

As it follows from the film surface profiles, the increasing of the precursor amount in the original film-forming solution correlates with increases of the film's surface roughness. As the precursor concentration decreases (up to1%) the film shows a developed surface, with large agglomerates ~ 200 nm and with the grain diameter of ~ 20 nm. At 5% of BADCT the surface roughness increases, although the films become more homogeneous. It is seen the reduction in the agglomerate size up to 100 nm, and the grain apparent size is in the range of 15 – 20 nm. At the highest concentration of precursor (10%) in this series of films the decrease in grain size and an increase in surface roughness are observed. Thus, the agglomerates in the film are virtually absent.

The topology of the first series of films is well explained by the peculiarities of the used precursor - hydrated air-dried BADCT(IV) (9). The water in its composition loosens film during annealing and prevents the formation of large agglomerates. Smaller step of roughness is a consequence of loosening in the films in this series. Loosening also leads to decrease the roughness step and increase the unevenness height in films with increasing concentration of the precursor.

Fig.2 shows a 3-D AFM image of tin dioxide films derived from film-forming solutions with different precursor's concentrations of complex № 2 (dried in vacuum BADCT (IV)).

The precursor concentration Studied area 45x45 μm 5x5 μm

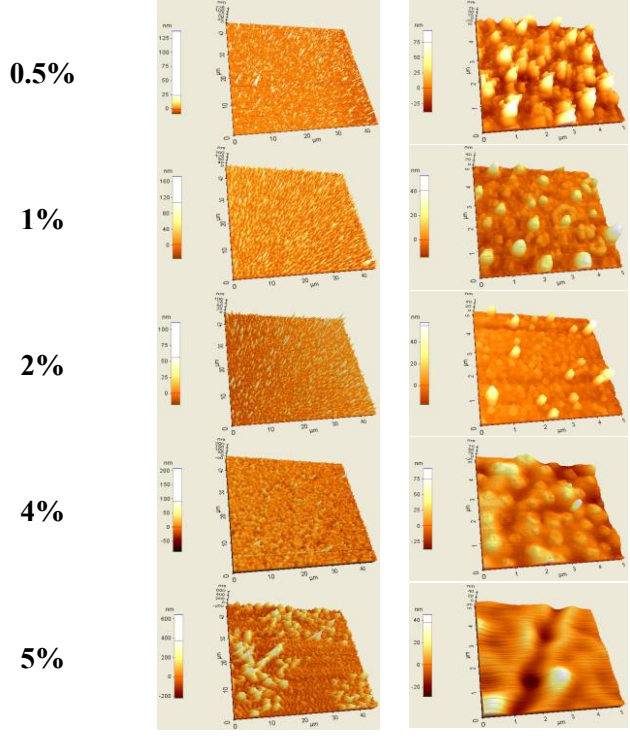

Fig.2 **3-D AFM image of tin dioxide films for different concentrations of the precursor № 2 in the coating solution.**

As it is evident from Fig.2, there is a correlation between the precursor concentration in the original film-forming solution and the surface roughness of tin dioxide films. At low concentrations of precursor (0.5% and 1%) films have a developed surface and consist of agglomerates of grains with a columnar structure. The agglomerate size varies between 100 – 400 nm. The precursor's concentration increasing gives the film crystallites growth in size, appearance of the cluster structure of the film and the agglomerate size reaches the values ~ 1 mkm.

This series of films has an additional feature. The histogram of the film approximated by Gaussian function (solution of 4%, complex № 2 in [12]) shows that the film consists of two groups of clusters occupying approximately equal space. The first group contains clusters ranging from several nanometers to 200 nanometers size, and the second one covers the cluster sizes more than 200 nm. The presence of two groups of clusters has been confirmed in [12] by the polarization modulation of electromagnetic radiation method (SPR-research). Existence of two groups of clusters, established in [12], is observed in the AFM images of films (see Fig.2).

As it can be seen, the films made of vacuum-dried precursor differ both in grain and agglomerate sizes, and also in the surface development. In the case of a precursor complex № 1 surface development is increased and the agglomerate and grain sizes are decreased. In the case of the precursor complex № 2 the surface development is reduced, and agglomerates' and grains' sizes are increased. Because the precursor is non-hydrated, the second series films have a higher density and do not loosen during annealing. The result is grain coarsening and agglomeration with increasing concentration of the precursor.

Fig.3 shows films' surface images and profiles for the complex № 3 (based on BADCT (IV) films.

The last series images in Fig.3 differ a lot from the previous ones. Prepared from solutions with the smallest amount of precursor BADCT (II) films have the cluster-like structure with cluster size of 60 – 80 nm. Presented images don't allow to suppose the structure of the cluster. At higher concentrations of the precursor (5%), the cluster size significantly decreases (20 – 50 nm), but the surface roughness is not substantially increased. At the concentration of precursor equal to 10% the cluster size increases up to 100 nm, wherein the surface roughness also increases. It can be seen that clusters of this film series have a petalous shape, unlike clusters of another film series. Cluster form may be determined by the existing direction of crystallite growth in the film derived from the solution containing the precursor complex № 3.

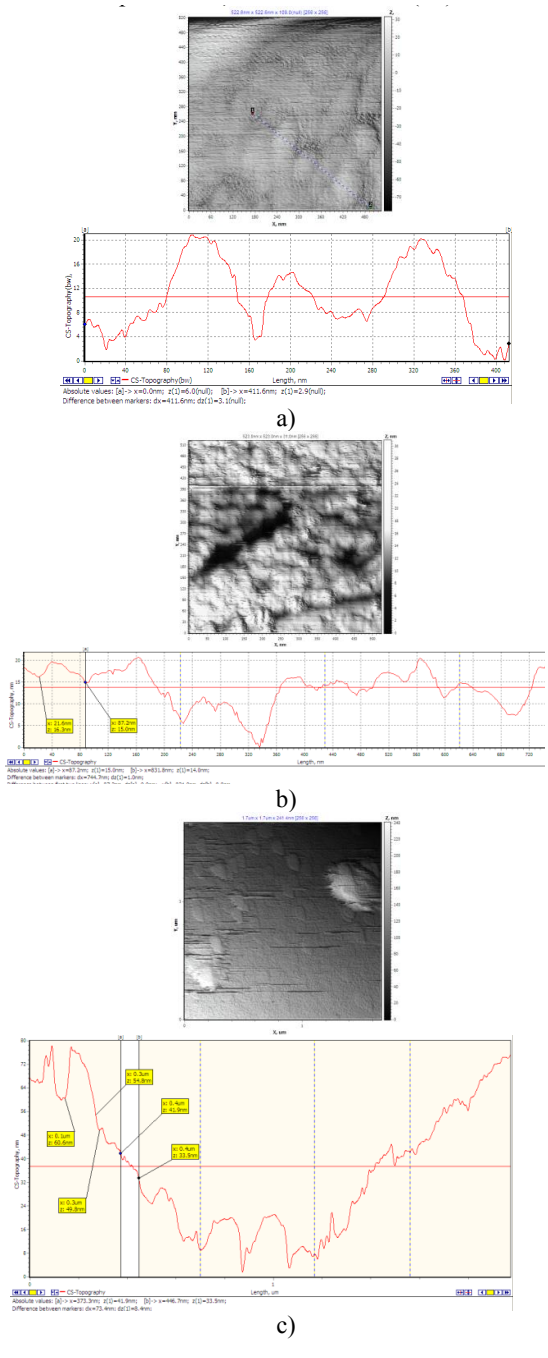

a)

b)

c)

Fig.3. **AFM image of the surface of the films obtained from solutions containing: a) 1%, b) 5%, and c) 10% of BADCT (II).**

Conclusion

Studies of tin dioxide films established a correlation between their surface morphology and concentration of tin dioxide precursor in the coating solution. However, this correlation is not one the same for all three types of precursors. Consequently, not only the quantity of the precursor in the coating solution determines the structure type (and hence different physical properties of films), but also the precursor preparation process.

References

1. D. S. Ginley, H. Hosono, D. C. Paine (Eds.), Handbook of Transparent Conductors, Springer Science+Business Media, New York, 2010.
2. J. Huang and Q. Wan. Gas Sensors Based on Semiconducting Metal Oxide One-Dimensional Nanostructures Sensors 2009, 9, 9903-9924; doi:10.3390/s91209903.
3. M. Batzill, U. Diebold. Progress in Surface Science, 79, 47 (2005).
4. J. Gong, Q. Chen. Sol-Gel Prepared Single Wall Carbon Nanotube SnO_2 Thin Film for Micromachined Gas Sensor// Nanotech. – 2004. – Vol. 3. – P. 232 – 235.
5. В. В. Иванов, И. А. Сидорак, А. А. Шубин, Л. Т. Денисова. Получение порошков SnO_2 разложением термически нестабильных соединений // Journal of Siberian Federal University. Engineering & Technologies. – 2010. – Vol. 2, №3. – P. 189-213.
6. Filevskaya L. N., Smyntyna V. A., Grinevich V. S. Morphology of nanostructured SnO_2 films prepared with polymers employment// Photoelectronics. - 2006. - №15. – P.11-14.
7. V. S. Grinevych, V. A. Smyntyna, L.M. Filevska. Influence of a precursor properties on the surface morphology of nanoscale tin dioxide films. Photoelectronics. Odessa. 21 (2012), P. 13-17.
8. B. Ulug, H. M. Türkdemir, A. Ulug, O. Büyükgüngör, M.B. Yücel, V.A. Smyntyna, V.S. Grinevich, L.N. Filevskaya. Structure, spectroscopic and thermal characterization of bis(acetylacetonato)dichlorotin(IV) synthesized in aqueous solution // Ukrainian chemical journal. – 2010. – T. 76, №7. – C. 12-17.
9. В. С. Гриневич, В. А. Смынтына, С. Н. Савин, Л. Н. Филевская, Б. Улуг, М. Х. Туркдемир, А. Улуг, С. Ялткая. Термогравиметрические исследования комплексов прекурсора для получения наноразмерных пленок двуокиси олова. Сенсорная электроника и микросистемные технологии. 2011, № 2. – С.69-75.
10. Борило Л. П. Синтез и физико-химические закономерности формирования золь-гель методом тонкопленочных и дисперсных наноматериалов оксидных систем элементов III-V групп. Автореферат диссертации на соискание ученой степени доктора химических наук. – Томск. 2003. – 29 с.
11. С. А. Кузнецова, Т. Д. Малиновская, В. И. Сачков, Влияние строения комплексных частиц в пленкообразующем растворе на структуру и свойства пленок In_2O_3:Sn и SnO_2:Sb. Известия Томского политехнического университета. 2004. Т. 307. № 2, с.105-108.
12. V.S. Grinevich, L. M. Filevska, I. E. Matyash, L. S. Maximenko, O. N. Mischuk, S. P. Rudenko, B. K. Serdega, V. A. Smyntyna, B. Ulug. Surface plasmon resonance investigation procedure as a structure sensitive method for SnO_2 nanofilms. Thin Solid Films 522 (2012) 452–456.

The article is received in editorial 17.06.2013

UDC 54.03, PACS 81.70.Pg

V. A. Smyntyna, L. M. Filevska, O. V. Sviridova

TOPOLOGICAL FEATURES OF TIN DIOXIDE FILMS OBTAINED FROM THE BIS(ACETYLACETONATO)DICHLOROTIN COMPLEXES

Abstract

The paper presents the surface morphology studies of tin dioxide nanoscale films produced from Bis(acetylacetonato)dichlorotin complexes of different concentrations. The films are agglomerates of several nanoscale grains. The film's grain size dependence on the number of Bis(acetylacetonato) dichlorotin in the initial solution is established. Dependencies for each type of precursors differ from each other.

Keywords: tin dioxide, Bis(acetylacetonato)dichlorotin, thin film, surface morphology.

УДК 54.03, PACS 81.70.Pg

В. А. Смынтына, Л. Н. Филевская, О. В. Свиридова

ТОПОЛОГИЧЕСКИЕ ОСОБЕННОСТИ ПЛЕНОК ДИОКСИДА ОЛОВА, ПОЛУЧЕННЫХ ИЗ КОМПЛЕКСОВ ДИХЛОРДИАЦЕТИЛАЦЕТОНАТА

Аннотация

В работе представлены результаты исследований морфологии поверхности наноразмерных пленок двуокиси олова, полученных из комплексов дихлордиацетилацетоната олова различной концентрации. Пленки состоят из агломератов нескольких зерен наноразмера. Установлена зависимость размера зерна в исследуемых пленках от количества дихлордиацетилацетоната в исходном растворе для их получения. Зависимости для каждого из типов прекурсоров отличаются друг от друга.

Ключевые слова: диоксид олова, дихлордиацетилацетонат олова, тонкие пленки, морфология поверхности.

УДК 54.03, PACS 81.70.Pg

В. А. Сминтина, Л. М. Філевська, О. В. Свиридова

ТОПОЛОГІЧНІ ОСОБЛИВОСТІ ПЛІВОК ДІОКСИДУ ОЛОВА, ОТРИМАНИХ З КОМПЛЕКСІВ ДІХЛОРДІАЦЕТІЛАЦЕТОНАТА

Анотація

У роботі представлені результати досліджень морфології поверхні нанорозмірних плівок двоокису олова, отриманих з комплексів діхлордіацетілацетоната олова різної концентрації. Плівки складаються з агломератів декількох зерен нанорозміру. Встановлено залежність розміру зерна в досліджуваних плівках від кількості діхлордіацетілацетоната у вихідному розчині для їх отримання. Залежності для кожного з типів прекурсорів відрізняються одна від одної.

Ключові слова: діоксид олова, діхлордіацетілацетонат олова, тонкі плівки, морфологія поверхні .

UDC 539.182

P. A. Kondratenko, Yu. M. Lopatkin, T. N. Sakun

National Aviation University, 1, Konarova av., Kiev, Ukraine
Sumy State University, Sumy, Ukraine
e-mail: quantlop@mail.ru

ELECTRON STRUCTURE AND RELAXATION PROCESSES IN RESAZURIN IN A HIGHLY EXCITED STATE

It has been performed the theoretical studying the electron structure and relaxation processes in resazurin with using the quantum-chemical calculation methods (MNDO/d and AM1). It is shown that that the quantum transition So → S (σσ *) is characterized by rather intense absorption band in contrast to the quantum transitions in S (πσ *) or S (σπ *) state, which corresponds to the oscillator strength close to 0. Dissociation of the C-O bond in the highly excited molecule of the resazurin occurs with high efficiency (no potential barrier in the triplet state). Calculations show that the absorption band that corresponds So → S (σσ *) quantum transition is in the range from 292 to 317 nm, which is consistent with experimental data on the photochemical activity.

The behavior of molecules in the highly excited states is relevant fundamental problem of modern physics, chemistry and engineering [1-12]. By this time, the relaxation process of excitation of molecules has been given very little attention. It was believed that the laws are strictly photochemistry and, in particular, the fourth law, which states that the vast majority of photochemical processes occurring in solutions of organic molecules involved only excited in S1 or T1 state of the molecule [1]. It was long thought that it should be so, since relaxation processes are mostly fast and non-equilibrium and equilibrium all possible processes can take place only with the S1 or T1 states of the molecule. And not despite the fact that the fading of dyes on fabrics under the influence of solar radiation known.

Later there appeared numerous experimental data showing that the excitation relaxation processes do not prevent leakage of important science and practice processes in the highly excited states such as generation of carriers, photochemical and radiation-chemical processes. For example, studying a photoconductivity of the polyacene linear crystals (anthracene, tetracene, pentatsen) [2] showed that its high quantum efficiency is observed only under irradiation of the highly excited molecules when there is possible a birth of holes and free electrons. During the process of relaxation from the highly excited state a molecule can stay at an intermediate state corresponding to electron transfer between the molecule and the crystal. Let us remind that the processes of charge separation in the non-equilibrium relaxation of highly excited state are theoretically considered already in the works by Onsager [3].

Another group of the known processes accompanying a relaxation of molecule from the highly excited state is a fluorescence of the S2 → S0 type in a solutions of the azulene molecules and polymethine dyes [8]. The specificity of the energy structure of these molecules is that they are characterized by high power distance between states S2 and S1, which makes non-competitive channel of the non-radiative relaxation. There is the third group of processes that appeared in the study of spectral sensitivity of the photo-dissociation processes in the azides dyes [224]. In this case, it appears that during exposure of the azides solution by a monochromatic light with a wave-

length region of the absorption band, the photodissociation quantum yield did not exceed 0.01 , while irradiating with light of $\lambda < \lambda_{kr}$ (λ_{kr} = 350 nm - the critical value of the wavelength of radiation) the quantum yield increases significantly (almost to unity at low temperatures). Similarly, the study of photochemical processes in the methylene blue [4,5] showed that the dye has not the photochemical activity in the long-wave absorption band (λ = 667 nm) at low excitation intensity, but it has the photochemical activity at high intensities (two-quantum processes) of the visible light range, or at arbitrary intensities in the ultraviolet region of the spectrum ($\lambda \leq 330$ nm). It lead to that the photochemical conversion of molecules is realized in the highly excited state. This work is devoted to theoretical studying the electron structure and relaxation processes in resazurin with using the quantum-chemical calculation methods: methods MNDO/d and AM1.

In order to carry out the theoretical study of the energy structure of the resazurin we have applied the quantum calculation methods (methods MNDO / d and AM1 [6,7]). In quantum-chemical calculation there are included 42 fully filled π- and σ-MO and all un-filled π^*- and σ^*-MO. In order to optimize the structure, there are firstly used the methods of molecular mechanics and then the methods MNDO/d or AM1 with configuration interaction (counted 12 occupied and 12 unoccupied MO). Such a calculation procedure allowed to find the geometric structure of the anion resazurin with minimal energy. Anion resazurin has the plain structure, symmetry C2v. As photo-dissociation processes occur in the highly excited state it should be understood why the excitation of the higher states does not relaxes into the S1-state by non-equilibrium way. If the total time of relaxation of the excitation from S_n (n> 1) into S1-state is equal to 5 ps (usually this value for different molecules is in the range $10^{-11} \div 10^{-13}$ s), and the energy difference E_n-E_1=25,000 cm-1, then the uniform filling the gap by vibrational states with $\hbar w$=100 cm^{-1} (vibration period T = 3 $\cdot$ 10^{-13} s) is m = 250 and average time of excited vibrational state will be near $\Delta t = 2 \cdot 10^{-14}$ s, i.e. in 15 times less than the period of oscillation. Using the uncertainty relation ship it is easily to find that ΔE=270cm^{-1}, i.e. the instantaneous state is spreading in the scale of energies. Obviously, the relaxation process can not be an equilibrium one for such proportions of ΔE and energy of a single oscillation.

Excitation will not feel the discrete energy structure and quickly relaxes to the the lower excited state. It is remained the only requirement that the conversion of the S_n-excitation rund at once into the vibrational state S(1,m). Low-energy vibrations are usually delocalized throughout the molecule. In this case, the wave functions of the same vibrational state of different molecules overlap significantly. Therefore, fluctuations between the neighboring molecules will experience a strong bond that will lead to a small relaxation time. If the interval E_n - E_1 is filled by the vibrational states with $\hbar w$=1000 cm^{-1} (T = 3 $\cdot$ 10^{-14} s), then there are only 25 states with an averaged time of the molecule in the single state $\Delta t = 2 \cdot 10^{-13}$s and the uncertainty of energy will be ΔE=27 cm^{-1}. This process will not be non-equilibrium, since the system in each state is able to make about 7 complete oscillations before transmitting the energy because of the collision with a neighboring molecule. So now one will deal with a quasi-equilibrium relaxation process.

The relatively long residence time in the vibrational state is due to the fact that high-frequency vibrations are localized on individual bonds in the molecule, resulting vibrational wave functions of different molecules weakly overlap and the probability of energy transfer fluctuations is reduced.

We suppose that the n-th excited electronic state of the molecule can not relax directly to the S1-state. This follows from the fact that such large difference in energy between S1 and S2-states of internal conversion is less likely, because there is always S2 → S0-fluorescence [8]. On the other hand, relaxation (internal conversion) Sn→S1 can occur only through iso-energetic transition from $S_n(0)$ to $S_1(m)$ state (m - number of vibrational states). The conversion probability p can be found if it is known the perturbation operator that causes the conversion:

$$p = \left| \int \psi_{S_n} \hat{p} \psi_{S_1} dV \right|^2 .$$

Using the Born-Oppengeymer approximation, one could write: $\psi_{S_i} = \chi_{S_i}\varphi_{S_i}$, where c and j - are the wave functions of the vibrational and electronic states, further one could find:

$$p = \left| \int \varphi_{S_n} \hat{p} \varphi_{S_1} dV_e \int \chi_{S_n} \chi_{S_1} dV_v \right|^2,$$

ie , the value of p is determined by the overlapping integral of the vibrational functions. Thus , the probability of internal conversion is determined by the overlapping integral of the vibrational states. Since the wave function of m-th vibrational state within its limits m- 1 times changes sign, then the value of the overlapping integral , and hence the probability of quantum transition will quickly decrease with increasing quantum number m.

These estimates show that the relaxation of the excitation of molecule occurs only with all the electronic states of molecules that lie between S_n and S_1- states. Of course , the lifetime of a molecule in a given intermediate state will depend on the distance to the nearest lower state, and the probability of non-radiative quantum transition between these states .

So one could expect that in some areas the relaxation of excitation will be presented as a quasi-equilibrium process, and unbalanced one in other. In particular, the process is non-equilibrium in the case when the surface energy of the lower state will intersect with the surface of the upper classes in the vicinity of its minimum. Often these are the processes of transition from the excited state to the binding dissociative state.

It would be logical to expect that the photo-dissociation of molecules is possible from the excited state formed due to the excitation of an electron from the fully occupied binding MO, partially or completely localized at dissociation bond, free anti-bonding MO, localized on the same bond.

It was found that for the equilibrium configuration of the anion resazurin there are two fully occupied delocalized σ-MO (Fig.1: № 33 and № 36), the first of which contains a small contribution to binding connection NO, and the second - is localized mainly due to NO and is loosening.

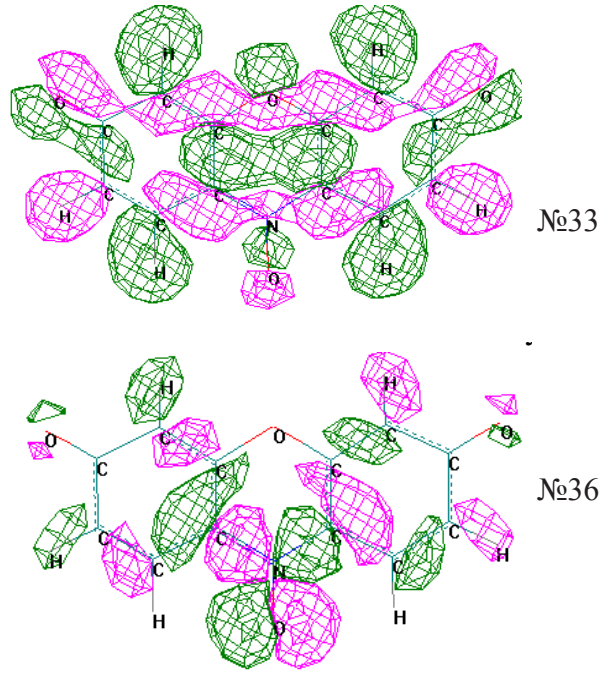

Fig.1. Two fully occupied delocalized σ-MO of the anion resazurin

Among unoccupied MO is a π *-MO (№ 43) and one σ *-MO (№ 47), which contain contributions due antibonding NO. Note that in the dissociation of σ *-MO completely localized on the NO-bond. Our calculation has showed that the quantum transition from σ- MO number 33 or the π- IU π *- MO number 43 and σ *- MO number 47 can not cause dissociation of NO- bond, since the corresponding potential surface has large potential barrier. The only quantum transition, which may cause dissociation of the molecule is a transition from σ- MO number 36 on the σ *- MO number 47.

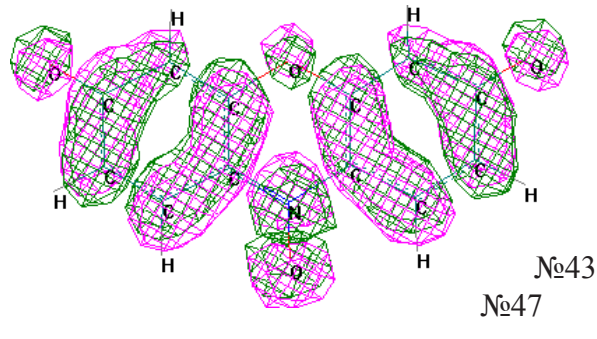

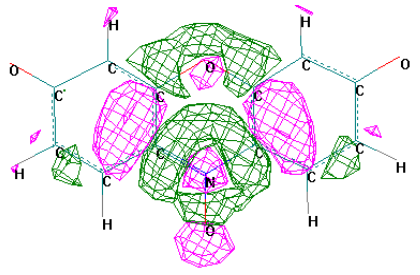

Fig.2. **The unoccupied MO of the anion resazurin**

The corresponding energy diagram for NO- bond is shown in Fig. 3,4 and for the CO- bond – in Fig.5. Fig.3 shows the dissociation of NO- bond in cation of resazurin and Fig .4 – a case of the neutral molecule.

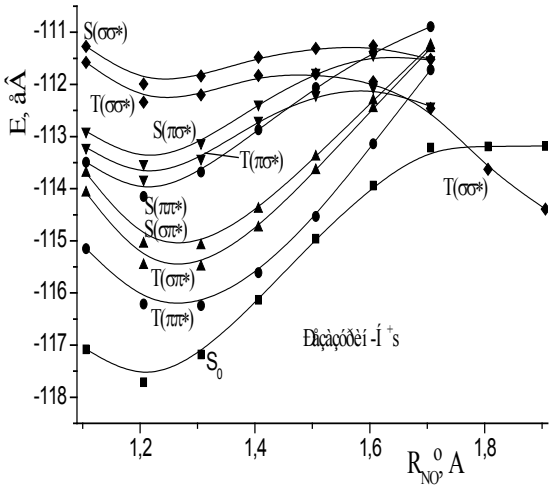

Fig. 3. **Energy diagram of the cation resazurin (calculated by the method AM1)**

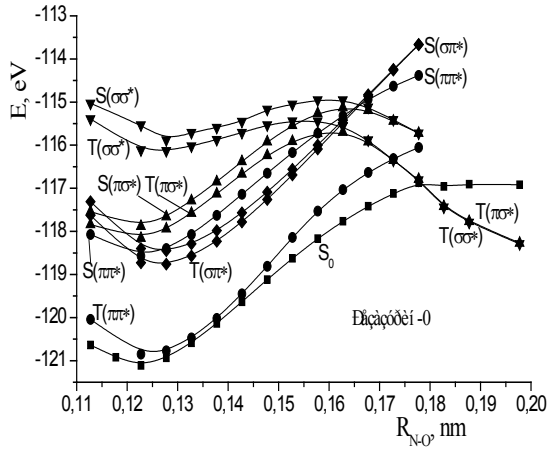

Fig.4. **Energy diagram of neutral form of the resazurin (calculated by the method AM1)**

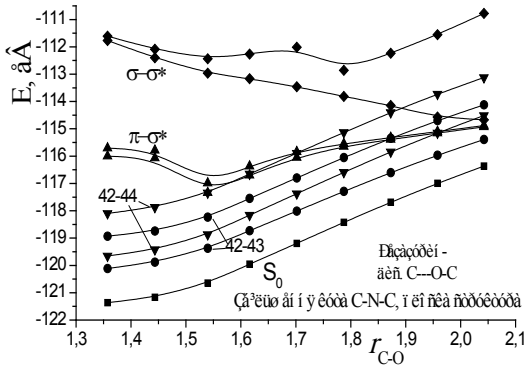

Fig. 5 **Energy diagram for the resazurin anion for a case of dissociation of the C-O-bond in the molecule (calculated by the method AM1)**

From these figures it follows that there is very significant potential barrier for dissociation of molecules with σσ * - status : the cation (for the triplet state 0.54 eV for singlet - 0.73 eV) and a neutral molecule (respectively , 0, 69 and 0.93 eV). It is implied that during the excitation into S (σσ *) state, the dissociation of the molecule can be inhibited due to the presence of a small barrier. Only the quantum transition into the T (σσ*) state leads to dissociation of NO- bond without barrier to form oxygen atom in the triplet state and molecule of resazurin.

Specified threshold could influence the dissociation with decreasing temperature in the condensed state. In the normal conditions (say, the room temperature) during relaxation of excitation there are two effects that can negate the presence of this barrier. On the one hand, the process of dissociation can occur from the non-thermalized state S (σσ *) or T (σσ *) where the barrier is not essential , and the second - the geometry of the molecule in the process of relaxation of excitation may be far from optimal structure . The latter, as shown by calculations leads to the fact that the size threshold may vary over a wide range (eg ± 1 eV). Therefore, there is always a finite probability that the dissociation of S (σσ *) or T (σσ *) state will in any structure of the resazurin.

One could draw attention to the fact that the quantum transition So → S (σσ *) is characterized by rather intense absorption band in contrast to the quantum transitions in S (πσ *) or S (σπ *) state, which corresponds to the oscillator strength close to 0 (look Table 1).

Table 1. **Quantum transitions in the symmetrized anion of the resazurin (AM1)**

№	Quantum transition	Calculation + corection		oscillator strength
		λ,nm	ν, cm^{-1}	
1	42 → 43 (π→π*)	635	15737	0.7358
2	36 → 43 (σ_{NO}→π*)	453	22072	0.0000
3	42 → 47 (π→ σ_{NO}*)	445	22463	0,0000
4	38 → 43 (π→π*)	444	22498	0,0000
5	42 → 47 36 → 43 (σ_{NO}→π*)	436	22957	0,0000
6	42 → 44 42 → 45 (π→π*)	421	23770	0.0682
7	42 → 46, 41 → 44 (π→π*)	398	25102	0.0101
8	41 → 43, (π→π*)	379	26393	0.1049
9	41 → 47 40 → 47 (π→σ_{NO}*)	365	27388	0.0042
10	42 → 44, 42 → 45 (π→π*)	345	29014	0.0758
11	40 → 43 (π→π*)	321	31174	0.3329
12	36 →47 (σ_{NO}→σ_{NO}*)	317	31546	0.1709
13	42 → 48 (π→π*)	313	31942	0.2129
14	40 → 44, 37 →43 (π→π*)	299	33469	0.2128
15	41 → 44, 37 →43 (π→π*)	274	36524	0.7375

Dissociation of the C-O bond in the highly excited molecule of the resazurin (look Fig.5) also occurs with high efficiency (in the triplet state no potential barrier). However, in this study the dissociation of the molecule requires significantly more energy quanta of light. If to explore the state of the molecule at higher excitation energies, one can find states from which dissociation occur from other possible bonds. Calculations show that the absorption band that corresponds So → S (σσ *) quantum transition is in the range from 292 to 317 nm, which is consistent with experimental data on the photochemical activity for the resazurin.

References

1. Kondratenko P. A., Photochemical action of light./ (Tutorial).- Kiev: Publishing center "Kyiv University".-2005.– 401P.
2. Siliņš E A. The electronic states of organic molecular crystals. – Riga: Zinatne.-1978.-344.
3. Onsager L. Initial recombination of ions // Physical Review. - 1938. - Vol.54. - P.554-557.
4. Kondratenko P. A., Lopatkin Yu. M., Single and double quantum processes in solid solutions of dyes // Physics and Chemistry of Solids.-2004.-Vol.5, № 3.-P.474-480.
5. Kondratenko P. A., Maksimyuk V. A., Tantsyura L.Y., Two-photon processes in the methylene blue in photo-thermoplastic environment // Chemical Physics.- 1983.- N7.-P.955-962.
6. Dewar M. J. S., Zoebisch E. G., Healy E. F., Stewart J. J. P., AM1: A new general quantum mechanical molecular model// Journal of Amer.Chem.Soc.-1985.-Vol.107,N3.-P. 3902-3909.
7. Dewar M. J. S., Thiel W., Ground states of molecules. 38. The MNDO method. Applications and parameters // Journal of Amer. Chem.Soc.-1977.-Vol.99, N15.- P.4899-4907.
8. Turro N., Molecular Photochemistry.-M.:Mir, 1967-328P.
9. Kondratenko P. A., Lopatkin Yu. M, Sakun T. N., Relaxation Processes in Highly Excited

Molecules of Resazurin // Physics and Chemistry of Solids -2007.-Vol.8,№1.-P.100-108
10. Kondratenko P. A., Lopatkin Yu. M, Sakun T. N., Spectroscopic properties of the resazurin in liquid and solid solutions// Physics and Chemistry of Solids.-2006.-Vol.7,N4. – P.695-700.
11. Glushkov A. V., Kondratenko P.A., Lepikh Ya. I., Fedchuk A. P., Lopatkin Yu. M., Svinarenko A. A., The Green's functions and density functional approach to vibrational structure in the photoelectron spectra: Molecules of CH, HF // Photoelectronics.-2011.-Vol.20.-P. 58-62.
12. Glushkov A. V., Svinarenko A. A., Fedchuk A. P., Lepikh Ya. I., Lopatkin Yu. M., Loboda A. V., The Green's functions and density functional approach to vibrational structure in the photoelectron spectra of carbon oxide molecule // Photoelectronics.-2010.-N19.-P.115-120.
13. Glushkov A. V., Kondratenko P. A., Lepikh Ya.vI. , Fedchuk A.vP., Svinarenko A. and Lovett L., Electrodynamical and quantum - chemical approaches to modelling the electrochemical and catalytic processes on metals, metal alloys and semiconductors // International Journal of Quantum Chemistry.-2009.-Vol.109,N14.- P. 3473-3481.

The article is received in editorial 05.06.2013

UDC 539.184

P. A. Kondratenko, Yu. M. Lopatkin, T. N. Sakun

ELECTRON STRUCTURE AND RELAXATION PROCESSES IN RESAZURIN IN A HIGHLY EXCITED STATE

Abstract

It has been performed the theoretical studying the electron structure and relaxation processes in resazurin with using the quantum-chemical calculation methods (MNDO/d and AM1). It is shown that that the quantum transition So → S (σσ *) is characterized by rather intense absorption band in contrast to the quantum transitions in S (πσ *) or S (σπ *) state, which corresponds to the oscillator strength close to 0. Dissociation of the C-O bond in the highly excited molecule of the resazurin occurs with high efficiency (no potential barrier in the triplet state). Calculations show that the absorption band that corresponds So → S (σσ *) quantum transition is in the range from 292 to 317 nm, which is consistent with experimental data on the photochemical activity

Key words: electronic structure, processes of relaxations, molecule in a highly excited state

УДК 541.27

П. А. Кондратенко, Ю. М. Лопаткин, Т. Н. Сакун

ЭЛЕКТРОННАЯ СТРУКТУРА И ПРОЦЕССЫ РЕЛАКСАЦИИ В РЕЗАЗУРИНЕ В ВЫСОКО ВОЗБУЖДЕННОМ СОСТОЯНИИ

Резюме

Выполнено теоретическое изучение электронной структуры и релаксационных процессов в резазурине с использованием квантово-химических методов расчета (MNDO / d и AM1). Показано, что, что квантовый переход So → S (σσ *) характеризуется достаточно интенсивной по-

лосой поглощения в отличие от квантовых переходов в S (πσ *) или S (σπ *) состояния, которым соответствует сила осциллятора близкая к 0. Диссоциации связи CO в сильно возбужденных молекулах резазурина происходит с высокой эффективностью. Расчеты показывают, что полоса поглощения, соответствующая квантовому переходу So→S(σσ*) находится в диапазоне от 292 до 317 нм, что согласуется с экспериментальными данными по фотохимической активности.

Ключевые слова: электронная структура, процессы релаксации, молекулы в высоко возбужденном состоянии

УДК 539.184

П. О. Кондратенко, Ю. М. Лопаткін, Т. М. Сакун

ЕЛЕКТРОННА СТРУКТУРА ТА РЕЛАКСАЦІЙНІ ПРОЦЕСИ У РЕЗАЗУРИНІ У ВИСОКО ЗБУДЖЕНОМУ СТАНІ

Резюме

Виконано теоретичне вивчення електронної структури та релаксаційних процесів у резазурині з використанням квантово-хімічних методів розрахунку (MNDO/d і AM1). Показано, що квантовий перехід So → S (σσ *) характеризується досить інтенсивною смугою поглинання на відміну від квантових переходів в S (πσ *) або S (σπ *) стани , яким відповідає сила осцилятора близька до 0. Дисоціації зв'язку CO у сильно збуджених молекулах резазуріна відбувається з високою ефективністю. Розрахунки показують, що смуга поглинання, що відповідає квантовому переходу So→S(σσ*) знаходиться у діапазоні від 292 до 317 нм, що узгоджується з експериментальними даними по фотохімічної активності .

Ключові слова: електронна структура, процеси релаксації, молекули у високо збудженому стані

UDC 539.135

Yu. V. Dubrovskaya

Odessa National Polytechnical University, 1, Shevchenko av., Odessa, Ukraine
Odessa State Environmental University, 15, Lvovskaya str., Odessa, Ukraine
e-mail: nucdubr@mail.ru

ATOMIC CHEMICAL COMPOSITION EFFECT ON THE BETA DECAY PROBABILITIES

Within a new theoretical scheme for sensing the atomic chemical environment effect on the beta decay characteristics there are presented numerical results for chemical environment effect on the beta decay in the fluorine, sulphur and nickel. Despite on the relative smallness of the atomic chemical environment effect on the b

1. Introduction

Though in a modern nuclear physics there is a number of principally new problems, connected with an unprecedented progress in the physical experiment, nevertheless the classical problems, including the beta decay or low energy nucleus-nucleus collision etc. are remained under intensive theoretical and experimental interest (c.f.[1-11]). This paper goes on our investigations on estimating the beta decay characteristics and sensing an influence of the chemical environment on the b decay parameters with using an optimal theoretical schemes (c.f.[11-16]). In last years a calculating the b decay processes and sensing an influence of the chemical environment on the beta b characteristics attracts a great interest especially due to the new experimental studies of the b decay for a number of nuclei [1-10]. A number of experimental and theoretical papers appeared where the different aspects of the b decay theory and accounting for different factors are considered. One of the important topics is problem to get the data about the neutrino mass from the beta decay spectra shape. An exact value of the half-decay period for the whole number of heavy radioactive nuclei is important for standardisation of data about their properties. Disagreement between different experimental data regarding the b-decay in heavy radioactive nuclei is provided by different chemical environment radioactive nucleus. For example, such disagreement in data on the half-decay period for the ^{241}Pu (see, for example, ref. [1,5,8,9]) is explained in some papers by special beta decay channel. The beta particle in this channel does not transit into free state, but it occupies the external free atomic level. According to ref. [1-5], differences in population of these levels are to be a reason of an influence of the chemical environment on the beta decay. So, a sensing the chemical environment effect on the beta decay is very important to be studied as within a consistent, high accurate theoretical calculation scheme as experimental high precise measurement. Under theoretical consideration of the problem, one has to consider the following effects:

i.). A changing electron wave functions because of the changing atomic electric field due to the difference in the valence shells occupation numbers in different chemical substances;

ii). A changing up limit of integration under calculating the Fermi integral function in different chemical substances [1,6].

As a rule, the beta particle and neutrino bring away the difference between energies of the mother and daughter atoms. This difference energy is equal to sum of values, provided by atomic nucleus reconstruction and atomic electron shell reconstruction. The entire energy of electron shell of an atom in the different chemical compounds is different. Due to the changing the nuclear charge Z on unite during the beta decay, this entire en-

ergy of electron shell of an atom changes in different chemical compounds by different way; iii). Together with beta decay and ejection of the beta particle out atom it is possible additional channel when the beta electron occupies non-occupied place on the bonded external orbitals of atom. As a rule, special tables [9] for the Fermi function and integral Fermi function is used for calculating the beta spectrum shape. In ref. [9] calculation scheme is based on the non-relativistic Hartree-Fock-Slater approach, but the finite size of nucleus is taken into account. In paper [4] the relativistic Dirac-Fock (DF) method was used. Note that the DF approach is the most wide spread method of calculation, but, as a rule, the corresponding orbitals basis's are not optimized. Some problems are connected with correct definition of the nuclear size effects, QED corrections etc. We are applying below the gauge invariant DF (GIDF) type approach [11-17] for estimating the atomic chemical environment effect on the b decay characteristics for fluorine, , sulphur and nickel.

2. Method

As it is well known a distribution of the b particles on energy in the permitted transitions is as follows [9]:

$$dW_\beta(E)/dE = \frac{1}{2\pi^3} G^2 \cdot F(E,Z) \cdot E \cdot p \cdot (E_0 - E)^2 \cdot |M|^2 . \quad (1)$$

Here G is the weak interaction constant; E and $p=(E^2-1)^{1/2}$ are an entire energy and pulse of beta particle; $E_0=1+(E_{bn}/m_e c^2)$, E_{bn} is the boundary energy of β-spectrum; |M| is a matrix element, which is not dependent upon an energy in a case of the permitted β- transitions.

As usually for calculation of the b decay shape and decay half period one should use the tables of the Fermi function and integral Fermi function. The Fermi function F and integral Fermi function f are defined as follows:

$$F(E,Z) = \frac{1}{2p^2}(g_{-1}^2 + f_{+1}^2), \quad (2a)$$

$$f(E_0,Z) = \int_1^{E_0} F(E,Z) \cdot E \cdot p \cdot (E_0 - E)^2 dE . \quad (2b)$$

Here f_{+1} and g_{-1} are the relativistic electron radial functions; the indexes $\pm l=c$, where $c=(l-j)/(2j+1)$. Two schemes of calculation are usually used: i). the relativistic electron radial wave functions are calculated on the boundary of the spherical nucleus with radius R_0 (it has done in ref. [4]); ii). the values of these functions in the zero are used (see ref.[9]).

The normalisation of electron radial functions f_i and g_i provides the behaviour of these functions for large values of radial valuable as follows:

$$g_i(r) \rightarrow r^{-1}[(E+1)/E]^{1/2} \sin(pr + d_l), \quad (3a)$$

$$f_i(r) \rightarrow r^{-1}(i/|i|)\,[(E-1)/E]^{1/2} \cos(pr + d_l) \quad (3b)$$

An effect of interaction in the final state between beta electron and atomic electrons with an accuracy to $(aZ/v)^2$ is manifested and further accounted for in the first non-vanishing approximation [8]. This contribution changes the energy distribution of the beta electron on value:

$$\frac{dW_\beta(E)/dE}{dW_\beta^{(0)}(E)/dE} = 1 - (\alpha E/p)^2 < \Psi_{in} \sum_j^z (a_B/|r_j|)\,|\Psi_{in}> \quad (4)$$

Here y_{in} – the wave function of atom initial state, z is a number of electrons, a_B is the Bohr radius. As method of calculation of the relativistic atomic fields and electron wave functions, we have used the GIDF approach [10,11]. The potential of Dirac equation includes also the electric and polarization potentials of a nucleus (the gaussian form of charge distribution in the nucleus was used). All correlation corrections of the PT second and high orders (electrons screening, particle-hole interaction etc.) are accounted for [5]. The GIDF equations for N-electron system are written and contain the potential: $V(r)=V(r|nlj)+V_{ex}+V(r|R)$, which includes the electrical and polarization potentials of the nucleus. The part V_{ex} accounts for exchange inter-electron interaction. Note that a procedure of the exchange account in the GIDF scheme is similar to one in the usual DF

approach. Regarding the GIDKS scheme, it is similar to usual DKS scheme. The optimization of the orbital basises is realized by iteration algorithm within gauge invariant QED procedure (look its application in the beta-decay theory [5]). Approach allows calculating the continuum wave functions, taking into account fully an effect of exchange of the continuum electron with electrons of the atom. Note that this is one of the original moments of the paper. Another original moment is connected with using the consistent QED gauge invariant procedure for optimization of the electron functions basis's. Numerical calculation and analysis shows that used methods allow getting the results, which are more precise in comparison with analogous data, obtained with using non-optimized basis's. The details of the numerical procedure are presented in ref. [11-17].

3. Results and conclusions

In Table 1 we present presents our data on the atomic chemical environment effect on the probability of β decay $^{17}F \rightarrow ^{17}O$. It is easy to see that the quantitative effect of the chemical environment of part of the decay is sufficiently small.

Table 1. The atomic chemical environment effect on the b decay probability $^{17}F \rightarrow ^{17}O$; Changing the half-period $T_{1/2}$ **(our data)**

Decay of neutral atom		
Atom	E_{bn}, eV	$\Delta f/f$. %
$F(^0)$	1748000 1748100	0,006
Decay of ionized atom		
Ion	E_{bn} , eV	$\Delta f/f$. %
$F(^{-1})$	1747900 1748000	0,006

The situation (compared ^{17}F) changes in the transition to the consideration of the decay $^{35}S®^{35}Cl$, $^{63}Ni®^{63}Cu$**.** In Table 2 there are presented the corresponding results for the decay $^{35}S®^{35}Cl$, including the value of $\Delta f/f = -\Delta T_{1/2}/T_{1/2}$. In the case of the decay of $S^{(0)}$ as the value of the boundary energy it is taken value 167450 eV, and the decay of the ion $S^{(+2)}$ - on 30 eV less. Accordingly, in the second version, the energy calculation is based on the value of 167390 eV in the case of the decay $S^{(+2)}$, and for the decay of $S^{(0)}$ - - 167420 30 eV.

Analysis for two versions of data shows that there are obtained give similar results, and, in particular, very similar values for the changing $T_{1/2}$ when the ionic parameter is changed. Regarding the value of the integral Fermi function, the characteristic value for the decay of ionized sulfur is less than in the case of neutral sulfur, respectively sulfur ionized decay is slower. The value of the Fermi function is greater for the neutral sulfur and, therefore, β-decay of the neutral sulfur is faster. As it can be seen from Table 2, the corresponding difference in the values of $T_{1/2}$ is about 0,04%. The similar data for the decay of $^{63}Ni®^{63}Cu$ are listed in the Table 3.

The difference in values of $T_{1/2}$ for $^{63}Ni®^{63}Cu$ is about ~0,1% (see table 3) for the twice-ionized atom of Ni in comparison with a decay of neutral nickel.

Table 2. **The atomic chemical environment effect on the b decay probability $^{33}P^{(0)} \rightarrow ^{33}S$ Changing the half-period $T_{1/2}$ (our data)**

Decay of neutral atom			
Atom	E_{bn}, eV	$f(E_{bn},Z)$	$\Delta f/f$. %
$S^{(0)}$	167420 167450	1,36849(-2) 1,36935(-2)	0,037
Decay of ionized atom			
Ion	E_{bn} , eV	$f(E_{bn},Z)$	$\Delta f/f$. %
$S^{(2+)}$	167390 167420	1,36798(-2) 1,36884(-2)	0,037

Correspondingly, the Fermi function value for for two-ionized atom of Ni is less on ~0,1%. It means that the decay of the neutral nickel runs faster in comparison with twice-ionized atom. In conclusion let us note that our conclusions fully coincide with analysis and conclusions, presented in [1].

Despite on the relative smallness of the atomic chemical environment effect on

Table 3. **The atomic chemical environment effect on the b decay probability ^{63}Ni®^{63}Cu ;**

Changing the half-period $T_{1/2}$ **(our data)**

Decay of neutral atom				
Atom	E_{bn}, eV	$f(E_{bn},Z)$	$\Delta f/f$. %	
$Ni^{(0)}$	65800 65825	1,38463(-3) 1,38599(-3)	0,095	
Decay of ionized atom				
Ion	E_{bn} , eV	$f(E_{bn},Z)$	$\Delta f/f$. %	
$Ni^{(+2)}$	65777 65800	1,38332(-3) 1,38478(-3)	0,095	

the b decay probabilities for corresponding decays, the situation may be significantly changed under consideration of the beta decay for the heavy elements.

References

1. Glushkov A. V., Khetselius O. Yu., Lovett L., Electron-b-nuclear spectroscopy of atoms and molecules and chemical environment effect on the b-decay parameters // Advances in the Theory of Atomic and Molecular Systems Dynamics, Spectroscopy, Clusters, and Nanostructures. Series: Progress in Theoretical Chemistry and Physics, Eds. Piecuch P., Maruani J., Delgado-Barrio G., Wilson S. (Berlin, Springer).-2009.-Vol. 20.-P. 125-172.
2. Tegen R., Beta decay of the free neutron and a (near) degenerate neutrino mass // Nucl. Phys.A.-2002.-Vol.706.-P.193-202.
3. Izosimov I. N., Kazimov A. A., Kalinnikov V. G., Solnyshkin A. A. and Suhonen J., Beta-decay strength measurement, total beta-decay energy determination and decay-scheme completeness testing by total absorption gamma-ray spectroscopy // Phys. Atom. Nucl.-2004.-Vol. 67, N10.-1876-1882.
4. Kopytin I. V., Karelin K. N., and Nekipelov A. A. Exact inclusion of the coulomb field in the photobeta decay of a nucleus and problem of bypassed elements // Phys. Atom. Nucl.-2004.-Vol.67,N8.-P.1429-1441.
5. Band I.M., Listengarten M.A., Trzhaskovskaya M.B., Possibility of beta decay in model of atom of the Hartree-Fock-Dirac and influence of chemical composition on the beta decay // Izv. AN USSR.-1987.-Vol.51,N11.-P.1998-200
6. Glushkov A.V., Laser- electron-b-nuclear spectroscopy of atomic and molecular systems and chemical environment effect on the b-decay parameters:Review //Photoelectronics -2010.-N19.-P.28-42.
7. Karpeshin F.,Trzhaskovskaya M.B., Gangrskii Yu.P.,Resonance Internal Conversion in Hydrogen-Like Ions // JETP.-2004.-Vol.99, N2.-P.286-289.
8. Kaplan I., Endpoint energy in the molecular beta spectrum, atomic mass defect &negative $m^2_{\nu_e}$ puzzle// J. Phys G:Nucl.Part.Ph.-1997.-Vol.23.-P.683-692.
9. Drukarev E.G., Strikman M.I., Final state interactions of beta electrons and related phenomena// JETP.-1986. –Vol.64(10).-P.1160-1168.
10. Gelepov B.C., Zyryanova L.N., Suslov Yu.P. Beta processes.-Leningrad: Nauka, 1972.-372p.
11. Malinovskaya S.V., Dubrovskaya Yu.V., Vitavetskaya L.A., Advanced quantum mechanical calculation of the beta decay probabilities // Low Energy Antiproton Phys. (AIP).-2005.-Vol.796-P.201-205.
12. Malinovskaya S.V., Dubrovskaya Yu.V., Zelentzova T.N., The atomic chemical environment effect on the b decay probabilities: Relativistic calculation // Kiev Univ.Bulletin. Series Phys.-Math.–2004.-№4 .-C.427-432.

13. Glushkov A.V., Malinovskaya S.V., Dubrovskaya Yu.V., Sensing the atomic chemical composition effect on b decay probabilities // Sensor Electr. & Microsys.Tech.-2005.-N1.-P.16-20.
14. Dubrovskaya Yu. V., The atomic chemical environment and beta electron final state interaction effect on bdecay probabilities// Photo-electronics.-2005.- N14.-P.86-88.
15. Dubrovskaya Yu. V., The beta electron final state interaction effect on beta decay probabilities // Photoelectronics. - 2006 .-N15.-P.92-94.
16. Turin A. V., Khetselius O. Yu.,. Dubrovskaya Yu. V, The beta electron final state interaction effect on beta decay probabilities for ^{42}Se nucleus within relativistic Hartree-Fock approach // Photoelectronics.-2007.-N16.-P.120-122..
17. Dubrovskaya Yu. V., Sukharev D. E., Vitavetskaya L. A., Relativistic theory of the beta decay: Environment and final state interaction effects // Photoelectronics.-2011.-Vol.20.-P.113-116.

The article is received in editorial 29.07.2013

UDC 539.135

Dubrovskaya Yu. V.

ATOMIC CHEMICAL COMPOSITION EFFECT ON THE BETA DECAY PROBABILITIES

Abstract

Within a new theoretical scheme for sensing the atomic chemical environment effect on the beta decay characteristics there are presented numerical results for chemical environment effect on the beta decay in the fluorine, sulphur and nickel. Despite on the relative smallness of the atomic chemical environment effect on the b decay probabilities for corresponding decays, the situation may be significantly changed under consideration of the beta decay for the heavy elements

Key words: atomic chemical composition effect, beta decay probability

УДК 539.135

Дубровская Ю. В.

АТОМНЫЙ ЭФФЕКТ ВЛИЯНИЯ ХИМИЧЕСКОГО ОКРУЖЕНИЯ НА ВЕРОЯТНОСТЬ БЕТА РАСПАДА

Резюме

В рамках новой теоретической схемы вычисления эффекта влияния химического окружения на характеристики b распада представлены численные оценки влияния химического окружения на b распад фтора, серы, никеля. Несмотря на относительную малость влияния атомного эффекта химической связи на вероятности бета распада, ситуация может быть значительно измениться в случае бета-распада тяжелых элементов.

Ключевые слова: влияние химического окружения, вероятность бета распада.

УДК 539.135

Дубровська Ю. В.

АТОМНИЙ ЕФЕКТ ВПЛИВУ ХІМІЧНОГО ОТТОЧЕННЯ НА ІМОВІРНІСТЬ БЕТА РОЗПАДУ

Резюме

На основі нової теоретичної схеми обчислення ефекту впливу хімічного отточення на характеристики b розпаду представлені чисельні оцінки впливу хімічного отточення на b розпад фтору, сіри та нікелю. Незважаючи на відносну малість атомного ефекту хімічного середовища на ймовірності b розпаду, ситуація може бути значно змінитися у випадку бета-розпаду важких елементів

Ключові слова: вплив хімічного отточення, імовірність бета розпаду

UDC 621.315.592

Myndrul V. B., Bak A. YU., Karakis YU. N., Kutalova M. I., Zatovskaya *N. P., Zubritskii S. V.,*

Odessa I. I. Mechnikov National University, e-mail: ndl_lepikh@onu.edu.ua

DETERMINATION IN MOBILITY OF NON-EQUILIBRIUM CARRIERS CONSIDERING MOTION VELOCITY DISTRIBUTION

The particularities of contact influence on processes of current rise in crystal at the expense of non-equilibrium charge were investigated. The procedure to determine carrier active mobility for the case of considerable asymmetry in their velocity distribution was developed

The mobility of charge carriers is one of the most important values that characterized the electric properties of semiconductors. This value determines such device qualities as sluggishness, frequency response, etc.

The value of mobility μ is defined as drift velocity v_{dr} fall at the unit of external field strength E:

$$\mu = \frac{v_{\partial p}}{E} \qquad (1)$$

And drift velocity is realizes as such medium rate being equal for all carriers at which they transfer the same electric charge between contacts at distance l [1, 2]:

$$v_{\partial p} = \frac{l}{t} \qquad (2)$$

Where t is time to pass this distance for current rise carriers. If voltage U is applied to contacts we obtain:

$$\mu = \frac{l^2}{U \cdot t} \qquad (3)$$

The l and U appeared in this equation are the large-scale parameters and measure experimentally. Drift time t – large-scale parameter too, and owing to thermal motion this time is different for each carrier. Calculation of active number for value μ offers the main difficulty to define mobility and crystal conductivity σ:

$$\sigma = e n \mu . \qquad (4)$$

The selective approach both for carriers already located in element at the moment of field connection and carriers injected from contact was used in our work.

During the first test we studied equilibrium carriers, during the second one – non-equilibrium carriers because their energy is not ---- and does not depend on energy of sample crystal lattice. For equilibrium carriers already located in crystal at the moment of field connection the symmetric distribution in velocities is characteristic phenomenon (Fig. 1a). The group of particles has the medium velocity v_0 with some quantity of slower and quicker participants.

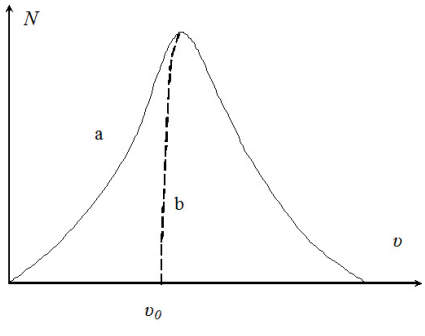

Fig. 1. **The distribution for N quantity of particles for different velocities υ in case of equilibrium (a) and injected (b) charge carriers**

When field of the corresponding polarity is connected they begin to move to cathode. The quicker particles reach cathode first. As their quantity is small (the right part of curve 1a) collector potential increases comparatively slowly. Then the basic group of carriers with velocity ~ υ_0 reaches cathode and potential of contact increases with maximum rate. The slower carriers reach cathode the latter (the left part of curve 1a) and collector potential again rises slowly. The time dependence of signal change is of S-shape [3, 4] and is shown in Fig. 2a.

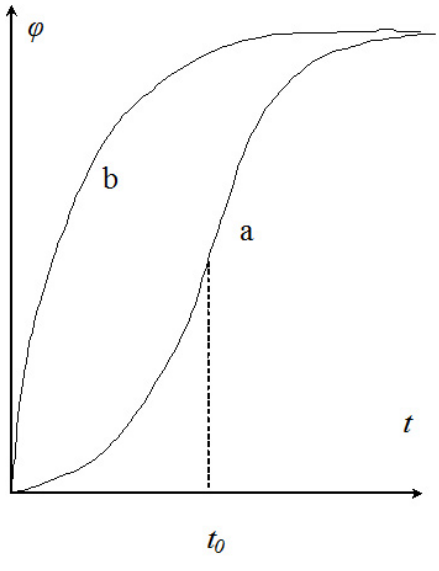

Fig. 2. **Increase of collector potential from the moment of field connection (t = 0) for equilibrium (a) and contact introduced (b) charge**

One should note that the shape of curve 2a is not the direct reflection of 1a distribution because of two reasons. Firstly, if the vector of additional velocity for carriers at the expense of field draw effect is equal in value and direction, then the vector of thermal velocity directed chaotically increases the variation in values of total velocity for each particle. Secondly, charge space distribution influences too. Independently on primary velocity the quick and slow charge carriers were located uniformly. As the result, the slower particles from distribution 1a at the moment of field connection can be located nearer to the probe and contributed quickly to raise of its potential $\varphi(t)$.

The shape of curve $\varphi(t)$ in Fig. 2a makes possible to determine the characteristic time of drift t_0 from inflection point at the moment when the basic number of charge carriers reach the probe. This parameter is observed as current forming value. The practical study of $\varphi(t)$ oscillograms gives the active value of mobility for equilibrium carriers.

The situation changes when non-equilibrium carriers entered crystal from the contact are observed. High-ohmic samples are usually investigated. It means that concentration of intrinsic charge n_0 is not high comparing with concentration of introduced charge Δn: $n_0 << \Delta n$. Non-equilibrium charge Δn just defines in this case the conductivity of crystal.

Moreover, the charge Δn should overcome energy barrier at metal-semiconductor boundary to enter the sample even for good ohmic contacts. The carriers with low velocities (and small energy too) cannot overcome the barrier. Especially as the presence of ohmic contact is the utmost situation. In practice the contacts to sample are more or less ohmic. This increases the height of barrier and decreases the portion of injected charge.

This is the cause that polarity of applied voltage is selected in such a way that polarity of external field was opposite to barrier field. Its height decreases simultaneously. But there is the limitation to apply the high injecting voltages. In this case the contribution of equilibrium carriers raises with arbitrary coordinate, the opposite collecting barrier, thermal effects influence at higher values of current. So, one cannot correct the emitter barrier. As result, the distribution in Fig. 1 for emitter contacted carriers is observed as curve 1b [5, 6].

We note that the transition from curve 2a to plot 2b can be the criteria for contact quality. This is of the special interest as the test procedure. But the parameters can not be always improved to reach the ideal shape of curve 2a. This is impossible if one needs to study the mobility in quantity-produced or operating device.

Let`s study the abscissa axis. The absolute value on vertical scale either in Figure 1 or in Fig. 2 was taken in arbitrary units comparing with the maximum value.

The changes in distribution of N particle number (Fig. 1b) are represented in curve of Fig. 2. The slow carriers are already absent. Large quantity of high-velocity carriers reach collector immediately. And signal increases quickly as shown in Fig. 2b.

Besides, curve 2b should be slightly shifted relatively to the origin of coordinates. Carriers located previously in crystal were distributed homogeneously along the volume. Part of them was located in the vicinity of contact to collector. So, curve 2a raises from the moment $t = 0$. On the contrary, all the added carriers at zero time locate from collector at distance equal to intra-probe one. And they need some time to overcome it. The graph 2b will be observed later. But probes are usually located rather nearer to each other and velocity of injected carriers is primarily high, practically this shift in curve 2b is observed comparative with thickness of oscillogram line and did not presented in Fig. 2.

The shape of dependence 2b hampers to determine value t_0 because there is no characteristic point in curve being evidently observed.

As criteria to look-up value t_0 we propose to search point on curve 2b where the square of inscribed rectangle would be the maximal. And both criteria to shape current will be taken into consideration (see equations 3 and 4): maximum number of participating carriers (vertical axis) and optimal short time of their motion (abscise line).

The task comes to geometric examination. And the axis of time is suitable to swing to the opposite way, i.e. to count off not from the moment of field connection but the opposite one – to the moment when equilibrium was attained. In this case the plot is completed between scales. We also note that traditionally used shape of plots 1 and 2 is mirror. In Fig. 1 from the left to the right we at first show the carriers with slow velocities, then – with higher ones. In Fig. 2, on the contrary, the high-rate carriers do their contribution, and then the insertion of charge with slow drift velocities is observed.

In Fig 3 one should search the point with maximal square of inscribed rectangle $S(t_0) = \varphi(t_0) \cdot t_0$. It is obvious that this point will tend to zero at the edges of plot when $\varphi \to 0$ or $t \to 0$ (dash-dot line $S(t)$). In operating point t_0 show the highest value.

For this point

$$\frac{d\,S(t)}{d\,t} = \frac{d}{d\,t}[\varphi(t)\cdot t] = 0 \qquad (5)$$

The shape of $\varphi(t)$ dependence is not prescribed. So,

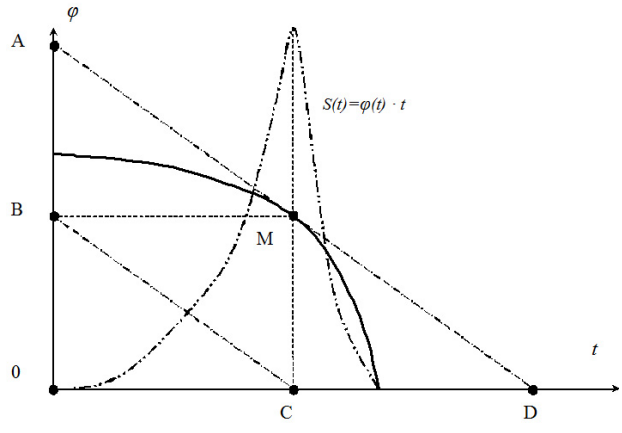

Fig. 3. The criteria to search operating point t_0 for non-equilibrium carriers

$$\frac{d\varphi(t)}{d\,t}\cdot t + \varphi(t) = 0 \qquad (6)$$

or

$$\frac{d\varphi(t)}{d\,t} = -\frac{\varphi(t)}{d\,t}\,. \qquad (7)$$

The sign «–»has no physical meaning. It simply describes the fact that the value of function along vertical scale decreases with increase of the value along X-axis in the chosen reading system.

In equation (7) the left value is the slope of tangent line to plot $\varphi(t)$ in operation point. And the left value is the slope of diagonal in rectangle $OBMC$, inscribed in operating point. Or $\angle BCO = \angle ADO$. The straight lines BC and AD are parallel. As $CM \parallel OB$ and $BM \parallel OD$ in plotting, then the boxes $BCMA$ and $BCDM$ are parallelograms. So, $BC = AM$ and $BC = MD$. Or $AM = MD$. The tangent line in operating point divides in two within the ranges of oscillogram changes.

The developed criteria to search the operating points for samples with non-ideal contacts are highly suitable to be applied in practice. For oscillograms obtained in real conditions and taking into account the particularities of carrier injection into crystal when the curves of shape 2b are observed one should choose such value of effective time for carrier drift between contacts t_0 when tangent line to plot $\varphi(t)$ divides in two in the point $t = t_0$.

We note that the present result was obtained without application of manifested appearance for function *φ(t)*. This means that the developed procedure is universal for wide class of smooth curves described the raise of collector potential ignoring the specificity of diffusion and recombination processes in crystal itself and depends only on changes of carrier dispersion in velocities when emitter contact was overcome.

The suggested model efficiently allows determining the transit time, and thus the carrier mobility from the distribution maximum (fig. 1b).

It should be pointed out that just because of the velocity distribution of the particles there is neither average nor typical mobility. It appears to be different depending on the carrier groups of different velocity intervals in Fig. 1b. Under this conditions, it is possible only to speak about some effective mobility value, which can adequately reflect the conditions of current transfer.

It is possible to get the calculation of the contribution of all the fractions from the range of possible velocities only by taking as the time of passing the distance between the emitter and the collector where

$$t = \frac{S}{\Delta t}, \qquad (8)$$

S - is the area under the curve of the function *U(t)* (fig. 2b) on the increasing curve section during the time *Δt* from the process start till the saturation beginning.

Graphically, it corresponds to the point of intersection on the graph with the side of an equivalent rectangle. Physically, this approach means that the model is accepted when all carriers are moving at the same drift speed. And the magnitude of this velocity provides the conductivity actually observed in accordance with (4, 1).

REFERENCES

1. Yu Y.P., Cardon M. Fundamentals of semiconductors: Physics and materials Properties// 2010 Berlin: Springer 775 p.
2. Л.И. Поморцева Подвижность носителей заряда при низком уровне инжекции в полупроводниках ФТП 2011, т. 45, вып. 4, С. 446 – 452
3. Г.Г. Чемересюк, Ю.Н.Каракис Методические указания к лабораторным работам по спецпрактикуму “Фотоэлектрические явления в полупроводниках” часть П // Одесса: “Одесский национальный университет”, 2012. – 60 с.
4. Принц В.Я., Панаев И.А. Неразрушающий способ определения подвижности носителей заряда в полупроводниковых структурах на изолирующих подложках и устройство для его осуществления. // Институт физики полупроводников СО РАН. Патент Российской федерации № 2097872, класс HO1L21/66, номер заявки 95103452/25 от 10.03.2010.
5. Тунг Тура Исследование влияния анизотропии на подвижность носителей заряда в алмазоподобных кристаллах. // Дисс. на соискание степени канд. физ-мат наук. ЬГТУ, г. Калуга 2012 г. 117 с.
6. Hadii A., Badieyan F. Analysis of steady-state transient transport within bulk // Maejo J. Sci.Technol. 2010, v.4, №1, P. 159-168.

The article is received in editorial 21.07.2013

UDC 621.315.592

Myndrul V. B., Bak A. Yu., Karakis Yu. N., Kutalova M. I., Zatovskaya N. P., Zubritskii S. V.

DETERMINATION IN MOBILITY OF NON-EQUILIBRIUM CARRIERS CONSIDERING MOTION VELOCITY DISTRIBUTION

Abstract

The particularities of contact influence on processes of current rise in crystal at the expense of non-equilibrium charge were investigated. The procedure to determine carrier active mobility for the case of considerable asymmetry in their velocity distribution was developed.

Key words: the contacts, the current, the mobility, the crystals.

УДК 621.315.592

Мындрул В. Б., Бак А. Ю., Каракис Ю. Н., Куталова М. И., Затовская Н. П., Зубрицкий С. В.

ОПРЕДЕЛЕНИЕ ПОДВИЖНОСТИ НЕРАВНОВЕСНЫХ НОСИТЕЛЕЙ С УЧЁТОМ РАСПРЕДЕЛЕНИЯ СКОРОСТЕЙ ИХ ДВИЖЕНИЯ

Резюме

Изучены особенности влияния контактов на процессы формирования тока в кристаллах за счёт неравновесного заряда. Указан способ определения действующей подвижности носителей для случая значительной несимметрии их распределения по скоростям.

Ключевые слова: ток, контакты, кристаллы, подвижность

УДК 621.315.592

Миндрул В. Б., Бак А. Ю Каракіс Ю. М., Куталова М. І., Затовська Н. П., Зубрицький С. В.

ВИЗНАЧЕННЯ РУХЛИВОСТІ НЕРІВНОВАЖНИХ НОСІЇВ З УРАХУВАННЯМ РОЗПОДІЛУ ШВИДКОСТЕЙ ЇХ РУХУ

Резюме

Розглянуто особливості впливу контактів на процеси формування струму в кристалі за рахунок нерівноважного заряду. Вказано засіб визначення дієвої рухливості носіїв у випадку значної несіметрії їх розподілу за швидкостями.

Ключеві слова: струм, контакти, кристали, рухливість

UDC 539.27

L. V. Nikola

I. Mechnikov Odessa National University, 2, Dvoryanskaya str., Odessa, Ukraine
e-mail: quantnik@mail.ru

*A*UGER-ELECTRON SPECTROSCOPY OF TRANSIENT METALS

The calculated data on the Auger-transition energies for a number of metals (Fe, Co, Cu, Zn) are presented and compared with theoretical data by the semi-empirical method by Larkins as well as experimental data. As basic approach to calculating the Auger spectra of solids we use a new approach, basing on the S-matrix formalism by Gell-Mann and Low and relativistic perturbation theory formalism.

This work goes on our investigation of the characteristics for the Auger effect in atomic systems and solids [1-7]. As introduction let us remind [1] that the Auger electron spectroscopy remains an effective method to study the solids electron structure, chemical composition of solid surfaces and near-surface layers [8-12]. Sensing the Auger spectra in atomic systems and solids gives the important data for the whole number of scientific and technological applications. So called two-step model is used most widely when calculating the Auger decay characteristics [8-13]. Since the vacancy lifetime in an inner atomic shell is rather long (about 10^{-17} to 10^{-14}s), the atom ionization and the Auger emission are considered to be two independent processes. In the more correct dynamic theory of the Auger effect [9] the processes are not believed to be independent from one another. The fact is taken into account that the relaxation processes due to Coulomb interaction between electrons and resulting in the electron distribution in the vacancy field have no time to be over prior to the transition. In fact, a consistent Auger decay theory has to take into account correctly a number of correlation effects, including the energy dependence of the vacancy mass operator, the continuum pressure, spreading of the initial state over a set of configurations etc.

Now it is clear that an account of the relativistic and exchange-correlation effects is very important for the adequate description of the Auger spectra of atoms and solids. This problem is partly solved in this paper. As basic approach to calculating the Auger spectra of solids we use a new approach [1-7], basing on the S-matrix formalism by Gell-Mann and Low and relativistic perturbation theory (PT) formalism [13]. Earlier the method has been applied to calculation of the Auger-electron spectra (transitions), the ionization cross-sections of inner shells in various atomic systems and solids [1-7]. In this paper we apply this method to studying the Auger –electron parameters fro a number for a number of the transient metals.

As the key aspects of our approach have been earlier described [1-7], here we are limited by a brief consideration. Within the frame of the relativistic many-body theory , the Auger transition probability and the Auger line intensity are defined by the square of an electron interaction matrix element having the form:

$$V^{\omega}_{1234} = [(j_1)(j_2)(j_3)(j_4)]^{1/2}\sum_{\lambda\mu}(-1)^{\mu}\begin{pmatrix} j_1 j_3 & \lambda \\ m_1 - m_3 & \mu \end{pmatrix}\cdot \\ \cdot \operatorname{Re} Q_{\lambda}(1234) \\ Q_{\lambda} = Q_{\lambda}^{\mathrm{Qul}} + Q_{\lambda}^{\mathrm{Br}}. \qquad (1)$$

The terms $Q_{\lambda}^{\mathrm{Qul}}$ and Q_{λ}^{B} correspond to subdivision of the potential into Coulomb part $cos|w|r_{12}/r_{12}$ and Breat one, $cos|w|r_{12}\boldsymbol{a}_1\boldsymbol{a}_2/r_{12}$. The real part of the electron interaction matrix element is determined using expansion in terms of Bessel functions:

$$\frac{\cos|\omega|r_{12}}{r_{12}} = \frac{\pi}{2\sqrt{r_1 r_2}}\sum_{\lambda=0}(\lambda)J_{\lambda+1/2}(|\omega|r_{<}) \\ J_{-\lambda-1/2}(|\omega|r_{>})P_{\lambda}(\cos\mathbf{r}_1\mathbf{r}_2) \qquad (2)$$

where J is the 1st order Bessel function, (l)=2l+1.

The Coulomb part Q_λ^{Qul} is expressed in terms of the radial integrals R_l and the angular coefficients S_l [13]:

$$\begin{aligned}\mathrm{Re}\,Q_\lambda^{\mathrm{Qul}} = \frac{1}{Z}\mathrm{Re}\{R_l(1243)S_\lambda(1243)+ + \\ + R_\lambda(\tilde{1}24\tilde{3})S_\lambda(\tilde{1}24\tilde{3})+ \\ + R_\lambda(1\tilde{2}4\tilde{3})S_\lambda(1\tilde{2}4\tilde{3})+ R_\lambda(\tilde{1}\tilde{2}4\tilde{3})S_\lambda(\tilde{1}\tilde{2}4\tilde{3})\}\end{aligned} \tag{3}$$

As a result, the Auger decay probability is expressed in terms of $\mathrm{Re}Q_l(1243)$ matrix elements:

$$\begin{aligned}\mathrm{Re}\,R_\lambda(1243) = \iint dr_1 r_1^2 r_2^2 f_1(r_1) f_3(r_1). \\ f_2(r_2) f_4(r_2) Z_\lambda^{(1)}(r_<) Z_\lambda^{(1)}(r_>)\end{aligned} \tag{4}$$

where f is the large component of radial part of single electron state Dirac function; function Z and angular coefficient are defined in refs. [2-4,13]. The other items in (3) include small components of the Dirac functions; the sign «~» means that in (3) the large radial component f_i is to be changed by the small g_i one and the moment l_i is to be changed by $\tilde{l}_i = l_i - 1$ for Dirac number æ$_i$> 0 and l_i+1 for æ$_i$<0.

The Breit interaction is known to change considerably the Auger decay dynamics in some cases. The Breit part of Q is defined in [7,13]. The Auger width is obtained from the adiabatic Gell-Mann and Low formula for the energy shift [7]. Namely, according to [1,7], the Auger level width with a vacancy $n_a l_a j_a m_a$ can be represented as:

$$\sum_\lambda \frac{2}{(\lambda)(j_\alpha)} \sum_{\beta\gamma\le f\, k>f} Q_\lambda(\alpha k\gamma\beta) Q_\lambda(\beta\gamma k\alpha) \quad , \tag{5}$$

$$\frac{2}{(j_\alpha)} \sum_{\lambda_1\lambda_2} \sum_{\beta\gamma\le f\, k>f} Q_{\lambda_1}(\alpha k\gamma\beta) Q_{\lambda_2}(\beta\gamma k\alpha) \begin{Bmatrix} j_\alpha & j_\gamma & \lambda_2 \\ j_k & j_\beta & \lambda_1 \end{Bmatrix} \tag{6}$$

The partial items of the $\sum_{\beta} \sum_{k}$ sum answer to contributions of a^{-1}®(bg)^{-1}K channels resulting in formation of two new vacancies bg and one free electron k: w_k=w_a+w_b–w_a. The final expression for the width in the representation of jj-coupling scheme of single-electron moments is given by the corresponding sum on over all possible decay channels.

The basis of the electron state functions was determined by the solution of Dirac equation (integrated numerically using the Runge-Cutt method). The contribution of the lower order PT corrections to the energies of the auger transitions is carried out according to the methodology [11,12,14]. The calculation of radial integrals **Re**R_l(1243) is reduced to the solution of a system of differential equations [13]:

$$\begin{aligned} y_1' &= f_1 f_3 Z_\lambda^{(1)}(\alpha|\omega|r) r^{2+\lambda} \\ y_2' &= f_2 f_4 Z_\lambda^{(1)}(\alpha|\omega|r) r^{2+\lambda} \\ y_3' &= [y_1 f_2 f_4 + y_2 f_1 f_3] Z_\lambda^{(2)}(\alpha|\omega|r) r^{1-\lambda} \end{aligned} \tag{7}$$

In addition, $y_3(\infty)$=**Re**R_l(1243), y_1(¥)=X_l(13). The formulas for the Auger decay probability include the radial integrals R_a(a$k$gb), where one of the functions describes electron in the continuum state.

The energy of an electron formed due to a transition jkl is defined by the difference between energies of atom with a hole at j level and double-ionized atom at kl levels in final state:

$$E_A(jkl, {}^{2S+1}L_J) = E_A^+(j) - E_A^{2+}(kl, {}^{2S+1}L_J) \tag{8}$$

In order to take into account the dynamic correlation effects, the equation (8) can be rewritten as:

$$E_A(jkl, {}^{2S+1}L_J) = E(j) - E(k) - E(l) - \Delta(k,l, {}^{2S+1}L_J) \tag{9}$$

where the item D takes into account the dynamic correlation effects (relaxation due to hole screening with electrons etc.) To take these effects into account, the set of procedures elaborated in the atomic theory [2,3] is used. For solid phase, the more precise form of equation (9) is as follows:

$$E^s{}_A(jkl, {}^{2S+1}L_J) = E_A(jkl, {}^{2S+1}L_J) + \Delta E^s + R_{rel} + e\Phi \tag{10}$$

where DE^s is a correction for the binding energy change in the solid; R_{rel}, the same for out-of-atom relaxation; eF takes into account the work of output. Other details can be found in Refs. [1-7].

In table 1 we present our calculation data on Auger-electron energies (column B) and also the semi-empirical method under Larkins' equivalent core approximation (from [8,9] (column A) as well as experimental data [2].

The calculation accuracy using the Larkins' method is within about 2 eV as an average. Our approach provides more accurate results that is due to a considerable extent to more correct accounting for the exchange-correlation effects.

Table 1. **Experimental and theoretical data for Auger electron energy: Exp-experiment; A, semi-empirical method - [8,9]; B- present paper;**

Solid	Auger line	Exp	Theory: A	Theory: D
Fe	$L_3M_{4,5}M_{4,5}\ ^1G_4$	701.2	702.8	701.3
Co	$L_3M_{4,5}M_{4,5}\ ^1G_4$	772.5	772.8	772.7
Cu	$L_3N_{4,5}N_{4,5}\ ^1G_4$	919.0	922.5	919.1
Zn	$L_3N_{4,5}N_{4,5}\ ^1G_4$	991.8	994.0	991.8

References

1. Nikola L. V., Ignatenko A. V., Shakhman A. N., Relativistic theory of the auger (autoionization) decay of excited states in spectrum of multicharged ion // Photoelectronics.-2010.-N19.-P.61-64.
2. Nikola L.V., Resonant Auger spectroscopy of the atoms of inert gases // Photoelectronics.-2011.-Vol.20.-P. 104-108.
3. Svinarenko A. A., Nikola L. V., Prepelitsa G.P., Tkach T., Mischenko E., The Auger (autoionization) decay of excited states in spectra of multicharged ions: Relativistic theory // Spectral Lines Shape (AIP, USA).-2010.-Vol.16.-P. 94-98.
4. Ambrosov S. V., Glushkov A. V., Nikola L.V., Sensing the Auger spectra for solids: New quantum approach // Sensor Electr. and Microsyst. Techn.-2006.-N3.-P. 46-50.
5. Nikola L. V., Quantum calculation of Auger spectra for Na, Si atoms and solids // Photoelectronics.-2007.-N16.-P. 102-105.
6. Khetselius O.Yu., Nikola L.V., Turin A.V., Sukharev D.E., Sensing the finite size nuclear effect in calculation of the Auger spectra for atoms and solids // Sensor Electr. and Microsyst. Techn.-2007.-N1.-P. 18-21..
7. Glushkov A. V., Khetselius O. Yu., Nikola L. V., Dubrovskaya Yu. V., Quantum calculation of Auger spectra for atoms and semiconductors: New approach // Photoelectronics.-2008.-N17.-P.12-16.
8. Kulekshov V. F., Kukharenko Yu. A., Fridrikhov S.A. et al. Spectroscopy and Electron Diffraction in Solid Surfaces Studies. Nauka: Moscow, 1985.
9. Aberg T., Hewat G. Theory of Auger effect. Springer-Verlag: Berlin, 1979.
10. Amusia M. Ya. Atomic photoeffect. Acad.Press: N.-Y., 1988.
11. Letokhov V. Nonlinear Selective Photoprocesses in Atoms and Molecules.-Moscow, 1987.
12. Aglitsky E. V., Safronova U. I. Spectroscopy of Autoionization states of atomic systems. Energoatomizd.: Moscow, 1992.
13. Glushkov A. V., Relativistic Quantum Theory. Quantum Mechanics of Atomic Systems.- Odessa: Astroprint, 2008.-704p.

The article is received in editorial 02.06.2013

UDC 539.27

L. V. Nikola

AUGER-ELECTRON SPECTROSCOPY OF TRANSIENT METALS

Abstract

The calculated data on the Auger-transition energies for a number of metals (Fe, Co, Cu, Zn) are presented and compared with theoretical data by the semi-empirical method by Larkins as well as experimental data. As basic approach to calculating the Auger spectra of solids we use a new approach, basing on the S-matrix formalism by Gell-Mann and Low and relativistic perturbation theory formalism.

Key words: Auger-transitions, transient metals

УДК 539.27

Л. В. Никола

ОЖЕ-ЭЛЕКТРОННАЯ СПЕКТРОСКОПИЯ ПЕРЕХОДНЫХ МЕТАЛЛОВ

Резюме

Приведены результаты расчета энергий Оже-переходов для ряда металлов (Fe, Co, Cu, Zn) и проведено их сравнение с теоретическими данными, полученными на основе полуэмпирического метода с Ларкинса , а также экспериментальными данными. Для расчета параметров Оже-спектров твердых тел использован новый подход, который базируется на S-матричном формализме Гелл-Манна и Лоу и формализме релятивистской теории возмущений.

Ключевые слова: Оже-переходы, переходные металлы

УДК 539.27

Л. В. Нікола

ОЖЕ-ЕЛЕКТРОННА СПЕКТРОСКОПІЯ ПЕРЕХІДНИХ МЕТАЛІВ

Резюме

Наведені результати розрахунку енергій Оже-переходів для ряду металів (Fe, Co, Cu, Zn) та проведено їх порівняння з теоретичними даними, отриманими на основі напівемпіричного методу Ларкінса, а також експериментальними даними. Для розрахунку параметрів Оже-спектрів твердих тіл використаний новий підхід, який базується на S-матричному формалізмі Гелл-Манна і Лоу і формалізмі релятивістської теорії збурень.

Ключові слова: Оже-переходи, перехідні метали

UDC 539.182

Yu. M. Lopatkin, V. I. Mikhailenko, A. A. Svinarenko

Sumy State University, Sumy, Ukraine
Odessa National Maritime Academy, 4, Didrikhsona str., Odessa, Ukraine
Odessa State Environmental University, 15, L'vovskaya str., Odessa, Ukraine
e-mail: quantsvi@mail.ru

SPECTROSCOPY OF THE SPECTRAL LINES BROADENING AND SHIFT FOR HEAVY ELEMENTS IN THE BUFFER GAS

A new relativistic approach, based on the gauge-invariant perturbation theory (PT), is applied to calculating the spectral line collisional broadening and shifts for the heavy atom (thallium) in an atmosphere of the buffer inert gases. It is shown that the relation of the adiabatic broadening to collisional shift is ~ 1/55 for the system TI - He, 1/80 for the system TI - Kr and ~ 1/65 system TI-Xe, i.e. the known Folly spectral relationship is not correct in a case of the thallium hyperfine lines.

1. Introduction

High precision data for collisional shifts and broadening the hyperfine structure lines of heavy elements (alkali, alkali-earth, lanthanides, actinides and others) in an atmosphere of the inert gases are of a great interest for modern quantum chemistry, atomic and molecular spectroscopy, astrophysics and metrology as well as for studying a role of weak interactions in atomic optics and heavy-elements chemistry [1-15]. As a rule, the cited spectral lines shift and broadening due to a collision of the emitting atoms with the buffer atoms are very sensitive to a kind of the intermolecular interaction. Besides, calculation of the hyperfine structure line shift and broadening allows to check a quality of the wave functions and study a contribution of the relativistic and correlation effects to the energetic and spectral characteristics of the two-center (multi-center) atomic systems. From the applied point of view, the mentioned physical effects form a basis for creating an atomic quantum measure of frequency [8,9]. The corresponding phenomenon for the thallium atom has attracted a special attention because of the possibility to create the thallium quantum frequency measure. Alexandrov et al [8] have realized the optical pumping thallium atoms on the line of 21GHz, which corresponds to transition between the components of hyperfine structure for the Tl ground state. These authors have measured the collisional shift of this hyperfine line in the atmosphere of the He buffer gas.

The detailed non-relativistic theory of collisional shift and broadening the hyperfine structure lines for simple elements (such as light alkali elements etc.) was developed by many authors (see, for example, Refs. [1-14]). However, until now an accuracy of the corresponding available data has not been fully adequate to predict or identify transitions within accuracy as required for many applications. It is obvious that correct taking into account the relativistic and correlation effects is absolutely necessary in order to obtain sufficiently adequate description of spectroscopy of the heavy atoms in an atmosphere of the buffer gases. This stimulated our current investigation whose goals were to apply a relativistic PT approach [15,16] to calculating the interatomic potentials and hyperfine structure line collision shifts for some complicated (Tl, Pb) atoms in an atmosphere of the inert gases. The basic expressions for the collision shift and broadening hyperfine structure spectral lines are taken from the kinetic theory of spectral lines [2,5,7]. The exchange perturbation theory (the modified version EL-HAV) has been used to calculate the corresponding potentials (see de-

tails in [1]). Finally, new data on the oscillator strength of the forbidden transition in the lead are presented too.

2. Relativistic theory of spectral line shift for system "heavy atom-inert gas"

In order to calculate a collision shift of the hyperfine structure spectral lines one can use the following expression known in the kinetic theory of spectral lines shape (see Refs. [5,7]):

$$f_p = \frac{D}{p} = \frac{4\pi w_0}{kT}\int_0^\infty dw(R)\exp\left(-U(R)/kT\right)R^2 dR \qquad (1)$$

Here *U(R)* is an effective potential of interatomic interaction, which has the central symmetry in a case of the systems *A—B (*in our case, for example, *A*=Rb,Cs*; B*=He*)*; *T* is a temperature, w_0 is a frequency of the hyperfine structure transition in an isolated active atom; $dw(R)=Dw(R)/w_0$ is a relative local shift of the hyperfine structure line. The local shift is caused due to the disposition of the active atoms (say, the atoms of lead Pb and helium He) at the distance *R*. In order to calculate an effective potential of the interatomic interaction further we use the exchange PT formalism (the modified version EL-HAV) [1]. The relative local shift of the hyperfine structure line is defined as follows:

$$\delta\omega(R) = \frac{S_0}{1-S_0} + \Omega_1 + \Omega_2 - \frac{C_6}{R^6}\left(\frac{2}{\bar{E}_a} + \frac{1}{\bar{E}_a + \bar{E}_B}\right),$$
$$\bar{E}_{a,b} = \left(I_{a,b} + E_{1a,b}\right)/2. \qquad (2)$$

Here S_0 is the overlapping integral; C_6 is the van der Waals coefficient; *I* is the potential of ionization; $E_{1a,b}$ is the energy of excitation to the first (low-lying) level of the corresponding atom. The values W_1, W_2 in Eq. (2) are the first order non-exchange and exchange non-perturbation sums correspondingly [1,5,6]. These values are defined as follows:

$$\Omega_1 = \frac{2}{N(1-S_0)\rho_0}\sum_k{}' \frac{\langle \Phi_0'(1)\left|H_{HF}'\right|\Phi_k'(1)\rangle V_{k0}}{E_0 - E_k}$$
$$\Omega_2 = \frac{2}{N(1-S_0)\rho_0}\sum_k{}' \frac{\langle \Phi_0'(1)\left|H_{HF}'\right|\Phi_k'(1)\rangle U_{k0}}{E_0 - E_k}$$
$$\rho_0 = <\Phi_0^1(1)\left|H_{HF}'\right|\Phi_0'(1)\rangle / <\Phi_0^1(1)\left|\Phi_0'(1)\right\rangle$$

where $\acute{I}_{HF}'$ is the operator of hyperfine interaction; *N* is the total number of electrons, which are taken into account in the calculation; E_k, $\Phi_k'(1) = F_{k_a}'(1)\varphi_{k_b}(2\ldots N)$ are an energy and a non-symmetrized wave function of state $k=\{k_a,k_b\}$ for the isolated atoms *A* and *B*. The non-exchange matrix element of the Coulomb interatomic interaction is as:

$$V_{ko} = <\Phi'_k(1) \mid V(1) \mid \Phi'_0(1)>.$$

Correspondingly the exchange matrix element is as follows:

$$U_{k0} = \sum_{i=2}^{N}\langle \Phi_k'(1)\left|V(i)\right|\Phi_0'(i)\rangle$$

The operator *V (i)* (for example, in a case of the system Tl-He), as follows:

$$V(i) = U_{SCF}(r_{a3}) + U_{SCF}(r_{a4}) - 2U_{SCF}(R) + \frac{1}{r_{bi}} \qquad (3)$$

where $U_{SCF}(r)$ is the self-consistent field, created by the lead atomic core.

Let us return to consideration of the van der Waals coefficient C_6 for the interatomic *A-B* interaction. As a rule, one could use the approximate values for the van der Waals constant C_6. However, sufficiently large error in definition of the van der Waals constants could provide a low accuracy of calculating the interatomic potentials. The van der Waals coefficient may be written as [2,9]:

$$C_6(L,M) = C_{6,0}(L) - \frac{3M^2 - L(L+1)}{(2L-1)(2L+3)}\cdot C_{6,2}(l) \qquad (4)$$

where $C_{6,0}$ *(L)* is the isotropic component of the interaction and $C_{6,2}$ *(L)* is the component corresponding to the $P_2(cosq)$ term in the expansion of the interaction in Legendre polynomials, where the angle specifies the orientation in the space-fixed frame. The dispersion coefficients $C_{6,0}$ *(L)* and $C_{6,2}$

(L) may be expressed in terms of the scalar and tensor polarizabilities $\alpha_0(L;iw)$ and $\alpha_2(L;iw)$ evaluated at imaginary frequencies [9]. In particular, one may write in the helium case as follows:

$$C_{6,0}(L) = \frac{3}{\pi} \cdot \int_0^\infty \alpha_0(L;iw)\overline{\alpha}_{He}(iw)dw \qquad (5)$$

where $\overline{\alpha}_{He}$ is the dynamic polarizability of He. The polarizabilities at imaginary frequencies are defined in atomic units by the following formula:

$$\alpha_{\|}(L,M;iw) = 2\sum_{\gamma,M_\gamma} \frac{(E_\gamma - E_L)|< LM|\hat{z}|L_\gamma M_\gamma >|^2}{(E_\gamma - E_L)^2 + w^2} \qquad (6)$$

where E_g is the energy of the electronically excited state $|L_g M_g >$ and the z axis lies along the internuclear axis. As a rule, (see, for example, Refs. [2,6-10]), the non-relativistic Hartree-Fock or the non-relativistic Kohn-Sham (KS) density functional or relativistic Dirac-Fock methods were used for calculating the corresponding wave functions. Another variant is using the relativistic wave functions as the solutions of the Dirac equations with the corresponding density functionals (Dirac-Kohn-Sham=DKS theory) and effective correlation potentials [14,15]. In our calculation we have used the relativistic PT with the optimized DKS zeroth approximation. The detailed approbation of method in studying spectra and radiative parameters the atoms is given in Refs. [15-18].

3. Results and conclusions

In Table 1 we present the results of our calculating energies of levels in ^{205}Tl: experimental data and the results of the calculation method in the framework of the relativistic Hartree-Fock (RHF), the time-dependent theory of RHF (TDRHF), RMBPT-DF (see [23] and references therein) and our theory. Our data are in quite good agreement with the experimental data and data by the RMBPT-DF.

Table 1. **Energy (cm-1) levels for ^{205}Tl: experiment and theor.data: RHF, TDRHF, RMBPT-DF and our theory (see text)**

	RHF	TDR HF	RPT DF	Exp	Our
7s	21100	22952	22818	22786	22809
$6p_{1/2}$	43909	50654	-	49264	49308
$7p_{1/2}$	14282	15203	-	15104	15154
$6p_{3/2}$	36670	42704	41432	41471	41501
$7p_{3/2}$	13359	14224	-	14103	14145
$6d_{3/2}$	12218	13130	13175	13146	13167
$6d_{5/2}$	12167	13042	-	13064	13083

Table 2. **E1 amplitudes (in units ea_B) for Tl: Experiment and calculation data by RHF (RHF), DF plus cong. interaction (DF + CI), TDRHF, and our data**

	L V	RHF	DF-CI	TDR HF	Our.	Exp.
$6p_{1/2}$-7s	L	2.50	2.32	2.14	2.21	2.23
	V	2.00	1.92	2.15	2.21	(6)
$6p_{3/2}$-7s	L	3.43	3.10	2.81	2.82	2.83
	V	2.75	2.55	2.84	2.81	(6)
$6p_{1/2}$-8s	L	0.80	0.71	0.64	0.67	0.67
	V	0.61	0.56	0.65	0.66	(3)
$6p_{1/2}$-8s	L	0.86	0.77	2.63	0.65	-
	V	0.64	0.61	0.65	0.65	
$7p_{1/2}$-7s	L	-8.14	-7.52	-7.20	-7.25	-7.27
	V	-7.72	-7.07	-7.13	-7.24	(7)
$7p_{3/2}$-7s	L	-7.65	-7.08	-6.85	-6.81	-6.84
	V	-7.22	-6.86	-6.79	-6.80	(7)

In table 2 there listed the theoretical and experimental data in the amplitudes E1 transitions in thallium, in particular it is clear that methods of the RHF type without accounting correlation effects does not provide a precise description of the desired amplitude accuracy.

In Table 3 we present our theoretical results for the collisional shift f_p (Hz / Torr) in a case of the pairs: TI - He, TI - Kr, Tl-Xe at T = 700K: Experiment by Chorou-Scheps-Galagher (Virginia group); Theory: A- DF method [7], B-optimized KS method with approximate estimate the constant C_6 [10] (see also[21,22]) and our theory. The important feature of our scheme is correct taking into account the correlation (polarization) effects with using special effective functionals from [15,19].

Table 3. **Collisional shift f_p (Hz / Torr) in a case of the pairs: TI - He, TI - Kr, Tl-Xe at T = 700K: Experiment by Chorou-Scheps-Galagher;**
Theory: A- DF method, B-optimized KS method with approximate estimate the constant C_6 and our theory.

Pair	T1-He	T1-Kr	T1-Xe
Exp.	130 ± 30	-490±20	-1000±80
Th:A	155.0	-850.0	-1420.0
Th:B	137.2	-504	-1052
Our: C	135.4	-501	-1036

Table 4 shows our values (C) of the collisional shift of the hyperfine lines for thallium at different temperatures (T, K) for the systems TI-He,

Table 4. **Collisional shift f_r (Hz/Torr) of the hyperfine lines for thallium at different temperatures (T, K) for the systems TI-He, Kr, Xe**

Pair	T1-He	T1-He	T1-He
T, K	Th:A	Th:B	Th:C
700	155	137,2	135,4
800	151	134,1	132,9
900	147.5	131,4	129,5
1000	143	126,2	124,4
Pair	T1-Ar	T1-Kr	T1-Xe
T, K	Th:C	Th:C	Th:C
700	-112	-501	-1036
800	-107	-418	-878
900	-102	-357	-772
1000	-94	-304	-694

Kr, Xe with alternative data from theories: A- DF approach [6] , B - optimized KS method [10]. The difference between our theoretical data and other calculation results can be explained by using different PT schemes and different approximations for calculating the wave functions. It is obvious that the using correct version of the exchange PT will be necessary for an adequate description of the energetic and spectral properties of the heavy atoms in an atmosphere of the inert gases. In Table 5 we list our (C) calculated values for the reduced adiabatic broadening of G_a/p for the thallium hyperfine line at different temperatures for the systems: TI - He. TI - Kr, TI-Xe together with results of other theories (theory A- DF approach [6] , B - optimized KS method [10]).

Table 5. **The adiabatic broadening G_a/p for the thallium hyperfine line at different temperatures in the the systems: TI - He. TI - Kr, TI-Xe (results of different theories: theory A- DF approach [6] , B - optimized KS method [10].**

T	TI-He A	TI-He B	TI-He C	TI-Kr C	TI-Xe C
700	2.83	2.51	2.45	6.50	15.9
800	2.86	2.54	2.48	5.58	13.8
900	2.90	2.58	2.51	4.98	11.4
10^3	2.89	2.56	2.48	4.28	10.0

The important aspect of the theory is an estimate of the ratio of $[G_a/p]/f_p$. According to our data this ratio is as follows: $G_a/p / f_p \sim 1/55$ for the system TI - He, $G_a/p / f_p \sim 1/80$ for the system TI - Kr and $(G_a/p / f_p) \sim 1/65$ system TI-Xe, i.e. the known Folly relationship ($G_a/p \sim f_p$) is not correct in a case of the thallium hyperfine line.

It is obvious that the pair “Tl-inert gas” is sufficiently complicated system, for example in comparison with such a systems as the pair of “alkali atom-atom of inert gas”. Obviously more detailed experimental studying as this atom as other interesting heavy atoms is very desirable.

Nevertheless, we believe that our data may be considered as very useful reference especially if there will be performed the further measurement of the temperature dependence for the collisional shift and adiabatic broadening parameters in a wide interval of the thermodynamical parameters.

References

1. Kaplan I. G., Theory of intermolecular interactions.-Moscow: Nauka, 1985.
2. Torrens I. M., Interatomic potentials.-N-Y.: Academic Press, 1972.
3. Sobel'man, I. I. Introduction to theory of atomic spectra.- Moscow: Nauka, 1977.
4. Khetselius O. Yu., Hyperfine structure of atomic spectra.-Odessa: Astroprint, 2008.
5. Freeman A. J., Frankel R. H., Hyperfine interactions.- N-Y.: Plenum, 1987.
6. Batygin V. V., Gorny M. B., Gurevich B. M., Interatomic potentials, shifts of hyperfine structure lines and diffusion coefficients of atoms of rubidium and caesium in the buffer helium // J.Techn.Phys.-1978.-Vol.48 - P. 1097-1105.
7. Batygin V. V., Sokolov I. M., Collisional shift and adiabatic broadening of line of the hyperfine transition in the ground state of thallium in an atmosphere of the buffer helium, krypton and xenon // Opt. Spectr.-1983.-Vol.55.-P. 30-38.
8. Alexandrov E. B., Popov V. I., Yakobson N.N., The optical pumping of the thallium atoms on the line of 21GHz// Opt. Spectr.-1979.-Vol.46.-P. 404-408.
9. Chi X., Dalgarno A., Groenenborn G.C., Dynamic polarizabilities of rare-earth-metal atoms and dispersion coefficients for their interaction with helium atoms // Phys. Rev. A.-2007.-Vol.75.-P. 032723.
10. Glushkov A.,Khetselius O., Mischenko E., Gurnitskaya E., Loboda A., Florko T., Sukharev D., Collisional shift of the Tl hyperfine lines in atmosphere of inert gases // Spectral Line Shapes (AIP).-2008.-Vol. 15.-P. 231-233.
11. Glushkov, A. V. Relativistic quantum theory. Quantum mechanics of atomic systems, Odessa: Astroprint, 2008.
12. Ehrlacher E., Huennekens J., Noble-gas broadening rates for barium transitions involving the metastable 6s5d ^3D_j levels // Phys.Rev.A.-1992.-Vol.46.-P. 2642-2648.
13. Franzke J., Wizemann H. D., Niemax K., Vadla C., Impact broadening and shift rates for the $6p^2\ ^3P_{J¢}$ ®$7s\ ^3P_J^o$ transitions of lead induced by collisions with argon and helium//
14. Kötteritzsch M., Gries W., Hese A., Foreign gas broadening and shift in the lead resonance line at lambda =283.3 nm // J. Phys. B:At. Mol. Opt. Phys.-1992.-Vol.25.-P. 913-918.
15. Malinovskaya S., Glushkov A., Svinarenko A., Khetselius O., Mischenko E., Florko T.A., Optimized perturbation theory scheme for calculating the interatomic potentials and hyperfine lines shift for heavy atoms in the buffer inert gas // Int. Journ. of Quantum Chemistry.-2009.-Vol.109,N14.-P. 3325-3329
16. Svinarenko A. A., Mischenko E. V., Loboda A. V., Dubrovskaya Yu.V., Quantum measure of frequency and sensing the collisional shift of the ytterbium hyperfine lines in medium of helium gas // Sensor Electronics and Microsystem Techn.- 2009.- N1.-P. 25-29.
17. Glushkov A. V., Svinarenko A. A., Ignatenko A. V., Spectroscopy of autoionization resonances in spectra of the lanthanides atoms // Photoelectronics.-2011.-Vol.20.- P. 90-94.
18. Svinarenko A. A., Nikola L. V., Prepelitsa G. P., Tkach T., Mischenko E., The Auger (autoionization) decay of excited states in spectra of multicharged ions: Relativistic theory // Spectral Lines Shape.-2010.- Vol. 16.-P. 94-98
19. Glushkov A. V., Ivanov L. N., Ivanova E. P., Radiation decay of atomic states. Generalized energy approach // Autoionization Phenomena in Atoms.-M.: Moscow State Univ.-1986.
20. Ivanov L.N., Letokhov V.S. Spectroscopy of autoionization resonances in heavy elements atoms // Com.Mod. Phys.D.: At. Mol. Phys. - 1985.-Vol.4.-P. 169-184.
21. Jamieson M. J., Drake G. W. F., Dalgarno A., Variational calculation of the dynamic polarizabilities of rare-earth

metal atoms / // Phys.Rev. A.-1995.-Vol.51.-P. 3358-3370.
22. Buchachenko A. A., Szczesniak M. M., Chalasinski G., Calculation of the Van der Waals coefficients for interaction of rare-earth metal atoms with helium atoms // J. Chem. Phys.-2006.-Vol.124.-P. 114301.
23. Dzuba V. A., Flambaum V. V., Silvestrov P.G., Sushkov D.E.Many-body perturbation theory calculations in atoms with open shells // Phys.Rev.A-1991.-Vol.44.-P. 2828-2831.

The article is received in editorial 29.07.2013

UDC 539.184

Yu. M. Lopatkin, V. I. Mikhalenko, A. A. Svinarenko

SPECTROSCOPY OF THE HYPERFINE LINES SHIFT FOR HEAVY ELEMENTS IN THE BUFFER INERT

Abstract

A new relativistic approach, based on the gauge-invariant perturbation theory (PT), is applied to calculating the spectral line collisional broadening and shifts for the heavy atom (thallium) in an atmosphere of the buffer inert gases. It is shown that the relation of the adiabatic broadening to collisional shift is ~ 1/55 for the system TI - He, 1/80 for the system TI - Kr and ~ 1/65 system TI-Xe, i.e. the known Folly spectral relationship is not correct in a case of the thallium hyperfine lines.

Key words: spectral lines shift, broadening, heavy elements, buffer gas, relativistic theory

УДК 539.184

Ю. М. Лопаткин, В. И. Михайленко, А. А.Свинаренко

СПЕКТРОСКОПИЯ СДВИГОВ ЛИНИЙ СВЕРХТОНКОЙ СТРУКТУРЫ ТЯЖЕЛЫХ ЭЛЕМЕНТОВ В БУФЕРНОМ ГАЗЕ

Резюме

Новый релятивистский подход, основанный на калибровочно-инвариантной теории возмущений, применен для расчета столкновительного сдвига и адиабатического уширения спектральных линий тяжелого атома (таллий) в атмосфере буферных инертных газов. Показано, что отношение адиабатического уширения к столкновительному сдвигу составляет ~ 1/55 для системы TI-He, ~ 1/80 для системы TI-Kr и ~ 1/65 для системы TI-Xe, что подтверждает некорректность известного спектрального отношения Фоли в случае линий сверхтонкой структуры таллия.

Ключевые слова: сдвиг, уширение спектральных линий, тяжелые элементы, буферный газ, релятивистская теория

УДК 539.184

Ю. М. Лопаткін, В. І. Міхайленко, А. А. Свинаренко

СПЕКТРОСКОПІЯ ЗСУВІВ ЛІНІЙ НАДТОНКОЇ СТРУКТУРИ ВАЖКИХ ЕЛЕМЕНТІВ В БУФЕРНОМУ ГАЗІ

Резюме

Новий релятивістський підхід, який базується на калібрувально-інваріантної теорії збурень, застосовано для розрахунку зсуву та адіабатичного уширення за рахунок зіткнень для важкого атома (таллій) в атмосфері буферних інертних газів. Показано, що відношення адіабатичного уширення для зсуву за рахунок зіткнень складає ~ 1/55 для системи TI -He, 1/80 для системи TI-Kr та ~ 1/65 для системи TI-Xe, що підтверджує некоректність відомого спектрального відношення Фолі у випадку надтонких ліній таллія.

Ключові слова: зсув, уширення спектральних ліній,, важкі елементи, буферний газ, релятивістська теорія

UDC 539.184

O. Yu. Khetselius

I. Mechnikov Odessa National University, 2, Dvoryanskaya str., Odessa, Ukraine
Odessa State Environmental University, 15, Lvovskaya str., Odessa, Ukraine
e-mail: nuckhet@mail.ru

HYPERFINE STRUCTURE PARAMETERS OF THE HEAVY ISOTOPES: CONSISTENT NUCLEAR-QED THEORY

It is presented the new, consistent theoretical nuclear-QED approach to estimating parameters of the hyperfine structure of the heavy isotopes, which is based on the relativistic mean field theory of a nucleus and QED perturbation theory. The hyperfine structure parameters for the heavy isotopes of ^{205}Tl and ^{169}Tm are calculated. The theoretical values of the relative contribution into the hyperfine structure due to the effect of the distribution of the magnetic moment of the nucleus are listed too.

1. Introduction

A development of a new effective nuclear schemes and technologies for sensing different nuclear properties, studying the properties of heavy isotopes is of a great importance in the modern atomic, nuclear physics and technologies [1-3]. Among the most important problems one could mention the studying of nuclei, which are available in the little quantities (for example, the lanthanides isotopes, radioactive nuclei far of the stability boundary), search of the super dense nuclei and its sensing, laser governing by parameters of the proton and other beams and sensing their characteristics etc [1-17]. Such possibilities are provided by the modern laser methods and technologies (see, for example, [1,2]). A high sensibility and resolution ability of laser spectroscopy methods allows investigating the characteristics of nuclei available in the little quantities, heavy isotopes. As an example (see ref. [1-6]) one can mention the CERN technical device for studying the short-lived nuclei which are obtained on the mass-separator in the line with synchrocyclotrone on 600 MeV (ISOLDE apparatus [1]). The shocking results have been obtained in studying of the odd neutron-deficit non-stable isotopes of $^{182-190}$Hg. The intensity of the ion beams of these isotopes with life time 1-60 min was 10^7-10^9 ions/s. Under excitation of fluorescence by dye pulsed laser radiation the second harmonics of radiation was tuning to region of 2537A and the measurement of the hyperfine structure for this line of Hg was carried out during 1-2 min disposing about 10^8 of the mercury isotope atoms. During transition from nucleus ^{186}Hg to nucleus ^{185}Hg it has been discovered the sharp changing of the middle square of the nuclear radius which is interpreted as sharp changing of the nuclear form (increasing of non-soherity and electric quadrupole moment) during decreasing the neutrons number. In refs. [17-25] (see also [4,5]) we have developed new effective theoretical scheme with possibility of advancing corresponding nuclear technology for sensing different spectral parameters, including the hyperfine structure ones, for heavy isotopes and elements available in the little quantities. It is based on the experimental receiving the isotope beams on the CERN ISOLDE type apparatus (see detailed description in refs. [1,3,4]) and the précised theoretical and laser spectroscopy empirical estimating the hyperfine structure parameters, magnetic and electric moments of a nucleus of isotopes. We have carried out sensing and estimating the hyperfine structure parameters, magnetic and electric moments of a nucleus for ^{235}U, ^{201}Hg and rare cosmic isotopes. Theory of the hyperfine structure calculation is based on developed ear-

lier gauge-invariant QED PT formalism with an precise account of the exchange-correlation (inter electron interaction corrections), nuclear and QED effects and nuclear relativistic mean field (RMF) theory. In this paper we consider its application to studying hyperfine structure parameters for some heavy isotopes, in particular, the corresponding data for the ^{205}Tl and ^{169}Tm isotopes are listed.

Let us also remind that the accurate measurements of the hyperfine structure parameters for a whole number of heavy isotopes (e.g. [1,6,16]) not only provide the possibility for testing the quantum electrodynamics (QED) in strong fields, but also sensing the hyperfine structure parameters of spectra for heavy atomic systems, electric charge and magnetic moment distributions inside the nucleus [5-10]. Theoretical calculations fulfilled during the last several years apart from the basis Fermi-Breit relativistic contributions also include the magnetic dipole moment distribution inside the nucleus (Bohr-Weisskopf effect) and radiative QED corrections (e.g. [1-6]). In calculations of the heavy ions the well known multiconfiguration (MC) Dirac-Fock (DF) approach is widely used (e.g.[14-20]).

2. Theoretical approach to calculating hyperfine structure parameters

Let us describe the key moments of the theoretical scheme. Full details of the whole method of calculating the hyperfine structure constants can be found in [4,5,17-24]. The wave electron functions zeroth basis is found from the Dirac equation solution with potential, which includes the core ab initio potential, electric, polarization potentials of nucleus. All correlation corrections of the second and high orders of PT (electrons screening, particle-hole interaction etc.) are accounted for [17]. The concrete nuclear model is used as described below. A quantitative estimate of the nuclear moments demands realistic proton single-particle wave functions which one could obtain by employing the RMF model of a nucleus. Though we have no guaranty that these wave-functions yield a close approximation to nature, the success of the RMF approach supports our choice (e.g.[26]). These wave functions do not suffer from known deficiencies of other approaches, e.g., the wrong asymptotics of wave functions obtained in a harmonic oscillator potential. The RMF model has historically been designed as a renormalizable meson-field theory for nuclear matter and finite nuclei. The realization of nonlinear self-interactions of the scalar meson led to a quantitative description of nuclear ground states. As a self-consistent mean-field model (for a comprehensive review see Ref. [25]), its ansatz is a Lagrangian or Hamiltonian that incorporates the effective, in-medium nucleon-nucleon interaction. Recently self-consistent models have undergone a reinterpretation which explains their quantitative success in view of the facts that nucleons are composite objects and that the mesons employed in RMF have only a loose correspondence to the physical meson spectrum [25-28]. RMF models are effective field theories for nuclei below an energy scale of 1GeV, separating the long- and intermediate-range nuclear physics from short-distance physics, involving, i.e., short-range correlations, nucleon form factors, vacuum polarization etc, which is absorbed into the various terms and coupling constants. As it is indicated in refs.[27] the strong attractive scalar (*S:* -400 MeV) and repulsive vector (*V:* +350 MeV) fields provide both the binding mechanism (*S* + *V:* -50 MeV) and the strong spin-orbit force (*S* – *V:* -750 MeV) of both right sign and magnitude. In our calculation we have used so called NL3 (c.f.[25]), which is among the most successful parametrizations available.

The scheme of accounting for the finite size effect is in details described in ref. [17]. Here we only note that if the point-like nucleus possesses by some central potential *W(R)* then transition to potential of the finite nucleus is realized by substitution *W(r)* on

$$W(r|R) = W(r)\int_0^r dr\, r^2 \rho(r|R) + \int_r^\infty dr\, r^2 W(r)\rho(r|R) \ .$$

In our case the Coulomb potential for spherically symmetric density $\rho(r|R)$ is:

$$V_{nucl}(r|R) = -\left((1/r)\int_0^r dr'\, r'^2 \rho\left(r'\middle|R\right) + \int_r^\infty dr'\, r'\, \rho\left(r'\middle|R\right)\right.$$

Further the standard Dirac-Fock -like equations for a multi-electron system {core-*nlj*} are solved. Formally they fall into one-electron Dirac equations for the orbitals *nlj* with potential: $V(r)=2V(r|SCF)+V(r|nlj)+V_{ex}+V(r|R)$. It includes the electrical and polarization potentials of a nucleus with a finite size. The part V_{ex} accounts for exchange inter-electron interaction. The exchange effects are accounted for in the first two PT orders by the total inter-electron interaction [17]. The core electron density is defined by iteration algorithm within QED procedure [4]. The radiative QED (the self-energy part of the Lamb shift and the vacuum polarization contribution) are accounted for within the QED formalism [4,25]. The hyperfine structure constants are defined by the radial integrals of the known type (e.g. [29,17]):

$$A=\{[(4{,}32587)10^{-4}Z^2cg_I]/(4c^2\text{-}1)\}$$
$$\int_0^\infty drr^2F(r)G(r)U(1/r^2,R)$$
$$B=\{7.2878\ 10^{-7}\ Z^3Q/[(4c^2\text{-}1)I(I\text{-}1)\}$$
$$\int_0^\infty drr^2[F^2(r)+G^2(r)U(1/r^2,R)$$

Here I is a spin of nucleus, g_I is the Lande factor, Q is a quadruple momentum of nucleus; radial integrals are calculated in the Coulomb units ($=3.57\times10^{20}Z^2m^{-2}$; $=6.174\ \ 10^{30}\ Z^3m^{-3}$). Radial parts F and G of two components of the Dirac function for electron, which moves in the potential are defined by solution of the Dirac equations (PT zeroth order). The other details can be found in refs. [17-25].

3. Estimating the hyperfine structure parameters and conclusions

Earlier we have studied the hyperfine structure of spectra for the elements Be, C, Al, U, which have above cited rare, cosmic isotopes. Here we present the results of studying (the Superatom package [4,5] is used) the hyperfine structure parameters for the heavy isotopes of ^{205}Tl and ^{169}Tm. In table 1 we present the values of the hyperfine splitting Dn(F, F') (in MHz) for ^{169}Tm ($^2F_{7/2}$) (nuclear spin 1/2) with available theoretical (MCDF) and experimental or compilation data [30].

Table 1. **The hyperfine splitting Dn(F, F') (in MHz) of levels for ^{169}Tm ($^2F_{7/2}$)**

Isotope; Spin of nucleus	Term	Quantum numbers total moment F, F'	$\Delta\nu(F, F')$, MHz [30]	Theory, MCDF	Theory, Present Wok
^{169}Tm ($^2F_{7/2}$) 1/2	4 $^2F_{7/2}$	(4, 3)	1496.55	1484.8	1496.12

Table 2 lists the experimental (A^{Exp}) and theoretical values of the constant A (in GHz) for the valence states ^{205}Tl, in particular, the theoretical value obtained by calculation within the method of single DF (A^{DF}), the method including single- and double- excited states (A^{SD}), DF method, taking into account the configuration interaction (A^{DF+C}), multiconfiguration DF method (A^{MCDF}), relativistic cluster-coupled method, taking into account the finite size of the nucleus ($A^{RCC\text{-}FS}$), a modified Hartree-Fock (A^{gHF}), the time-dependent relativistic Hartree-Fock theory (A^{TDRHF}), the same method, but taking into account the correlations and the finite size of the nucleus ($A^{TDRHF+C}$) and the nuclear-QED theory ($A^{N\text{-}QED}$) (from [14 -18]). Analysis of the data shows that an account of the interelectron correlation effects is crucial in the calculation of the hyperfine structure parameters and therefore the conventional methods such as the method of DF (of single approximation) as well as the method with the limited accounting the exchange-correlation effects do not give a sufficiently high accuracy. Significantly better data in terms of accuracy and consistency to the experiment results are obtained on the basis of the calculation in the framework of the relativistic cluster-coupled method, taking into account the finite size of the nucleus ($A^{RCC\text{-}FS}$), the time-dependent relativistic theory with accounting the correlations and the finite size of the nucleus ($A^{TDRHF+C}$) and nuclear-QED theory. Naturally, a precise agreement between theory and experiment can be reached by means accounting for not

only the relativistic and exchange-correlation effects, but the radiative QED corrections, the nuclear effects of Bohr-Weisskopf, Breit-Rosenthal-Crawford-Schawlow etc too.

Table 2. **Experimental (A^{Exp}) and theoretical values of the constant A (in GHz) for the valence states of ^{205}Tl (see text)**

Method/State	$6p_{1/2}$	$6p_{3/2}$	$7s_{1/2}$
A^{DF}	17.68	1.304	7.78
A^{DF+C}	20.86	0.256	12.67
A^{RCC+FS}	21.43 21.30	0.317 0.339	12.92 12.76
A^{SD-DF}	18.73	1.381	-
A^{MCDF}	20.32	1.485	-
A^{gHF}	20.89	0.895	-
A^{RMBPT}	21.663	0.248	12.666
A^{TDRHF} $A^{TDRHF+C}$	24.06 21.30	-1.885 0.600	13.06 12.56
A^{N-QED}	21.3098	0.2535	12.2713
A^{exp}	21.3108	0.2650	12.2972

In Table 3 we list the theoretical value of the relative contribution (the value of $D/l_{c,m}$) into the hyperfine structure due to the effect of the distribution of the magnetic moment of the nucleus. There are presented data, estimated by the different methods, namely, the single-configuration Dirac-Fock (DF) method, the relativistic cluster-coupled method, taking into account the finite size of the nucleus (ARCC-FS) and nuclear-QED theory (see [14-18]). The cited parameter has a simple physical meaning. The shift in the hyperfine structure constant for two different isotopes (nuclear $g=m/I$ factor) is usually estimated as: A_1g_2/A_2g_1-1=D.

On the other hand, the variation of the charge distribution in a nucleus core, as known from the theory of the isotope shift, leads to the known correction: $l_{c,m}=k_c<d<(r_c)^2>$, where the k_c factor takes into account the higher moments of the distribution of the charge. For ^{205}Tl there are known the experimental data on the parameters D and $l_{c,m}$, derived from the values of the magnetic moments ^{203}m =1.622258m_N и ^{205}m =1.638315m_N [16]. The analysis shows that the contribution to the «perturbation» of the hypefine structure for the thallium has roughly equal to the effects of Bohr-Weisskopf and Breit-Rosenthal-Crawford-Schawlow.

Table 3. **Experimental and theoretical values for the $D/l_{c,m}$ (10^{-4}/fm^2) for the valence states of the ^{205}Tl: single-configuration Dirac-Fock (DF), relativistic cluster-coupled method with accounting the finite size effect (A^{RCC-FS}) and nuclear-QED theory (A^{N-QED})**

Method/State	$6p_{1/2}$	$6p_{3/2}$	$7s_{1/2}$
$(\Delta/\lambda_{c,m})^{DF}$	-2.26	-	-7.95
$(\Delta/\lambda_{c,m})^{RCC+FS}$	-2.48	43.0	-7.62
$(\Delta/\lambda_{c,m})^{N-QED}$	-2.4735	42.68	-7.54
Experiment Δ $\lambda_{c,m}$	-2.4762 -1.04 0.42	42.79 16.26 0.38	-7.56 -3.4(18) 0.45(24)

References

1. Letokhov V. S., Non-linear selective photoprocesses in atoms and molecules.- Moscow: Nauka, 1987.- 380 P.
2. Klaft I., Borneis S., Engel T., Fricke B., Grieser R., Huber G., Kuhl T., Marx D., Neumann R., Schroder S., Seelig P., Volker L. Precision laser spectroscopy of ground state hyperfine splitting of H-like $^{209}Bi^{82+}$ // Phys.Rev.Lett.-1994.- Vol. 73.-P. 2425-2427.
3. Glushkov A.V., Relativistic and correlation effects in spectra of atomic systems.-Odessa: Astroprint, 2006.- 400 P.
4. Glushkov A.V., Khetselius O.Yu., Ambrosov S.V., Loboda A.V., Gurnitskaya E.P., QED calculation of heavy ions with account for the correlation, radiative and nuclear effects // Recent Adv. in Theor. Phys. and Chem. Systems (Springer). - 2006.-Vol. 15.-P. 285-300.
5. Glushkov A. V., Khetselius O. Yu., Ambrosov S. V., Loboda A. V., Chernyako-

va Yu.G., Svinarenko A. A., QED calculation of the superheavy elements ions: energy levels, radiative corrections and hfs for different nuclear models// Nucl. Phys.A.: Nucl.and Hadr. Phys. –2004.-Vol.734.-P. 21-28.
6. Freeman A. J., Frankel R. H., Hyperfine interactions.-N-Y.: Plenum, 1987.-340P.
7. Nagasawa T., Haga A., Nakano M., Hyperfine splitting of hydrogenlike atoms based on relativistic mean field theory // Phys.Rev.C.-2004.-Vol.69.-P. 034322:1–10.
8. Tomaselli M, Kuhl T., Nortershauser W., Borneis S., Dax A., Marx D, Wang H, Fritzsche S., Hyperfine splitting of hydrogenlike thallium // Phys. Rev.A-2002.-Vol. 65.-P. 022502.
9. Tomaselli M., Kuhl T., Seelig P., Holbrow C. and Kankeleit E., Hyperfine splittings of hydrogenlike ions and the dynamic-correlation model for one-hole nuclei // Phys.Rev.C.-1998.-Vol.58, N3.-P. 1524-1534.
10. Tomaselli M., Schneider S. M., Kankeleit E., Kuhl T., Ground state magnetization of ^{209}Bi in a dynamic-correlation model // Phys.Rev.C.-1995.-Vol. 51, N 6.-P. 2989-2997.
11. Benczer-Koller N., The role of magnetic moments in the determination of nuclear wave functions of short-lived excited states // J.Phys.CS.-2005.-Vol. 20.-P. 51-58.
12. Bieron J., Pyykko P., Degree of accuracy in determining the nuclear electric quadrupole moment of radium // Phys. Rev. A.- 2005.-Vol. 71.-P. 032502.
13. Derevianko A., Porsev S. G., Dressing lines and vertices in calculations of matrix elements with the coupled-cluster method and determination of Cs atomic properties // Phys.Rev. A.-2005.-Vol.71.-P. 032509.
14. Safronova M. S., Johnson W. R., Safronova U. I., Excitation energies, hyperfine constants, E1,E2,M1 transition rates and lifetimes of $6s^2nl$ states in TlI and PbII // Phys.Rev.A.-2005.-Vol. 71.-P. 052506.
15. Martensson A. M., Gouch D. S., Hanaford P., Relativistic coupled-cluster approach to hyperfine structure of Tl atom // Phys. Rev.A.1993 -.Vol. 49.-P. 3351-3360.
16. Martensson A. M., Magnetic moment distributions in Tl nuclei // Phys. Rev. Lett.-1995.-Vol. 74.-P. 2184-2188.
17. Khetselius O. Yu., Hyperfine structure of atomic spectra.-Odessa: Astropritn, 2008.-210 P.
18. Khetselius O. Yu., Relativistic perturbation theory calculation of the hyperfine structure parameters for some heavy-element isotopes // Int. Journ. of Quantum Chemistry.-2009.-Vol. 109.- N14.-P. 3330-3335
19. Khetselius O. Yu., Gurnitskaya E. P., Sensing the electric and magnetic moments of a nucleus in the N-like ion of Bi // Sensor Electr. and Microsyst. Tech.- 2006.-N 3.-P. 35-39.
20. Khetselius O. Yu., Gurnitskaya E. P., Sensing the hyperfine structure and nuclear quadrupole moment for radium // Sensor Electr. and Microsyst. Techn.-2006.-N 2.-P. 25-29.
21. Glushkov A. V., Khetselius O. Yu., Gurnitskaya E. P., Florko T. A., Sensing of nuclei available in little quantities by means of laser spectroscopy of hyperfine structure for isotopes: new theoretical scheme (U ,Hg) // Sensor Electr. and Microsyst. Techn.- 2007.-N 3.-P. 21-26.
22. Khetselius O. Yu., On possibility of sensing nuclei of the rare isotopes by means of laser spectroscopy of hyperfine structure // Sensor Electr. and Microsyst. Techn.-2007.-N4.-P. 11-16.
23. Khetselius O. Yu., Hyperfine structure of energy levels for isotopes ^{73}Ge, ^{75}As, ^{201}Hg // Photoelectronics.-2007.-N16.-P. 129-132.
24. Khetselius O. Yu., Hyperfine structure of radium // Photoelectronics.-2005.-

N14.-P.83-85.
25. Khetselius O.Yu., Quantum structure of electroweak interaction in heavy finite ermi-systems.-Odessa: Astroprint, 2011.
26. Serot B. D., Advances in Nuclear Physics Vol. 16: The Relativistic Nuclear Many Body Problem / Serot B. D., Walecka J. D.-Plenum Press, New York, 1986.
27. Burvenich T. J., Evers J., Keitel C. H., Dynamic nuclear Stark shift in superintense laser fields // Phys.Rev.C.-2006.-Vol.74.-P. 044601-1-044601-10.
28. Dikmen E., Novoselsky A., Vallieres M., Shell model calculation of low-lying states of ^{110}Sb // J.Phys.G.: Nucl. Part. Phys.- 2007.-Vol. 34.-P. 529-535.
29. Sobel'man I. I. Introduction to theory of atomic spectra.-Moscow: Nauka.- 1977.
30. Radtsig A. A.,Smirnov B. M., Parameters of atoms and ions. – Moscow, 1986.

The article is received in editorial 15.07.2013

UDC 539.184

O. Yu. Khetselius

HYPERFINE STRUCTURE PARAMETERS OF THE HEAVY ISOTOPES: CONSISTENT NUCLEAR-QED THEORY

Abstract

It is presented the new, consistent theoretical nuclear-QED approach to estimating parameters of the hyperfine structure of the heavy isotopes, which is based on the relativistic mean field theory of a nucleus and QED perturbation theory. The hyperfine structure parameters for the heavy isotopes of ^{205}Tl and ^{169}Tm are calculated. The theoretical values of the relative contribution into the hyperfine structure due to the effect of the distribution of the magnetic moment of the nucleus are listed too.

Key words: hyperfine structure, heavy isotopes, nuclear-QED approach

УДК 539.184

О. Ю. Хецелиус

ПАРАМЕТРЫ СВЕРХТОНКОЙ СТРУКТУРЫ ТЯЖЕЛЫХ ИЗОТОПОВ В РАМКАХ ПОСЛЕДОВАТЕЛЬНОЙ ЯДЕРНО-КЭД ТЕОРИИ

Резюме

Представлен новый, последовательный теоретический ядерно-КЭД подход к оценке параметров сверхтонкой структуры тяжелых изотопов, основанный на релятивистской теории среднего поля ядра и КЭД теории возмущений. Рассчитаны параметры сверхтонкой структуры спектров тяжелых изотопов ^{205}Tl и ^{169}Tm. Также приведены оценки теоретических значений относительного вклада в значения параметров сверхтонкой структуры вследствие эффекта распределения магнитного момента в ядре.

Ключевые слова: сверхтонкая структура, тяжелые изотопы, ядерно-КЭД теория

УДК 539.184

О. Ю. Хецеліус

ПАРАМЕТРИ НАДТОНКОЇ СТРУКТУРИ ВАЖКИХ ІЗОТОПІВ В РАМКАХ ПОСЛІДОВНОЇ ЯДЕРНО-КЕД ТЕОРІЇ

Резюме

Розвинуто новий послідовний теоретичний ядерно-КЕД підхід до оцінки параметрів надтонкої структури важких ізотопів, який базується на релятивістській теорії середнього поля ядра і КЕД теорії збурень. Розраховані параметри надтонкої структури спектрів важких ізотопів ^{205}Tl і ^{69}Tm. Також наведені оцінки теоретичних значень відносного внеску до параметрів надтонкої структури завдяки ефекту розподілу магнітного моменту в ядрі.

Ключові слова: надтонка структура, важкі ізотопи, ядерно-КЕД теорія

ІНФОРМАЦІЯ ДЛЯ АВТОРІВ НАУКОВОГО ЗБІРНИКА «PHOTOELECTRONICS»

У збірнику «Photoelectronics» друкуються статті, які містять результати наукових досліджень та технічних розробок у таких напрямках:

- Фізика напівпровідників, гетеро- і низькорозмірні структури;
- Фізика мікроелектронних приладів;
- Квантова оптика і спектроскопія ядер, атомів, молекул та твердих тіл;
- Оптоелектроніка , квантова електроніка і сенсоріка;
- Фотофізика ядра, атомів, молекул;
- Взаємодія інтенсивного лазерного випромінювання з ядрами, атомними системами, речовиною.

Збірник включено до Переліку спеціальних видань ВАК України з фізико-математичних та технічних наук.

Рукописи надсилаються на адресу: відповід. секретарю Куталовій М. І., вул. Пастера, 42, Одеський національний університет імені І. І. Мечникова, м. Одеса, 65026, http://www. photoelectronics.onu.edu.ua

Комп'ютерне верстання – О. І. Карличук

Підп.до друку 05.09.2013. Формат 60×84/8. . Умов.-друк.арк. 17,9. Тираж 100 прим.
Замов. № 783.

Видавець і виготовлювач
«Одеський національний університет»
Свідоцтво ДК № 4215 від 22.11.2011 р.

65082, м. Одеса, вул. Єлісаветинська, 12, Україна
Тел.: (048) 723 28 39, e-mail: druk@onu.edu.ua